De la constante de Rydberg à la métrologie des constantes fondamentales

François Nez

Université Pierre et Marie Curie

Mémoire d'habilitation à diriger des recherches

François Nez

soutenue, le 27 juin 2005, devant le jury composé de :

Alfred MAQUET, président du jury
Christian CHARDONNET, rapporteur
Jacques VIGUÉ, rapporteur
Christoph WESTBROOK, rapporteur
Barry TAYLOR
François BIRABEN

Table des matières

Curriculum vitae

NEZ François (41 ans)

Section 04

27 Juin 2004 : Habilitation à Diriger des Recherches.

1998 : passage CR1.

1994 : recrutement CR2.

1993/1994 : post-doc au Laboratoire Primaire du Temps et des Fréquences (maintenant BNM-SYRTE).

1990/1993 : thèse de doctorat de l'Université Paris 6 au Laboratoire de Spectroscopie Hertzienne de l'Ecole Normale Supérieure (maintenant Laboratoire Kastler Brossel).

1989/1990 : service national.

1989 : diplôme d'ingénieur de l'Ecole Supérieure d'Optique.

Coordonnées professionnelles

Laboratoire Kastler Brossel - UMR 8552
4 place Jussieu, pyramide 13-24
75252 Paris Cedex 05
Téléphone :
+33 1 44 27 72 48 (bureau)
+33 1 44 27 26 67 (laboratoire)
Courriel : nez@spectro.jussieu.fr

LISTE DES TRAVAUX, PUBLICATIONS ET COMMUNICATIONS A DES CONGRES

Thèse de doctorat de l'Université Paris 6 : "Chaîne de fréquence optique pour mesurer les transitions 2S-8S/8D dans l'atome d'hydrogène ; mesure de la constante de Rydberg en unité de fréquence." (27 Octobre 1993)

Publications dans des revues à comité de lecture :

1. F. BIRABEN, L. JULIEN, J. PLON et F. NEZ, Europhys. Lett., 15 (1991) p.831 : "Compensation of the second Doppler effect in two photon spectroscopy of atomic hydrogen".
2. F. BIRABEN, D. JASMIN, L. JULIEN, F. NEZ et J. VIGUE, Optics Comm., 92 (1992) p.135 : "Hyperfine structure of the A3 1 of IBr".
3. F. NEZ, M. D. PLIMMER, S. BOURZEIX, L. JULIEN, F. BIRABEN, R. FELDER, O. ACEF, J.J. ZONDY, P. LAURENT, A. CLAIRON, M. ABED, Y. MILLERIOUX, et P. JUNCAR, Phys. Rev. Lett., 69 (1992) p.2326 : Precise frequency measurement of the 2S-8S/8D transitions in atomic hydrogen : new determination of the Rydberg constant".
4. S. BOURZEIX, M.D. PLIMMER, F. NEZ, L. JULIEN et F. BIRABEN., Optics Comm., 99 (1993) p.89 : "Efficient frequency doubling of a continuous wave titanium-sapphire laser in an external enhancement cavity".
5. F. NEZ, F. BIRABEN, R. FELDER et Y. MILLERIOUX, Optics Comm., 102 (1993) p.432 : "Optical frequency determination of the hyperfine components of the 5S1/2-5D3/2 two photon transitions in rubidium".
6. F. NEZ, M.D. PLIMMER, S. BOURZEIX, L. JULIEN, F. BIRABEN, R. FELDER, Y. MILLERIOUX et P. de NATALE, Europhys. Lett., 24 (1993) p.635 : "First pure frequency measurement of an optical transition in atomic hydrogen : better determination of the Rydberg constant".
7. O. ACEF, L. HILICO, M. BAHOURA, F. NEZ et P. de NATALE., Optics Comm., 109 (1994) p.428 : "Comparaison between MIM and

Schottky diodes as harmonic mixers for visible lasers and microwave sources".

8. O. ACEF, F. NEZ et G.D. ROVERA, Optics Lett., 19 (1994) p.1275 : "Optical heterodyning with a frequency difference of 1 THz in the 850 nm range".
9. L. HILICO, D. TOUAHRI, F. NEZ et A. CLAIRON, Rev. Sci. Instrument. 65 (12), (1994) p.3628 : "Narrow line, low amplitude noise semiconductor laser oscillator in the 780 nm range".
10. S. BOURZEIX, B. de BEAUVOIR, F. NEZ, M.D. PLIMMER, F. de TOMASI, L. JULIEN, F. BIRABEN et D.N. STACEY, Phys. Rev. Lett., 76 (1996) p.384 : "High resolution spectroscopy of the hydrogen atom : determination of the 1S Lamb shift".
11. S. BOURZEIX, B. de BEAUVOIR, F. NEZ, F. de TOMASI, L. JULIEN et F. BIRABEN, Optics Comm., 133 (1997) p. 239 : "Ultra-violet light generation at 205 nm by two frequency doubling steps of a CW titanium-sapphire laser".
12. D. TOUAHRI, O. ACEF, A. CLAIRON, J.J. ZONDY, R. FELDER, L. HILICO, B. de BEAUVOIR, F. BIRABEN et F. NEZ, Optics Comm., 133 (1997) p. 471 : "Frequency measurement of the 5S1/2(F=3)-5D5/2(F=5) two-photon transition in rubidium".
13. B. de BEAUVOIR, F. NEZ, L. JULIEN, B. CAGNAC, F. BIRABEN, D. TOUAHRI, L. HILICO, O. ACEF, A. CLAIRON et J.J. ZONDY, Phys. Rev. Lett., 78 (1997) p 440 : "Absolute frequency measurement of the 2S-8S/D transitions in hydrogen and deuterium : new determination of the Rydberg constant".
14. C. DORRER, F. NEZ, B. DE BEAUVOIR, L. JULIEN et F. BIRABEN, Phys. Rev. Lett., (1997), 78, p 3658 : "Accurate determination of the 23S1-33D1 two-photon transition frequency in helium : new determination of the 23S1 Lamb shift".
15. B. de BEAUVOIR, F. NEZ, L. HILICO, L. JULIEN, F. BIRABEN, B. CAGNAC, J.J. ZONDY, D. TOUAHRI, O. ACEF et A. CLAIRON, Eur. Phys. J. D. 1 (1998), p 227 "Transmission of an optical frequency through a 3 km long optical fiber".
16. G. HAGEL, C. NESI, L. JOZEFOWSKI, C. SCHWOB, F. NEZ et F. BIRABEN, Optics Comm., 160 (1999), p. 1 "Accurate measurement of the frequency of the 6S-8S two photon transition in Cesium".

17. C. SCHWOB, L. JOZEFOWSKI, B. de BEAUVOIR, L. HILICO, F. NEZ, L. JULIEN, F. BIRABEN, O. ACEF et A. CLAIRON, Phys. Rev. Lett, 82 (1999) p.4960-4963 : "Optical frequency measurement of the 2S-12D transitions in hydrogen and deuterium : Rydberg constant and Lamb shift determinations ".
18. B. De BEAUVOIR , C. SCHWOB , O. ACEF , L. JOZEFOWSKI , L. HILICO , F. NEZ , L. JULIEN, A. CLAIRON et F. BIRABEN , Eur. Phys. J. D 12 (2000) p.61-93 : "Metrology of the hydrogen and deuterium atoms : determination of the Rydberg constant and Lamb shifts".
19. G. HAGEL, R. BATTESTI, F. NEZ, L. JULIEN et F. BIRABEN, Phys. Rev. Lett. 89 (2002) p. 203001 : " Observation of a motional Stark effect to determine the second order Doppler effect ".
20. G. HAGEL, F. NEZ et F. BIRABEN, Applied Optics 41 (2002) pp. 7702-7706 : " Analysis and observation, on an atomic resonance, of the frequency shift due to the length modulation of an optical cavity ".
21. R. Battesti, P. Cladé, S. Guellati-Khélifa, C. Schwob, B. Grémaud, F. Nez, L. Julien and F. Biraben, Phys.Rev. Lett. 92 (2004) p. 253001 : " Bloch oscillations of ultracold atoms : a tool for a metrological determination of h/mRb ".
22. P. Cladé, S. Guellati-Khélifa, C. Schwob, F. Nez, L. Julien and F. Biraben, Eur. Phys. J. D. (à paraître) : "Noise sensitivity of an atomic velocity sensor".

Publications dans des actes de colloques

1. F. BIRABEN, L. JULIEN et F. NEZ Proceeding of Laser Spectroscopy X, édités par M. Ducloy, E. Giacobino et G. Camy, World Scientific (1992) p.104 : "High resolution spectroscopy of the hydrogen atom".
2. F. NEZ, M.D. PLIMMER, S. BOURZEIX, L. JULIEN, F. BIRABEN, B. CAGNAC, R. FELDER, P. JUNCAR et Y. MILLERIOUX, IEEE Transactions on Instrumentation and Measurements, 42 (1993) p.217 : "Towards a frequency measurement of the Rydberg constant using the 2S-8S and 2S 8D transitions of hydrogen".
3. F. NEZ, M.D. PLIMMER, S. BOURZEIX, L. JULIEN et F. BIRABEN, Proceedings of the XIIIth International Conference on Atomic

Physics, H. Walther, T.W. Hänsch et B. Neizert Ed., American Institute of Physics, 275 (1993) p.20 : "Frequency measurement of the Rydberg constant via the 2S 8S/D transitions in atomic Hydrogen".

4. F. NEZ, M.D. PLIMMER, S. BOURZEIX, L. JULIEN et F. BIRABEN, Proceedings of the International School of Physics "Enrico Fermi", Course "Frontiers in Laser Spectroscopy", Rendiconti S.I.F. CXX (1994) p.287 : "High resolution spectroscopy of the Hydrogen atom : measurement of the Rydberg constant".
5. F. NEZ, M.D. PLIMMER, S. BOURZEIX, L. JULIEN, F. BIRABEN, R. FELDER, Y. MILLERIOUX et P. de NATALE, Proceeding of Laser Spectroscopy XI, American Institute of Physics, 290 (1994) p.11 : "Absolute frequency measurement of the 2S-8S/D transitions in atomic hydrogen".
6. F. NEZ, S. BOURZEIX, L. JULIEN, F. BIRABEN, R. FELDER et Y. MILLERIOUX, Proceeding of Laser Spectroscopy XI, American Institute of Physics, 290 (1994) p.9 : "Frequency measurement of the 5S-5D two-photon transition in rubidium and prospects for measuring (He-Ne)/I2 lasers at $\lambda = 633nm$".
7. F. NEZ, M.D. PLIMMER, S. BOURZEIX, L. JULIEN, F. BIRABEN, R. FELDER, Y. MILLERIOUX et P. de NATALE, IEEE Transactions on Instrumentation and Measurements, 44 (1995) p.568 :"Determination of the Rydberg constant by direct frequency measurement".*
8. D.TOUAHRI, F. NEZ, M. ABED, J.J. ZONDY, O. ACEF, L. HILICO, A. CLAIRON, Y. MILLERIOUX, F. BIRABEN, L. JULIEN et R. FELDER, IEEE Transactions on Instrumentation and Measurements, 44 (1995) p.170 : "LPTF frequency synthesis chain : results and improvements for the near future".
9. D. TOUAHRI, M. ABED, L. HILICO, J.J. ZONDY, O. ACEF, A. CLAIRON, Y. MILLERIOUX, R. FELDER, F. NEZ, F. BIRABEN. et L. JULIEN, Proceedings of the VIII European Frequency and Time Forum : "Absolute frequency measurement in the visible and near infrared range".
10. J.J ZONDY, D. TOUAHRI, O. ACEF, L. HILICO, M. ABED, A. CLAIRON, Y. MILLERIOUX, R. FELDER, B. de BEAUVOIR, F. NEZ, F. BIRABEN et L. JULIEN, Proceedings of the Photonic West 95 Conference, SPIE95 2378 (1995) p.147 : "Absolute frequency mea-

surement of a diode laser locked on a hyperfine component of 5S-5D two-photon transitions of rubidium".

11. R. FELDER, D. TOUAHRI, O. ACEF, L. HILICO, J.J. ZONDY, A. CLAIRON, B. de BEAUVOIR, F. BIRABEN, L. JULIEN, F. NEZ et Y. MILLERIOUX, Proceedings of the Photonic West 95 Conference, SPIE95 2378 (1995) p.52 : "Performance of a GaAlAs laser diode stabilized on a hyperfine component of two-photon transitions of rubidium at 778 nm".
12. S. BOURZEIX, B. de BEAUVOIR, F. NEZ, M.D. PLIMMER, F. de TOMASI , L. JULIEN, F. BIRABEN et D.N. STACEY, Proceedings of Laser Spectroscopy XII, édités par M. Inguscio, M. Allegrini et A. Sasso, World Scientific (1996) p.79-82 : "High resolution spectroscopy of the hydrogen atom : determination of the 1S Lamb shift".
13. S. BOURZEIX, B. de BEAUVOIR, F. NEZ, M.D. PLIMMER, F. de TOMASI, L. JULIEN et F. BIRABEN, Proceedings of the Fifth Symposium on Frequency Standards and Metrology, édité par J.C. Bergquist, World Scientific (1996) p.145-150 : "High resolution spectroscopy of the hydrogen atom".
14. B. CAGNAC, F. BIRABEN, L. JULIEN, F. NEZ et S. BOURZEIX, In "Modern Problems of Laser Physics", édité par Bagayev S.N. et Denisov V.I., (1996) pp. 19-28 : "Two-photon spectroscopy of optical frequencies in rubidium and hydrogen".
15. F. BIRABEN, B. de BEAUVOIR, F. NEZ, L. HILICO, L. JULIEN, B. CAGNAC, D. TOUAHRI, O. ACEF, A. CLAIRON et J.J. ZONDY, Proceedings of Laser Spectroscopy XIII, ed. Z. J. Wang et Z. M. Zhang (World Scientific) p. 93-96 : "Accurate spectroscopy of simple atomic systems : metrology of fundamental constants and test of quantum electrodynamics".
16. F. BIRABEN, F. NEZ, L.JULIEN, Proceedings of the Third Euroconference on Atomic Physics with Highly Charged Ions, Hyperfine Interactions 114 (1998) p. 71-86 : "Experimental tests of quantum elctrodynamics in weak field".
17. B. de BEAUVOIR, L. HILICO, L. JULIEN, F. BIRABEN, B. CAGNAC, F. NEZ, J.J. ZONDY, D. TOUAHRI, O. ACEF et A. CLAIRON, Proceedings of the international symposium on Modern Problems of Laser Physics (MPLP'97), ed. S.N. Bagayev et V.I. Denisov,

p.79-86 : "High resolution spectroscopy of hydrogen and deuterium atoms".

18. C. SCHWOB, L. JOZEFOWSKI, O. ACEF, L. HILICO, B. de BEAUVOIR, F. NEZ, L. JULIEN, A. CLAIRON et F. BIRABEN, IEEE Transactions on Instrumentation and Measurements, 48 (1999) p.178-181 : :"Frequency measurement of the 2S-12D transitions in hydrogen and deuterium, new determination of the Rydberg constant".
19. C. SCHWOB, L. JOZEFOWSKI, B. de BEAUVOIR, L. HILICO, F. NEZ, L. JULIEN, F. BIRABEN, O. ACEF et A. CLAIRON, Proceedings of the XXXIVth Rencontres de Moriond, Gravitationnal Waves and experimental gravity, , édité par J. Trân Thanh Vân, J. Dumarchez, S. Reynaud, C. Salomon, S. Thorsett et J.Y. Vinet, World Publishers, Hanoi, Vietnam, p.427-432 :"Metrology of the hydrogen atom : Rydberg constant determination and Lamb shift".
20. C. SCHWOB, L. MASSON, B. GREMAUD, S. GUELLATI, F. NEZ, L. JULIEN et F. BIRABEN , Actes de COLOQ6, Journal de physique IV 10 (2000) p.153-154 : "Accélération d'atomes ultrafroids : mesure de h/MA".
21. R. POHL, F. BIRABEN, C.A.N. CONDE, C. DONCHE-GAY, T.W. HANSCH, F.J. HARTMANN, P. HAUSER, V.W. HUGHES, O. HUOT, P. INDELICATO, P. KNOWLES, F. KOTTMANN , Y.W. LIU, F. MULHAUSER, F. NEZ, C. PETITJEAN, P. RABINOWITZ , J.M.F. DOS SANTOS, L.A. SCHALLER, Y.H. SCHNEUWL, W. SCHOTT , L.M. SIMONS, D. TAQQU, F. TREHIN, J.F.C.A. VELOSO, Hyperfine-Interactions 127 (2000) p. 161-166. : "Experiment to measure the Lamb shift in muonic hydrogen".
22. F. BIRABEN, T.W. HÄNSCH, M. FISCHER, M. NIERING, R. HOLZWARTH, J. REICHERT, Th. UDEM, M. WEITZ, B. de BEAUVOIR, C. SCHWOB, L. JOZEFOWSKI , L. HILICO, F. NEZ, L. JULIEN, O. ACEF et A. CLAIRON, Proceedings of the conference Hydrogen Atom II, actes : "Precision spectroscopy of atomic hydrogen".
23. G. HAGEL, R.BATTESTI, C. SCHWOB, F. NEZ, L. JULIEN, F. BIRABEN, O. ACEF, J.J. ZONDY, A. CLAIRON, Proceedings of the conference Hydrogen Atom II, actes à paraître sur cdrom : "Absolute frequency measurement of the 1S-3S transition in hydrogen".
24. R. POHL, F. BIRABEN, C.A.N. CONDE, C. DONCHE-GAY, T.W. HÄNSCH, F.J. HARTMANN, P. HAUSER, V.W. HUGHES, O. HUOT,

P. INDELICATO, P. KNOWLES, F. KOTTMANN, Y.W. LIU, F. MULHAUSER, F. NEZ, C. PETITJEAN, P. RABINOWITZ, J.M.F. Dos SANTOS, L.A. SCHALLER, H. SCHNEUWLY, W. SCHOTT, L. SIMONS, D. TAQQU et J.F.C.A. VELOSO, Proceedings of the conference Hydrogen Atom II, actes : "Towards a measurement of the Lamb shift in muonic hydrogen".

25. G. HAGEL, C. SCHWOB, L. JOZEFOWSKI, B. de BEAUVOIR, L. HILICO, F. NEZ, L. JULIEN, F. BIRABEN, O. ACEF et A. CLAIRON, Proceedings of the Third international symposium Modern Problems of Laser Physics (Novosibirsk, 2000), à paraître : "Metrology of hydrogen atom : determination of the Rydberg constant and Lamb shifts".
26. G. HAGEL, C. SCHWOB, L. JOZEFOWSKI, B. de BEAUVOIR, L. HILICO, O. ACEF, F. NEZ, L. JULIEN, A. CLAIRON et F. BIRABEN, Proceedings of the Conference QED 2000 (Trieste, 2000), Frontier Tests of Quantum Electrodynamics and Physics of the Vacuum, édité par G. Cantatore, à paraître : "Metrology of hydrogen atom : determination of the Rydberg constant and Lamb shifts".
27. G. HAGEL, C . SCHWOB, L. JOZEFOWSKI, B. de BEAUVOIR, L. HILICO, O. ACEF, F. NEZ, L. JULIEN, A. CLAIRON et F. BIRABEN, Proceedings SPIE 4269 (San Jose, 2001) : "Metrology of hydrogen atom : determination of the Rydberg constant and Lamb shifts".
28. BIRABEN F., HÄNSCH T.W., FISCHER M., NIERING M., HOLZWARTH R., REICHERT J., UDEM Th., WEITZ M., de BEAUVOIR B., SCHWOB C., JOZEFOWSKI L., HILICO L., NEZ F., JULIEN L., ACEF O. et CLAIRON A., Lecture Notes in Physics (Springer), The Hydrogen Atom, Precision Physics of Simple Atomic Systems, édité par S.G. Karshenboïm, F.S. Pavone, G.F. Bassani, M. Inguscio and T.W. Hänsch, LNP 570 (2001) p. 17-41 : "Precision spectroscopy of atomic hydrogen".
29. HAGEL G., BATTESTI R., SCHWOB C., NEZ F., JULIEN L., BIRABEN F., ACEF O., ZONDY J.J., CLAIRON A., Lecture Notes in Physics (Springer), The Hydrogen Atom, Precision Physics of Simple Atomic Systems, édité par S.G. Karshenboïm, F.S. Pavone, G.F. Bassani, M. Inguscio and T.W. Hänsch, LNP 570 (2001) sur cdrom : "Absolute frequency measurement of the 1S-3S transition in hydrogen".

30. POHL R., BIRABEN F., CONDE C.A.N., DONCHE-GAY C., HÄNSCH T.W., HARTMANN F.J., HAUSER P, HUGHES V.W., HUOT O., INDELICATO P., KNOWLES P., KOTTMANN F., LIU Y.W., MULHAUSER F., NEZ F., PETITJEAN C., RABINOWITZ P., Dos SANTOS J.M.F., SCHALLER L.A., SCHNEUWLY H., SCHOTT W., SIMONS L., TAQQU D.et VELOSO J.F.C.A., Lecture Notes in Physics (Springer), The Hydrogen Atom, Precision Physics of Simple Atomic Systems, édité par S.G. Karshenboïm, F.S. Pavone, G.F. Bassani, M. Inguscio and T.W. Hänsch, LNP 570 (2001) sur cdrom : "Towards a measurement of the Lamb shift in muonic hydrogen".
31. HAGEL G., SCHWOB C., JOZEFOWSKI L., de BEAUVOIR B., HILICO L., NEZ F., JULIEN L., BIRABEN F., ACEF O. et CLAIRON A., Proceedings of the Third international symposium Modern Problems of Laser Physics (Institute of Laser Physics, Novosibirsk, 2000), édité par S.N. Bagayev et V.I. Denisov, pp. 40-51 ; publié aussi dans Laser Physics 11 (2001) pp. 1076-1082 : "Metrology of hydrogen atom : determination of the Rydberg constant and Lamb shifts".
32. KOTTMANN F., BIRABEN F., CONDE C.A.N., DONCHE-GAY C., HÄNSCH T.W., HARTMANN F.J., HAUSER P, HUGHES V.W., HUOT O., INDELICATO P., KNOWLES P., LIU Y.W., MARKUSHIN V.E., MULHAUSER F., NEZ F., POHL R., RABINOWITZ P., Dos SANTOS J.M.F., SCHALLER L.A., SCHNEUWLY H., SCHOTT W., TAQQU D.et VELOSO J.F.C.A., Proceedings of the Conference QED 2000 (Trieste, 2000), Quantum Electrodynamics and Physics of the Vacuum, édité par G. Cantatore, AIP-Conference proceedings 564 (2001) p.13-20 : "Towards a Lamb shift measurement in muonic hydrogen".
33. HAGEL G., SCHWOB C., JOZEFOWSKI L., de BEAUVOIR B., HILICO L., ACEF O., NEZ F., JULIEN L., CLAIRON A. et BIRABEN F., Proceedings of the Conference QED 2000 (Trieste, 2000), Quantum Electrodynamics and Physics of the Vacuum, édité par G. Cantatore, AIP-Conference proceedings 564 (2001) p.231-238 : "Metrology of hydrogen atom : determination of the Rydberg constant and Lamb shifts".
34. HAGEL G., SCHWOB C., JOZEFOWSKI L., de BEAUVOIR B., HILICO L., ACEF O., ZONDY J.-J., NEZ F., JULIEN L., CLAIRON A. et BIRABEN F., Proceedings SPIE 4269 (2001) p.25-31 : Metrology of hydrogen atom : determination of the Rydberg constant and Lamb shifts".

35. F. Kottmann, W. Amir, F. Biraben, C.A.N. Conde, S. Dhawan, T.W. Hänsch, F.J. Hartmann, V.W. Hughes, O. Huot, P. Indelicato, L. Julien, P. Knowles, S. Kazamias, Y.-W. Liu, F. Mulhauser, F. Nez, R. Pohl, P. Rabinowitz, J.M.F.D. Santos, L.A. Schaller, H. Schneuwly, W. Schott, D. TaqquetJ.F.C.A. Veloso. Hyp. Int. 138 (2001), p. 55-60 : "The Muonic Hydrogen Lamb Shift Experiment at PSI".
36. HAGEL G., SCHWOB C., JOZEFOWSKI L., de BEAUVOIR B., HILICO L., NEZ F., JULIEN L., BIRABEN F., ACEF O., ZONDY J.-J. and CLAIRON A., ., Proceedings of the Sixth Symposium on Frequency Standards and Metrology (St-Andrews, 2001), édité par P. Gill, World Scientific (2002), pp. 222-229 : "Metrology of hydrogen atom : determination of the Rydberg constant and Lamb shifts".
37. BATTESTI R., SCHWOB C., GRÉMAUD B., GUELLATI S., NEZ F., JULIEN L. et BIRABEN F. : Proceedings of the Sixth Symposium on Frequency Standards and Metrology (St-Andrews, 2001), édité par P. Gill, World Scientific (2002), pp. 535-537 : "Acceleration of rubidium cold atoms : determination of ".
38. R. BATTESTI, P. CLADÉ, S.GUELLATI-KHÉLIFA, C. SCHWOB, B. GRÉMAUD, F. NEZ, L. JULIEN AND F. BIRABEN, J. Opt. B : Quantum Semiclass. Opt. 5 (2003) pp. 178-182 : " Acceleration of ultracold atoms : towards a measurement of h/MRb ".
39. R. BATTESTI, P. CLADE, C. SCHWOB, B. GREMAUD, S. GUELLATI-KHELIFA, F. NEZ, L. JULIEN ET F. BIRABEN, actes de COLOQ8, à paraître : "Accélération d'atomes ultra froids : vers une mesure de h/MA".

Publications dans des revues de diffusion de l'information scientifique :

1. O. ACEF, B. de BEAUVOIR, F. BIRABEN, B. CAGNAC, A. CLAIRON, L. HILICO, L. JULIEN, F. NEZ, D. TOUAHRI et J.J. ZONDY, Lettre Ultimatech, 6 (1997) pp. 16-18 :"Mesure de fréquences optiques : réalisation d'un étalon de fréquence à 385 THz".
2. B. de BEAUVOIR, F. NEZ, L. JULIEN, L. HILICO, F. BIRABEN, B. CAGNAC, D. TOUAHRI, O. ACEF, A. CLAIRON et J.J. ZONDY,

Bulletin du Bureau National de Métrologie, 108 (1997)p. 17-25 : "La métrologie des fréquences lumineuses fait progresser notre connaissance de la constante de Rydberg".

Conférences invitées :

Les communications que j'ai présenté personnellement sont suivies d'une astérisque.

1. L. JULIEN, F. NEZ, M.D. PLIMMER, S. BOURZEIX, F. BIRABEN, XIII International Conference on Atomic Physics, (1992) : "Frequency measurement of the Rydberg constant via the 2S-8S, 8D transitions in atomic hydrogen" (Münich - Allemagne).
2. L.JULIEN, F. NEZ, M.D. PLIMMER, S. BOURZEIX, F. BIRABEN, International School of Physics "Enrico Fermi" (1992) : "High resolution spectroscopy of the hydrogen atom ; measurement of the Rydberg constant (Course "Frontiers in Laser Spectroscopy ", Varenna - Italie).
3. F. NEZ, M.D. PLIMMER, S. BOURZEIX, L. JULIEN, F. BIRABEN, R. FELDER, Y. MILLERIOUX et P. de NATALE, International Conference on Laser Spectroscopy (1993) : "Absolute frequency measurement of the 2S-8S/D transitions in atomic hydrogen" (Hot Springs - USA).
4. * F. NEZ., M.D. PLIMMER, S. BOURZEIX, L. JULIEN, F. BIRABEN, R. FELDER, Y. MILLERIOUX et P. de NATALE, Conference on Precision Electromagnetic Measurements (1994) :"Determination of the Rydberg constant by direct frequency measurement" (Boulder - USA).
5. S. BOURZEIX, B. de BEAUVOIR, F. NEZ, M.D. PLIMMER, F. de TOMASI, L. JULIEN, F. BIRABEN et D.N. STACEY D, International Conference on Laser Spectroscopy XII (1995) : "High resolution spectroscopy of the hydrogen atom : determination of the 1S Lamb shift" (Capri - Italie).
6. B. CAGNAC, F. BIRABEN, L. JULIEN, F. NEZ et S. BOURZEIX, International symposium on Modern Problems of Laser Physics (1995) : : "Two-photon spectroscopy of optical frequencies in rubidium and hydrogen" (Novossibirsk - Russie).
7. S. BOURZEIX, B ; de BEAUVOIR, F. NEZ, M.D. PLIMMER, F. TOMASI, L. JULIEN et F. BIRABEN., Fifth Symposium on Frequency

Standards and Metrology (1995) : "High resolution spectroscopy of the hydrogen atom" (Woods Hole -USA).

8. * B. de BEAUVOIR, L. HILICO, L. JULIEN, F. BIRABEN, B. CAGNAC, F. NEZ, J.J. ZONDY, D. TOUAHRI, O. ACEF et A. CLAIRON, International symposium on Modern Problems of Laser Physics (1997) : "High resolution spectroscopy of hydrogen and deuterium atoms" (Novossibirsk - Russie).
9. F. BIRABEN, F. NEZ et L. JULIEN Third Euroconference of Atomic Physics with Highly charged ions (1997) : "Experimental tests of quantum electrodynamics in weak field" (Ferrara - Italie).
10. C. SCHWOB, L. JOZEFOWSKI, L. HILICO, B. de BEAUVOIR, F. NEZ, L. JULIEN, F. BIRABEN, O. ACEF et A. CLAIRON, International Conference on Coherent and Nonlinear Optics (ICONO'98) (1998) : "Optical frequency measurement in hydrogen and deuterium. Determination of the Rydberg constant" (Moscou - Russie).
11. C. SCHWOB, L. JOZEFOWSKI, O. ACEF, L. HILICO, B. de BEAUVOIR, F. NEZ, L. JULIEN, A. CLAIRON et F. BIRABEN, Sixth European Conference on Atomic and Molecular Physics (1998) : "Frequency measurement of the 2S-12D transitions in hydrogen and deuterium. Determination of the Rydberg constant" (Sienne - Italie)
12. * C. SCHWOB, L. JULIEN, L. HILICO, B. CAGNAC, F. BIRABEN, F. NEZ, O. ACEF, A. CLAIRON, D. TOUAHRI, S. BOURZEIX, B. de BEAUVOIR, F de TOMASI et L. JOZEFOWSKI, Quantum Optics (1998) : "Metrology of hydrogen atom : Determination of the Rydberg constant and QED test" (Pise - Italie).
13. C. SCHWOB, L. JOZEFOWSKI, B. de BEAUVOIR, L. HILICO, F. NEZ, L. JULIEN, F. BIRABEN, O. ACEF et A. CLAIRON, XXXIVth Rencontres de Moriond, Gravitationnal Waves and experimental gravity, (1999) :"Metrology of the hydrogen atom : Rydberg constant determination and Lamb shift" (Moriond - Suisse).
14. C. SCHWOB, L. JOZEFOWSKI , B. de BEAUVOIR, L. HILICO, F. NEZ, L. JULIEN , F. BIRABEN, O. ACEF et A. CLAIRON, First Russian-French Workshop, Les Houches, France, 1999 : "High resolution spectroscopy of hydrogen atoms".
15. G. HAGEL, C. SCHWOB, L. JOZEFOWSKI, B. de BEAUVOIR, L. HILICO, F. NEZ, L. JULIEN, F. BIRABEN, O. ACEF et A. CLAI-

RON : Third international symposium Modern Problems of Laser Physics, Novosibirsk, Russie, 2000, "Metrology of hydrogen atom : determination of the Rydberg constant and Lamb shifts".

16. G. HAGEL, C. SCHWOB, L. JOZEFOWSKI, B. de BEAUVOIR, L. HILICO, O. ACEF, F. NEZ, L. JULIEN, A. CLAIRON et F. BIRABEN, Conference QED 2000, Frontier Tests of Quantum Electrodynamics and Physics of the Vacuum, Trieste, Italie, 2000 (actes : "Metrology of hydrogen atom : determination of the Rydberg constant and Lamb shifts".
17. G. HAGEL, C. SCHWOB, L. JOZEFOWSKI , B. de BEAUVOIR, L. HILICO, O ; ACEF, F. NEZ, L . JULIEN, A. CLAIRON et F. BIRABEN , Conference SPIE LASE 2001, Laser frequency stabilization, standards, measurement, and applications, San Jose, USA, 2001 (actes) : "Metrology of hydrogen atom : determination of the Rydberg constant and Lamb shifts".
18. HAGEL G., SCHWOB C., JOZEFOWSKI L., de BEAUVOIR B., HILICO L., ACEF O., ZONDY J.-J., NEZ F., JULIEN L., CLAIRON A. et BIRABEN F. ,Second Russian-French Laser Symposium, Vladimir, Russie, octobre 2001. : " Precision spectroscopy of hydrogenic systems ".
19. P. CLADE, R. BATTESTI, S. GUELLATI, C. SCHWOB, B. GREMAUD, F. NEZ, L. JULIEN ET F. BIRABEN, Congrés de la Société Française de Physique, Lyon, juillet 2003 : "Accélération d'atomes ultra froids : vers une mesure de la constante de structure fine".
20. R. BATTESTI, P. CLADE, C. SCHWOB, B. GREMAUD, S. GUELLATI-KHELIFA, F. NEZ, L. JULIEN ET F. BIRABEN, Symposium Laser Franco Russe (RFLS), Moscou, octobre 2003 : "Towards a measurement of the fine structure constant with ultracolds atoms".
21. R. BATTESTI, P. CLADE, S. GUELLATI-KHELIFA, C. SCHWOB, B. GREMAUD, F. NEZ, L. JULIEN ET F. BIRABEN, Forth international symposium Modern Problems of Laser Physics, Novosibirsk, Russie, 22-27 aôut 2004. : "Preliminary measurement of h/mRb using Bloch oscillations of ultracold atoms".

Autres exposés oraux

- F.BIRABEN, L. JULIEN et F. NEZ, Congrès de la SFP : nouvelles tendances en physique atomique et moléculaire, Caen, France, 1991 : "Spectroscopie à haute résolution de l'atome d'hydrogène".
- F. NEZ, M.D. PLIMMER, S. BOURZEIX, L. JULIEN, F. BIRABEN, B. CAGNAC, R. FELDER, P. JUNCAR, Y. MILLERIOUX, Conference on Precision Electromagnetic Measurements, Paris, 1992 : "Towards a frequency measurement of the Rydberg constant using the 2S-8S and 2S-8D transitions of hydrogen".
- F. NEZ, M.D. PLIMMER, S. BOURZEIX, L. JULIEN et F. BIRABEN Eighteenth International Quantum Electronics Conference, Vienne, Autriche, 1992 : "Frequency measurement of the Rydberg constant".
- F. NEZ, M.D. PLIMMER, S. BOURZEIX, L. JULIEN, F. BIRABEN, R. FELDER, Y. MILLERIOUX et P. De NATALE, European Quantum Electronic Conference, Florence, Italie, 1993 (15 mn) : "Optical frequency measurement in atomic hydrogen and rubidium".
- D. TOUAHRI, M. ABED, L. HILICO, J.J. ZONDY, O. ACEF, A. CLAIRON, Y. MILLERIOUX, R. FELDER, F. NEZ, F. BIRABEN et L. JULIEN , Eight European Frequency and Time Forum, Munich, Allemagne, 1994 : "Absolute frequency measurement in the visible and near infrared range".
- Y. MILLERIOUX, R. FELDER, D. TOUAHRI, O. ACEF, L. HILICO, A. CLAIRON, BIRABEN F., B. de BEAUVOIR, L. JULIEN et F. NEZ, Conference on Precision Electromagnetic Measurements, Boulder - USA, 1994 : "A potential new frequency-wavelength standard at 778 nm : Doppler free two-photon transition in rubidium".
- S. BOURZEIX, B. de BEAUVOIR, F. NEZ, M.D. PLIMMER, F. de TOMASI, L. JULIEN, F. BIRABEN et B. CAGNAC, Conference on Precision Electromagnetic Measurements, Braunschweig, Allemagne, 1996 : "High resolution spectroscopy of the hydrogen atom".
- F. BIRABEN, B. de BEAUVOIR, F. NEZ, L. HILICO, L. JULIEN, B. CAGNAC, D. TOUAHRI, O. ACEF, A. CLAIRON et J.J. ZONDY, International Conference on Laser Spectroscopy, Hangzhou, Chine, 1997 : "Accurate spectroscopy of simple atomic systems : metrology of fundamental constants and test of quantum electrodynamics".
- C. SCHWOB, L. JOZEFOWSKI, O. ACEF, L. HILICO, B. de BEAUVOIR, F. NEZ, L. JULIEN, A. CLAIRON et F. BIRABEN, Conference

on Precision Electromagnetic Measurements, Washington, USA, 1998 : "Frequency measurement of the 2S-12D transitions in hydrogen and deuterium. New determination of the Rydberg constant" (Actes).

- P. HAUSER, C. PETITJEAN, L. SIMONS, D. TAQQU, F. KOTTMANN, R. POHL, C. DONCHE-GAY, O. HUOT, P. KNOWLES, F. MULHAUSER, L.A. SCHALLER, H. SCHNEUWLY, F.J. HARTMANN, W. SCHOTT, F. BIRABEN, P. INDELICATO, F. NEZ, F. TREHIN, C.A.N. CONDE, J.MF. Dos SANTOS, J.F.C.A. VELOSO, T.W. HÄNSCH, P. RABINOWITZ, V.W. HUGHES, EGAS, Marseille, France, 1999 : "Laser spectroscopy of the Lamb shift in muonic hydrogen".
- C. SCHWOB, L. JOZEFOWSKI, B. de BEAUVOIR, L. HILICO, F. NEZ, L. JULIEN, F. BIRABEN, O. ACEF et A. CLAIRON, Hydrogen Atom II, Castiglione della Pescaia, Italie, 2000 : "High resolution spectroscopy of hydrogen".
- R. POHL, F. BIRABEN, C.A.N. CONDE, C. DONCHE-GAY, T.W. HÄNSCH, F.J. HARTMANN, P. HAUSER, V.W. HUGHES, O. HUOT, P. INDELICATO, P. KNOWLES, F. KOTTMANN, Y.W. LIU, F. MULHAUSER, F. NEZ, C. PETITJEAN, P. RABINOWITZ, J.M.F. Dos SANTOS, L.A. SCHALLER, H. SCHNEUWLY, W. SCHOTT, L. SIMONS, D. TAQQU et J.F.C.A. VELOSO : Hydrogen Atom II, Castiglione della Pescaia, Italie, 2000 : "Towards a measurement of the Lamb shift in muonic hydrogen".
- G. HAGEL, C. SCHWOB, L. JOZEFOWSKI, B. DE BEAUVOIR, L. HILICO, O. ACEF, J.-J. ZONDY, F. NEZ, L. JULIEN, A. CLAIRON AND F. BIRABEN, Sixth Symposium on Frequency Standards and Metrology, St Andrews, Ecosse, 2001 (exposé oral, 30 mn). : "Metrology of hydrogen atom : determination of the Rydberg constant and Lamb shifts".
- R. BATTESTI, P. CLADE, C. SCHWOB, B. GREMAUD, S. GUELLATI-KHELIFA., F. NEZ, L. JULIEN ET F. BIRABEN, Conference on Precision Electromagnetic Measurements, Londres, 27 juin- 2 juillet 2004 (exposé oral, 20 mn). "Accélération d'atomes ultra froids : vers une mesure de h/MA".
- P. CLADE, R. BATTESTI, S. GUELLATI-KHELIFA, C. SCHWOB, B. GREMAUD, F. NEZ, L. JULIEN AND F. BIRABEN Eight European Conference on Atomic and Molecular Physics, Rennes, 6-10 juillet 2004 (exposé oral et affiche). : "A preliminary measurement of h/mRb

using ultracold atoms".
- R. POHL, F.D. AMARO, A. ANTOGNINI, , F. BIRABEN, J.M.R. CARDOSO, C.A.N. CONDE, A. DAX, S. DHAWAN, L.M.P. FERNANDES, T.W. HÄNSCH, F.J. HARTMANN, V.-W. HUGHES, O. HUOT, P. INDELICATO, L. JULIEN, P.E. KNOWLES, F. KOTTMANN, Y.-W. LIU, L. LUDHOVA, C.M.B. MONTEIRO, F. MULHAUSER, F. NEZ, P. RABINOWITZ, J.M.F. DOS SANTOS, L.A. SCHALLER, C. SCHWOB, D. TAQQU, AND J.F.C.A. VELOSO, Hydrogen Atom III, Mangaratiba, Rio de Janeiro, 1-4 aôut 2004 "The muonic hydrogen lamb shift experiment".
- O. ARNOULT, C. SCHWOB, F. NEZ, L. JULIEN AND F. BIRABEN, Hydrogen Atom III, Mangaratiba, Rio de Janeiro, 1-4 aôut 2004 : "Absolute frequency measurement of the 1S-3S line in atomic hydrogen".

Affiches

- F. BIRABEN, L. JULIEN et F. NEZ, International Conference on Laser Spectroscopy X, Font-Romeu, France, 1991 (actes) : "High resolution spectroscopy of the hydrogen atom".
- F. NEZ, M.D. PLIMMER, S. BOURZEIX, L. JULIEN, F. BIRABEN, Fourth European Conference on Atomic and Molecular Physics, Riga, 1992 : "Frequency measurement of the Rydberg constant in atomic hydrogen".
- BOURZEIX S., PLIMMER M.D., NEZ F., BIRABEN F. et JULIEN L., Twenty-fifth EGAS Conference, Caen, France, 1993 : "Towards a measurement of the 1S Lamb shift in hydrogen and deuterium".
- F. NEZ, M.D. PLIMMER, S. BOURZEIX, L. JULIEN, F. BIRABEN, R. FELDER, Y. MILLERIOUX et P. de NATALE , Twenty-fifth EGAS Conference, Caen, France, 1993 : "Frequency Measurement of the Rydberg Constant in atomic Hydrogen".
- S. BOURZEIX, B. de BEAUVOIR, F. NEZ, L. JULIEN et F. BIRABEN, COLOQ3, Limoges, France, 1993 : "Réalisation d'une source continue à 205 nm pour la spectroscopie de l'atome d'hydrogène".
- F. NEZ, S. BOURZEIX, L. JULIEN, F. BIRABEN, R. FELDER et Y. MILLERIOUX, International Conference on Laser Spectroscopy, Hot Springs, USA, 1993 : "Frequency measurement of the 5S-5D two-photon transition in rubidium and prospects for measuring (He-Ne)/I2 lasers

at $\lambda = 633nm$".

- D. TOUAHRI, F. NEZ, M. ABED, J.J. ZONDY, O. ACEF, L. HILICO, A. CLAIRON, Y. MILLERIOUX, F. BIRABEN, L. JULIEN et R. FELDER, Conference on Precision Electromagnetic Measurements, Boulder - USA, 1994 : "LPTF frequency synthesis chain : results and improvements for the near future".
- B. CAGNAC, B. de BEAUVOIR, F. NEZ, F. BIRABEN, L. JULIEN, L. HILICO, Y. MILLERIOUX, D. TOUAHRI, A. CLAIRON et R. FELDER, Fourteenth International Conference on Atomic Physics, Boulder, USA, 1994 : "High resolution spectroscopy and absolute frequency measurement of 5S-5D two-photon transition in rubidium".
- B. de BEAUVOIR, F. NEZ, L. JULIEN, F. BIRABEN et B. CAGNAC, International Conference on Laser Spectroscopy, Capri, Italie, 1995 : "Accurate frequency standard using a laser diode stabilized on a Doppler free two-photon transition in rubidium".
- B. de BEAUVOIR, F. NEZ, L. JULIEN, F. BIRABEN, B. CAGNAC, D. TOUAHRI, J.J. ZONDY, O. ACEF, M. ABED, A. CLAIRON, Y. MILLERIOUX et R. FELDER, Journées ULTIMATECH, Paris, France, 1995 : "Techniques de mesure de fréquences dans le domaine optique - Laser étalon de fréquence à 385 THz ($\lambda = 778nm$)".
- B. de BEAUVOIR, F. NEZ, L. JULIEN, F. BIRABEN, B. CAGNAC, D. TOUAHRI, J.J. ZONDY, O. ACEF, M. ABED, A. CLAIRON, Y. MILLERIOUX et R. FELDER, COLOQ4, Palaiseau, France, 1995 : "Techniques de mesure de fréquences dans le domaine optique - Laser étalon de fréquence à 385 THz ($lambda = 778nm$)".
- B. de BEAUVOIR, F. NEZ, L. JULIEN, F. BIRABEN, B. CAGNAC, J.J. ZONDY, D. TOUAHRI, O. ACEF, L. HILICO et A. CLAIRON, Conference on Precision Electromagnetic Measurements, Braunschweig, Allemagne, 1996 : "Transmission of an optical frequency through a 3 km long optical fiber : application to absolute frequency measurements in hydrogen".
- F. BIRABEN, B. de BEAUVOIR, F . NEZ, L. HILICO, L. JULIEN, B. CAGNAC, D. TOUAHRI, O. ACEF, A. CLAIRON et J.J. ZONDY, COLOQ 5, Strasbourg, France, 1997 : "Métrologie des systèmes atomiques simples et tests de l'électrodynamique quantique".
- C. SCHWOB, L. MASSON, B. GREMAUD, S. GUELLATI, F. NEZ, L. JULIEN et F. BIRABEN, COLOQ 6, Bordeaux, France, 1999 : "Accélération d'atomes ultra-froids : Mesure de h/MA" (Actes).

- G. HAGEL, C. SCHWOB, F. NEZ, L. JULIEN, F. BIRABEN, O. ACEF, J.J. ZONDY, A. CLAIRON, EGAS, Marseille, France, 1999 : "Towards an absolute frequency measurement of the 1S-3S transition in hydrogen".
- G. HAGEL, R. BATTESTI, C. SCHWOB, F. NEZ, L. JULIEN, F. BIRABEN, O. ACEF, J.J. ZONDY, A. CLAIRON, Hydrogen Atom II, Castiglione della Pescaia, Italie, 2000 : "Absolute frequency measurement of the 1S-3S transition in hydrogen" (Actes sur cdrom).
- Y.W. LIU, F. BIRABEN, C.A.N. CONDE, C. DONCHE-GAY, T.W. HÄNSCH, F.J. HARTMANN, P. HAUSER, V.W. HUGHES, O. HUOT, P. INDELICATO, P. KNOWLES, F. KOTTMANN, F. MULHAUSER, F. NEZ, C. PETITJEAN, P. RABINOWITZ, R. POHL, J.M.F. Dos SANTOS, L.A. SCHALLER, H. SCHNEUWLY, W. SCHOTT, L. SIMONS, D. TAQQU, F. TREHIN et J.F.C.A VELOSO, Seventeenth International Conference on Atomic Physics, Florence, Italie, 2000 : "The laser system for the muonic hydrogen Lamb shift measurement".
- S. GUELLATI, C. WINISDOERFFER, C. SCHWOB, B. GREMAUD, F. NEZ, L. JULIEN et F. BIRABEN, Seventeenth International Conference on Atomic Physics, Florence, Italie, 2000 : "Acceleration of ultracold atoms : measurement of h/MA".
- R. BATTESTI, C. SCHWOB, B. GRÉMAUD, S. GUELLATI-KHÉLIFA, F. NEZ, L. JULIEN ET F. BIRABEN, : Sixth Symposium on Frequency Standards and Metrology, St Andrews, Ecosse, 2001 "Acceleration of rubidium cold atoms : determination of α".
- R. BATTESTI, P. CLADE, C. SCHWOB, B. GREMAUD, S. GUELLATI-KHELIFA, F. NEZ, L. JULIEN ET F. BIRABEN, Conference on Precision Electromagnetic Measurements, Ottawa, Canada, 2002 (affiche)."Measurement of h/MRb with ultracold atoms".
- S. GUELLATI-KHÉLIFA, C. SCHWOB, R. BATTESTI, P. CLADÉ, B. GRÉMAUD, F. NEZ, L. JULIEN ET F. BIRABEN : 7th International Workshop on Atom Optics and Interferometry, Lunteren 2002, Pays-Bas, 28 septembre-2octobre 2002 "Measurement of h/MRb with ultracold atoms".
- P. CLADÉ, R. BATTESTI, S. GUELLATI-KHÉLIFA, C. SCHWOB, B. GRÉMAUD, F. NEZ, L. JULIEN AND F. BIRABEN COLOQ 8, Toulouse, septembre 2003 : "A preliminary measurement of h/mRb using ultracold atoms".
- O. ARNOULT, C. SCHWOB, F. NEZ, L. JULIEN AND F. BIRABEN ,

Eight European Conference on Atomic and Molecular Physics, Rennes, 6-10 juillet 2004 "Ultrahigh resolution spectroscopy of the 1S-3S line in hydrogen".

- P. CLADE, R. BATTESTI, S. GUELLATI-KHELIFA, C. SCHWOB, B. GREMAUD, F. NEZ, L. JULIEN ET F. BIRABEN :XIX International Conference on Atomic Physics, Rio de Janeiro, Brésil, 25-30 juillet 2004 "Bloch oscillations of ultracold atoms : a tool for a h/mRb measurement".
- A. ANTOGNINI, F.D. AMARO, F. BIRABEN, J.M.R. CARDOSO, C.A.N. CONDE, A. DAX, S. DHAWAN, L.M.P. FERNANDES, T.W. HÄNSCH, F.J. HARTMANN, V.-W. HUGHES, O. HUOT, P. INDELICATO, L. JULIEN, P.E. KNOWLES, F. KOTTMANN, Y.-W. LIU, L. LUDHOVA, C.M.B. MONTEIRO, F. MULHAUSER, F. NEZ, R. POHL, P. RABINOWITZ, J.M.F. DOS SANTOS, L.A. SCHALLER, C. SCHWOB, D. TAQQU, AND J.F.C.A. VELOSO, XIX International Conference on Atomic Physics, Rio de Janeiro, Brésil, 25-30 juillet 2004, "Lamb shift in muonic hydrogen".
- O. ARNOULT, C. SCHWOB, F. NEZ, L. JULIEN AND F. BIRABEN, XIX International Conference on Atomic Physics, Rio de Janeiro, Brésil, 25-30 juillet 2004, "Absolute frequency measurement of the 1S-3S line in atomic hydrogen".
- A. ANTOGNINI, F.D. AMARO, F. BIRABEN, J.M.R. CARDOSO, C.A.N. CONDE, A. DAX, S. DHAWAN, L.M.P. FERNANDES, T.W. HÄNSCH, F.J. HARTMANN, V.-W. HUGHES, O. HUOT, P. INDELICATO, L. JULIEN, P.E. KNOWLES, F. KOTTMANN, Y.-W. LIU, L. LUDHOVA, C.M.B. MONTEIRO, F. MULHAUSER, F. NEZ, R. POHL, P. RABINOWITZ, J.M.F. DOS SANTOS, L.A. SCHALLER, C. SCHWOB, D. TAQQU, AND J.F.C.A. VELOSO, XIX International Conference on Atomic Physics, Rio de Janeiro, Brésil, 25-30 juillet 2004 "The laser system for the muonic hydrogen lamb shift experiment".
- A. ANTOGNINI, F.D. AMARO, F. BIRABEN, J.M.R. CARDOSO, C.A.N. CONDE, A. DAX, S. DHAWAN, L.M.P. FERNANDES, T.W. HÄNSCH, F.J. HARTMANN, V.-W. HUGHES, O. HUOT, P. INDELICATO, L. JULIEN, P.E. KNOWLES, F. KOTTMANN, Y.-W. LIU, L. LUDHOVA, C.M.B. MONTEIRO, F. MULHAUSER, F. NEZ, R. POHL, P. RABINOWITZ, J.M.F. DOS SANTOS, L.A. SCHALLER, C. SCHWOB, D. TAQQU, AND J.F.C.A. VELOSO, Hydrogen Atom III, Mangaratiba, Rio de Janeiro, 1-4 aôut 2004 : "The laser system for

the muonic hydrogen lamb shift experiment".

– A. ANTOGNINI, F.D. AMARO, F. BIRABEN, J.M.R. CARDOSO, C.A.N. CONDE, A. DAX, S. DHAWAN, L.M.P. FERNANDES, T.W. HÄNSCH, F.J. HARTMANN, V.-W. HUGHES, O. HUOT, P. INDELICATO, L. JULIEN, P.E. KNOWLES, F. KOTTMANN, Y.-W. LIU, L. LUDHOVA, C.M.B. MONTEIRO, F. MULHAUSER, F. NEZ, R. POHL, P. RABINOWITZ, J.M.F. DOS SANTOS, L.A. SCHALLER, C. SCHWOB, D. TAQQU, AND J.F.C.A. VELOSO, Hydrogen Atom III, Mangaratiba, Rio de Janeiro, 1-4 aôut 2004 "Lamb shift in muonic hydrogen".

Résumé des travaux de recherche

Mon travail de recherche s'effectue dans le groupe de métrologie des systèmes simples et fondamentaux sous la direction de F.Biraben. Je suis impliqué dans les trois expériences de notre groupe. Les deux premières expériences, relatives à la métrologie de l'atome d'hydrogène, sont décrites dans le premier chapitre. La nouvelle expérience développée pour déterminer la constante de structure fine en mesurant le rapport h/M_{Rb} est présentée dans le deuxième chapitre. Sont reportées dans l'annexe, quelques expériences complémentaires à nos expériences principales.

Dès ses débuts, la spectroscopie de l'atome d'hydrogène a suscité de nombreux développement théoriques. Cet atome étant le plus simple, des calculs très précis peuvent être faits pour le décrire. Des nouvelles théories ont été développées pour expliquer le spectre de raies expérimental de cet atome (comme par exemple l'introduction de la constante de structure fine ou l'électrodynamique quantique). Ces calculs de plus en plus précis ont stimulés le développement de nouvelles techniques expérimentales afin d'affiner la comparaison théorie-expérience (voir chapitre 1). Nos expériences se situent dans cette dynamique. Chaque nouveau développement de notre expérience a permis d'améliorer l'incertitude des mesures de fréquence des transitions (2S-nS/nD) ceci dans le cadre d'une compétition intense avec l'équipe de T.W.Hänsch travaillant sur la transition 1S-2S.

L'expérience sur l'hydrogène a commencé au LKB en 1983. C'est l'époque pionnière de cette étude spectroscopique. Durant cette période, le jet d'atomes dans l'état métastable 2S a été mis au point par F.Biraben et L.Julien et les premiers signaux observés. L'équipe a ensuite réalisé des mesures très précises des longueurs d'onde des transitions 2S-8D,10D,12D sur l'hydrogène et le deutérium à l'aide de deux cavités Fabry-Perot. Ces mesures ont constitué le travail de thèse de J.C. Garreau [*Gar89*]. Les limitations de ces mesures provenaient de l'incertitude sur le laser HeNe stabilisé sur l'iode et de la

méthode interférométrique.

Cette méthode consistait à comparer les longueurs d'onde de deux lasers à l'aide d'un interféromètre de Fabry-Perot. La mesure de fréquence se fait elle en comparant la fréquence inconnue à celle d'un laser de référence via un mélange hétérodyne sur une photodiode rapide. La différence de fréquence résultante est simplement comptée sur un fréquence-mètre. La bande passante des photodiodes étant de l'ordre du GHz, cette méthode très précise nécessite un laser de référence proche de celui à mesurer. C'est dans ce contexte que je suis arrivé au Laboratoire de Spectroscopie Hertzienne de L'Ecole Normale Supérieure (maintenant laboratoire Kastler Brossel) en avril 1989 en stage de fin d'étude de L'Ecole Supérieure d'Optique. Le but de stage était d'étudier la possibilité de faire un laser étalon de fréquence à 778 nm à partir d'une diode laser asservie sur une transition de la molécule IBr [*Bir92*](voir l'annexe).

Finalement, la fréquence du laser HeNe/I_2 a été re-mesurée par le Laboratoire Primaire du Temps et des Fréquences (LPTF) [*Ace92*]. Nous avons entrepris en parallèle la construction d'une chaîne de fréquence optique reliant la fréquence des transitions 2S-8S/8D à celle des lasers étalons (HeNe/CH_4 et HeNe/I_2). La période (1990-1993) a constitué mon travail de thèse dont le sujet était : "Chaîne de fréquence optique pour mesurer les transitions 2S-8S/8D dans l'atome d'hydrogène ; mesure de la constante de Rydberg en unité de fréquence" [*Nez93b*]. Hormis la réalisation de la partie laser de cette chaîne, la principale difficulté de cette expérience a été de raccorder en fréquence deux lasers distants de 89 GHz. Ce mélange hétérodyne des 2 lasers et d'une source hyper-fréquence à 89 GHz a finalement été fait à l'aide d'une diode Schottky. Cette étape a permis la première mesure en fréquence d'une transition de l'atome d'hydrogène [*Nez93a*][1]. Grâce à cette chaîne, les fréquences absolues de certaines transitions 5S-5D de l'atome de rubidium ont aussi été mesurées [*Nez93c*][2]. Ces mesures ont conduit au développement d'un nouveau laser étalon à 778 nm stabilisé sur ces transitions à deux photons du rubidium (voir l'annexe).

J'ai ensuite effectué un séjour post-doctoral d'un an au LPTF pour mettre au point une partie de la nouvelle chaîne laser destinée à mesurer le laser étalon à rubidium [*Tou97*]. Avec O.Acef, j'ai aussi exploré les limites de mesures de fréquence optique avec les diodes Schottky [*Ace94b*].

[1] F. Nez et al., Europhys. Lett. 24, 635 (1993) *article joint à la fin du manuscrit.*
[2] F. Nez et al., Opt. Commun. 102, 432 (1993) *article joint à la fin du manuscrit.*

Parallèlement à ma thèse, une autre expérience sur l'hydrogène a été développée dans l'équipe, à partir de 1991. En comparant les fréquences des transitions 1S-3S et 2S-6S/6D (qui sont approximativement dans un rapport 4), on peut en déduire une mesure du déplacement de Lamb de l'état fondamental 1S. Ceci a constitué le travail de thèse de S.Bourzeix durant lequel un jet atomique dans l'état 1S et une source laser à 205 nm ont été construits et les premiers signaux de la transition 1S-3S observés [*Bou95*]. Recruté au CNRS en 1994, j'ai participé aux mesures de cette expérience déterminant très précisément le déplacement de Lamb de l'état 1S [*Bou96*][3].

En 1996, nous avons mesuré à nouveau les fréquences des transitions 2S-8S/8D dans l'hydrogène et le deutérium à partir du nouvel étalon de fréquence à 778 nm. J'ai co-encadré le travail de thèse de B. de Beauvoir [*Bea96*]. Durant cette mesure, pour la première fois, la fréquence d'un laser étalon a été mesurée sans le déplacer, via une fibre optique reliant notre laboratoire au Laboratoire Primaire du Temps et des Fréquences (LPTF) (maintenant laboratoire BNM-SYRTE) [*Bea98*]. Suite à cette thèse il est apparu qu'il serait très difficile d'améliorer l'incertitude de nos mesures.

Malgré cela les fréquences des transitions 2S-12S/12D ont été mesurées en fréquence. En effet la chaîne de fréquence pour cette mesure n'étant pas trop compliquée, cette étude a permis de valider l'analyse des champs électriques parasites dans notre jet atomique 2S et donc les corrections Stark faites sur les mesures précédentes [*Sch99*][4].

Depuis 1997, la fréquence de la transition 1S-2S est aussi mesurée en unité de fréquence [*Ude97*] et en particulier depuis 1999, à l'aide de la technique révolutionnaire de peigne de fréquence optique [*Ude99*, *Rei00*]. Cette fréquence est la mieux mesurée dans l'atome d'hydrogène. Cependant cette donnée seule n'est pas suffisante pour déterminer R_∞ avec une bonne incertitude. Actuellement, la constante de Rydberg la plus précise est déduite d'un ajustement de type moindre carré sur toutes les fréquences des transitions 1S-2S, 2S-8S/8D, 2S-12D (hydrogène et deutérium) et la donnée théorique L_{1S}-8L_{2S} (où L_{nS} représente le déplacement de Lamb du niveau nS) (hydrogène et deutérium) [*Bea00*][5].

Afin d'améliorer les données spectroscopiques sur l'hydrogène, nous avons

[3] S. Bourzeix et al., Phys. Rev. Lett. 76, 384 (1996) *article joint à la fin du manuscrit.*
[4] C. Schwob et al., Phys. Rev. Lett. 82, 4960 (1999) *article joint à la fin du manuscrit.*
[5] B. de Beauvoir et al., Eur. Phys. J. D 12, 61 (2000) *article joint à la fin du manuscrit.*

reporté nos efforts sur l'étude de la transition 1S-3S. Pour cela, nous avons mis en place une méthode pour compenser l'effet Doppler du deuxième ordre proposée en 1991 [*Bir91*] et réalisée en 2001 [*Hag02b*][6]. Ce travail que j'ai co-encadré correspond à la thèse de G.Hagel [*Hag01*].

Depuis 2002, un nouvel étudiant en thèse O. Arnoult (co-encadré avec F.Biraben) travaille sur la mesure absolue de fréquence de la transition 1S-3S. Nous disposons maintenant d'un laser femtoseconde référencé, via la fibre optique, à l'horloge à césium du BNM-SYRTE (anciennement LPTF). Il suffit donc que tous les éléments nécessaires à la mesure fonctionnent en même temps pour enfin réaliser une mesure absolue de fréquence de cette transition...

Parallèlement aux études sur l'hydrogène, deux nouvelles expériences ont été entreprises dès 1999 : la spectroscopie de l'hydrogène muonique et la mesure du rapport h/M à l'aide d'atomes froids.

L'expérience de spectroscopie de l'hydrogène muonique est motivée par le fait que la comparaison théorie-expérience est maintenant limitée en partie par la connaissance de la taille de la distribution de charge du proton. Dans le cadre d'une collaboration internationale, nous avons commencé la spectroscopie de l'hydrogène muonique à l'institut Paul Scherrer (PSI, Villigen, Suisse). L'hydrogène muonique est formé d'un muon (μ^-) et d'un proton. L'image simple que l'on peut avoir du système est la suivante. Comme la masse du muon est 207 fois plus élevée que celle de l'électron, le rayon de son orbite autour du proton est $\sim$ 200 fois plus petit et donc "l'influence" de la distribution de charge du proton est plus grande. Nous avons eu la responsabilité d'une partie de la chaîne laser : la partie "laser titane-saphir". Ce système laser a été mis au point dans notre laboratoire [*Kaz00*, *Ami00*] puis mis en place près de la source de muons. Les deux périodes de prises de données à PSI (juillet - octobre 2002 et mi-juin - mi-novembre 2003), ont mis en évidence la bonne conception de l'expérience avec cependant quelques faiblesses. A ce jour, il n'y a aucune indication claire que la transition recherchée ait été observée. Cette absence de signal est très probablement due à une statistique de signal trop faible. Les solutions techniques existant, cette expérience devrait se poursuivre...

Notre nouvelle expérience, à l'aide d'atomes froids de masse M, a pour but de déterminer le rapport h/M (h étant la constante de Planck). Comme

[6] G. Hagel et al, Phys. Rev. Lett. 89, 203001 (2002) *article joint à la fin du manuscrit.*

les rapports de masse sont mesurés très précisément, la mesure du rapport h/M est un moyen via la constante de Rydberg, de déterminer la valeur de la constante de structure fine α. Celle-ci est déterminée dans différents domaines de la physique. La dispersion des différentes mesures est de l'ordre de 2×10^{-7}. Le but premier de notre expérience est de contribuer au diagramme des différentes mesures de α. La valeur actuelle de α est essentiellement déterminée à partir d'une mesure très précise du moment magnétique anormal de l'électron à l'aide de calculs d'électrodynamique quantique. Une mesure extrêmement précise et indépendante pourrait donc être vue comme un test de cette théorie.

Une première expérience a été réalisée pendant la thèse de R.Battesti [*Bat03*] à l'aide d'une cellule à atomes froids conçue pour une autre expérience. L'idée simple de l'expérience est la mesure de la vitesse de recul d'un atome lorsqu'il absorbe un photon puis émet de manière stimulée un autre photon. Plus le nombre d'absorptions-émissions stimulées est grand, meilleure est l'incertitude sur la mesure de la vitesse de recul. Notre première mesure, en géométrie horizontale, a mis en évidence l'excellente efficacité du processus utilisé dans notre expérience (oscillations de Bloch [*Bat04*][7]). Par contre, cette mesure a été entachée d'effets systématiques que nous cherchons à comprendre tout en entamant des mesures en géométrie verticale qui seront bientôt réalisées dans une nouvelle cellule à atomes froids.

[7]R. Battesti et al., Phys. Rev. Lett. 92, 253001-1 (2004) *article joint à la fin du manuscrit.*

Plan du mémoire

Le mémoire se découpe en plusieurs chapitres qui servent d'introduction aux différents articles joints. Ceux ci, cités dans le texte, sont mis à la fin du mémoire.

Le premier chapitre est consacré à la spectroscopie de l'atome d'hydrogène. Cet atome, constitué d'un électron et d'un proton est le plus simple des systèmes atomiques, ce qui en fait un outil privilégié pour confronter théorie et expérience. Depuis le début du siècle, la spectroscopie de l'atome d'hydrogène a ainsi conduit à des avancées spectaculaires de la physique de l'atome de Bohr jusqu'à l'électrodynamique quantique. C'est pourquoi l'atome d'hydrogène fut qualifié de "pierre de Rosette de la physique moderne"[*Hän79*]. Ce chapitre suit un plan "historique" en 7 parties :

- la première partie donne quelques rappels concernant l'atome d'hydrogène,
- la seconde partie décrit les expériences réalisées sur les transitions faites à partir du niveau métastable 2S,
- quelques autres mesures de fréquences sur l'hydrogène de part le monde sont présentées dans la troisième partie,
- la quatrième partie traite de la contribution des mesures de fréquence à la spectroscopie de l'hydrogène,
- la cinquième partie est consacrée à l'étude en cours de la transition 1S-3S,
- la sixième partie décrit l'expérience en cours de spectroscopie de l'hydrogène muonique,
- enfin une conclusion et une perspective sont ébauchées dans la septième partie.

Dans la suite, il ne sera fait mention que de l'hydrogène atomique étant entendu que la plupart du temps l'expérience a été faite aussi avec le deutérium. La philosophie de ces expériences a été celle de la métrologie. A chacune des

étapes, nous avons cherché à tirer le meilleur parti de l'expérience pour valider l'étape. Les limitations de l'expérience susceptibles d'être améliorées ont donné lieu soit à un développement nouveau de l'expérience soit à de nouvelles expériences.

Notre nouvelle expérience pour déterminer la constante de structure fine α à l'aide d'atomes froids est décrite dans le deuxième chapitre.

Une brève introduction fait le point sur les différentes déterminations de α. Je décris ensuite brièvement notre mesure préliminaire réalisée pendant la thèse de R.Battesti et donne les derniers développements et les perspectives de cette nouvelle expérience.

Enfin, la troisième partie tente d'ébaucher une conclusion de ce travail de recherche.

L'annexe est consacrée aux travaux de recherche menés en parallèle ou en complément à la spectroscopie de l'hydrogène et à la mesure de la constante de structure fine. Quelques mesures présentées ont été faites grâce à notre cavité Fabry-Perot FPR. Il serait alors exact de parler de mesure de longueur d'onde avec notre interféromètre FPR. La culture de mesure de fréquence optique imprègne maintenant complètement notre équipe, ce qui se manifeste aussi dans ce manuscrit....

Le premier paragraphe traite d'une étude spectroscopique de l'hélium sur la transition à deux photons $2^3S_1 - 3^3D_1$. Cette expérience faite pour comparer théorie-expérience a pour la première fois utilisé l'atome d'hydrogène comme référence optique.

Dans le second paragraphe, je décris notre recherche de références atomiques et moléculaires pour réaliser un laser étalon de fréquence proche de nos transitions atomiques dans l'hydrogène.

Chapitre 1

Métrologie de l'atome d'hydrogène

1.1 Quelques rappels sur l'atome d'hydrogène

1.1.1 Une théorie simplifiée

De manière très schématique, les niveaux d'énergie de l'atome d'hydrogène s'expriment comme la somme de trois termes :

$$E_{n,L,J} = E^{\mu}_{nJ}(Dirac) + E_n(recul) + E(Lamb) \tag{1.1}$$

où

- n désigne le nombre quantique principal
- L désigne le nombre quantique associé au moment cinétique orbital
- J est associé au moment cinétique total de l'électron $\overrightarrow{J} = \overrightarrow{L} + \overrightarrow{S}$
- μ désigne la masse réduite du système formé d'un électron (de masse m) et d'un proton (de masse M) $\mu = \frac{mM}{m+M}$

La résolution de l'équation de Dirac pour un proton infiniment lourd donne une expression de $E^{m}_{nJ}(Dirac)$. Pour tenir compte de la masse finie du proton, on procède en deux étapes :

- en substituant m par μ dans l'expression de $E^{m}_{nJ}(Dirac)$
- en ajoutant un terme correctif $E_n(recul)$.

Le dernier terme $E(Lamb)$ contient par convention toutes les autres contributions, c'est à dire les effets de recul relativistes d'ordres supérieurs, ainsi que les corrections radiatives et l'effet de taille finie du noyau.

L'expression des deux premiers termes, proportionnels à la constante de Rydberg R_∞, est exacte.

Le troisième terme donne lieu à un intense travail théorique depuis plusieurs décennies. Les calculs de grande précision sur des états liés sont très compliqués (une présentation très claire du problème a été faite dans la thèse de S.Bourzeix [*Bou95*]). Ces calculs diffèrent de ceux décrivant un système libre. Sur un tel système, le calcul est perturbatif et peut donc être développé en série (par exemple le moment magnétique anormal de l'électron (a_e) ; voir chapitre 2 partie 2.1). Ce n'est pas le cas dans les systèmes liés de sorte qu'un diagramme de Feynmann peut se décomposer en un terme principal et une infinité de termes correctifs qui contribuent tous à un ordre donné. De plus on peut trouver des regroupements de diagrammes astucieux tels que les termes principaux s'éliminent... Cette situation a été résumée par le théoricien P. Sapirstein dans un article de revue [*Sap90*] :"il y a de nombreux chemins qui mènent à la bonne réponse, mais pas tous avec le même bonheur". Le lecteur trouvera dans les articles [*Moh00*], [*Moh02*] une présentation complète de tous les termes correctifs connus. Notons simplement que la plupart de ces corrections varient comme $1/n^3$, propriété qui sera utile pour la suite de l'exposé.

Les inconnues déterminées à partir de la spectroscopie d'une transition de l'atome sont donc la constante de Rydberg et/ou l'ensemble des corrections d'électrodynamique quantiques en incluant l'effet de taille de la distribution de charge du proton (appelée par la suite l'effet du "rayon du proton").

1.1.2 Un bref historique

Le spectre de raies de l'atome d'hydrogène couvrant un large domaine de fréquence de l'ultraviolet jusqu'aux micro-ondes, la mesure de fréquence de n'importe laquelle de ces raies donne accès à la constante de Rydberg ou aux corrections d'électrodynamique quantique. Nos expériences se font dans le domaine optique.

Jusque dans les années 1970, l'élargissement dû à l'effet Doppler du premier ordre limitait à environ 10^{-7} la résolution des spectres obtenus dans le domaine optique. L'avènement des sources lasers et l'apparition de techniques spectroscopiques sans effet Doppler ont permis une amélioration très rapide de cette résolution. Dans le cas de l'atome d'hydrogène, le progrès est presque de quatre ordres de grandeur en trente ans (figure 1.1). Les transitions étudiées dans notre groupe sont des transitions à deux photons. Nos expériences

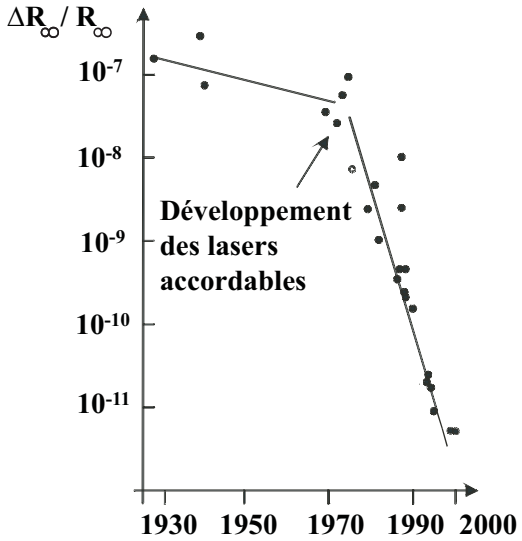

FIG. 1.1 – Cette figure montre clairement l'influence des techniques spectroscopiques sans effet Doppler sur la précision de la constante de Rydberg.

se font avec des jets atomiques. Plusieurs mesures ont été effectuées, chaque étape permettant d'améliorer un ou plusieurs points particuliers de l'expérience.

1.1.3 La spectroscopie à deux photons

La méthode utilisée dans notre groupe et dans celui de T.Hänsch pour s'affranchir de l'effet Doppler du premier ordre est la spectroscopie à deux photons [*Cag73*, *Vas70*].

Il est possible avec une source intense d'exciter une transition à deux photons entre niveaux de même parité. Soit ω_0 la fréquence d'une telle transition atomique dans le domaine optique. Considérons le cas où cette transition est excitée par deux ondes laser de même fréquence ω se propageant en sens opposés dans le milieu atomique. Dans le référentiel d'un atome se déplaçant à la vitesse $\overrightarrow{v}$, les vibrations ont pour fréquences $\omega - k \times v_z$ et $\omega + k \times v_z$ où v_z est la projection de $\overrightarrow{v}$ sur l'axe commun de propagation des faisceaux. Si l'atome absorbe un photon de chaque onde, alors les décalages Doppler du premier ordre se compensent exactement quelque soit v_z. On observe donc un signal sans élargissement Doppler pour $\omega = \frac{\omega_0}{2}$. Les probabilités de transitions à

deux photons étant souvent petites, il faut des puissances lasers importantes. Ce champ lumineux intense conduit à un déplacement des niveaux d'énergie appelé déplacement lumineux proportionnel à l'intensité laser. Cependant, contrairement aux autres méthodes de spectroscopie sans effet Doppler (jet atomique et faisceau laser perpendiculaires et absorption saturée), tous les atomes quelle que soit leur vitesse contribuent au signal. L'effet Doppler du deuxième ordre est pris en compte dans le calcul des formes de raies (voir le paragraphe 1.2.2).

Notre groupe a plus particulièrement étudié les transitions à partir du niveau métastable 2S-nS/nD (n=8,10,12), alors que le groupe de T.Hänsch a travaillé sur la transition 1S-2S. La largeur naturelle (Γ) de cette transition est de 1,3 Hz, tandis que pour les transitions 2S-nS/nD l'ordre de grandeur de Γ est plusieurs centaines de kHz. Ainsi on peut pointer la raie 1S-2S avec une meilleure incertitude. Cependant, à partir des transitions 2S-nS/nD, la constante de Rydberg peut être déduite directement des mesures de fréquence, les déplacements de Lamb étant suffisamment bien connus, soit expérimentalement pour le niveau (L_{2S}) [*Lun81*, *Pal85*], soit théoriquement ($L_{nS/nD}$) [*Eri77*]. Ce n'est pas le cas pour la transition 1S-2S où il y a deux inconnues dans l'équation de fréquence (R_∞ et le déplacement de Lamb du niveau 1S L_{1S}).

1.2 Nos expériences sur les transitions 2S-nS/nD

Après avoir décrit le jet atomique et le traitement des signaux atomiques, les chaînes de fréquences lasers nécessaires sont présentées. Nous avons mesuré deux fois la fréquence des transitions 2S-8S/8D, en 1993 et 1996. Les niveaux n=12 étant plus sensibles au champ électrique, l'expérience sur les transitions 2S-12D a permis en 1998 de valider les corrections Stark faites sur les mesures précédentes.

1.2.1 Description générale de l'expérience

Nos expériences utilisent un jet d'atomes d'hydrogène dans l'état métastable 2S, obtenu par bombardement électronique d'un jet atomique dans l'état fondamental 1S (voir figure 1.2).

Ce jet est réalisé à partir d'hydrogène moléculaire dissocié dans une décharge radio-fréquence. Lors de leurs collisions inélastiques avec les électrons,

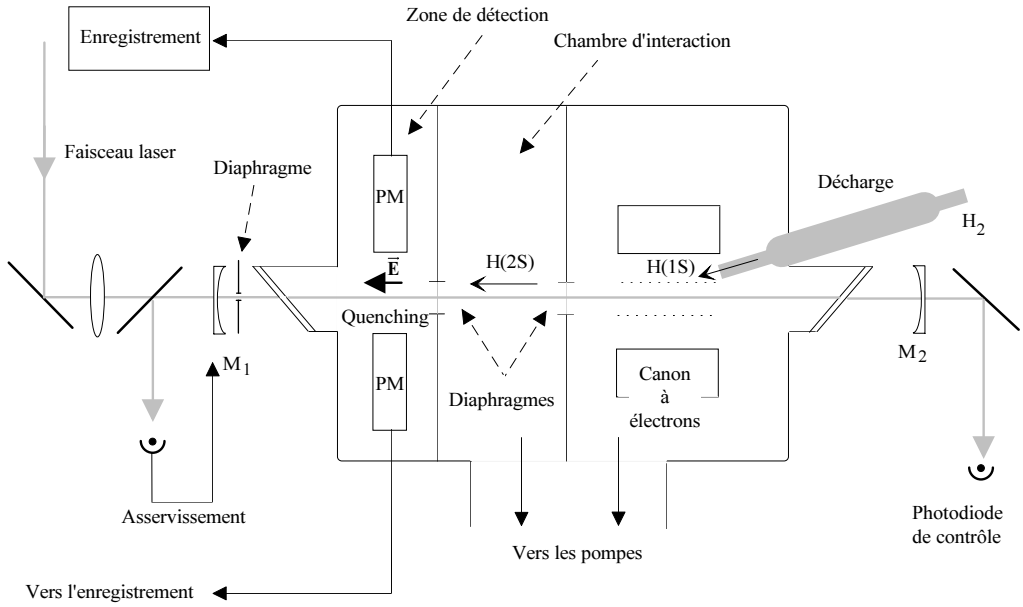

FIG. 1.2 – Schéma du jet atomique 2S.

les atomes d'hydrogène sont déviés de sorte que le jet d'atomes métastables 2S fait avec le jet d'atomes incidents un angle d'environ 20°. Les atomes entrent ensuite dans la zone d'interaction atome-laser délimitée par deux diaphragmes. En appliquant un champ électrique à l'extrémité du jet, on mélange les états 2S et 2P. La désexcitation de l'état 2P vers le niveau 1S produit des photons Lyman α qui sont détectés par deux photomultiplicateurs placés à l'extrémité du jet. Lorsque la transition à deux photons vers les niveaux supérieurs a lieu, le nombre d'atomes dans l'état 2S diminue. On observe cette diminution sur le signal donné par les photomultiplicateurs (des exemples de signaux expérimentaux sont donnés dans les articles joints à la fin du manuscrit voir par exemple [*Bea00*][1].

Pour l'expérience de 1993, aucune modification n'a été apportée au jet par rapport à la mesure précédente.

En 1994, nous avons essayé, sans succès, d'augmenter le nombre d'atomes métastables produits en améliorant l'efficacité du bombardement électronique. Par ailleurs, un blindage en mu-métal placé dans la zone d'interac-

[1]B. de Beauvoir et al., Eur. Phys. J. D 12, 61 (2000) *article joint à la fin du manuscrit.*

tion atome-laser a réduit les champs magnétiques parasites à mieux que le milligauss.

1.2.2 Les formes de raie des transitions 2S-nS/nD

Dans une expérience de haute résolution, il faut définir très précisément la position en fréquence de la raie observée. Cependant plusieurs effets parasites déplacent et élargissent les raies étudiées. Pour s'affranchir de ces effets, une forme de raie théorique, calculée en tenant compte des données expérimentales, est ajustée sur le signal atomique observé. L'ajustement donne la position de la raie corrigée de ces effets.

Le calcul de ces formes de raies a été développé pendant la thèse de J.C. Garreau [*Gar89*] puis amélioré pendant la thèse de B. de Beauvoir [*Bea96*]. La forme de raie décrit la probabilité de destruction des atomes métastables intégrée le long de toutes les trajectoires atomiques possibles entre les deux diaphragmes de la zone interaction atome-laser du jet.

1.2.3 Dépouillement des signaux expérimentaux

Pour améliorer le rapport signal à bruit, le signal expérimental que l'on ajuste est la moyenne de 10 enregistrements successifs obtenus en passant 10 fois de suite sur la résonance atomique. L'ajustement des profils de raies sur les signaux expérimentaux donne la position de la raie corrigée (ν_0) des différents effets qui la déplacent. Notons que la position ν_0 représente la position de la raie atomique par rapport à un pic de cavité Fabry Perot. La fréquence absolue est mesurée à l'aide de chaînes de fréquence décrites dans le paragraphe suivant.

Chaque campagne de mesures donne lieu à de nombreux enregistrements avec différentes puissances lumineuses. Typiquement, la puissance lumineuse vue par les atomes varie de 15 W à 130 W. La donnée utile est la position de la raie à puissance lumineuse nulle. Cette position est obtenue en extrapolant à zéro les positions ν_0.

1.2.4 Le laser d'excitation

Pour réaliser une spectroscopie de haute résolution, il faut disposer d'un laser d'excitation de largeur de raie inférieure à celle de la transition atomique et balayable finement autour d'une longueur d'onde déterminée. Pour cela

nous disposons d'un laser en anneau Titane-Saphir (TiSa) développé sur la base d'un laser à colorant conçu par F. Biraben.

Le laser Titane-Saphir

Le laser à colorant a été utilisé jusqu'en 1990 sur l'expérience. Un laser solide étant plus simple et plus fiable d'utilisation, une première version du laser TiSa a été mise au point pendant mon service militaire par F. Biraben. Pour ma thèse, il a fallu construire un autre laser Titane-Saphir (voir la figure 1.3). Nous en avons profité pour améliorer la base mécanique de laser. C'est cette "version" du laser que nous utilisons actuellement sur nos trois expériences en cours. La description complète de ce laser se retrouve dans toutes les thèses soutenues dans l'équipe depuis 1993 [*Nez93b*, *Bou95*, *Bea96*, *Hag01*, *Bat03*].

Stabilisation en fréquence du laser TiSa

Ce laser est ensuite asservi sur une cavité Fabry Perot de "haute finesse" (FPA) pour réduire les fluctuations instantanées de fréquence (appelée gigue du laser ou "jitter" en anglais). Pour réduire le bruit acoustique, le montage mécanique est très soigné. Deux méthodes ont été utilisées pour asservir le laser sur cette cavité : la méthode Hänsch-Couillaud (HC) et la méthode des bandes latérales (BL).

Le principe de la méthode HC repose sur l'analyse de la polarisation réfléchie par la cavité FPA [*Hän80*]. Les avantages de cette méthode sont la simplicité du matériel utile à sa réalisation et le fait qu'il n'est pas nécessaire de moduler la fréquence du laser pour l'asservir. L'inconvénient majeur réside dans l'obtention du signal d'erreur à partir de la différence de deux signaux importants : une dérive très légère d'un des signaux décale rapidement le zéro d'asservissement (par exemple une vibration sur un miroir de renvoi devant l'une des deux photodiodes servant à analyser la polarisation...). Avec cette méthode nous avons observé, un signal de battement de largeur 100 kHz entre deux lasers TiSa identiques asservis sur deux cavités FPA indépendantes. En faisant l'hypothèse que ces deux lasers sont indépendants, on en déduit que la largeur de raie d'un tel laser est donc d'environ 70 kHz. Cette valeur est à comparer à la largeur typique des signaux atomiques sur l'hydrogène qui vaut environ 1 MHz.

La méthode HC n'étant pas parfaite, nous avons utilisé la méthode des

bandes latérales [*Dre83*]. Un calcul complet du signal d'erreur est développé dans la thèse de M.Houssin [*Hou96*]. Malgré la complication matérielle, cette méthode présente l'énorme avantage de fournir une courbe en dispersion idéale pour l'asservissement. Le signal d'erreur a une pente importante au voisinage de la résonance et une large plage de capture en fréquence. Nous avons de nouveau analysé le signal de battement entre deux lasers TiSa identiques asservis sur deux cavités FPA indépendantes avec la même méthode. La largeur de raie d'un tel laser est inférieure à 10 kHz [*Bou93*].

Stabilisation à long terme du laser et balayage du laser

La stabilisation à long terme du laser se fait par l'intermédiaire d'une cavité Fabry-Perot (FPR). Cette cavité est décrite dans les thèses [*Gar89*, *Nez93b*]. Cette cavité est asservie sur un laser HeNe asservi sur l'iode. Ceci confère à la cavité la stabilité long terme de ce laser étalon. La fréquence d'un pic de cette cavité est donc fixe au cours du temps. Un pic de cette cavité nous sert de référence de fréquence depuis plusieurs années. La dérive de fréquence de ce pic au cours du temps est présentée dans l'article [*Bea00*][2]. Elle est de 100 kHz sur 5 ans et est probablement due au vieillissement du dépôt métallique des miroirs. Le balayage du laser se fait par l'intermédiaire d'un modulateur acousto-optique piloté par un synthétiseur de fréquence. Ce modulateur monté en double passage décale la fréquence du faisceau laser entrant dans la cavité FPR. Comme la longueur de la cavité est fixe, quand la fréquence du modulateur acousto-optique est décalée de $\delta\nu$, c'est la fréquence laser qui doit se déplacer de 2 $\delta\nu$ pour rester en coïncidence avec le pic de la cavité FPR. Ce montage permet un balayage extrêmement précis et reproductible du laser.

1.2.5 Les chaînes de fréquences pour les transitions 2S-nS/nD

Toutes nos mesures de fréquences optiques sur les transitions 2S-nS/nD ont été faites avec des chaînes de multiplications de fréquences. Ce ne serait plus le cas maintenant, la révolution du peigne de fréquence optique étant passée par là...

[2] B. de Beauvoir et al., Eur. Phys. J. D 12, 61 (2000) *article joint à la fin du manuscrit.*

Une mesure de fréquence d'un oscillateur ν se fait en comparant cette fréquence à celle connue d'un autre oscillateur ν_0 via un mélange hétérodyne. Ce mélange fournit un signal de battement radio-fréquence $(\nu - \nu_0)$. L'erreur sur le comptage des cycles de ce battement n'est limitée que par le rapport signal à bruit du battement et par l'incertitude sur la référence.

Dans le domaine optique, il est relativement aisé de mesurer une différence de fréquence $(\nu - \nu_0)$ de l'ordre du GHz. Cependant pour mesurer une fréquence optique à partir de celle de référence donnée par l'horloge à césium (∼9,192 GHz), le problème est autrement complexe. Il n'existe pas de multiplicateur direct des fréquences radio-fréquences vers les fréquences optiques. La multiplication doit être décomposée en plusieurs étapes via des dispositifs non linéaires. Ces dispositifs étant peu efficaces il faut utiliser de nombreux oscillateurs intermédiaires pour relier l'étalon primaire de fréquence à la fréquence laser à mesurer. C'est dans ce contexte que nous avons réalisé la première mesure en fréquence des transitions 2S-8S/8D de l'hydrogène. Une mesure plus précise de cette transition a ensuite été faite à partir d'un nouveau laser étalon à 778 nm. Enfin la fréquence absolue d'une autre transition (2S-12D) a été faite en 1999, validant ainsi les mesures précédentes. Les chaînes de fréquences sont présentées chronologiquement dans les paragraphes suivants.

Première mesure de fréquence des transitions 2S-8S/8D (H)

Le schéma proposé par A.Clairon tire profit de la quasi-coïncidence entre la fréquence à deux photons des transitions 2S-8S/8D et la différence de fréquence du laser étalon HeNe/I_2 à 633 nm et du laser HeNe/CH_4 à 3,39 μm.

$$\nu_{2S-8S/8D} + \nu_{HeNe/CH_4} \approx \nu_{HeNe/I_2} \tag{1.2}$$

Cette équation n'a de sens que si les incertitudes sur les fréquences des deux lasers HeNe sont suffisamment petites. Ce n'était pas le cas avec le laser HeNe/I_2. Le Laboratoire Primaire du Temps et des Fréquences a développé une chaîne de multiplication de fréquence pour mesurer la fréquence de ce laser à partir de celle d'un laser à CO_2/OsO_4. Cette chaîne extrêmement plus compliquée que la nôtre est décrite dans la thèse de M.Abed [*Abe93*]. La fréquence du laser à CO_2 a été mesurée par rapport à celle de l'horloge à césium avant et après la mesure de fréquence du laser HeNe/I_2. Le laser HeNe/I_2 mesuré par cette chaîne est le laser INM12 de l'Institut National

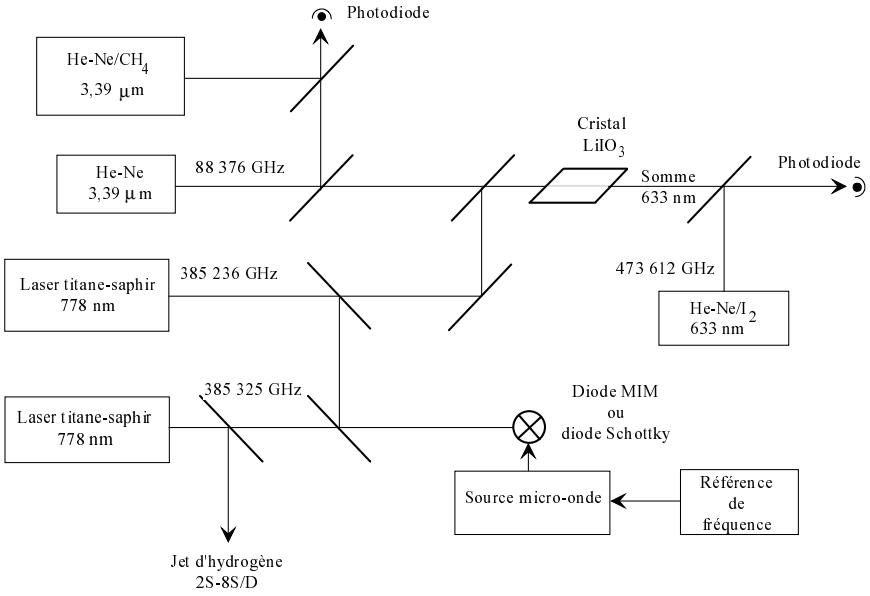

FIG. 1.3 – Schéma de la chaîne de fréquence utilisée en 1993

de Métrologie [*Ace92*]. Ce laser a été transporté dans notre laboratoire puis comparé par battement à nos deux lasers HeNe/I_2.

Concrètement, l'équation 1.2 est réalisée à l'aide de 5 lasers et d'une source micro-onde à 89 GHz (voir figure 1.3). Comme toute la puissance du laser TiSa d'excitation est utilisée pour induire la transition à deux photons, nous avons construit un deuxième laser TiSa pour réaliser la somme de fréquences avec le laser HeNe à 3,39 μm. La puissance du laser étalon HeNe/CH_4 n'étant pas suffisante, il a fallu construire au laboratoire un laser HeNe infrarouge puissant. La somme de fréquences dans un cristal de $LiIO_3$ génère une radiation à 633 nm [*Nez93b*]. Le laser HeNe auxiliaire à 3,39 μm est asservi en fréquence sur le laser HeNe/CH_4. La fréquence de l'onde générée dans le cristal de $LiIO_3$ est mesurée via un battement avec notre laser HeNe/I_2. Ainsi la fréquence du deuxième laser TiSa est connue.

Le raccordement en fréquence entre ces deux lasers est plus délicat. Dans un premier temps nous avons mesuré cet écart de 89 GHz à l'aide de la cavité FPR [*Nez92*][3].

[3]F. Nez et al., Phys. Rev. Lett. 69, 2326 (1992) *article joint à la fin du manuscrit.*

Puis, pour mesurer cette différence de fréquence, nous avons utilisé successivement deux dispositifs : une diode MIM (Métal Isolant Métal) et une diode Schottky. Ces diodes pointes réalisent le mélange des 2 ondes optiques et de l'onde hyper-fréquence à 89 GHz. Les ondes lumineuses sont couplées à la diode via un objectif de microscope. L'onde hyper-fréquence est détectée par l'antenne formée par la pointe.

Les diodes MIM sont souvent employées dans le domaine infra-rouge lointain (par exemple pour mesurer la fréquence du laser à CO_2/OsO_4 [*Ace99*]). Quelques essais dans le domaine visible ont montré qu'un tel battement pouvait être réalisé [*Dru83*]. La diode est formée par une pointe de tungstène qui vient pénétrer plus ou moins l'oxyde de nickel formé à la surface du barreau de nickel. Nous nous sommes donc lancés dans l'aventure des diodes MIM... L'éphémère signal de battement à 3 ondes est présenté dans ma thèse [*Nez93b*].

Grâce à M. Inguscio et P. de Natale du Laboratoire Européen de Spectroscopie Non Linéaire (LENS, Florence), nous avons pu essayer une diode Schottky qui leur avait été prêtée par K. Evenson (NIST). Dès la première mise en oeuvre, nous avons pu réaliser ce mélange à 3 ondes... L'intérêt essentiel de cette diode réside dans sa structure. La diode Schottky est une jonction métal-semiconducteur. La diode est propre à la structure, la pointe de tungstène ne servant qu'à faire le contact électrique en plus de sa fonction d'antenne hyper-fréquence. Une comparaison des deux dispositifs est présentée dans l'article [*Ace94a*].

Mesure de fréquence des transitions 2S-8S/8D (H,D) à partir d'un nouveau laser étalon

Durant la première mesure de fréquence, nous avons aussi mesuré avec notre chaîne de fréquence la fréquence d'une transition à deux photons dans l'atome de rubidium (voir l'annexe). A partir de cette mesure, un nouveau laser étalon à 778 nm a été construit dans notre laboratoire [*Bea96*] et au LPTF [*Mil94*]. La chaîne de fréquence du LPTF a été adaptée pour mesurer ce laser. Elle est décrite dans la thèse de D.Touahri [*Tou96*].

D'autre part, depuis 1995, deux fibres optiques longues de 3 km relient notre laboratoire au LPTF. Cela évite les éventuelles dérives de fréquence liées au transport du laser étalon mesuré par la chaîne vers notre laboratoire. Une étude brève a montré que le décalage induit par cette fibre est au plus de 3 Hz. Ce dernier est très inférieur à l'incertitude visée (400 Hz) [*Bea98*]. Enfin

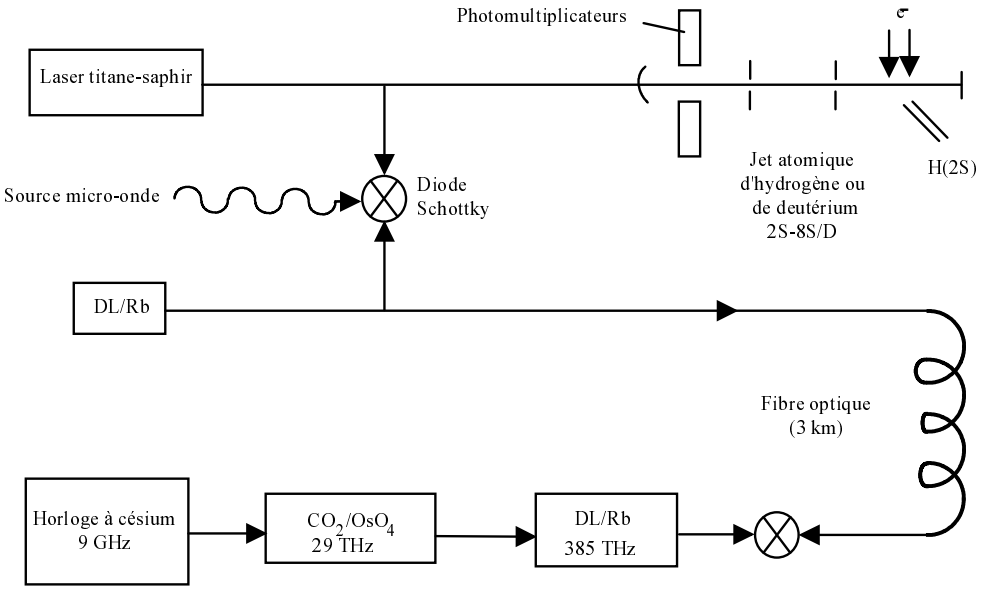

FIG. 1.4 – Schéma simplifié de la chaîne de fréquence utilisée en 1996

cette fibre permet dans le principe une comparaison de l'atome d'hydrogène à l'horloge à césium. Dans la réalité, il n'était pas matériellement possible de faire fonctionner la chaîne de fréquence du LPTF de l'horloge à césium jusqu'au laser étalon à rubidium. Là encore le laser CO_2/OsO_4 a servi de relais entre les extrémités de la chaîne. Quelques heures d'enregistrement des signaux sur l'hydrogène ont même été réalisées avec comme laser source le laser à CO_2. La relative proximité du laser étalon à rubidium avec celle du laser TiSa d'excitation simplifie grandement la chaîne de fréquence située dans notre laboratoire (voir figure 1.4). L'équation de fréquence pour les lasers devient :

$$H : \nu_{2S-8S/8D} \approx \nu_{DL/Rb_{5S-5D}} + 44\ GHz \tag{1.3}$$

$$D : \nu_{2S-8S/8D} \approx \nu_{DL/Rb_{5S-5D}} + 144\ GHz \tag{1.4}$$

Pour cette mesure, nous avons développé au laboratoire un chaîne de multiplication de fréquence sur le même modèle que celle utilisée en 1993. L'ensemble des sources hyper-fréquences qui ont été utilisées pour cette mesure sont décrites dans la thèse [*Bea96*]. Là encore, une diode Schottky a

permis de comparer en fréquence les lasers distants de plusieurs dizaines de GHz.

Mesure de fréquence des transitions 2S-12D (H,D)

Pour tester la validité des corrections Stark induites par les champs électriques parasites présents dans le jet, nous avons réalisé la mesure de fréquence absolue des transitions 2S-12D (les niveaux n=12 étant beaucoup plus sensibles aux champs électriques que les niveaux n=8). Cette fois ci, l'équation de fréquence est un peu plus complexe [*Sch99*][4]. Elle nécessite deux lasers étalons : la diode laser stabilisée sur la transition 5S-5D du rubidium et le laser CO_2/OsO_4. On a :

$$\nu(2S-12D)+\nu(DLint)\approx 2\nu(DL/Rb(5S-5D)) \tag{1.5}$$

$$\nu(2S-12D)-\nu(DLint)\approx \nu(CO_2) \tag{1.6}$$

Cependant grâce aux fibres optiques et à l'utilisation de nombreux éléments existants, la chaîne de fréquence pour mesurer la fréquence de ces transitions a pu être mise en place relativement facilement. Pour cette mesure, nous avons doublé en fréquence l'étalon à rubidium. L'onde à 778 nm est d'abord amplifiée en injectant une diode laser esclave par la diode laser étalon. L'onde amplifiée est ensuite doublée en fréquence dans un cristal de LBO placé dans une cavité externe générant ainsi une onde à 389 nm. La fréquence de cette onde est comparée avec celle de la radiation produite par somme de fréquence dans un cristal de LBO entre un laser TiSa à 750 nm et une diode laser intermédiaire à 809 nm. La deuxième équation est réalisée au LPTF. Une partie du faisceau de la diode laser à 809 nm est envoyée dans la fibre optique, la diode laser à 809 nm locale est alors asservie en phase sur la diode laser du LKB. La somme de fréquence dans un cristal de $AgGaS_2$ avec un laser à CO_2 produit un faisceau à 750 nm. Une diode laser à 750 nm est alors asservie en phase sur cette somme et renvoyée dans notre laboratoire. Ainsi tous les battements de fréquence sont mesurés dans le même laboratoire. L'utilisation du laser à CO_2 P(8) pour l'hydrogène (respectivement R(4) pour le deutérium) est nécessaire pour avoir une bonne coïncidence de fréquence. L'écart de fréquence résiduel entre les deux lasers TiSa est de 2,5 GHz pour l'hydrogène (respectivement 41,3 GHz pour le

[4]C. Schwob et al., Phys. Rev. Lett. 82, 4960 (1999) *article joint à la fin du manuscrit.*

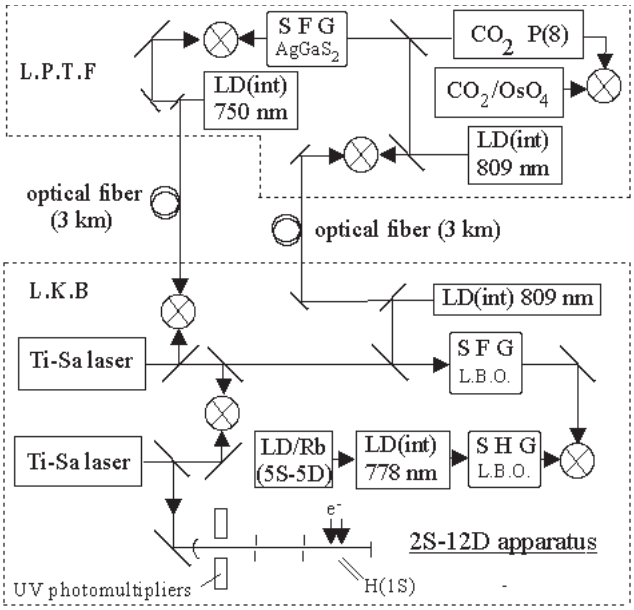

FIG. 1.5 – Schéma de la chaîne de fréquence utilisée en 1998 [*Sch99*]

deutérium). Un battement sur une photodiode rapide ou la diode Schottky permet de mesurer ces écarts.

Cette mesure de fréquence a été la dernière faite avec notre jet d'atomes métastables. Dans l'état actuel, il n'est plus possible d'améliorer l'incertitude sur les fréquences des transitions (2S-nS/nD). La contribution à la spectroscopie de l'hydrogène des mesures de fréquences des transitions 2S-nS/nD est présentée dans la partie 1.4, après la description d'autres mesures de fréquence faites sur l'hydrogène.

1.3 Les autres mesures de fréquence sur l'hydrogène

1.3.1 L'expérience de T.Hänsch sur la transition 1S-2S

Cette transition est étudiée depuis 1975 [*Hän75*]. Comme rappelé précédemment, l'intérêt premier de cette transition est sa faible largeur naturelle 1,3 Hz.

Le groupe de T.Hänsch à Garching a d'abord comparé les transitions 1S-2S et 2S-4S/4D pour en déduire le déplacement de Lamb de l'état fondamental [*Wei92*]. Une mesure interférométrique de la transition 1S-2S a été faite en 1992 [*And92*]. Depuis 1997, la fréquence de cette transition 1S-2S a été mesurée en unité de fréquence :

- par une chaîne laser avec comme laser de référence un laser HeNe/CH_4 [*Ude97*],
- puis à l'aide d'un peigne de fréquence optique avec le même laser de référence [*Rei00*]
- et enfin avec le peigne de fréquence optique référencé par l'horloge transportable à atomes froids du BNM-SYRTE [*Nie00*].

Le laser d'excitation (à 243 nm) est un laser à colorant doublé en fréquence dans un cristal de BBO. La fréquence de ce laser est mesurée en utilisant un peigne de fréquence optique généré par un laser femtoseconde (technique mise au point dans le groupe de T.Hänsch [*Ude99*]).

Les atomes d'hydrogène dans l'état fondamental sont produits par dissociation de di-hydrogène dans une décharge radio-fréquence. Dès 1992, la vitesse des atomes, via l'effet Doppler du 2ème ordre, a joué un rôle important dans la forme de raie des signaux observés [*And92*]. Actuellement les atomes 1S sont guidés vers les zones d'excitation et de détection par une buse refroidie à 5-6 K dans un cryostat fonctionnant à l'hélium liquide [*Nie00*]. De plus, seuls les atomes les plus lents sont sélectionnés. Ainsi l'effet Doppler du second ordre et l'élargissement par temps de transit se trouvent réduits. Une analyse très poussée de la forme de raie permet d'atteindre une très bonne incertitude dans le pointé de la raie.

Grâce à cette expérience, la fréquence de la transition 1S-2S est connue avec une incertitude relative record de $1{,}9\times10^{-14}$ [*Nie00*].

1.3.2 Spectroscopie des états circulaires

Une manière élégante de mesurer directement la constante de Rydberg est d'utiliser une transition entre états circulaires de nombres quantiques principaux élevés. Une expérience a été développée dans notre laboratoire sur l'atome de lithium [*Gro89*]. Une expérience sur l'hydrogène (n=27 à 30) menée pendant de longues années dans le groupe de D.Kleppner a donné récemment une mesure de la constante de Rydberg avec une incertitude relative de $2{,}1\times10^{-11}$ [*Moh02*]. Cette expérience présente de nombreux avantages par rapport aux expériences optiques. La mesure est indépendante des mesures

faites dans le domaine optique. Elle dépend très peu des corrections QED et des corrections de taille du noyau (qui varient en $1/n^3$), la fréquence théorique de la transition peut donc être calculée très précisément. Comme elle varie en $1/n^5$, la largeur naturelle des niveaux impliqués dans la transition est très petite. D'un point de vue pratique, la fréquence de ces transitions étant dans le domaine hyper-fréquence, le raccordement à l'horloge à césium est relativement aisé. Par contre la préparation des atomes dans l'état n=27 est difficile à réaliser d'un point de vue laser (laser à 121nm [*Kle00*]). En plus les niveaux étant très proches les uns des autres, le contrôle et l'analyse des effets systématiques sont très pointus.

1.4 Contributions de nos expériences à la détermination de la constante de Rydberg

Le graphique suivant représente l'évolution de l'incertitude sur la constante de Rydberg depuis 30 ans. Le début du graphique correspond approximativement à l'utilisation des techniques de spectroscopie sans effet Doppler. A partir de 1986, seules les mesures faites par spectroscopie à deux photons sont représentées.

Depuis 1992, hormis une mesure faite à l'université de Yale [*Ber95*], deux groupes ont principalement contribué à la diminution de l'incertitude sur R_∞, notre groupe et celui de T.Hänsch. La manière d'extraire la constante de Rydberg des mesures a évolué avec la précision des mesures de fréquences. Ceci peut être mis en évidence à l'aide de nos trois mesures de fréquences absolues.

1993 : La constante de Rydberg est déduite directement des fréquences des transitions 2S-8S/8D en utilisant la moyenne des valeurs expérimentales du déplacement de Lamb $2S_{1/2}$-$2P_{1/2}$ et les valeurs théoriques des corrections radiatives pour les niveaux $2P_{1/2}$, $8S_{1/2}$, $8D_{3/2}$ et $8D_{5/2}$. La valeur de R_∞ est alors : R_∞=109 737, 315 683 4(24)cm^{-1} [*Nez93a*][5].

1996 : Comme en 1993, il est possible d'extraire de ν_H(2S-nS/nD), avec une bonne incertitude, la constante de Rydberg à l'aide des "mesures 2S-2P" faites dans l'hydrogène. Ce n'est pas le cas pour les mesures faites sur le

[5]F. Nez et al., Europhys. Lett. 24, 635 (1993) *article joint à la fin du manuscrit.*

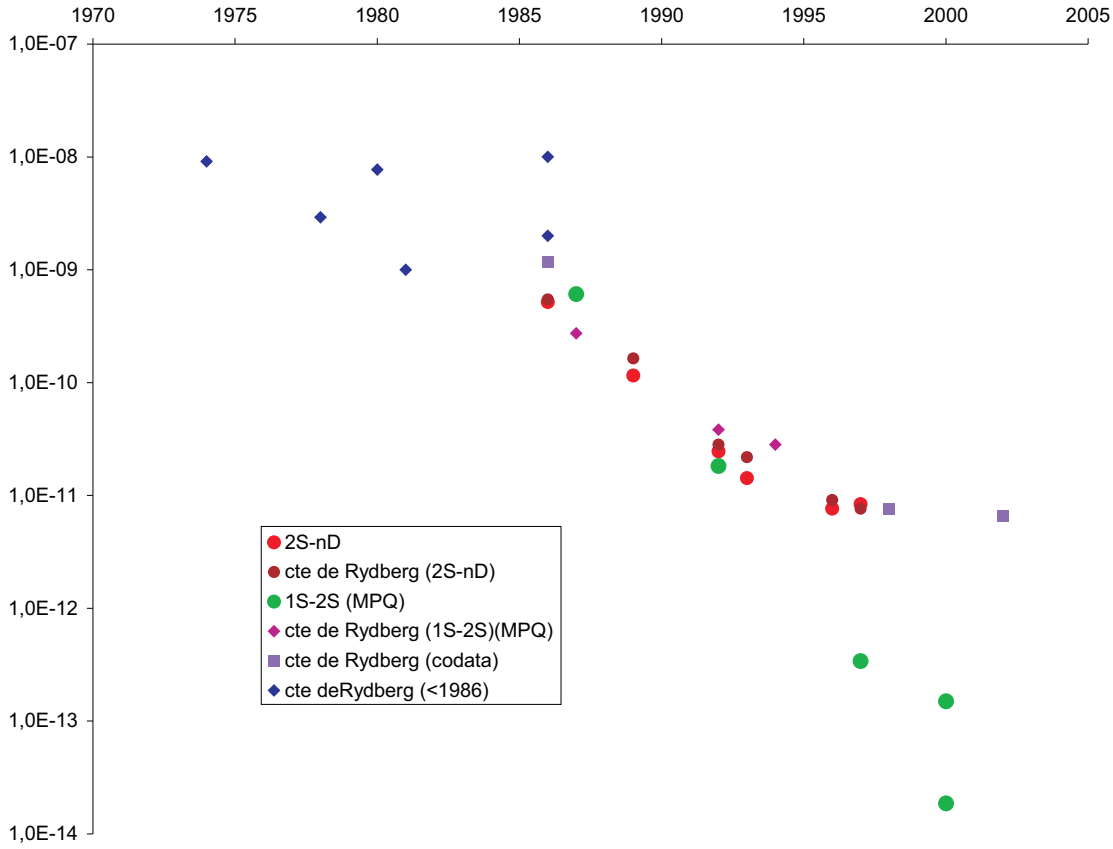

FIG. 1.6 – Evolution en fonction du temps de l'incertitude relative des fréquences des transitions 2S-nS/nD, de la fréquence 1S-2S mesurée à Garching, et de la constante de Rydberg.

deutérium. Il faut utiliser la donnée théorique L_{1S}-$8L_{2S}$ (où L_{nS} représente le déplacement de Lamb du niveau nS) et la combinaison de fréquences $7\nu_D$(2S-nS/nD)-ν_D(1S-2S) pour déterminer la constante de Rydberg. Cette combinaison linéaire fait en effet apparaître la quantité L_{1S}-$8L_{2S}$, ce qui permet d'éliminer les déplacements de lamb des niveaux 1S et 2S. La moyenne pondérée de ces deux déterminations donne : R_∞=109 737, 315 685 9(10)cm^{-1} [*Bea97*][6] .

1999 : La constante de Rydberg la plus précise ne peut être déduite que d'un ajustement de type moindres carrés sur toutes les fréquences des transitions 1S-2S, 2S-8S/8D, 2S-12D (hydrogène et deutérium) et la donnée théorique L_{1S}-$8L_{2S}$ (où L_{nS} représente le déplacement de Lamb du niveau nS) (hydrogène et deutérium). La constante de Rydberg a alors pour valeur : R_∞=109 737, 315 685 16(84)cm^{-1} [*Sch99*][7].

Une analyse faite dans l'article [*Moh00*] montre que sans les mesures de fréquences sur les transitions 2S-nS/nD, l'incertitude sur la constante de Rydberg serait multipliée par 2 alors que sans les mesures sur la transition 1S-2S elle le serait de 1,3. Cela montre l'intérêt de nos expériences.

Depuis 1999, l'incertitude de la fréquence de la transition 1S-2S a été améliorée d'un facteur 20. Différents calculs de QED ont donné un même résultat confirmant ainsi la validité de ces calculs. Enfin une "nouvelle valeur du rayon du proton" a été déduite des expériences de diffusion électron-proton (voir le paragraphe 1.6). Malgré toutes ces améliorations, l'incertitude relative sur la constante de Rydberg n'a été améliorée que de 18 % [*Moh02*]. Pour l'améliorer notablement, il faudrait disposer de la fréquence d'une autre transition de l'hydrogène avec une incertitude relative de 10^{-13} (ce que nous essayons de réaliser avec la transition 1S-3S, voir paragraphe 1.5).

D'autre part, un examen plus attentif de la comparaison théorie-expérience montre que la mauvaise connaissance du rayon de la distribution de charge du proton limite cette comparaison. Là encore, une nouvelle expérience pour le mesurer a été entreprise, expérience à laquelle nous participons. Cette expérience est décrite dans le paragraphe 1.6.

Le rôle de R_∞ ne se limite pas à la spectroscopie de l'hydrogène. Elle a une place importante dans l'ajustement des constantes fondamentales.

[6]B. de Beauvoir et al., Phys. Rev. Lett. 78, 440 (1997) *article joint à la fin du manuscrit.*
[7]C. Schwob et al., Phys. Rev. Lett. 82, 4960 (1999) *article joint à la fin du manuscrit.*

Plus ou moins régulièrement depuis 1969, une analyse de toutes les mesures de constantes fondamentales est faite dans le cadre du "sous-groupe des constantes fondamentales du Codata " auquel j'appartiens depuis janvier 1998. Le but premier de cette analyse est de donner la meilleure estimation possible des valeurs des constantes fondamentales à partir des mesures existantes. En supposant les mesures exactes, cette analyse permet aussi de tester la validité des relations entre constantes fondamentales. Depuis 1986, l'incertitude relative sur R_∞ a toujours été l'une des plus petites parmi celles des constantes fondamentales. Le rôle de R_∞ dans l'ajustement de 1998 est souligné ; elle fait partie des 4 données qui ont contribué à l'amélioration des constantes fondamentales de 1986 à 1998 [*Moh00*]. L'expression de R_∞ est :

$$R_\infty = \frac{\alpha^2 mc^2}{2(hc)} \tag{1.7}$$

Cette constante relie donc entre elles la constante de structure fine α, la masse de l'électron m et la constante de Planck h (depuis 1983, la vitesse de la lumière c est fixée). Ainsi R_∞ est utilisée pour déterminer la constante de structure fine α à partir du rapport h/M (voir chapitre 2), la constante de Planck à partir du volume molaire du silicium [*Moh00*, *Moh02*] et la masse de l'électron [*Moh00*, *Moh02*].

1.5 L'expérience actuelle sur la transition 1S-3S

L'effet systématique principal sur l'étude des transitions 2S-nS/nD est le déplacement lumineux induit par le laser d'excitation. La forte puissance lumineuse, nécessaire à l'obtention d'un bon signal à bruit "compense en partie" le faible nombre d'atomes disponibles dans l'état 2S. Malgré tous nos efforts, nous n'avons jamais réussi à augmenter l'efficacité du bombardement électronique excitant les atomes d'hydrogène dans l'état métastable [*Bea96*]. L'étude d'une transition à partir de l'état fondamental permet de disposer d'un plus grand nombre d'atomes et donc d'avoir un bon rapport signal à bruit avec moins de puissance lumineuse d'excitation. Nous essayons donc maintenant de mesurer la fréquence absolue de la transition 1S-3S.

Cette expérience a commencé en 1991. L'objectif était alors la mesure du déplacement de Lamb de l'état 1S par comparaison des fréquences des

transitions 1S-3S et 2S-6S/6D (qui sont approximativement dans un rapport 4). Ce travail a constitué la thèse de S.Bourzeix [*Bou95*] et a permis de mesurer le déplacement de Lamb de l'état 1S avec une très bonne incertitude [*Bou96*][8]. Dans les paragraphes suivants, ne sont décrits que les éléments utilisés dans le montage expérimental actuel.

1.5.1 Le jet d'atomes d'hydrogène dans l'état fondamental

Pour les expériences sur la transition 1S-3S, un nouveau jet atomique a été construit pendant la thèse de S.Bourzeix [*Bou95*]. Ce jet utilise une source d'atomes dans l'état 1S identique à celle du jet 2S. Le tube à décharge est placé perpendiculairement à l'axe optique de la cavité Fabry-Perot de surtension. Les atomes sont maintenant déviés par une buse en téflon. Cette géométrie limite la lumière parasite de la décharge vue par le photomultiplicateur [*Bou95*] ; par contre une partie des atomes se recombine sur les parois. Différents matériaux ont été essayés sans surpasser le téflon [*Hag01*].

La détection de la transition se fait en observant via un photomultiplicateur, placé au dessus de la zone de focalisation, la fluorescence soit 3S-2P à 656 nm, soit 2P-1S à 121 nm.

1.5.2 La source laser à 205 nm

L'excitation à deux photons de la transition 1S-3S nécessite une source laser à 205 nm. Celle-ci est réalisée en quadruplant la fréquence du laser TiSa à 820 nm.

Le premier doublage de fréquence se fait dans un cristal de LBO placé dans une cavité de surtension en anneau. L'onde à 410 nm sort de la cavité grâce à un miroir dichroïque. Un long travail d'optimisation [*Bou95*] a permis d'obtenir 500 mW d'onde à 410 nm à partir 2 W de laser TiSa [*Bou93*]. Avec un nouveau cristal, 960 mW de radiation à 410 nm ont été obtenus avec 2,3 W d'onde à 820 nm [*Hag01*].

Le second doublage est beaucoup plus délicat : c'est le point faible de cette expérience. Le seul cristal capable de générer l'onde à 205 nm par doublage de fréquence est le cristal de BBO [*Bou95*]. Malheureusement, à la longueur d'onde de 205 nm, nous sommes très proches de la limite d'absorption de

[8] S. Bourzeix et al., Phys. Rev. Lett. 76, 384 (1996) *article joint à la fin du manuscrit.*

ce matériau et de la limite au delà de laquelle il n'est plus accordable en phase. Le cristal est là encore placé dans une cavité en anneau. Le faisceau à 205 nm est prélevé dans la cavité à l'aide d'un prisme. Cette cavité est enfermée dans une enceinte à vide remplie d'oxygène, ce qui diminue les détériorations de surface du cristal. Un autre effet parasite vient diminuer l'efficacité de ce doublage de fréquence : l'effet photoréfractif. Il se met en place en quelques dizaines de secondes. Le réseau d'indice créé dans le cristal réfléchit la moitié environ de l'onde à 410 nm, diminuant ainsi la puissance de l'onde générée à 205 nm. Pour s'en affranchir, la longueur de la cavité est fortement modulée autour d'une résonance (via un miroir (M_{mod}) collé sur une cale piézoélectrique). Comme le temps pendant lequel la cavité est résonnante est court, l'effet photoréfractif n'a pas le temps de se mettre en place. L'inconvénient bien sûr est de produire des impulsions à 205 nm et non plus un faisceau continu [*Bou97*]. De nombreuses tentatives ont été entreprises pour améliorer l'efficacité de ce doublage sans donner de résultats spectaculaires [*Hag01*].

Cette onde à 205 nm est envoyée dans la cavité Fabry-Perot placée autour du jet atomique. L'asservissement un peu particulier de cette cavité sur l'onde incidente est très bien expliqué dans la thèse [*Hag01*].

L'effet Doppler induit par le mouvement aller-retour de M_{mod} produit un élargissement du signal atomique. En sélectionnant les impulsions soit aller soit retour, deux courbes de résonance 1S-3S décalées en fréquence peuvent être mises en évidence. Une analyse complète de cet effet est donnée dans l'article [*Hag02a*].

1.5.3 Mesure de la distribution de vitesse

Avec la méthode de spectroscopie à deux photons, il subsiste un effet Doppler du deuxième ordre. L'expression du déplacement de fréquence (δ_{Dopp}) induit par cet effet est :

$$\delta_{Dopp} = -\nu_0 \frac{v^2}{c^2} \tag{1.8}$$

où ν_0 désigne la fréquence de la transition atomique, v la vitesse des atomes et c la vitesse de la lumière.

Pour corriger la fréquence mesurée de cet effet systématique, il faut connaître la distribution de vitesse du jet atomique. Or l'absorption à un photon à partir de l'état 1S n'est pas facile à mettre en oeuvre ($\lambda \leq$121 nm). En 1991,

notre groupe a proposé une méthode pour compenser l'effet Doppler du second ordre en spectroscopie à deux photons de l'hydrogène [*Bir91*]. L'idée consiste à appliquer un champ magnétique $\overrightarrow{B}$ transverse par rapport au jet atomique. Soit $\overrightarrow{v}$ la vitesse des atomes. Le champ motionel induit a pour expression :

$$\overrightarrow{E} = \overrightarrow{v} \wedge \overrightarrow{B} \tag{1.9}$$

Ce champ électrique couple les niveaux d'énergie de l'atome par effet Stark. Le déplacement δ_{Stark} du niveau S couplé à au niveau P peut se mettre sous la forme :

$$\delta_{Stark} \propto \frac{E^2}{\Delta\nu_{SP}} = \frac{v^2 B^2}{\Delta\nu_{SP}} \tag{1.10}$$

où $\Delta\nu_{SP}$ est l'écart d'énergie entre les niveaux S et P.

Il apparaît donc clairement que le décalage Stark peut compenser l'effet Doppler du second ordre... Pratiquement cette idée est un peu plus compliquée à mettre en oeuvre qu'il n'y paraît. Les calculs complets faits par G.Hagel pendant sa thèse montrent que le décalage Doppler ne peut pas être totalement compensé. La courbe en dispersion représentant la position de la raie 1S-3S(F=1, $m_F \pm 1$) en fonction de $\overrightarrow{B}$ étant précisément calculée [*Hag01*], nous l'avons utilisée pour mesurer le décalage Doppler du second ordre [*Hag02b*][9].

Cette expérience se poursuit. Une caméra CCD plus efficace que le photomultiplicateur est utilisée pour détecter la fluorescence Balmer-α. Nous disposons maintenant d'un laser femtoseconde référencé via la fibre optique à l'horloge à césium du BNM-SYRTE. Il suffit donc que tous les éléments nécessaires à la mesure fonctionnent en même temps pour enfin réaliser une mesure absolue de fréquence de cette transition...

1.6 La spectroscopie de l'hydrogène muonique

Je décris ici l'expérience en cours sur l'hydrogène muonique. Cette expérience a lieu à l'Institut Paul Scherrer (PSI) à Villigen (Suisse) dans le cadre d'une collaboration regroupant différents équipes de plusieurs pays (Allemagne, Etats Unis, France, Portugal, Taïwan, Suisse). Le but de cette expérience est la détermination du rayon de la distribution de charge du proton

[9] G. Hagel et al, Phys. Rev. Lett. 89, 203001 (2002) *article joint à la fin du manuscrit.*

avec une incertitude relative de 10^{-3} à partir de la mesure du déplacement de Lamb (2S-2P).

1.6.1 Présentation de l'expérience

Grâce aux mesures absolues de fréquences dans l'hydrogène et le deutérium, la comparaison théorie-expérience est devenue extrêmement précise. Ainsi la constante de Rydberg est connue avec une incertitude de 6,6 10^{-12} [*Moh02*]. Cet accord est obtenu en réalisant un ajustement de moindres carrés utilisant la théorie la plus complète et toutes les mesures précises de l'hydrogène. Les paramètres ajustés sont :

- la constante de Rydberg R_∞,
- la constante de structure fine α,
- le rapport de la masse de l'électron à celle du proton,
- le rayon de la distribution de charge du proton r_p.

La plupart des corrections d'électrodynamique quantique (QED) et la correction de "taille finie du proton" suivent la même loi d'échelle (en $1/n^3$). Ainsi en supposant les corrections QED exactes ou même si les corrections QED sont incomplètes ou inexactes, un accord parfait peut être réalisé en ajustant aussi la donnée r_p. Nous appellerons $r_p^{spectro}$ la valeur de r_p ainsi obtenue. Cette valeur a évolué au gré des nouvelles corrections QED calculées. La valeur spectroscopique la plus récente est $r_p^{spectro}$=0,8736(77)fm [*Moh02*].

Initialement le "rayon du proton" a été mesuré par diffusion élastique électron-proton (appelé r_p^{diff} par la suite). Le principe de l'expérience est d'envoyer un faisceau d'électrons d'énergie bien définie dans une cible contenant de l'hydrogène liquide. Les électrons diffusés sont détectés pour différents angles de diffusion en s'assurant que leur énergie est identique à celle incidente (diffusion élastique). Deux époques doivent être considérées (∼1960, ∼1980). L'analyse des mesures de la première époque conduit à r_p^{diff}=0,809(11) fm [*Han63*]. Pendant la deuxième époque, des mesures ont été faites avec des électrons de basse énergie (ces électrons étant plus "sensibles" à la taille du proton) [*Bor74*, *Bor75*]. De plus les données de cette expérience, archivées sur ordinateur, ont été mises à la disposition de toute la communauté scientifique. Une première analyse des données a conduit à : r_p^{diff}=0,862(12) fm [*Sim80*]. De nombreux théoriciens ont travaillé à l'analyse des résultats. La dernière analyse faite par I. Sick prenant en compte toutes les mesures réalisées à basse énergie (même celles de la première période)

donne : r_p^{diff}=0,895(18) fm [*Sic03*].

Cette valeur diffère de la valeur spectroscopique ; une nouvelle expérience est donc nécessaire. A l'aide d'atomes exotiques, il est possible de s'affranchir partiellement de certaines corrections QED. En effet elles varient comme $(\mu/m)^i$ (μ désigne la masse réduite du système formé d'un électron (de masse m) et d'un noyau (de masse M), l'exposant i étant un entier). Quand l'électron ou le proton est remplacé par une particule exotique, l'importance de certaines corrections QED est atténuée ou amplifiée. Des expériences sur le muonium et le positronium ont été menées dans ce sens [*Maa94*], [*Fee93*].

L'expérience du PSI se fait avec l'hydrogène muonique (μ^--p), à savoir un système formé d'un muon négatif (μ^-) et d'un proton (p). L'image simple que l'on peut avoir du système est la suivante. Comme la masse du muon est 207 fois plus élevée que celle de l'électron, le rayon de son orbite autour du proton est $\sim$ 200 fois plus petit et donc "l'influence" de la distribution de charge du proton est plus grande. Les corrections QED de ce système sont relativement bien connues [*LeB04*] (effet du facteur d'échelle) et contrairement à l'atome d'hydrogène (e-p) le niveau 2P est au dessus du niveau 2S (voir figure 1.7). La longueur d'onde d'excitation de la transition 2S-2P est 6 μm. La largeur naturelle de la transition est proportionnelle à m donc dans notre cas 207 fois celle de l'hydrogène à savoir environ 20 GHz. Par contre, à cause de la dépendance en $1/m^3$ de la force d'oscillateur, la probabilité de transition est environ 10^7 plus petite que celle de l'hydrogène normal. Compte tenu du faible nombre d'atomes d'hydrogène muonique, cette expérience représente un certain défi expérimental...

Les techniques requises sont inhabituelles pour notre équipe :

- travail sur accélérateur pour produire l'hydrogène muonique,
- laser en impulsion (à cause de la probabilité de transition),
- analyse de signaux extrêmement faibles (typiquement quelques coups par heure).

Pour déterminer le "rayon du proton" avec une incertitude relative de 10^{-3}, il faut mesurer la fréquence de la transition 2S-2P avec une incertitude relative de 3.10^{-5} soit $\sim$ 2 GHz, ce qui correspond à environ un dixième de la largeur naturelle de la transition [*Kot99*]. Pour ne pas dégrader la précision sur la mesure de r_p, une incertitude de 100 MHz sur la fréquence absolue du laser semble suffisante. Ceci est très différent des incertitudes requises pour nos expériences sur l'hydrogène (de l'ordre du kHz).

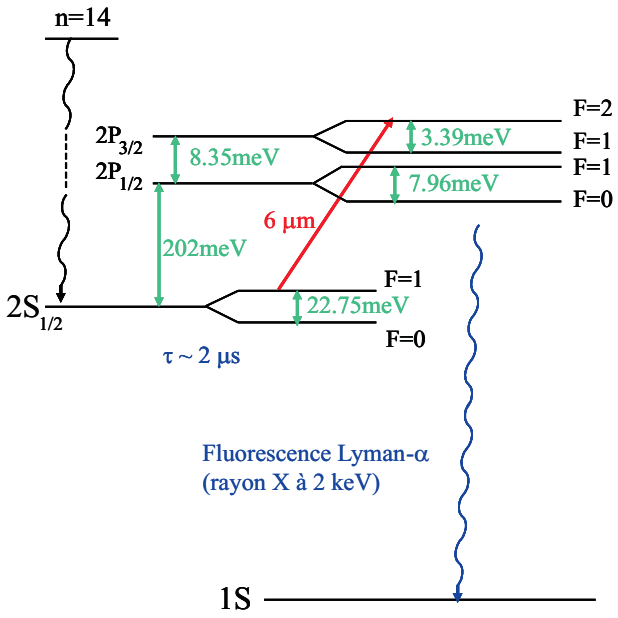

FIG. 1.7 – Schéma des niveaux d'énergie de l'hydrogène muonique

Le schéma initial de l'expérience est décrit dans le document [*Kot99*]. L'hydrogène muonique est formé en envoyant un faisceau de muons quasi-continu dans une cible de di-hydrogène. Le muon casse la molécule H_2 et éjecte un électron. Il est capturé dans un niveau très excité n∼14 ; une cascade radiative l'amène vers les états fondamentaux du système. Une toute petite proportion d'atomes seulement est formée dans l'état 2S. Typiquement la durée de vie d'un tel état est de l'ordre de la micro-seconde ; il faut donc tirer l'impulsion laser très rapidement. C'est le rôle du laser à excimère dont le tir est déclenché par l'arrivée aléatoire du muon dans la cible. Une chaîne laser convertit l'impulsion de 308 nm à 6 μm. Une cavité multi-passage à 6 μm permet d'illuminer tout le volume d'arrêt des muons dans la cible d'i-hydrogène. Des photodiodes à avalanches de grande surface (LAAPD) placées de part et d'autre de la cible viennent détecter la fluorescence 2P-1S à 2 keV [*Lud04*]. Le muon se désintègre ensuite en émettant un électron que l'on détecte. Tous les signaux sont enregistrés dans un ordinateur et archivés sur plusieurs disques durs. L'analyse des signaux se fait a posteriori. La présence de l'électron de désintégration, d'autres signaux dans des fenêtres temporelles bien précises et de conditions logiques sur ces signaux permettent

de filtrer les données et donc de réduire le bruit dans la fenêtre temporelle de la fluorescence à 2 keV.

Initialement, notre équipe a eu la responsabilité du système laser TiSa ; par la suite nous avons aussi pris en charge la mesure de fréquence du système laser complet, testé la cellule Raman et participé activement à l'alignement de la cavité multi-passage à 6 μm.

Le dispositif expérimental utilisé pour les deux périodes de recherche du signal (2003 et 2004) peut être décomposé en trois parties : production de l'hydrogène muonique, système de détection de fluorescence à 2 keV et chaîne laser. Par souci de simplicité, je ne décris dans la suite que la chaîne laser. Le dispositif complet est décrit dans les documents [*Kot99*, *Poh00*, *Kot02*] [*Poh05*][10] (voir aussi http ://muhy.web.psi.ch).

1.6.2 La chaîne laser

La chaîne laser est constituée de plusieurs étages (voir figure 1.8). Le point de départ est un laser à excimère à 308 nm (XeCl). A l'autre extrémité de cette chaîne se trouve une cellule Raman contenant de l'hydrogène moléculaire sous forte pression. Le faisceau à 6 μm est généré, après trois transitions Raman successives, à partir d'une impulsion laser à 708 nm. Pour que le processus soit efficace, la durée de l'impulsion laser incidente doit être inférieure à 8 ns, avec une énergie d'environ 10 mJ. C'est le rôle du système TiSa. L'oscillateur délivre l'impulsion courte, l'amplificateur fournit l'énergie, la fréquence du laser étant fixée par l'injection d'un laser TiSa continu. Les lasers TiSa en impulsion sont pompés par un laser à colorant lui-même pompé par le laser XeCl. Cette chaîne laser est décrite en détail dans l'article [*Ant04*] ; je n'en donne ici qu'un bref résumé en partant du laser à excimère.

Les lasers à excimère et les lasers à colorant

Ces lasers forment un ensemble complet, optimisé pour donner un maximum d'énergie à un taux de répétition élevé. Le choix du laser à excimère est dicté par :

- la capacité du laser à être déclenché sur un signal aléatoire,
- le délai de tir très rapide ($\leq 1\mu s$),
- la puissance disponible,

[10] R. Pohl et al, J. Can. Phys. xxx, xxx (2005) *article joint à la fin du manuscrit.*

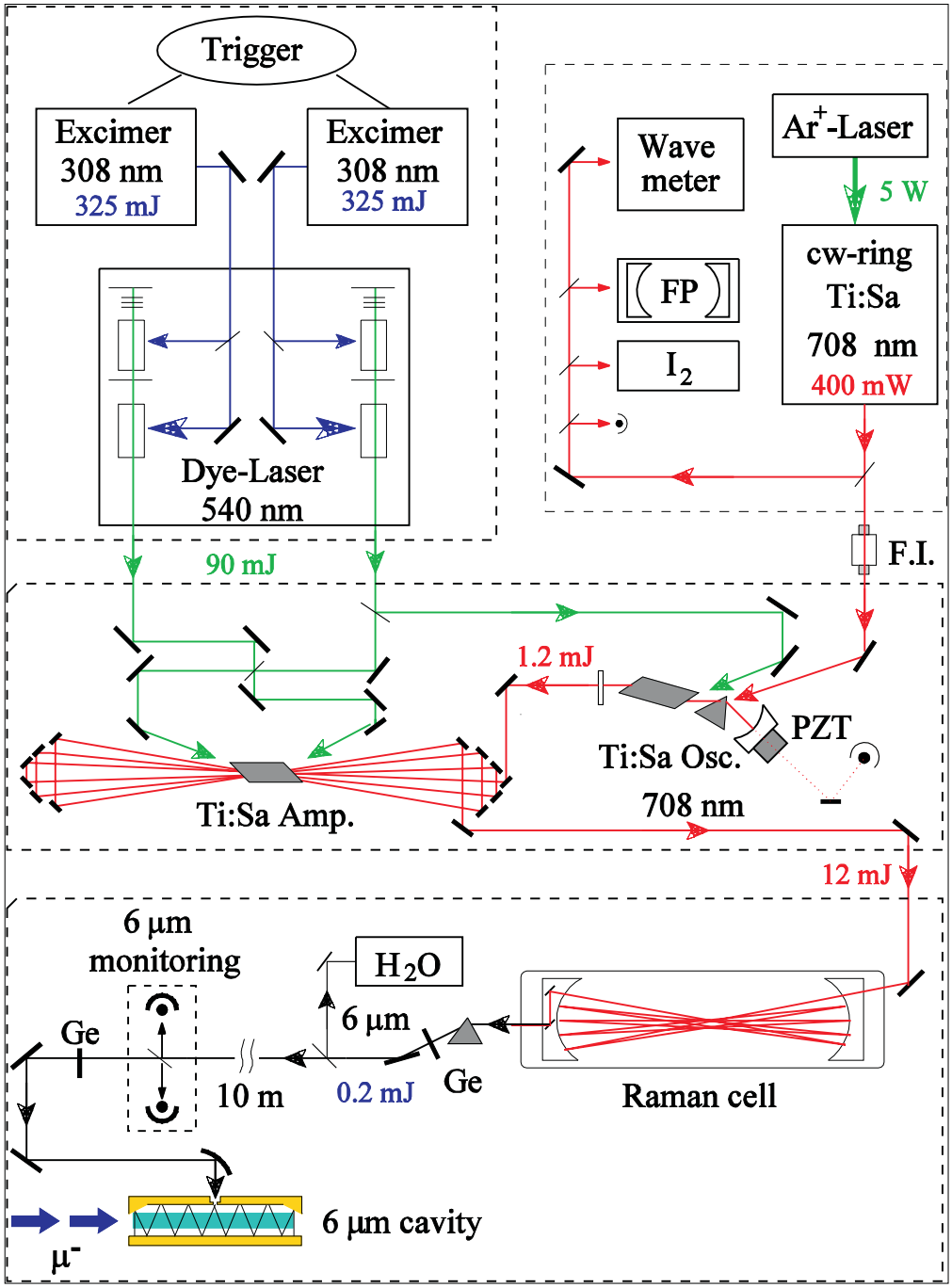

FIG. 1.8 – Schéma du dispositif de la chaîne laser [*Ant04*]

– le taux de répétition supérieur à 50 Hz,
– (et enfin la disponibilité d'un exemplaire (LPX 300) au PSI).

Durant la première recherche du signal, nous avons utilisé un laser LPX 300 reconditionné par la société Radiant Dye. Il produisait 600 mJ avec un taux de répétition de 50 Hz et malheureusement un délai de tir de 1 μs (au lieu des 300 ns promis)... Pour le deuxième temps de faisceau, ce laser a été remplacé par deux lasers LPX 210 et LPX 220 récupérés dans deux instituts (MPQ Garching et EPF Lausanne). Là encore un gros travail de maintenance journalier a été nécessaire au simple fonctionnement normal de ces lasers...

Les lasers à colorant ont évolué avec leurs lasers de pompe. Ils sont constitués d'un oscillateur et d'une cellule amplificatrice. L'oscillateur est formé d'une cellule de Béthune placée entre deux miroirs plans. A cause de sa relativement bonne durée de vie et de son spectre d'émission par rapport à celui d'absorption du Titane-Saphir, le colorant Coumarine 153 a été retenu. La mauvaise qualité du mode spatial de ces lasers fluctue avec le taux de répétition et de plus, évolue avec le vieillissement du colorant. En période d'enregistrement de signaux, il faut préparer 30 litres de colorant par jour...

Au mieux, les lasers à excimère (XeCl à 308 nm) donnent chacun 350 mJ. L'énergie délivrée par chacun des lasers à colorant est d'environ 45 mJ.

L'ensemble laser Tisa

La configuration retenue est celle d'un oscillateur injecté par un laser continu suivi d'un amplificateur multi-passages. Différents essais ont été réalisés dans notre laboratoire avec comme laser de pompe un vieux laser YAG (YG 481 Quantel) [*Kaz00*] [*Ami00*].

L'oscillateur TiSa

La fonction de l'oscillateur est de fournir une impulsion courte de longueur d'onde parfaitement définie à 708 nm avec suffisamment d'énergie pour obtenir plus de 10 mJ en sortie de l'amplificateur. L'idée initiale pour fabriquer cette impulsion était d'utiliser une cellule de Pockels dans l'oscillateur, montée en vanne optique pour vider la cavité. Les essais ont montré que le traitement anti-reflet de la cellule se détériorait très rapidement. L'idée est alors venue de raccourcir au maximum la longueur de la cavité pour diminuer la durée de l'impulsion (dans notre cas L_{cavit}=7 cm) ; c'est la dynamique du laser qui va générer cette impulsion courte. Ainsi la durée de l'impulsion

dépend notablement de la fluence de pompe. Une durée d'environ 7 ns est obtenue en pompant le cristal le plus fortement possible sans le casser... Les meilleurs résultats ont été obtenus avec les cristaux fabriqués par la société Saint-Gobain vendus par l'entreprise Roditi.

Le système TiSa doit fonctionner à 708 nm. Or à cette longueur d'onde le gain du TiSa est deux fois plus petit que le gain maximum. Il faut donc un élément dispersif dans la cavité pour forcer le laser à émettre à 708 nm. Compte tenu de la faible puissance de pompe à 540 nm, il nous a semblé difficile d'utiliser un réseau. Premièrement, un prisme en Flint est placé dans la cavité de l'oscillateur au minimum de déviation. Dans cette configuration, l'incidence sur le prisme est aussi très proche de celle de Brewster à 708 nm. Deuxièmement, la largeur de raie du laser est affinée par injection d'un laser TiSa continu. Ce dernier contrôle ainsi la fréquence émise par l'oscillateur. Le laser TiSa continu est construit selon le modèle standard à l'équipe (voir 1.2.4). Différents schémas pour l'injection ont été réalisés :

- Classiquement via un isolateur optique placé en sortie de l'oscillateur. Cette méthode a pour défaut d'introduire des pertes sur le trajet de l'impulsion, la transmission de l'isolateur étant de 80%.
- Simplement via une face du cristal qui est taillé à l'incidence de Brewster pour 800 nm. La faible efficacité de couplage est l'inconvénient de cette idée.
- Simplement et plus efficacement via une réflexion sur une face du prisme. Dans ce cas, le couplage du laser continu dans la cavité est meilleur que précédemment.

Cette injection permet aussi d'aligner très facilement les miroirs de la cavité de l'oscillateur. Cette dernière est maintenue à résonance avec le laser continu via un asservissement classique (miroir fixé sur une cale piézoélectrique et détection synchrone). Un aperçu de cet oscillateur est donné sur la figure 1.9.

L'amplificateur TiSa

L'amplificateur 8 passages est utilisé pour amener l'énergie de l'impulsion au voisinage de 10 mJ. La géométrie "papillon" de cet amplificateur est identique à celle utilisée sur les chaînes laser femtoseconde. Contrairement au montage présenté dans le document [*LeB93*], la position des faisceaux amplifiés dans le cristal TiSa n'est pas ajustée avec une caméra pour maximiser le recouvrement avec le faisceau de pompe. L'alignement se fait en optimisant

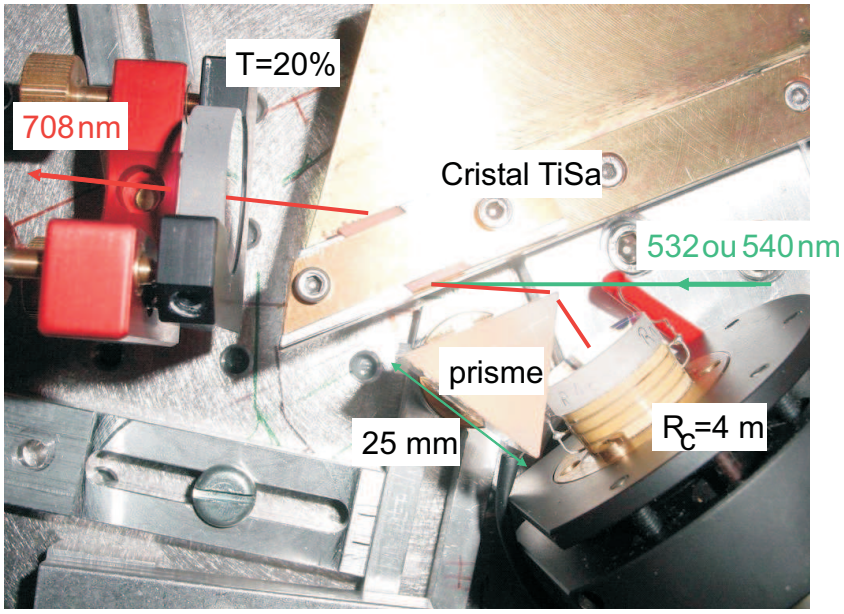

FIG. 1.9 – Photographie de l'oscillateur TiSa

l'énergie amplifiée à chaque passage. Comme l'amplification est plus efficace au début de l'impulsion qu'à la fin, la durée de l'impulsion est raccourcie à 6 ns.

Typiquement, le système TiSa délivre à 708 nm des impulsions de 6 à 7 ns d'énergie supérieure à 10 mJ, pour une énergie de pompe de 90 mJ à 100 mJ [*Ant04*].

La cellule Raman et la cavité à 6 μm

La cellule Raman [*Rab86*] convertit les photons à 708 nm en photons à 6 μm par 3 diffusions Raman stimulées successives dans un gaz d'H_2 sous forte pression (14 bars). Le photon incident est absorbé par la molécule qui passe dans un état excité. Elle se désexcite sur un niveau vibrationnel plus élevé (v=1) que celui d'origine (v=0). La différence d'énergie est le quantum de vibration moléculaire (σ_{Raman}=4155,2 cm^{-1}). Les longueurs d'onde des photons mis en jeu dans le processus sont 708 nm, 1 μm, 1,7 μm et 6 μm. L'énergie de l'impulsion émergeante à 6 μm est de 0,2 mJ pour 12 mJ incidents à 708 nm.

Un prisme en CaF_2 et deux lames en germanium traitées anti-reflet à

6 μm sont utilisés pour filtrer l'onde à 6 μm en sortie de cellule Raman.

L'impulsion à 6 μm est dirigée sur une autre cavité multi-passages via plusieurs miroirs en cuivre placés dans une enceinte en surpression d'azote sec afin d'éviter toute absorption parasite de H_2O.

Le rôle de cette autre cavité multi-passages non résonnante est d'illuminer, avec l'onde à 6 μm, tout le volume d'arrêt des muons dans la cible d'H_2 ($7 \times 15 \times 170$ mm^3). La géométrie de cette cavité est donc particulière. Le premier miroir est plan, ses extrémités étant terminées par deux parties courbes. Ceci assure le confinement latéral de l'onde infrarouge dans la cavité. Le confinement vertical est assuré par le deuxième miroir de forme cylindrique. La réflectivité nécessairement élevée (99,97%) est obtenue avec des couches diélectriques de ZnSe et ThF_4. Cependant la radioactivité du thorium endommage les détecteurs de rayons X ; d'autres couches diélectriques seront utilisés pour le prochain run. Un trou de diamètre 630 μm, situé au milieu du miroir plan, permet de coupler la lumière à la cavité. Le trou d'injection et l'approche non résonnante rendent cette cavité peu sensible aux défauts d'alignement, ce qui est indispensable puisqu'après réglage sur une table optique, cette cavité est enfermée dans le jet de muons au plus près de la cible de H_2. L'analyse du temps d'amortissement et de la forme de la distribution temporelle de l'onde émergente de la cavité permet d'estimer la qualité de l'injection dans la cavité.

Détermination de la fréquence de la source à 6 μm

La calibration de la fréquence absolue de la source à 6 μm est faite grâce au spectre de H_2O. Notre raie de référence (appelée 37 dans [*Pot98*]) est connue avec une incertitude de 2 MHz. Une absorption simple dans une cellule permet d'observer cette raie. D'autre part, la fréquence de cette source à 6 μm est contrôlée par celle du laser TiSa continu. La fréquence de ce laser est déterminée grâce à un interféromètre de Fabry Perot stable (FPS) à l'aide d'une cellule d'iode. Un lambdamètre construit au laboratoire permet de déterminer sans ambiguïté le numéro du pic de FPS sur lequel est asservi le laser continu. Le glissement de fréquence entre le laser continu et l'oscillateur en impulsion, mesuré en analysant simultanément l'absorption dans la cellule d'iode en continu et en impulsion vaut 110 MHz. Cette valeur est en bon accord avec celle estimée [*Ant04*]. Les calculs montrent que l'effet de glissement de fréquence est négligeable dans l'amplificateur [*Ant04*]. Il est donc possible de déterminer σ_{Raman} à partir de l'un de nos enregistrements

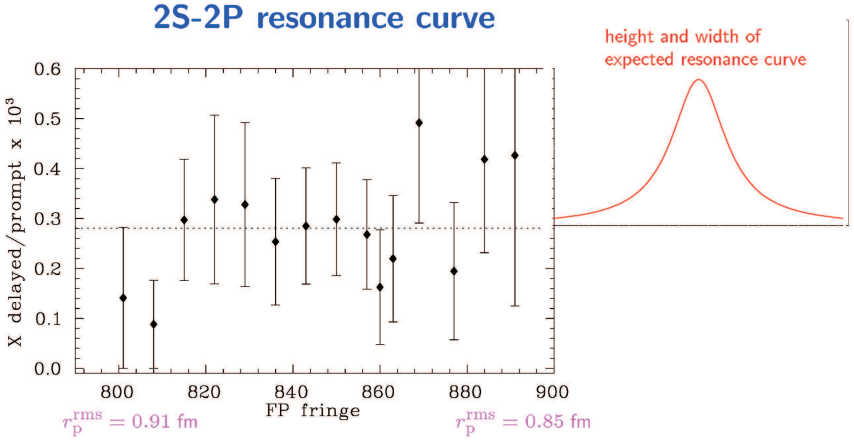

FIG. 1.10 – Evolution de la fluorescence 2P-1S en fonction de la fréquence laser. Le signal de résonance attendu est présenté à coté des points expérimentaux. Cette figure est extraite d'une présentation de F.Kottmann (Coimbra 2005).

de spectre de la raie 37 et des mesures de longueur d'onde à 708 nm. Notre mesure est en relativement bon accord avec celles connues [*Ant04*].

1.6.3 Résultats

Le résultat du premier run en 2002 a été de faire fonctionner toutes les parties du dispositif expérimental en même temps, validant ainsi la conception de l'expérience. Nous avons essayé d'améliorer les points défectueux de l'expérience avant le deuxième run prévu un an plus tard. Malgré cela des difficultés nouvelles sont apparues ce qui nous a obligé à utiliser certaines solutions de secours prévues.

Finalement 2×10^7 tirs lasers ont été utilisés pour chercher la résonance 2S-2P de l'hydrogène muonique [*Poh05*] Le laser a été utilisé avec 15 longueurs d'onde différentes. L'écart entre deux longueurs d'onde successives correspond à une demi largeur naturelle de la transition.

L'analyse des données n'a pas mis en évidence de résonance (voir figure 1.10). Ceci est dû à la trop faible amplitude de signal (environ 1 coup par heure à résonance) qui est à comparer au bruit de fond (1 coup par heure). La source principale de la faible statistique résultante est l'ensemble laser XeCl et laser à colorant (de par le délai de tir et le faible taux de répétition). Nous

étudions la possibilité de remplacer ces deux lasers par des lasers Yb :YAG à disque : ces lasers devraient permettre de réduire significativement le délai de déclenchement de l'impulsion laser et d'augmenter le taux de répétition. La maintenance de ce laser étant moins lourde, nous pourrons mieux utiliser le temps de faisceau en réduisant les temps morts.

1.7 Conclusion

Nos expériences ont permis d'améliorer la connaissance de la constante de Rydberg d'un facteur 25 en 15 ans. Nous avons réalisé la première mesure absolue de fréquence d'une transition de l'atome d'hydrogène. La compétition avec le groupe de T.W.Hänsch a stimulé le développement de nouveaux dispositifs de mesures de fréquences optiques (le laser étalon stabilisé sur une transition à deux photons du rubidium, le peigne de fréquence optique généré par laser femtoseconde...)

A ce jour, la spectroscopie de l'hydrogène sur jet est proche de ses limites. Une amélioration possible du jet (2S) consisterait à augmenter notablement le nombre d'atomes métastables produits réduisant ainsi les effets systématiques liés à la forte puissance lumineuse nécessaire au bon rapport signal à bruit des signaux détectés. Une méthode à base d'impulsions lumineuses et de passage adiabatique rapide est proposée dans la référence [*Yat99*]. Il faut cependant étudier plus en détail cette possibilité, les longueurs d'onde des lasers n'étant pas simples à générer. Une nouvelle voie de spectroscopie d'atomes d'hydrogène refroidis est en cours d'exploration dans le groupe de D.Kleppner [*Kle04*].

Comme pour l'hydrogène muonique, on peut essayer de contourner le problème en jouant sur les facteurs d'échelle que sont la masse du noyau ou la charge des systèmes hydrogénoïdes. La possibilité de spectroscopie d'états circulaires d'atomes hydrogénoïdes est en cours d'étude théorique dans notre laboratoire [*Ind05*]. Enfin, l'ion He^+ suscite l'intérêt de nombreuses équipes pour tester la QED à deux boucles et donc améliorer la détermination de la constante de Rydberg à l'aide de l'atome d'hydrogène (voir [*Rot05*] et les références citées).

D'un point vue théorique, les techniques actuelles de calcul des corrections d'électrodynamique quantique semblent aussi atteindre leurs limites. Le développement de nouvelles techniques permettant le calcul de toutes les corrections n'est pas envisageable dans le court terme, à ma connaissance.

Actuellement, la spectroscopie de l'hydrogène ne peut se passer d'une mesure précise de la distribution de charge du proton. Cette mesure permettra d'infirmer ou de confirmer les prédictions de l'électrodynamique quantique et donc éventuellement de stimuler de nouveaux développements théoriques et expérimentaux. Enfin une telle mesure est un petit pas vers une meilleure connaissance de la structure du proton et donc une détermination de α à partir de la structure hyperfine de l'état 1S de l'atome d'hydrogène.

Chapitre 2

Mesure de la constante de structure fine

2.1 Introduction

La constante de structure fine α a été introduite par A.Sommerfeld pour décrire la structure fine des raies spectrales de l'atome d'hydrogène. L'expression de α est :

$$\alpha = \frac{q^2}{4\pi\epsilon_0\hbar c} \tag{2.1}$$

où

- q est la charge de l'électron,
- ϵ_0 est la permittivité du vide,
- $\hbar$ est la constante de Planck réduite,
- et c est la vitesse de la lumière dans le vide.

Aujourd'hui, la signification de α a évolué. Elle est la constante de couplage qui caractérise l'interaction électromagnétique qui est l'une des interactions fondamentales avec les interactions gravitationnelle, faible et forte. Cette constante intervient dans différents domaines de la physique, comme nous allons le voir par la suite.

2.1.1 Les différentes mesures de α

La valeur de la constante de structure fine peut être déterminée à partir de mesures faites dans les domaines de la physique du solide ou de la physique

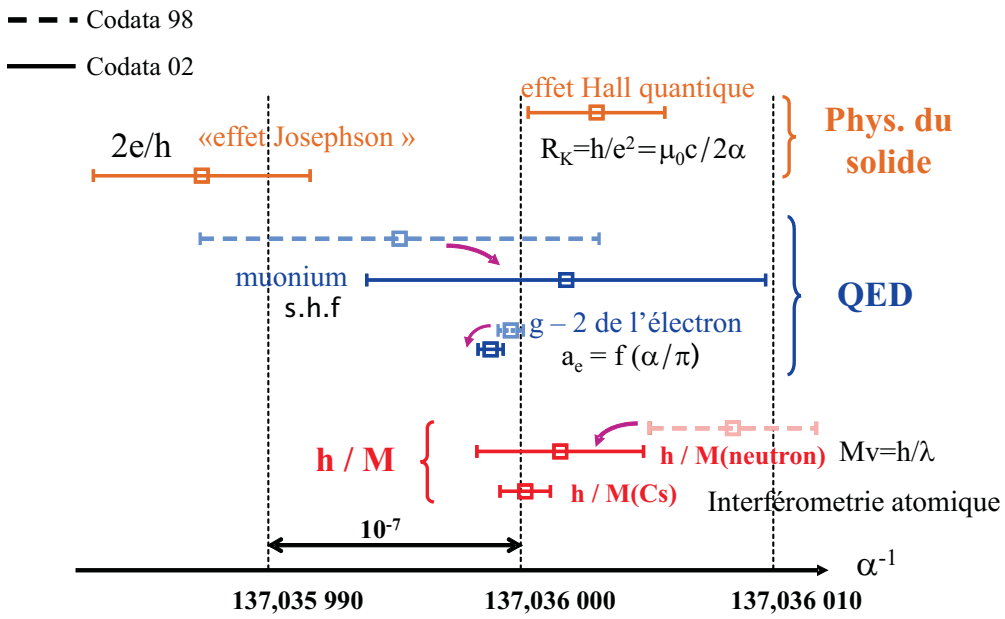

FIG. 2.1 – Différentes déterminations de α.

atomique (effet QED ou mesures de structure fine ou hyperfine) ou à partir de mesures du rapport h/M_X où M_X désigne la masse de la particule X.

Les expériences retenues par le Codata 2002 pour donner la meilleure estimation de α sont :

- l'effet Hall quantique caractérisé par la constante de Von Klitzing (R_K),
- le rapport gyromagnétique du proton qui s'exprime en fonction de R_K et de K_J (constante caractérisant l'effet Josephson),
- la structure hyperfine du muonium,
- le moment magnétique anormal de l'électron (a_e),
- le rapport h/M_n où M_n est la masse du neutron et h la constante de Planck,
- et le rapport h/M_{Cs} où M_{Cs} est la masse de l'atome de césium.

Quand notre expérience a débuté (1999), la dispersion totale de ces mesures était de l'ordre de $2{,}9\times10^{-7}$ alors que l'incertitude de chacune des mesures (hormis a_e) était de l'ordre de quelques 10^{-8} [*Moh00*].

Fin 2002, cette situation a légèrement évolué (voir figure 2.1).Des nouvelles corrections QED ont été ajoutées à l'expression théorique de la structure hyperfine du muonium, déplaçant ainsi la valeur de α déduite de cette

donnée. Une valeur très précise de α ne peut pas être déduite des mesures très précises de structure fine de l'hélium ([*Geo01*, *Pas01*]) et hyperfine de l'hydrogène car les expressions théoriques de ces structures ne sont pas suffisamment bien connues.

La mesure du rapport h/M_n est liée à la distance entre plans interréticulaires de cristaux de silicium (d_{220}) via la mesure de longueur d'onde des neutrons. Une longue analyse a montré que des erreurs ont probablement été faites dans certaines mesures de d_{220}. En ne prenant pas en compte ces données, l'accord entre les différentes déterminations de α est un peu meilleur [*Moh02*].

La valeur actuelle de α est essentiellement donnée par celle déduite de la mesure du moment magnétique anormal de l'électron ($a_e = f(\alpha/\pi)$). Les coefficients du développement en série de $f(\alpha/\pi)$ sont calculés par l'électrodynamique quantique. Très récemment, les calculs du dernier terme ont été réévalués, "déplaçant" ainsi la valeur de α. D'autres mesures de α sont donc nécessaires.

Le but premier de notre expérience est de contribuer à la connaissance de α avec une incertitude relative de quelques 10^{-8}, puis mieux si possible.

2.1.2 Principe de notre expérience

La mesure de α à partir de h/M_X se déduit de l'équation suivante :

$$\alpha^2 = \frac{2R_\infty}{c}\frac{M_p}{m}\frac{M_X}{M_p}\frac{h}{M_X} \tag{2.2}$$

où :
- R_∞ est la constante de Rydberg,
- M_p est la masse du proton,
- m est la masse de l'électron,
- M_X est la masse de la particule X,
- et h est la constante de Planck.

Les rapports de masse sont connus très précisément si bien que cette méthode conduit à une mesure très précise de α indépendante de la QED et de la physique du solide.

Le principe de notre expérience est la mesure du recul d'un atome. Lorsqu'un atome absorbe ou émet un photon de quantité de mouvement $\hbar\overrightarrow{k}$, il subit un effet de recul. Cet effet a été observé pour la première fois en 1976

[*Hal76*]. La vitesse qu'il acquiert est la vitesse de recul $\overrightarrow{v_r}$:

$$\overrightarrow{v_r} = \frac{\hbar \overrightarrow{k}}{M} \tag{2.3}$$

Il apparaît clairement que la mesure de v_r et k donne une mesure de h/M et donc de α via l'équation 2.2.

Pour faire cette expérience, il faut disposer d'atomes dont la distribution de vitesse est bien plus étroite que v_r (classe de vitesse sub-recul). La source atomique mono-cinétique doit donc être réalisée à partir d'atomes refroidis par laser (dans notre expérience, la classe de vitesse sub-recul est obtenue en ne sélectionnant qu'une petite partie des atomes froids). Après avoir sélectionné et mesuré la vitesse initiale des atomes, l'idée est de les accélérer de manière cohérente puis de mesurer leur vitesse finale.

Il est tentant de faire l'expérience avec un atome léger (H ou He), l'effet de recul à mesurer étant alors grand. Un premier inconvénient est la difficulté à refroidir simplement ces deux atomes. D'autre part, pour obtenir une bonne incertitude sur la mesure sur h/M, il faut transférer de manière cohérente le plus grand nombre possible de $\hbar k$ à l'atome. Or plus l'atome est léger, plus sa vitesse de recul est grande et donc plus l'atome va parcourir une grande distance pendant la phase d'accélération. Ceci conduit à une taille d'expérience qui n'est pas raisonnable et sur laquelle le contrôle des effets parasites devient très difficile.

Nous avons choisi l'atome de rubidium pour plusieurs raisons. Il possède deux isotopes stables (^{85}Rb et ^{87}Rb). Ces atomes peuvent être refroidis par le même système laser. L'expérience, qui dépend de la masse, peut donc être conduite sur l'un ou l'autre des isotopes. Enfin, de nombreuses expériences ont permis d'observer un condensat de ^{87}Rb. Ce condensat pourrait à terme servir de source atomique sub-recul. Notre expérience utilise des transitions Raman pour sélectionner et mesurer la distribution de vitesse des atomes. Enfin, l'autre originalité de notre expérience est l'emploi d'oscillations de Bloch pour accélérer les atomes.

Depuis maintenant plus 10 ans, l'équipe de S.Chu a entrepris une expérience d'interférométrie atomique sur l'atome de césium pour mesurer l'accélération locale de la gravité g [*Kas91b*] et le rapport h/M$_{Cs}$ [*Wei93*]. Ces expériences ont permis la mise au point de nouvelles techniques dans le domaine des atomes froids dont nous bénéficions en partie.

L'accélération g est mesurée grâce à un interféromètre ($\pi/2 - \pi - \pi/2$). Le dernier gravimètre développé dans cette équipe donne des résultats en

accord avec ceux des gravimètres classiques (du type coin cube en chute libre) à 7±7 10^{-9}g [*Pet01*]. Ceci montre qu'il est possible d'effectuer des mesures sensibles et exactes à l'aide d'interféromètre atomique.

L'expérience h/M_{Cs} utilise un interféromètre "Ramsey-Bordé" ($\pi/2 - \pi/2 - N \times \pi - \pi/2 - \pi/2$) [*Bor89*] . Ce dernier produit deux systèmes de franges séparés de 2 N v_r. Les deux couples d'impulsions $\pi/2$ servent à sélectionner puis mesurer la distribution de vitesse des atomes au sommet d'une fontaine atomique. L'avantage essentiel de cette expérience par rapport à la nôtre est la très faible largeur des franges d'interférence. Cependant le nombre d'impulsions π semblent limités à 30. Très récemment, l'expérience de mesure de h/M_{Cs} a donné un résultat préliminaire d'incertitude relative de 1,5 10^{-8} [*Wit01*]. La valeur de α tirée de cette mesure préliminaire est en bon accord avec la détermination la plus précise de la constante de structure fine [*Moh02*].

Rappelons que le but premier de notre expérience est de contribuer à la connaissance de α avec une incertitude relative de quelques 10^{-8}, puis mieux si possible. L'expérience de S.Chu montre que ce n'est pas irréaliste. Notons enfin qu'en prenant les valeurs connues de h et M_{Rb}, notre expérience peut aussi être employée pour mesurer g.

2.2 Notre expérience

Je présente ici brièvement les transitions Raman utilisées pour accélérer les atomes et mesurer très précisément leur vitesse. On donne aussi un bref aperçu du dispositif expérimental. Cette expérience préliminaire a donné une mesure de α avec une incertitude relative de 4×10^{-7}. La description très complète de cette mesure est présentée dans la thèse de Rémy Battesti [*Bat03*]. Ce chapitre se conclut en faisant le point sur l'avancement de l'expérience et sur les nouveaux développements envisagés.

2.2.1 Les transitions Raman

La sélection en vitesse des atomes, leur accélération et les mesures de vitesse se font à l'aide de transitions Raman. Ce sont des transitions à deux photons qui couplent des états de même parité. Dans notre expérience ces états sont les deux niveaux hyperfins de l'état fondamental de l'atome de rubidium (figure 2.2) ou un seul de ces niveaux hyperfins couplé à lui même.

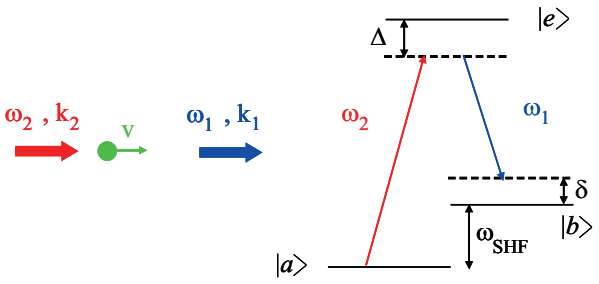

FIG. 2.2 – Schéma des niveaux.

Dans la cas où les faisceaux sont co-propageants ($\overrightarrow{k_1} \simeq \overrightarrow{k_2} \simeq \overrightarrow{k}$), la condition de résonance s'écrit :

$$\omega_2 - \omega_1 - \omega_{SHF} \sim 0. \tag{2.4}$$

Dans le cas contra-propageant ($\overrightarrow{k_1} \simeq -\overrightarrow{k_2}$), la condition de résonance devient :

$$\omega_2 - \omega_1 - \omega_{SHF} \sim 2k(v + v_r). \tag{2.5}$$

où v_r est la vitesse de recul (voir équation 2.3). Dans ce cas, l'effet Doppler est prédominant et les transitions sont sélectives en vitesse [*Kas91a*]. Cette sélectivité peut être rendue arbitrairement étroite car la largeur de la sélection n'est pas affectée par la largeur radiative quasi nulle des niveaux mis en jeu. Seul le temps d'interaction atome-laser limite la largeur de la distribution de vitesse sélectionnée.

L'efficacité de transfert de la population de l'état $|a\rangle$ vers l'état $|b\rangle$ dépend du produit $\Omega^{eff}_{a\to b}\, t$ où t est la durée de l'impulsion Raman, et $\Omega^{eff}_{a\to b}$ la pulsation de Rabi effective. L'expression de cette pulsation, en fonction des pulsations de Rabi de chaque onde (Ω_1 et Ω_2) est :

$$\Omega^{eff}_{a\to b} = -\frac{\Omega_1^* \, \Omega_2}{2\Delta} \tag{2.6}$$

Le transfert est maximum quand $\Omega^{eff}_{a\to b}\, t = \pi$. Une impulsion π réalisée par deux ondes contra-propageantes permet donc de sélectionner une classe de vitesse définie en la transférant complètement vers un autre niveau atomique.

Durant l'excitation Raman, il y a absorption puis émission induite de photons. Ainsi, contrairement au processus simple d'absorption à un pho-

ton suivie d'une émission spontanée (par nature isotrope), le transfert d'impulsion avec les transitions Raman est parfaitement défini. Une transition Raman d'un état atomique vers lui même laisse l'atome dans le même état atomique, mais sa quantité de mouvement varie de $2\hbar k$. Le processus peut être répété si la fréquence des ondes ω_1 et ω_2 est ajustée pour compenser l'effet Doppler induit par $2\hbar k$. Il suffit pour cela que la fréquence ω_2 varie linéairement dans le temps alors que ω_1 reste fixe

Pour maintenir la condition de résonance pendant les N transitions Raman, la différence de fréquence ($\delta' = \omega_1 - \omega_2$) doit suivre la relation :

$$\delta' = 2kv_r(2N - 1) \tag{2.7}$$

Dans le référentiel du laboratoire, l'atome est donc soumis à une accélération constante a :

$$a = \frac{1}{M}\frac{dp}{dt} = \frac{(2\hbar k)}{M}\frac{dN}{dt} = \frac{1}{2k}\frac{d\delta'}{dt}. \tag{2.8}$$

Ainsi les atomes peuvent être accélérés de manière cohérente par des faisceaux lumineux.

En terme d'atome habillé, ces transitions Raman successives peuvent être vues comme des passages adiabatiques rapides entre états d'impulsions différentes.

Un autre point de vue peut être développé. Durant l'accélération, les ondes ω_1 et ω_2 forment une onde stationnaire uniformément accélérée par rapport au référentiel du laboratoire. Dans le référentiel de l'onde, l'atome est alors soumis à une force d'inertie d'entraînement constante. Ce problème est analogue à celui d'électrons plongés dans un potentiel périodique (induit par un cristal) et soumis à une force constante (provoquée par un champ électrique constant). Dans un réseau cristallin idéal, les électrons oscillent sur place sans changer de bande d'énergie (soit τ_B la période des oscillations de Bloch). Une comparaison très détaillée de ces trois points de vue réalisée à partir d'une expérience d'atomes froids de césium est présentée dans l'article [*Pei97*]. Ce travail, fait dans notre laboratoire par l'équipe de C.Salomon, est le point de départ de notre expérience.

Pour faire ces passages adiabatiques rapides, il faut que la profondeur du potentiel lumineux induit par les faisceaux lasers d'accélération reste petite devant l'énergie de recul mais suffisamment grande pour pouvoir accélérer, pendant τ_B, tous les atomes sélectionnés. Du point vue des oscillations de Bloch, la première condition correspond à des électrons faiblement liés au

réseau et l'autre à un taux de transition inter-bandes par période de Bloch le plus faible possible.

L'accélération des atomes peut se faire selon l'axe de la pesanteur ou perpendiculairement. C'est la géométrie horizontale, expérimentalement plus simple, qui a été utilisée dans cette expérience préliminaire.

La distribution de vitesse des atomes est ensuite sondée par transition Raman sélective en vitesse entre les deux sous niveaux hyperfins de l'état fondamental.

2.2.2 Dispositif expérimental

Notre expérience utilise les techniques maintenant classiques des expériences d'atomes refroidis par lasers. Le lecteur trouvera dans la thèse de Rémy Battesti [*Bat03*] tous les détails de cette expérience. Le système laser de refroidissement est réalisé à l'aide de diodes lasers en cavité étendue (DLCE) injectant des diodes esclaves puissantes. Les diodes DLCE sont asservies en fréquence sur les transitions utilisées pour le piégeage du rubidium. Des modulateurs acousto-optiques permettent d'ajuster la fréquence des diodes lasers par rapport à celles des transitions de piégeage. Ces modulateurs servent aussi à contrôler la puissance des faisceaux lasers vue par les atomes.

Les faisceaux Raman sont générés par deux diodes DLCE asservies en phase à environ 6,8 GHz l'une de l'autre. La fréquence de cette micro-onde est accordable. En changeant cette fréquence, on règle l'écart à résonance des transitions Raman (δ voir figure 2.2), sondant ainsi la distribution de vitesse. Les diodes lasers sont ensuite amplifiées dans des amplificateurs à semi-conducteur (MOPA).

Un laser TiSa standard à notre équipe (voir la partie 1.2.4) est utilisé pour faire les oscillations de Bloch.

Ce laser et une des diodes Raman sont asservis en fréquence sur un pic d'un interféromètre de Fabry-Perot en zérodur, d'intervalle spectral libre connu. Ainsi la fréquence des ondes Raman et celle des ondes Bloch sont connues avec une incertitude relative meilleure que 10^{-8}.

Tous les faisceaux lasers sont dirigés vers l'enceinte ultra-vide contenant le rubidium via des fibres optiques polarisantes ou à maintien de polarisation. Cette enceinte nous a été prêtée par l'institut national de métrologie (BNM-INM). Elle a été utilisée pour réaliser un laser étalon asservi sur les transitions 5S-5D d'atomes de rubidium refroidis par lasers [*Fre97*]. Bien qu'elle ne soit

pas adaptée à notre expérience, elle nous a permis de réaliser une expérience préliminaire. Les atomes sont capturés et refroidis dans un piège magnéto-optique situé dans la partie haute de l'enceinte. La température du nuage atomique est mesurée par la technique de temps de vol. Une croix ultra-vide placée en dessous de l'enceinte sert de zone de détection. Deux nappes lumineuses permettent de détecter les populations des sous niveaux hyperfins. Cette détection est inspirée par celle des fontaines atomiques des étalons primaires de temps développés au BNM-SYRTE [*Cla95*].

L'expérience se déroule selon une séquence temporelle pilotée par ordinateur. Cette séquence comprend une phase d'accélération-décélération. Sans cette phase, le nombre d'oscillations de Bloch serait limité à 5, après quoi les atomes tomberaient à côté de la croix ultra-vide. Le nombre d'oscillations de Bloch est optimisé pour que le rapport signal à bruit des signaux détectés reste correct. La séquence temporelle se décompose donc de la manière suivante.

- *préparation des atomes froids*

Les atomes sont capturés dans un piège magnéto-optique et refroidis au mieux par une phase de mélasse optique. On dispose alors d'atomes froids ^{87}Rb dans l'état $5S_{1/2}(F = 2)$. La largeur de la distribution de vitesse (Δv) est alors de 3 à 4 v_r.

- *accélération des atomes*

Cette séquence décale le centre de la distribution de vitesse de $2 \times \mathrm{N} \times v_r^{Bloch}$ où v_r^{Bloch} désigne la vitesse de recul induite par le laser TiSa.

- *sélection d'une classe de vitesse*

Une transition Raman amène une partie des atomes dans l'état $F = 1$. La distribution de vitesse de ces atomes (typiquement $\Delta v = v_r/30$) est décalée de $2v_r^{Raman}$. Un faisceau laser vient ensuite pousser les atomes restant dans $F = 2$.

- *décélération de cette classe de vitesse*

Les atomes ($F = 1$) sont ensuite décélérés par N oscillations de Bloch.

- *détection par temps de vol.*

Une nouvelle impulsion Raman sélective en vitesse, de fréquence variable, ramène les atomes dans l'état $F = 2$. La population des deux sous-niveaux hyperfins est mesurée dans la zone de détection.

Pour s'affranchir de certains effets systématiques (par exemple la non horizontalité des faisceaux Bloch et Raman [*Bat03*]), l'expérience est répétée en accélérant puis décélérant les atomes en sens inverse.

L'écart entre les deux signaux donnent une mesure de h/M_{Rb}.

2.2.3 Résultats

Notre expérience préliminaire en géométrie horizontale

La mesure différentielle de h/M_{Rb} a été répétée 42 fois. En Mars 2003,la valeur moyenne pondérée de ces mesures donne une première mesure de h/M_{Rb} avec une incertitude relative de $4{,}2\times10^{-7}$ [*Bat04*][1], ce qui est très encourageant. Cependant la valeur absolue de h/M_{Rb} est décalée de 6×10^{-7} par rapport à la valeur la plus probable déterminée par le Codata 98 [*Moh00*]. Rappelons qu'il s'agit d'une expérience préliminaire. Cette expérience a mis en évidence la très grande efficacité (η) des oscillations de Bloch comme processus pour accélérer les atomes (η=99,5%). Cela signifie qu'un grand nombre d'oscillations de Bloch peuvent être réalisées sans perdre trop d'atomes, ce qui est très prometteur pour le futur de l'expérience.

Comparaison avec l'expérience de S.Chu

L'expérience de S.Chu, à Stanford se fait avec l'atome de césium, en utilisant un interféromètre atomique pour déterminer la vitesse de recul de l'atome de césium et donc h/M$_{Cs}$. Commencée en 1991, cette expérience a donnée récemment un très bon résultat [*Wit01*, *Wit02*]. Notre expérience est similaire puisque elle a pour but de déterminer h/M$_{Rb}$ à partir de la mesure de la vitesse de recul. Quelques différences sont à noter.

La largeur des franges d'interférences est de 8 Hz. Dans notre cas, la classe de vitesse sélectionnée a pour largeur environ 600 Hz, celle-ci étant limitée par le faible nombre initial d'atomes dans notre expérience. Rappelons que cette mesure préliminaire est faite avec une cellule ultra-vide qui n'est pas adaptée à cette expérience.

L'efficacité du taux de transfert d'une oscillation de Bloch est de 99,5%. Par contre elle vaut 94% pour les transitions adiabatiques résonnantes utilisées dans l'expérience de Stanford, limitant le recul à 120 transferts d'impulsion au maximum. Bien sûr, en disposant de plus d'atomes froids, il est possible d'augmenter le nombre de transferts.

[1] R. Battesti et al., Phys. Rev. Lett. 92, 253001-1 (2004) *article joint à la fin du manuscrit.*

2.3 Conclusion

En géométrie horizontale, le nombre oscillations de Bloch est limité par le temps de chute libre des atomes dans les faisceaux lasers. Ce n'est plus le cas en géométrie verticale. Nous étudions maintenant cette géométrie toujours à l'aide la cellule du BNM-INM, tout en préparant une nouvelle cellule à atomes froids. Dans cette géométrie, le nombre d'oscillations de Bloch est passé à 80. Comme précédemment, l'expérience se fait en accélérant les atomes "vers le haut ou vers le bas" ce qui permet de "s'affranchir" de la mesure de $\overrightarrow{g}$ pour déterminer h/M_{Rb}. L'expérience de compensation de la gravité par des oscillations de Bloch a aussi été réalisée.

Le but du travail actuel est non seulement de chercher à réduire l'incertitude sur cette mesure mais surtout de trouver le ou les effets qui décalent systématiquement la mesure. On peut s'affranchir de certains effets systématiques en inversant le sens des faisceaux Raman utilisés pour sélectionner et mesurer la vitesse des atomes. La différence entre les expériences de sélection-mesure dans un sens puis dans l'autre permet de "réduire" l'influence de certains effets systématiques (gradient de champ magnétique...). Actuellement, nous cherchons à contrôler en temps mais aussi en fréquence la coupure des oscillations de Bloch pour projeter de manière adiabatique les atomes dans un seul et même état d'impulsion.

Enfin, nous avons étudié la contribution non négligeable des vibrations du montage au bruit observé sur les distributions de vitesse. Le déménagement de l'expérience au rez de chaussée de l'université a déjà amélioré la situation. Une table anti-vibrations active devrait rajouter une isolation supplémentaire des vibrations. Les premiers essais avec cette table devraient être faits d'ici peu.

Une nouvelle cellule en titane a été réalisée en 2004. Elle est en cours d'installation. Elle constituera la zone de mesure de $\mathrm{h/M}_{Rb}$. Elle sera alimentée par un jet issu d'un piège magnéto-optique à 2 dimensions. Le blindage en μ-métal entourant la cellule d'expérience permettra de réduire les fluctuations de champ magnétique dans la cellule. Cet ensemble devrait conduire à une mesure de $\mathrm{h/M}_{Rb}$ avec une incertitude relative de quelques 10^{-8}.

Chapitre 3

Perspectives

Mon travail de recherche a commencé par la spectroscopie haute résolution de l'atome d'hydrogène. Il évolue maintenant vers la métrologie des constantes fondamentales d'un point de vue expérimental via la mesure de la constante de structure fine à l'aide du rapport h/M et d'un point de vue plus général par l'intermédiaire de ma participation au Codata.

Nos expériences et celles de T.W.Hänsch ont permis d'améliorer la connaissance de la constante de Rydberg de plus d'un facteur 20. La compétition intense entre nos deux groupes a permis l'apparition de nouveaux dispositifs de mesures de fréquences optiques (le laser étalon stabilisé sur une transition à deux photons du rubidium, le peigne de fréquence optique généré par laser femtoseconde...)

Parallèlement, des calculs d'électrodynamique quantique développés indépendamment ont convergé vers des valeurs identiques validant ainsi les résultats obtenus.

Pour affiner la comparaison théorie-expérience, il faut, de nos jours, déterminer très précisément la valeur du rayon de la distribution de charge du proton. Dans le cadre d'une collaboration internationale, une étude spectroscopique de l'hydrogène muonique a été entreprise. Les deux périodes passées sur l'accélérateur de l'institut Paul Scherrer n'ont pas permis de mettre en évidence la résonance atomique recherchée. L'arrivée récente de nouveaux membres dans la collaboration devrait permettre de résoudre les derniers problèmes techniques et financiers.

A ce jour, les expériences sur jet d'hydrogène sont très proches de leurs limites. Une amélioration possible du jet (2S) consisterait à augmenter notablement le nombre d'atomes métastables produits réduisant ainsi les effets

systématiques liés à la forte puissance lumineuse nécessaire au bon rapport signal à bruit des signaux détectés. Une méthode à base d'impulsions lumineuses et de passage adiabatique rapide [*Yat99*] a été proposée. Du point de vue laser, elle n'est cependant pas simple à mettre en oeuvre.

Par ailleurs, une nouvelle voie de spectroscopie d'atomes d'hydrogène refroidis est en cours d'exploration dans le groupe de D.Kleppner [*Kle04*].

Comme pour l'hydrogène muonique, on peut aussi essayer de contourner le problème en jouant sur les facteurs d'échelle que sont la masse du noyau ou sa charge pour un système hydrogénoïde. La possibilité d'une spectroscopie d'états circulaires d'atomes hydrogénoïdes est en cours d'étude théorique dans notre laboratoire [*Ind05*]. Enfin, l'ion He^+ suscite l'intérêt de nombreuses équipes pour déterminer en autres la constante de Rydberg (voir [*Rot05*] et les références citées).

Parallèlement à la spectroscopie haute résolution de l'atome d'hydrogène, nous avons développé une nouvelle expérience à base d'atomes froids pour déterminer le rapport h/M. La mesure de ce rapport permet de déterminer la constante de structure fine indépendamment de l'électrodynamique quantique. Les premiers résultats obtenus avec une enceinte à vide préliminaire sont très encourageants. Actuellement, l'étude des effets systématiques se poursuit tout en préparant une nouvelle enceinte à vide. Ceci devrait conduire à une mesure de h/M avec une incertitude relative de quelques 10^{-8}. Comme toujours en métrologie, c'est seulement à partir des résultats de cette nouvelle expérience, qu'il sera alors possible de savoir s'il est possible ou non de diminuer encore l'incertitude relative de la mesure de h/M.

Annexe : spectroscopie d'autres systèmes atomiques et moléculaires

Note : tous ces travaux de recherche ont été faits avant l'apparition des peignes de fréquences optiques générés par les lasers femtoseconde.

A1 Spectroscopie de l'hélium

A1.1 Motivation de l'expérience

Cette expérience est décrite dans l'article [*Dor96*][1]. La structure des niveaux d'énergie de l'hélium présente quelques analogies avec celle de l'hydrogène, le facteur d'échelle étant encore la constante de Rydberg. Les calculs de corrections d'électrodynamique quantique à plusieurs électrons sont plus compliqués et donc moins précis que ceux de l'hydrogène [*Dra93*]. Les données extraites des comparaisons expérience-théorie sont les déplacements de Lamb. La spectroscopie de l'hélium à partir du niveau fondamental est d'un point de vue laser très difficile (1S-2S à deux photons (λ=120 nm) [*Ber98*], 1S-2P à un photon (λ=58 nm) [*Eik96*]). A partir du niveau métastable $2^3\mathrm{S}_1$, les longueurs des transitions à deux photons tombent dans la domaine visible ou proche infra-rouge. La mesure du déplacement de Lamb du niveau $2^3\mathrm{S}_1$ de l'hélium à partir de la fréquence absolue des transitions $2^3S_1 - n^3D$ en utilisant la valeur théorique du déplacement n^3D est une façon de faire relativement simple.

Le but premier de cette expérience sur la transition $2^3\mathrm{S}_1$-$3^3\mathrm{D}_1$ était de

[1] C. Dorrer et al., Phys. Rev. Lett. 78, 3658 (1996) *article joint à la fin du manuscrit.*

tester la source atomique d'hélium pour effectuer par la suite, au BNM-INM, une mesure absolue de fréquence sur la transition 2^3S_1-4^3D à partir de celle du laser HeNe/I_2, les deux fréquences étant relativement proches (rappelons que la technique de peigne de fréquence optique n'était pas encore répandue).

A1.2 Résultats

Cette expérience très simple à mettre en oeuvre, a donné une mesure de la fréquence de la transition 2^3S_1-3^3D_1 avec une incertitude de $7{,}1\times10^{-11}$ avec pour la première fois à notre connaissance l'utilisation de l'atome d'hydrogène comme référence optique. Elle est en très bon accord avec la valeur précédente [*Gia82*] en utilisant l'écart de structure fine 3^3D_1-3^3D_3 donné dans [*Dra93*, *Dra96*].

La valeur du déplacement de Lamb du niveau 2^3S_1 ($L(2^3S_1)$ déduite de cette mesure est environ 100 fois plus précise que la valeur théorique et en très bon accord avec celle faite dans le groupe de M.Ingusio à Florence [*Pav94*].

Enfin la comparaison expérience-théorie du déplacement de Lamb du niveau n^3P ou du niveau n^3D à partir de cette mesure de $L(2^3S_1)$ et des fréquences mesurées des transitions $2\ ^3S_1$-n^3P ou $2\ ^3S_1$-n^3D) est présentée dans l'article [*Dor96*]. L'accord entre théorie et expérience est correct. Quelques mesures plus précises d'autres transitions $2\ ^3S_1$-n^3D permettraient d'affiner cette comparaison. Ceci est envisagé dans le groupe de Florence, à l'aide d'un peigne de fréquence optique [*CaP04*].

Du point de vue théorique, la possibilité de déterminer la constante de structure fine à partir de la mesure de la structure fine du niveau 2^3P [*Geo01*] a stimulée de nombreux calculs. Cependant des progrès importants doivent être faits car l'incertitude théorique est encore beaucoup trop grande pour que la comparaison avec l'expérience donne un résultat significatif sûr pour α (voir [*Moh02*] et les références citées).

A2 Recherche de références optiques dans le proche infrarouge

A2.1 Spectroscopie de la molécule IBr

Ce sujet a constitué mon premier travail de recherche. Le but de l'expérience à plus long terme était la réalisation d'un laser étalon dans la gamme

de longueur d'onde 750 nm à 780 nm proche des transitions 2S-nS/nD (n=8, 10, 12) dans l'hydrogène.

La molécule d'iode qui possède des raies dans cette région, est aussi un candidat à la réalisation d'un tel laser étalon. Cependant, pour observer ces raies il faut, pour avoir une pression d'iode suffisante, chauffer fortement la cellule afin d'avoir un signal d'absorption conséquent. Il nous a semblé intéressant d'étudier la molécule IBr. J'ai participé à la recherche et à l'enregistrement des signaux. Cette expérience a été faite avec le laser à colorant [*Bir82*] précédant le laser TiSa. La température du queusot est voisine de $0°C$ tandis que la cellule est chauffée à $100°C$. Dans ce cas l'absorption est d'environ 1,4% [*Bir92*].

Une analyse détaillée faite pendant mon service militaire, avec l'aide de J.Vigué, a permis de déterminer pour la première fois les 4 constantes de structure hyperfine de l'état excité $^3\Pi_1$(A') de cette molécule [*Bir92*]. La cellule est maintenant utilisée dans le groupe de D.Stacey. Elle sert de référence de fréquence pour l'expérience de violation de parité [*Sta04*].

A2.2 Spectroscopie à deux photons de l'atome de rubidium

La première étude a été faite en un mois à la fin de ma thèse. En contrepartie du prêt de la diode Schottky, il a fallu trouver un laser étalon de fréquence pour l'expérience de Florence sur la transition 2 $^3S_1$-3 ^3P de l'hélium [*Pav94*]. La première mesure en fréquence de la transition 5S-5D du rubidium a été réalisée à l'aide de la chaîne de fréquence utilisée en 1993 sur l'hydrogène [*Nez93c*][2]. Les résultats très encourageants de cette mesure ont conduit à la réalisation d'un laser étalon utilisé par exemple pour la spectroscopie de l'iode à 532 nm [*Hal99*] ou pour réaliser des lasers étalons dans le domaine de longueurs d'onde Telecom [*Ber00*] et bien sûr pour la spectroscopie de l'hydrogène [*Bea97*] [*Sch99*]. La radiation 5S-5D du rubidium est aussi recommandée pour la nouvelle mise en pratique de la définition du mètre [*Qui97*]. Enfin une application industrielle est réalisée avec cette transition. Une diode laser à 1,55 μm stabilisée sur cette transition est vendue par la société "DiCOS technologies". Ces diodes stables en fréquence sont utilisées pour synchroniser un réseau d'antennes millimétriques qui doit être construit à l'observatoire de radio-astronomie du Chili [*Cli04*].

[2]F. Nez et al., Opt. Commun. 102, 432 (1993) *article joint à la fin du manuscrit.*

La fréquence de notre laser étalon [*Bea96*] a été mesurée grâce à la chaîne de fréquence réalisée au LPTF [*Tou96*] [*Tou97*] sans le déplacer grâce à deux fibres optiques (L=3 km) reliant notre laboratoire au LPTF [*Bea98*]. La fréquence de notre laser asservi sur la transition $5S_{1/2}$(F=3)-$5D_{5/2}$(F=5) est connue avec une incertitude relative de 3×10^{-12}. Par la suite ce dispositif a été utilisé pour toutes les mesures ou calibrations de fréquences faites dans notre groupe [*Bea97*][3] [*Sch99*][4] [*Dor96*][5][*Hag99*] [*Bat04*][6].

A2.3 : Spectroscopie à deux photons de l'atome de césium

Dans l'atome de césium, il existe une transition à deux photons similaire à celle du rubidium. Là encore une petite expérience a été montée pour tester les qualités métrologiques de la transition 6S-8S pour réaliser un étalon de fréquence pour l'étude de la transition 1S-3S. Le montage est strictement identique à celui du rubidium. A l'aide du Fabry-Perot FPR, la fréquence des transitions 6S-8S (F=3, F=4) a été mesurée avec une incertitude relative de 3×10^{-10} ce qui est 70 fois plus précis que la mesure précédente. L'écart de fréquence entre les deux transitions est 4158,06(2) MHz, là encore en bon accord avec la mesure précédente (10 fois moins précise). En utilisant cette mesure et celle bien connue de la structure hyperfine de l'état fondamental 6S, une valeur du dipôle magnétique peut être extraite. Cette valeur, en très bon accord avec la mesure précédente, diffère légèrement des prédictions théoriques. Cependant, comme la largeur de raie est plus grande que celle du rubidium, un laser étalon asservi sur cette transition aurait des performances métrologiques un peu moins bonnes [*Hag99*].

[3]B. de Beauvoir et al., Phys. Rev. Lett. 78, 440 (1997) *article joint à la fin du manuscrit.*

[4]C. Schwob et al., Phys. Rev. Lett. 82, 4960 (1999) *article joint à la fin du manuscrit.*

[5]C. Dorrer et al., Phys. Rev. Lett. 78, 3658 (1996) *article joint à la fin du manuscrit.*

[6]R. Battesti et al., Phys. Rev. Lett. 92, 253001-1 (2004) *article joint à la fin du manuscrit.*

Bibliographie

[*Abe93*] M. Abed, thèse de doctorat de l'université Paris XI (1993).

[*Ace92*] O. Acef et al., Opt. Commun. 97, 29 (1992).

[*Ace94a*] O. Acef et al., Opt. Commun. 109, 428 (1994).

[*Ace94b*] O. Acef et al., Opt. Lett. 19, 1275 (1994).

[*Ace99*] O. Acef et al., IEEE Trans. Instr. Meas. 48, 567 (1999).

[*Ami00*] W. Amir, rapport de stage DEA Modélisation et Instrumentation en physique, 2000.

[*And92*] T. Andreae et al., Phys. Rev. Lett. 69, 1923 (1992).

[*Ant04*] A. Antognini et al, en cours de rédaction (2004).

[*Bat03*] R. Battesti, thèse de doctorat de l'université P. et M. Curie (2003).

[*Bat04*] R. Battesti et al., Phys. Rev. Lett. 92, 253001-1 (2004).

[*Bea96*] B. de Beauvoir, thèse de doctorat de l'université P. et M. Curie (1996).

[*Bea97*] B. de Beauvoir et al., Phys. Rev. Lett. 78, 440 (1997).

[*Bea98*] B. de Beauvoir et al., Eur. Phys. J. D 1, 227 (1998).

[*Bea00*] B. de Beauvoir et al., Eur. Phys. J. D 12, 61 (2000).

[*Ber95*] D.J. Berkeland, et al., Phys. Rev. Lett. 75, 2470 (1995).

[*Ber98*] S.D. Bergeson, et al., Phys. Rev. Lett. 80, 3475 (1998).

[*Ber00*] J.E. Bernard et al., Opt. Commun. 173, 357 (2000).

[*Bir82*] F. Biraben et al., Opt. Commun. 41, 49 (1982).

[*Bir90*] F. Biraben et al, Rev. Sci. Instrum. 61, 1468 (1990).

[*Bir91*] F. Biraben et al, Europhys. Lett. 15, 831 (1991).

[*Bir92*] F. Biraben et al., Opt. Commun. 92, 135 (1992).

[*Bor74*] F. Borkowski et al, Nucl. Phys. A 222, 269 (1974).

[*Bor75*] F. Borkowski et al, Nucl. Phys. B 93, 461 (1975).

[*Bor89*] C. Bordé, Phys. Lett. A 140, 10 (1989).

[*Bou93*] S. Bourzeix et al., Opt. Commun. 99, 89 (1993).

[*Bou95*] S. Bourzeix, thèse de doctorat de l'université P. et M. Curie (1995).

[*Bou96*] S. Bourzeix et al., Phys. Rev. Lett. 76, 384 (1996).

[*Bou97*] S. Bourzeix et al., Opt. Commun. 133, 239 (1997).

[*Bum61*] F.A. Bumiller et al, Phys. Rev. 124, 1623 (1961).

[*Cag73*] B. Cagnac, et al., J. Phys. (Paris) 34, 845 (1973).

[*CaP04*] P. Cancio Pastor et al., Phys. Rev. Lett. 92, 023001 (2004).

[*Cla95*] A. Clairon et al, IEEE trans. Instrum. Meas. 44, 128 (1995).

[*Cli04*] J. F. Cliche et al., CPEM 2004 digest (2004).

[*Dor96*] C. Dorrer et al., Phys. Rev. Lett. 78, 3658 (1997).

[*Dra93*] G.W.F. Drake, "Long Range Casimir Forces : Theory and Recent Experiments on Atomic Systems", edited by F.S. Levin and D.A. Micha (Plenum, New York, 1993).

[*Dra96*] , "Atomic, Molecular & Optical Physics Handbook", edited by G. W. F. Drake, (AIP, New York, 1996).

[*Dre83*] R.W.P. Drever et al, Appl. Phys. B31, 97 (1983).

[*Dru83*] R.E. Drullinger et al, Appl. Phys. Lett. 42, 137 (1983).

[*Eik96*] K.S.E. Eikema et al, Phys. Rev. Lett. 76, 1216 (1996).

[*Eri77*] G.W. Erickson, J. Phys. Chem. Ref. Data 6, 831 (1977).

[*Fee93*] M.S. Fee et al, Phys. Rev. A 48, 192 (1993).

[*Fre97*] E. Fretel, thèse de doctorat de Conservatoire National des Arts et Métiers (1997).

[*Gar89*] J.C. Garreau, thèse de doctorat de l'université P. et M. Curie (1989).

[*Ger78*] S. Gerstenkorn et P. Luc, "Atlas du spectre d'absorption de la molécule de l'iode entre 14000-15600cm^{-1}" Ed. CNRS, Paris (1978).

[*Geo01*] M.C. Georges et al, Phys. Rev. Lett. 87, 173002 (2001).

[*Gia82*] E. Giacobino et al, J. Phys. B 15, 385 (1982).

[*Gro89*] M.Gross et al, *The Hydrogen Atom* Springer, Berlin 134 (1989).

[*Hag99*] G. Hagel et al, Opt. Commun. 160, 1 (1999).

[*Hag01*] G. Hagel, thèse de doctorat de l'université P. et M. Curie (2001).

[*Hag02a*] G. Hagel et al, App. Opt. 41, 7702 (2002).

[*Hag02b*] G. Hagel et al, Phys. Rev. Lett. 89, 203001 (2002).

[*Hal76*] J.L. Hall et al, Phys. Rev. Lett. 37, 1339 (1976).

[*Hal99*] J.L. Hall et al, IEEE Trans. Inst. Meas. 44, 151 (1995).

[*Han63*] N. Hand et al, Rev. Mod. Phys. 35, 335 (1963) .

[*Hän75*] T.W. Hänsch et al, Phys. Rev. Lett. 34, 307 (1975).

[*Hän79*] T.W. Hänsch et al, Scientific American 240, 94 (1979).

[*Hän80*] T.W. Hänsch et B. Couillaud, Opt. Commun. 35, 441 (1980).

[*Her64*] D. Herriot et al, Appl. Opt. 3, 523 (1964).

[*Hou96*] M. Houssin, thèse de doctorat de l'université Paris 6 (1989).

[*Ind05*] P. Indelicato, communication privée.

[*Jan66*] T. Janssens et al, Phys. Rev. 142, 922 (1966).

[*Jen86*] D.E. Jennings et al, App. Opt. 25, 284 (1986).

[*Kar96*] S.G.Karsemboïm, J. Phys. B. 29, L29 (1996).

[*Kas91a*] M. Kasevich et al, Phys. Rev. Lett. 66, 2297 (1991).

[*Kas91b*] M. Kasevich et al, Phys. Rev. Lett. 67, 181 (1991).

[*Kat76*] Y. Kato et al, J. Opt. Soc. Am. 66, 490 (1976).

[*Kaz00*] S. Kazamias-Moucan, rapport de stage DEA physique quantique, 2000.

[*Kle00*] D. Kleppner et al, RLE progress Report n°142 Section 10.

[*Kle04*] D. Kleppner hydroIII brazil (à compléter).

[*Kot99*] F. Kottmann et al, PSI proposal (1999).

[*Kot02*] F. Kottmann et al, Proc. of EXA02 159 (2002).

[*LeB93*] C. Le Blanc, Annales de Physique 19, 1 (1994).

[*LeB04*] E.O. Lebigot, communication privée.

[*Lud04*] L. Ludhova et al, Nucl. Inst. Meth. A (2004).

[*Lun81*] S.R. Lundeen et F.M. Pipkin, Phys. Rev. Lett. 46, 232 (1981).

[*Maa94*] F.E. Maas et al, Phys. Lett. A 187, 247 (1994).

[*Moh00*] P. Mohr et B.N. Taylor, Rev. Mod. Phys. 72, 351 (2000).

[*Moh02*] P. Mohr et B.N. Taylor,Rev. Mod. Phys. 77, 1 (2005).

[*Mil94*] Y. Millerioux et al., Opt. Commun. 108, 91 (1994).

[*Nez92*] F. Nez et al., Phys. Rev. Lett. 69, 2326 (1992).

[*Nez93a*] F. Nez et al., Europhys. Lett. 24, 635 (1993).

[*Nez93b*] F. Nez, thèse de doctorat de l'université P. et M. Curie (1993).

[*Nez93c*] F. Nez et al., Opt. Commun. 102, 432 (1993).

[*Nie00*] M. Niering et al., Phys. Rev. Lett. 84, 5496 (2000).

[*Pal85*] V.G. Pal'chikov et al, Metrologia 21, 99 (1985).

[*Pas01*] P.C. Pastor et al, *The Hydrogen Atom : Precision Physics of Simple Atomic Systems* Springer, Berlin 314 (2001).

[*Pav94*] F.S. Pavone et al, Phys. Rev. Lett. 73, 42 (1994).

[*Pei97*] E. Peik et al, Phys. Rev. A, 55, 2989 (1997).

[*Pet01*] A. Peters et al, Metrologia 38, 25 (2001).

[*Poh00*] R. Pohl et al, Hyp. Int. 127, 161 (2001).

[*Poh05*] R. Pohl et al, J. Can. Phys. xxx, xxx (2005).

[*Pot98*] R. Poth, J. of Mol. Spect. 190, 379 (1998).

[*Qui97*] T.J. Quinn, Metrologia 36, 211 (1999).

[*Rab86*] P. Rabinowitz et al, IEEE Q.E. 22, 797 (1986).

[*Rei00*] J. Reichert et al., Phys. Rev. Lett. 84, 3232 (2000).

[*Rot05*] B. Roth et al., Phys. Rev. Lett. 04, 053001-1 (2005).

[*Sap90*] J.R. Sapirstein et D.R. Yennie, *Quantum Electrodynamics* World Publ. Co., Singapore(1990).

[*Sch99*] C. Schwob et al., Phys. Rev. Lett. 82, 4960 (1999).

[*ScK93*] F. Schmidt-Kaler, et al., Phys.Rev. Lett. 70, 2261 (1993).

[*Sic03*] I. Sick, Phys. Lett. B 576, 62 (2003).

[*Sim80*] G.G. Simon et al, Nucl. Phys. A 333, 381 (1980).

[*Sim81*] G.G. Simon et al, Nucl. Phys. A 364, 285 (1981).

[*Sta04*] D.N. Stacey commnuication ***(voir avec Lucile)***

[*Tou96*] D. Touahri, thèse de doctorat de l'université Paris XI (1996).

[*Tou97*] D. Touahri et al., Opt. Commun. 133, 471 (1997).

[*Ude97*] T. Udem et al., Phys. Rev. Lett. 79, 2646 (1997).

[*Ude99*] T. Udem, et al., Phys. Rev. Lett. 82, 3568 (1999).

[*Vas70*] L.S. Vasilenko, et al., JETP Lett. 12, 113 (1970).

[*Wei93*] D.S. Weiss et al, Phys. Rev. Lett. 70, 2706 (1993).

[*Wei92*] M. Weitz, et al., Phys. Rev. Lett. 68, 1120 (1992).

[*Wit01*] A. Witch, et al., Proceedings of 6^{th} Symposiusm Frequency Standards and Metrology, Ed. P.Gill, 193 (2001).

[*Wit02*] A. Witch, et al., Physica Scripta T102, 82 (2002).

[*Yat99*] L.P. Yatsenko et al, Phys. Rev. A, 60, R4237 (1999).

Articles joints

On trouvera dans les articles joints des détails supplémentaires concernant nos expériences de spectroscopie de l'atome d'hydrogène, l'expérience de mesure de h/M_{Rb} et nos expériences de spectroscopie de grande précision sur d'autres systèmes atomiques et moléculaires.

- F. Nez et al., Phys. Rev. Lett. 69, 2326 (1992).
- F. Nez et al., Europhys. Lett. 24, 635 (1993).
- F. Nez et al., Opt. Commun. 102, 432 (1993).
- S. Bourzeix et al., Phys. Rev. Lett. 76, 384 (1996).
- B. de Beauvoir et al., Phys. Rev. Lett. 78, 440 (1997).
- C. Dorrer et al., Phys. Rev. Lett. 78, 3658 (1997).
- C. Schwob et al., Phys. Rev. Lett. 82, 4960 (1999).
- B. de Beauvoir et al., Eur. Phys. J. D 12, 61 (2000).
- G. Hagel et al, Phys. Rev. Lett. 89, 203001 (2002).
- R. Battesti et al., Phys. Rev. Lett. 92, 253001-1 (2004).
- R. Pohl et al, J. Can. Phys. xxx, xxx (2005).

Precise Frequency Measurement of the $2S$-$8S/8D$ Transitions in Atomic Hydrogen: New Determination of the Rydberg Constant

F. Nez, M. D. Plimmer, S. Bourzeix, L. Julien, and F. Biraben
Laboratoire de Spectroscopie Hertzienne de l'Ecole Normale Supérieure, Université Pierre et Marie Curie, Tour 12 E01, 4 place Jussieu, 75252 Paris CEDEX 05, France

R. Felder
Bureau International des Poids et Mesures, Pavillon de Breteuil, 92312 Sèvres CEDEX, France

O. Acef, J. J. Zondy, P. Laurent,[a] A. Clairon, and M. Abed
Laboratoire Primaire des Temps et des Fréquences, Bureau National de Métrologie-Observatoire de Paris, 61 avenue de l'Observatoire, 75014 Paris, France

Y. Millerioux and P. Juncar
Institut National de Métrologie-Bureau National de Métrologie, 292 rue St. Martin, 75141 Paris CEDEX 03, France
(Received 5 August 1992)

We have measured the Rydberg constant by frequency comparison of the three transitions $2S_{1/2}$-$8S_{1/2}$, $2S_{1/2}$-$8D_{3/2}$, and $2S_{1/2}$-$8D_{5/2}$ in hydrogen with the difference of two optical standards, the methane-stabilized He-Ne laser and the iodine-stabilized He-Ne laser. The frequency of the iodine-stabilized He-Ne laser has been remeasured. The new value for the Rydberg constant, $R_\infty = 109\,737.315\,683\,0(31)\ \mathrm{cm}^{-1}$, is currently the most precise available.

PACS numbers: 06.20.Jr, 06.20.Hq, 31.30.Jv

The Rydberg constant R_∞ is important in many areas of physics and chemistry. During the last twenty years, the precise techniques of Doppler-free laser spectroscopy have been applied to atomic hydrogen and the uncertainty in R_∞ has been reduced drastically [1]. Yet there are several reasons to improve this precision even further. R_∞ is the natural energy scale of atomic physics. It plays a key role in the least-squares adjustment of the physical fundamental constants [2]. A very precise value of R_∞ is required to test quantum electrodynamics (QED) calculations on simple systems, for example, to determine the Lamb shift of the hydrogen $1S$ state [3,4]. Finally, the comparison of two Rydberg measurements deduced from different transitions in hydrogen provides a severe test of the $1/r$ dependence of the Coulomb potential [5]. From another point of view, this $1/r$ dependence can be supposed exact: As hydrogen has transitions with frequencies ranging from the microwave region (transition between circular Rydberg states [6]) to the visible, the hydrogen atom can be used to check the frequency chains connecting these two frequency domains [7,8].

Until very recently, the most precise Rydberg constant value was given by the 1988 measurement performed by our group in Paris on the $2S_{1/2}$-$nD_{5/2}$ two-photon transitions ($n=8,10,12$) in hydrogen and deuterium [9]. This measurement was based on an interferometric comparison between the excitation laser and the iodine-stabilized He-Ne laser (He-Ne/I_2) at 633 nm. The precision was limited by the uncertainty in the frequency of the He-Ne/I_2 laser (1.6×10^{-10}) which had been measured at the National Bureau of Standards (NBS) in 1983 [10]. Our precision relative to the standard was 4.3×10^{-11}.

The present experiment is based on a new determination of the He-Ne/I_2 standard frequency made at the Laboratoire Primaire des Temps et des Fréquences (LPTF) and on a frequency comparison between this standard and the $2S$-$8S$ and $2S$-$8D$ hydrogen transitions that we have performed at the Laboratoire de Spectroscopie Hertzienne (LSH). In this latest work, the frequency chain between the cesium clock and the frequencies of the $2S$-$8S/8D$ transitions is almost continuous and the interferometric method is only used to measure a small frequency splitting (88 GHz). Our measurement is the most precise to date with an uncertainty of 2.9 parts in 10^{11}.

The frequency chain of LPTF connects the He-Ne/I_2 laser at 473 THz to a standard at 29 THz which is a CO_2 laser stabilized on an OsO_4 line. The frequency of the latter had been measured previously with an uncertainty of 2.7×10^{-12} [11]. The details of this frequency chain will be published later. The frequency ν_f of the f hyperfine component of a He-Ne/I_2 laser of the Institut National de Métrologie (labeled INM12) has been measured:

$$\nu_f = 473\,612\,353\,586.0(3.4)\ \mathrm{kHz}.$$

We note that this value is 133 kHz redshifted with respect to the NBS value used in our previous measurement. In 1988 we compared our standard laser with the same INM12 laser. For this reason, we can now take into account the new value of the standard frequency to correct and improve our 1988 results. From frequency comparisons with other standard lasers, we can estimate the frequency stability of the INM12 laser, over the

1988–1992 period, to be better than 7 kHz. The corrected value of the 1988 Rydberg constant is thus $R_\infty = 109737.315681(5)\ \mathrm{cm}^{-1}$ with an uncertainty of 4.6×10^{-11}.

The frequency measurement of the $2S$-$8S/8D$ lines of hydrogen made at LSH involves two standard lasers, the He-Ne/I_2 laser and the methane-stabilized He-Ne laser (He-Ne/CH_4) at 88 THz ($\lambda = 3.39\ \mu$m). This frequency comparison takes advantage of the near coincidence (88 GHz) of the $2S$-$8S/8D$ frequency with the frequency difference between these two standards. The infrared He-Ne/CH_4 standard laser is the Bureau International des Poids et Mesures (BIPM) one labeled VB-BIPM. Its frequency is known with an uncertainty of 1 kHz [12]. The frequency of the He-Ne/I_2 standard used at LSH has been measured with respect to the INM12 laser. Taking into account the uncertainties due to this comparison and to possible frequency shifts of the lasers, we estimate the total uncertainty in the frequency of the LSH standard to be 7 kHz.

The scheme for the frequency comparison between the standard lasers and the $2S$-$8S/8D$ hydrogen frequencies is outlined in Fig. 1. We use two homemade Ti-sapphire lasers at 385 THz ($\lambda = 778$ nm), one (TiS1) for the excitation of the atomic transition and another one (TiS2) for the sum-frequency generation. For this sum frequency, we need a second, more powerful (20 mW output), He-Ne source at 3.39 μm and we detect the beat frequency $f_B(3.39)$ between this laser and the He-Ne/CH_4 standard. Its radiation is mixed with the output (about 1 W) of the TiS2 laser at 778 nm in a $LiIO_3$ crystal to obtain about 250 nW at 633 nm. This generated beam is heterodyned with that of our standard laser at 633 nm to provide the beat frequency $f_B(633)$. The residual frequency difference between the two Ti-sapphire lasers (88 GHz) is measured with a high-finesse, 50-cm-long, Fabry-Pérot reference cavity (FPR). This cavity is locked to the d hyperfine component of the He-Ne/I_2 laser and provides a frequency reference for the TiS1 laser. Since the FPR cavity remains locked to the iodine line d, we can calculate its length and hence—taking into account dispersive phase shifts—its free spectral range ν_0. The TiS1 laser is frequency shifted with respect to a peak of FPR using an acousto-optic modulator (AOM) [13]. In a first step we record the hydrogen resonance and we deduce the position of the $2S$-$8S/8D$ lines with respect to the FPR. In a second step, the TiS1 frequency is decreased by 295 times the free spectral range ν_0 of the FPR so that it lies close to the TiS2 frequency. Next we measure simultaneously the beat frequencies $f_B(633)$, $f_B(3.39)$, and $f_B(778)$ (between the two Ti-sapphire lasers) and we obtain the frequency of the TiS1 laser. Taking into account the frequency offset $295\nu_0$ we can derive the frequencies of the hydrogen lines.

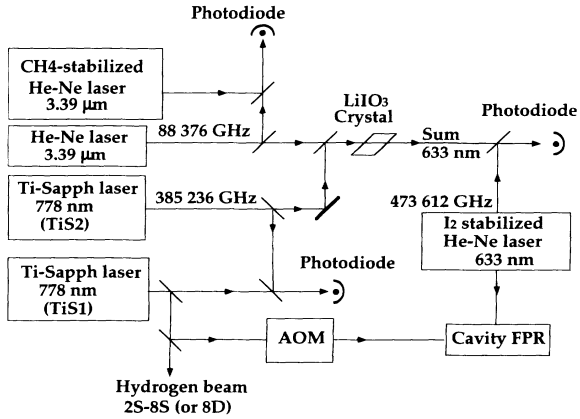

FIG. 1. Experimental setup for the frequency comparison between the $2S$-$8S/8D$ transition and the standard lasers.

The principle of the hydrogen experiment is the same as in our previous work [9,14]. In order to observe very narrow signals, with negligible collisional and transit time broadening, the two-photon transitions are induced in a metastable atomic beam collinear with two counterpropagating laser beams. The number of metastable atoms beyond the interaction region is measured via the Lyman-α fluorescence induced by a quenching electric field. As the excited nS or nD states decay preferentially to the $1S$ ground state, the optical excitation can be detected via the corresponding decrease of the $2S$ beam intensity. Since our last measurement, we have improved several parts of the apparatus in order to increase our signal-to-noise ratio and to reduce the observed linewidths. The metastable beam has been shortened from 96 to 56 cm to reduce the saturation of the signal due to the depletion of the metastable atoms along the laser beam. The dye laser has been replaced by a titanium-sapphire laser which gives both a higher power and a smaller frequency jitter: Inside the enhancement cavity surrounding the atomic beam the optical power can be as much as 100 W in each direction. The mirrors of this cavity have been changed to increase the waist of the laser beam from 600 to 860 μm and consequently to reduce the light shift. The analysis of the experimental data follows the same procedure as in 1988 [13]. Several effects shift the atomic signal.

(i) *Light shift* is the major source of the frequency shift. A detailed analysis of the recorded spectra is performed; calculated profiles are fitted to the experimental ones for different laser intensities and the light shift corrected line positions are deduced.

(ii) *The second-order Doppler effect* is evaluated from the velocity distribution of the metastable atoms. This distribution is measured by monitoring the Doppler-broadened $2S$-$6P$ transition at 410 nm with a collinear, frequency-doubled, Ti-sapphire laser beam. The measured mean square velocity is 3100(70) m/s and the second-order Doppler shift is -41 kHz.

(iii) *The Stark effect* due to stray electric fields is es-

TABLE I. Experimental determination of the $2S_{1/2}$-$8S/8D$ transition frequencies and of the Rydberg constant.

	$2S_{1/2}$-$8S_{1/2}$	$2S_{1/2}$-$8D_{3/2}$	$2S_{1/2}$-$8D_{5/2}$
Resonance frequency (MHz)	385 324 653.142	385 324 729.985	385 324 758.579
Resonance frequency × 2	770 649 306.284	770 649 459.971	770 649 517.159
$2S_{1/2}$ hyperfine splitting (MHz)	44.389	44.389	44.389
$8S/8D$ hyperfine splitting (MHz)	−0.694	0.028	−0.028
Second-order Doppler effect (MHz)	0.041	0.041	0.041
Stark effect (MHz)	−0.005	0.002	0.003
$2S_{1/2}$-$8S/8D$ experimental value of the energy splitting (MHz)	770 649 350.015	770 649 504.431	770 649 561.564
$R_\infty - 109\,737$ (cm^{-1})	0.315 684 2(47)	0.315 682 4(37)	0.315 683 0(32)

timated from the observation of the $2S$-$15D$ transition: From the linewidth we deduce a value of 8 mV/cm for the residual electric field, corresponding to a shift of about −3 kHz for the $8D_{5/2}$ level and 5 kHz for the $8S_{1/2}$.

We have studied the three $2S_{1/2}(F=1)$-$8S_{1/2}$, $2S_{1/2}(F=1)$-$8D_{3/2}$, and $2S_{1/2}(F=1)$-$8D_{5/2}$ two-photon transitions. For each transition the measured frequency is corrected for the second-order Doppler effect, for the Stark effect, and for the hyperfine structure of the metastable and excited states. Table I gives the details of the calculation of the Rydberg constant. We have used the experimental value of the hydrogen $2S$ Lamb shift [15] [1057.851(2) MHz] to deduce the $2P_{1/2}$-$8S/8D$ frequencies. Taking into account another less precise measurement of the $2S$ Lamb shift [16], we have adopted a 9-kHz uncertainty for this quantity. The $2P_{1/2}$-$8S/8D$ frequencies are compared to the ones calculated by Erickson [17] after correction for the 1986 recommended values of the fine structure constant and the proton/electron mass ratio [2], using the Rydberg constant as a scaling factor. By this procedure, the extraction of a value for the Rydberg constant relies on a knowledge of the Lamb shifts of the $2P_{1/2}$ and $8S/8D$ levels. Following Erickson the theoretical values of these corrections are $L_{2P_{1/2}} = -12.834(3)$ MHz, $L_{8S_{1/2}} = 16.506(2)$ MHz, $L_{8D_{3/2}} = -0.058(3)$ MHz, and $L_{8D_{5/2}} = 0.074(3)$ MHz. The total uncertainty given by this procedure (about 10 kHz) is the quadratic sum of the theoretical QED uncertainties for the $2P$ and $8S/8D$ terms (3 kHz for each term) with the experimental uncertainty for the $2S$ Lamb shift (9 kHz). The three Rydberg constant values deduced are quite self-consistent. The weighted mean value is $R_\infty = 109\,737.315\,683\,0(31)$ cm^{-1} with an uncertainty of 2.9×10^{-11} (1 standard deviation). The contributions to this uncertainty are listed in Table II. In Fig. 2, our results are compared with the other continuous-wave measurements made since 1986. Our new result agrees very well with our 1988 value (corrected with the new frequency value of the standard) and with the recent result of the group of Hänsch obtained from the $1S$-$2S$ transition [20]. Taking into account the disagreement (3.1 parts in 10^9) between the CODATA value [2] and the recent values, we see that the precision on the Rydberg has been improved by a factor of 100 since 1986.

The recent measurement of the $1S$-$2S$ frequency [20] and our results on the $2S$-$8S/8D$ transitions are precise

TABLE II. Uncertainty budget (parts in 10^{11}, 1 standard deviation).

Lamb shift and QED calculations	1.3
Electron-to proton mass ratio	1.1
Statistical uncertainty	0.9
Fits by theoretical profiles	0.5
Frequency of the He-Ne/I_2 laser	1.8
Methane-stabilized He-Ne laser	0.3
88-GHz measurement	0.8
Second-order Doppler effect	0.4
Stark effect	0.3
Global uncertainty	2.9

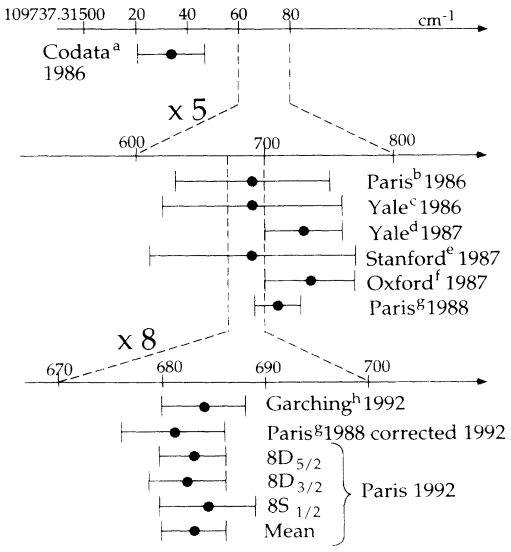

FIG. 2. Comparison of our result with recent high-precision measurements of the Rydberg constant: *a*, Ref. [2]; *b*, Ref. [18]; *c*, Ref. [19]; *d*, Ref. [8]; *e*, Ref. [3]; *f*, Ref. [4]; *g*, Ref. [9]; and *h*, Ref. [20].

enough to provide a new determination of the $1S$ Lamb shift. The result is 8172.804(83) MHz, in very good agreement with the recent result of Weitz, Schmidt-Kaler, and Hänsch [8172.82(11) MHz] [21]. From our results we can also deduce the interval $8S_{1/2}$-$8D_{5/2}$ [211.549(26) MHz] and an experimental value [16.517(26) MHz] of the $8S_{1/2}$ Lamb shift in agreement with theory (16.506 MHz).

In conclusion, we have performed a measurement of the Rydberg with an uncertainty of 2.9 parts in 10^{11}. This precision is now close to the limitations imposed by the measurements of the $2S$ Lamb shift and the electron/proton mass ratio. In the future, the comparison of different hydrogen optical frequencies will provide new measurements of the Lamb shift and it will be possible to achieve a precision of the order of 10^{12} on R_∞. To this end, a better determination of the electron/proton mass ratio is highly desirable.

The authors are indebted to B. Cagnac for many stimulating discussions during this experiment. They also thank T. W. Hänsch for fruitful advice. This work is partially supported by the Bureau National de Métrologie and by the Direction des Recherches et Etudes Techniques. Laboratoire de Spectroscopie Hertzienne de l'Ecole Normale Supérieure is a Laboratoire associé au CNRS URA 18.

[a]Permanent address: Lasers Ultra Stables-Etablissement Technique Central de l'Armement, Fort de Montrouge, 94114 Arcueil, CEDEX, France.

[1] See, for example, D. H. McIntyre and T. W. Hänsch, Metrologia **25**, 61 (1988); L. Julien, F. Biraben, and M. Allegrini, Comments At. Mol. Phys. **26**, 219 (1991).

[2] E. R. Cohen and B. N. Taylor, Rev. Mod. Phys. **59**, 1121 (1987).

[3] R. G. Beausoleil *et al.*, Phys. Rev. A **35**, 4878 (1987); **39**, 4591 (1989).

[4] M. G. Boschier *et al.*, Nature (London) **330**, 463 (1987); Phys. Rev. A **40**, 6169 (1989).

[5] D. F. Barlett and S. Lögl, Phys. Rev. Lett. **61**, 2285 (1988).

[6] R. G. Hulet and D. Kleppner, Phys. Rev. Lett. **51**, 1430 (1983); J. Liang, M. Gross, P. Goy, and S. Haroche, Phys. Rev. A **33**, 4437 (1986).

[7] L. Julien, F. Biraben, and B. Cagnac, Bulletin du Bureau National de Métrologie **66**, 31 (1986).

[8] P. Zhao, W. Lichten, H. P. Layer, and J. C. Bergquist, Phys. Rev. Lett. **58**, 1293 (1987); Phys. Rev. A **39**, 2888 (1989).

[9] F. Biraben, J. C. Garreau, L. Julien, and M. Allegrini, Phys. Rev. Lett. **62**, 621 (1989).

[10] D. A. Jennings *et al.*, Opt. Lett. **11**, 136 (1983).

[11] A. Clairon *et al.*, IEEE Trans. Instrum. Meas. **34**, 265 (1985); Metrologia **25**, 9 (1988).

[12] The frequency of this laser has been compared, via an intermediate standard laser, to a methane-stabilized standard laser (labeled M101) which has been measured with a frequency chain at the VNIISTRI in Moscow.

[13] J. C. Garreau, M. Allegrini, L. Julien, and F. Biraben, J. Phys. (Paris) **51**, 2263 (1990); **51**, 2275 (1990); **51**, 2293 (1990).

[14] F. Biraben, J. C. Garreau, L. Julien, and M. Allegrini, Rev. Sci. Instrum. **61**, 1468 (1990).

[15] V. G. Pal'chikov, Yu. L. Sokolov, and V. P. Yakovlev, Metrologia **21**, 99 (1985).

[16] S. R. Lundeen and F. M. Pipkin, Phys. Rev. Lett. **46**, 232 (1981).

[17] G. W. Erickson, J. Phys. Chem. Ref. Data **6**, 831 (1977).

[18] F. Biraben, J. C. Garreau, and L. Julien, Europhys. Lett. **2**, 925 (1986).

[19] P. Zhao, W. Lichten, H. P. Layer, and J. C. Bergquist, Phys. Rev. A **34**, 5138 (1986).

[20] T. Andreae *et al.*, Phys. Rev. Lett. **69**, 1923 (1992).

[21] M. Weitz, F. Schmidt-Kaler, and T. W. Hänsch, Phys. Rev. Lett. **68**, 1120 (1992). To be consistent with these authors we have used the value of Ref. [17] for the $2S$ Lamb shift to calculate the $1S$ Lamb shift.

EUROPHYSICS LETTERS 10 December 1993

Europhys. Lett., 24 (8), pp. 635-640 (1993)

First Pure Frequency Measurement of an Optical Transition in Atomic Hydrogen: Better Determination of the Rydberg Constant.

F. NEZ(*), M. D. PLIMMER(*), S. BOURZEIX(*), L. JULIEN(*)
F. BIRABEN(*), R. FELDER(**), Y. MILLERIOUX(***) and P. DE NATALE(*$_*$*)

(*) *Laboratoire de Spectroscopie Hertzienne de l'ENS*(§), *Université Pierre et Marie Curie*
4 place Jussieu, Tour 12 E01, 75252 Paris Cedex 05, France
(**) *Bureau International des Poids et Mesures*
Pavillon de Breteuil, 92312 Sèvres Cedex, France
(***) *Institut National de Métrologie-BNM*
292 rue St. Martin, 75141 Paris Cedex 03, France
(*$_*$*) *Laboratorio Europeo di Spettroscopie Non-Lineari*
Largo E. Fermi 2, Arcetri, I-50125 Firenze, Italia

(received 2 August 1993; accepted 21 October 1993)

PACS. 06.20J - Determination of fundamental constants.
PACS. 06.30F - Time and frequency measurement.
PACS. 12.20F - Experimental tests of quantum electrodynamics.

Abstract. - We have performed a pure frequency measurement of the $2S$-$8S/D$ two-photon transition in atomic hydrogen. The hydrogen frequencies are compared with the difference of two optical standards, the methane-stabilized He-Ne laser and the iodine-stabilized He-Ne laser. In this way, an optical frequency of atomic hydrogen is directly linked for the first time to the caesium clock without any interferometry. We deduce a new value for the Rydberg constant, $R_\infty = 109\,737.315\,683\,4(24)\,\mathrm{cm}^{-1}$ with an uncertainty of 2.2 parts in 10^{11}. This value is currently the most precise available.

Introduction. - The spectroscopy of atomic hydrogen is very important for the measurement of fundamental constants and as a test of quantum electrodynamics (QED). In the last decade, Doppler-free two-photon spectroscopy has been applied to the $1S$-$2S$ and $2S$-nS/D transitions of hydrogen and the resolution has been greatly increased [1]: the observed relative linewidths are now 2 parts in 10^{11} for the $1S$-$2S$ transition [2] and 2 parts in 10^{10} for the $2S$-$12S$ transition [3]. To take advantage of these improvements, interferometric measurements are no longer adequate and have to be replaced by accurate optical-frequency measurements. This kind of measurement needs frequency-multiplication chains which link the measured frequency to the caesium clock. In this paper we present the first pure frequency measurement of an optical frequency of atomic hydrogen, without any interferometry. We have built a frequency chain which connects, through two auxiliary standard lasers (namely the iodine-stabilized and the methane-stabilized He-Ne lasers), the frequencies of the $2S$-$8S/D$ two-photon transitions to the caesium clock. Our result for the $2S_{1/2}$-$8D_{5/2}$ frequency interval is $\nu(2S_{1/2}\text{-}8D_{5/2}) = 770\,649\,561\,571(12)$ kHz. This result, with a relative uncertainty of 1.6 parts in 10^{11}, is the most precise to date for an optical frequency of hydrogen.

This measurement provides a new value of the Rydberg constant, $R_\infty =$

(§) Laboratoire associé au CNRS URA 18.

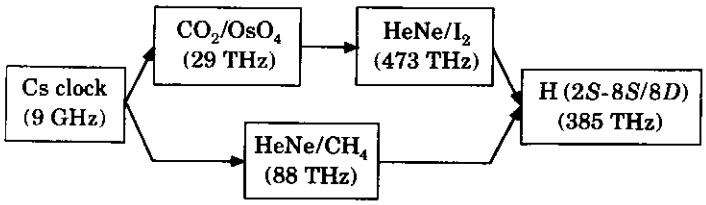

Fig. 1. – Outline of the frequency chain between the $2S$-$8S/D$ hydrogen frequencies and the caesium clock.

$= 109\,737.315\,6834(24)\ \mathrm{cm}^{-1}$. The Rydberg constant R_∞ is important in many areas of physics: the Rydberg constant is the natural energy scale of atomic physics, it plays a key role in the least-squares adjustment of the physical fundamental constants [4] and a very precise value of R_∞ is required to test QED calculations on simple systems. This new value of R_∞, with a relative uncertainty of 2.2 parts in 10^{11}, is currently the most precise available. This measurement, after the measurement of the electron g-factor, is the most accurate measurement of any fundamental constant.

Frequency measurements. – The principle of our frequency mesurement is the near coincidence (89 GHz) between the $2S$-$8S/D$ frequencies $\nu(2S\text{-}8S/D)$ and the frequency difference between two standard lasers, the iodine-stabilized and the methane-stabilized helium-neon lasers (frequencies ν_f and $\nu(CH_4)$, respectively):

$$\nu(2S\text{-}8S/D) \approx \nu_f - \nu(CH_4).$$

The frequency chain between the caesium clock and the hydrogen frequencies is outlined in fig. 1. It involves three intermediate standard lasers. The methane-stabilized He-Ne laser ($He\text{-}Ne/CH_4$) is the laser VB-BIPM from the Bureau International des Poids et Mesures (BIPM). Its frequency is known with an uncertainty of 1 kHz: $\nu(CH)_4 = 88\,376\,181\,602.6(1.0)$ kHz. The iodine-stabilized He-Ne laser ($He\text{-}Ne/I_2$) is the laser INM12 from the Institut National de Métrologie (INM). The frequency ν_f of the f hyperfine component of the (127)R11-5 iodine line has been measured in 1992 in the Laboratoire Primaire des Temps et des Fréquences (LPTF) [5]. This last measurement uses a frequency chain connecting the $He\text{-}Ne/I_2$ laser at 473 THz to a standard at 29 THz which is a CO_2 laser stabilized to an OsO_4 line. This last standard laser had been previously compared to the caesium clock [6]. The measured frequency for the laser INM12 is $\nu_f = 473\,612\,353\,586.9(3.4)$ kHz.

Figure 2 shows the experimental set-up. In addition to the two standard lasers, we use two titanium-shappire lasers and an auxiliary He-Ne laser at 3.39 μm. The first titanium-sapphire laser (labelled TiS1) is used to observe the two-photon transition in hydrogen. As the power of the $He\text{-}Ne/CH_4$ laser is only 100 μW, a second He-Ne laser at 3.39 μm, more powerful (about 15 mW), is frequency-locked to the $He\text{-}Ne/CH_4$ standard laser. The second titanium-shappire laser and this auxiliary He-Ne laser are mixed in a $LiIO_3$ crystal in order to generate a visible beam at 633 nm. This synthesized beam is heterodyned with that of the standard laser INM12 at 633 nm. In preliminary work, the frequency difference (about 89 GHz) between the two titanium-shappire lasers has been measured with a Fabry-Perot interferometer [7]. In the present work, we have used a Schottky diode [8]. The electrical contact is made with a tungsten whisker. The two titanium-sapphire laser beams (about 30 mW) are mode-matched and focused on the Schottky diode and the diode is simultaneously irradiated with a microwave source which is a Gunn diode at 88.6 GHz (about 20 mW). The low-frequency beat note is detected with 40 dB signal-to-noise ratio in a resolution bandwidth of 30 kHz.

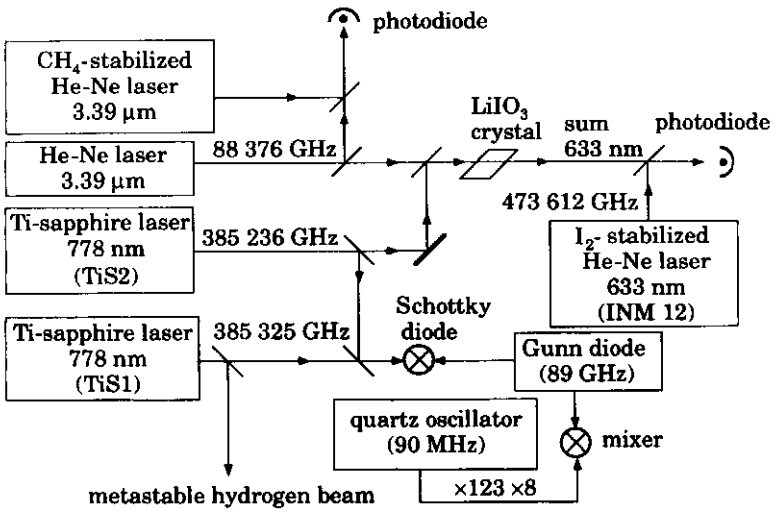

Fig. 2. – Experimental set-up for the frequency comparison between the $2S$-$8S/8D$ transition and the standard lasers.

The frequency measurements require counting and phase-locking techniques. The Gunn diode is phase-locked to the 984th harmonic of a low-phase noise quartz oscillator at 90 MHz. The frequency of this oscillator was measured during the experiment with a high-stability frequency counter (HP-5345A) which was checked before and after the data acquisition with a caesium clock. We estimate the final uncertainty on the Gunn diode frequency to be about 30 Hz. In the case of the beat note between the two He-Ne lasers at 3.39 μm, the signal-to-noise ratio is sufficient to count directly the beat frequency. In the other cases (that is to say the beat given by the Schottky diode and the beat between the synthesized beam at 633 nm and the INM12 laser), the signal-to-noise ratio is too small and we use tracking oscillators phase-locked to these beat signals. Finally, during the data acquisition of the hydrogen signals, we count simultaneously the three beat frequencies and we can deduce the frequency of the laser TiS1 from the frequencies of the two standard lasers. In this way, the frequency chain between the $2S$-$8S/D$ hydrogen frequencies and the two standard lasers is completed and these hydrogen frequencies are linked to the caesium clock.

The hydrogen experiment. – The principle of our hydrogen experiment has been described elsewhere [7, 9, 10]. The two-photon transitions are induced in a metastable atomic beam collinear with two counterpropagating laser beams. In this way, we reduce the broadening due to the collisions and due to the finite transit time of the atoms through the laser beams. At the end of the atomic beam we apply an electric field to quench the metastable atoms and we detect the Lyman-α fluorescence to measure the metastable yield. As the excited nS or nD states decay preferentially to the $1S$ ground state in a proportion of 95%, the optical excitation can be detected via the corresponding decrease of the $2S$ beam intensity. The metastable atomic beam is surrounded by an enhancement cavity; inside the cavity the optical power can be as much as 100 W in each direction with a beam waist of 650 μm. The recent improvements to our hydrogen experiment have been described elsewhere [7]. Since 1988, our metastable beam has been shortened from 96 to 56 cm to reduce the saturation of the signal due to the depletion of the metastable atoms along the laser beam. The dye laser has been replaced by a home-made titanium-shappire laser which provides a larger power. This laser is frequency-locked to an external cavity using an FM sideband method and its frequency jitter is reduced to a level of 2 kHz [11].

TABLE I. – *Experimental determination of the* $2S_{1/2}$-$8S/8D$ *transition frequencies* (MHz).

	$2S_{1/2}$-$8S_{1/2}$	$2S_{1/2}$-$8D_{3/2}$	$2S_{1/2}$-$8D_{5/2}$
resonance frequency	385 324 653.1385	385 324 729.9868	385 324 758.5848
resonance frequency × 2	770 649 306.2771	770 649 459.9737	770 649 517.1697
corrections for:			
$2S_{1/2}$ hyperfine splitting	44.3892	44.3892	44.3892
$8S/8D$ hyperfine splitting	− 0.6936	0.0277	− 0.0277
second-order Doppler effect	0.0402	0.0402	0.0402
$\nu(2S_{1/2}\text{-}8S_{1/2}/8D_J)$	770 649 350.0129	770 649 504.4308	770 649 561.5714
$8S_{1/2}/8D_{3/2}$-$8D_{5/2}$ splitting	211.5575	57.1285	
$\nu(2S_{1/2}\text{-}8D_{5/2}) = 770\,649\,561$	0.5704(150)	0.5593(130)	0.5714(120)

The acquisition and analysis of the experimental data follow the same procedure as in ref. [10]. The experimental linewidths vary with the light power because of the inhomogeneous light shift experienced by the atoms due to the laser beams. Typically the linewidths (in terms of the atomic frequency) are 1.3 MHz and 500 kHz for the $2S$-$8D$ and $2S$-$8S$ two-photon transitions (the natural widths are 572 kHz and 144 kHz, respectively). We have to take into account several effects which shift the atomic signal:

i) The light shift is the major source of the frequency shift; with a 100 W light power in each direction the shift of the line is about 400 kHz (in terms of the atomic frequency). For this reason we record the atomic signal for different laser intensities and we extrapolate the line position to zero light power. More precisely, we have performed a theoretical analysis of the line profile which takes into account the light shift and the saturation of the two-photon transition [10]. For each recording, the calculated profiles are fitted to the experimental curves. Each fit gives both the experimental line centre (half-maximum centre) and the line position corrected for light shift. A careful study of these data is made *vs.* the light power in order to deduce the unperturbed position of the line.

ii) The second-order Doppler effect is evaluated from the velocity distribution of the metastable atoms. This distribution is measured by monitoring the Doppler-broadened $2S$-$6P$ transition at 410 nm with a collinear, frequency-doubled, titanium-sapphire laser beam. We estimate the second-order Doppler shift at − 40.2(2.0) kHz. This value is very similar to our previous determinations of the second-order Doppler shift of the $2S$-$8D$ transition in hydrogen (− 40 kHz in our measurement of 1988 [9] and − 41 kHz in 1992 [7]). This result indicates that the velocity distribution of our atomic beam is very reproducible.

iii) The Stark effect due to stray electric fields is estimated from the linewidth of $2S$-$15D$ transition. In our preliminary work of 1992, this linewidth was about 1.23 MHz and we deduce a value of 8 mV/cm for the residual electric field. We have renewed since the graphite coating of our vacuum apparatus which was two years old and the linewidth of the $2S$-$15D$ transition has been reduced to about 530 kHz. Taking into account the other broadening effects, we can estimate that the stray electric fields are smaller than 3 mV/cm, corresponding to a shift of about − 400 Hz for the $8D_{5/2}$ level and 700 Hz for the $8S_{1/2}$. We have neglected these corrections in the analysis of the data.

Results. – We have studied the three $2S_{1/2}(F = 1)$-$8S_{1/2}$, $2S_{1/2}(F = 1)$-$8D_{3/2}$, and $2S_{1/2}(F = 1)$-$8D_{5/2}$ two-photon transitions. For each transition we have recorded the atomic signal for about twenty different light powers. The measured frequencies are corrected for the second-order Doppler effect and for the hyperfine structure of the metastable and excited

TABLE II. – *Uncertainty budget (parts in 10^{11}, one standard deviation).*

Lamb shift and QED calculations	1.3
electron-to-proton mass ratio	1.1
statistical uncertainty	0.7
fits to theoretical profiles	0.5
frequency of the He-Ne/I_2 laser	0.9
methane-stabilized He-Ne laser	0.3
second-order Doppler effect	0.3
Stark effect	0.2
total uncertainty	2.2

states. Table I gives the details of these corrections. The three experimental values can be intercompared by taking into account the theoretical value of the fine structure and of the QED corrections in the $n = 8$ levels. Following Erickson [12], the QED corrections of these levels are: $L_{8S_{1/2}} = 16.506(2)$ MHz, $L_{8D_{3/2}} = -0.058(3)$ MHz and $L_{8D_{5/2}} = 0.074(3)$ MHz. We can thus deduce three independent values of the $2S_{1/2}$-$8D_{5/2}$ interval (see table I). They are in very good agreement. The mean value is: $\nu(2S_{1/2}\text{-}8D_{5/2}) = 770\,649\,561\,567(10)$ kHz.

In order to deduce the Rydberg constant, we have used the experimental value of the hydrogen $2S$ Lamb shift [13] (1057.851(2) MHz). We have, however, adopted the more conservative error estimate of 9 kHz, which takes into account another less precise measurement of the $2S$ Lamb shift [14]. We thus deduce an experimental value for the $2P_{1/2}$-$8D_{5/2}$ frequency which we then compare to the one calculated by Erickson [12] after correction for the 1986 recommended values of the fine-structure constant and the proton/electron mass ratio [4], using the Rydberg constant as a scaling factor. The final result is $R_\infty = 109\,737.315\,6834(24)\,\mathrm{cm}^{-1}$ with an uncertainty of $2.2 \cdot 10^{-11}$ (one standard deviation). The contributions to this uncertainty are listed in table II. Our result is compared in table III with the other continuous wave measurements made since 1986. Our new result agrees very well with our preliminary result of 1992 [7] and with the recent result of the group of Hänsch obtained from the $1S$-$2S$ and $2S$-$4D$ transitions [2]. The slight disagreement with our previous work of 1988 [9] is due to the value of the frequency of the He-Ne/I_2 standard laser which was used to date [15]. With the new measurement of 1992 [5], this disagreement disappears. Taking into account the disagreement (3.1 parts in 10^9) between the CODATA value [4] and the recent values, we see that the precision on the Rydberg has been improved by a factor 140 since 1986. The recent measurement of the $1S$-$2S$ frequency [2]

TABLE III. – *Comparison with recent measurements of the Rydberg constant.*

Authors	Town	Transition	$(R_\infty - 109737)\,\mathrm{cm}^{-1}$
CODATA [4]			0.315 34(13)
Biraben *et al.* [16]	Paris	$2S$-$8D$ and $2S$-$10D$	0.315 69(6)
Zhao *et al.* [17]	Yale	$2S$-$3P$	0.315 69(7)
Zhao *et al.* [18]	Yale	$2S$-$4P$	0.315 73(3)
Beausoleil *et al.* [19]	Stanford	$1S$-$2S$	0.315 69(8)
Boshier *et al.* [20]	Oxford	$1S$-$2S$	0.315 735(35)
Biraben *et al.* [9]	Paris	$2S$-$8D/10D/12D$	0.315 709(18)
Andreae *et al.* [2]	Garching	$1S$-$2S$ and $2S$-$4D$	0.315 684 1(42)
Nez *et al.* [7]	Paris	$2S$-$8S/D$	0.315 683 0(31)
this work	Paris	$2S$-$8S/D$	0.315 683 4(24)

and our results on the $2S$-$8S/8D$ transition are precise enough to also provide a new determination of the $1S$ Lamb shift. The result is 8172.815(70) MHz, in very good agreement with the recent result of Hänsch (8172.820(110) MHz) [21].

In conclusion, we have performed the first measurement of an optical frequency in atomic hydrogen without any interferometry. This measurement provides a new value of the Rydberg constant which is the most precise available. In the near future, with new frequency chains, the relative uncertainty in frequency measurements in hydrogen could be reduced to 10^{-12}. For the determination of the Rydberg constant, the main limitations will be the measurements of the $2S$ Lamb shift and the electron/proton mass ratio, which are at the level of about one part in 10^{11}. Nevertheless, the comparison of different hydrogen optical frequencies and a better theoretical analysis of the QED corrections could give a precision of the order of 10^{-12} for the Rydberg constant for hydrogen R_H. To deduce R_∞ with the same precision, a better determination of the electron/proton mass ratio is needed.

* * *

The authors are indebted to B. CAGNAC for many stimulating discussions during this experiment. They also thank P. GOY for essential help in the phase-locking of the Gunn diode. We are also grateful to A. CLAIRON and his co-workers from the LPTF for stimulating discussions and expert technical assistance concerning the frequency measurement, and to D. N. STACEY for critical reading of the manuscript. This work is partially supported by the Bureau National de Métrologie, by the Direction des Recherches et Etudes Techniques and by the European Community in the frame of a SCIENCE cooperation contract no. SC1*-CT92-0816.

REFERENCES

[1] See, for example, MCINTYRE D. H. and HÄNSCH T. W., *Metrologia*, **25** (1988) 61; JULIEN L., BIRABEN F. and ALLEGRINI M., *Comments At. Mol. Phys.*, **26** (1991) 219.
[2] ANDREAE T. *et al.*, *Phys. Rev. Lett.*, **69** (1992) 1923.
[3] BIRABEN F., JULIEN L. and NEZ F., in *Laser Spectroscopy X*, edited by M. DUCLOY, E. GIACOBINO and G. CAMY (World Scientific) 1992, p. 104.
[4] COHEN E. R. and TAYLOR B. N., *Rev. Mod. Phys.*, **59** (1987) 1121.
[5] ACEF O. *et al.*, *Opt. Commun.*, **97** (1993) 29.
[6] CLAIRON A. *et al.*, *IEEE Trans. Instrum. Meas.*, **IM-34** (1985) 265; *Metrologia*, **25** (1988) 9.
[7] NEZ F. *et al.*, *Phys. Rev. Lett.*, **69** (1992) 2326.
[8] BERGQUIST J. C. and DANIEL H. U., *Opt. Commun.*, **48** (1984) 327.
[9] BIRABEN F., GARREAU J. C., JULIEN L. and ALLEGRINI M., *Phys. Rev. Lett.*, **62** (1989) 621.
[10] GARREAU J. C. *et al.*, *J. Phys. (Paris)*, **51** (1990) 2263, 2275, 2293.
[11] BOURZEIX S. *et al.*, *Opt. Commun.*, **99** (1993) 89.
[12] ERICKSON G. W., *J. Phys. Chem. Ref. Data*, **6** (1977) 831.
[13] PAL'CHIKOV V. G., SOKOLOV YU. L. and YAKOVLEV V. P., *Metrologia*, **21** (1985) 99.
[14] LUNDEEN S. R. and PIPKIN F. M., *Phys. Rev. Lett.*, **46** (1981) 232.
[15] JENNINGS D. A. *et al.*, *Opt. Lett.*, **11** (1983) 136.
[16] BIRABEN F., GARREAU J. C. and JULIEN L., *Europhys. Lett.*, **2** (1986) 925.
[17] ZHAO P., LICHTEN W., LAYER H. P. and BERGQUIST J. C., *Phys. Rev. A*, **34** (1986) 5138.
[18] ZHAO P., LICHTEN W., LAYER H. P. and BERGQUIST J. C., *Phys. Rev. Lett.*, **58** (1987) 1293; *Phys. Rev. A*, **39** (1989) 2888.
[19] BEAUSOLEIL R. G. *et al.*, *Phys. Rev. A*, **35** (1987) 4878; **39** (1989) 4591.
[20] BOSHIER M. G. *et al.*, *Nature*, **330** (1987) 463; *Phys. Rev. A*, **40** (1989) 6169.
[21] WEITZ M., SCHMIDT-KALER F. and HÄNSCH T. W., *Phys. Rev. Lett.*, **68** (1992) 1120. To be consistent with these authors we use the value of ref.[14] for the $2S$ Lamb shift to calculate the $1S$ Lamb shift.

Optics Communications 102 (1993) 432–438
North-Holland

OPTICS
COMMUNICATIONS

Optical frequency determination of the hyperfine components of the $5S_{1/2}$–$5D_{3/2}$ two-photon transitions in rubidium

F. Nez, F. Biraben

Laboratoire de Spectroscopie Hertzienne de l'ENS [1], *Université Pierre et Marie Curie, 4 place Jussieu, Tour 12 E01, 75252 Paris cedex 05, France*

R. Felder

Bureau International des Poids et Mesures (BIPM), Pavillon de Breteuil, 92312 Sèvres cedex, France

and

Y. Millerioux

Institut National de Métrologie (INM), 292 rue St Martin, 75141 Paris cedex 03, France

Received 28 May 1993

An absolute optical frequency measurement is made of the hyperfine components of the $5S_{1/2}$–$5D_{3/2}$ two-photon transitions in rubidium with an uncertainty of 1.3×10^{-11}. This is carried out in a simple way by taking advantage of the near coincidence between the two-photon frequency at $\lambda=778$ nm in Rb and the frequency difference of two HeNe lasers, stabilized respectively to an iodine line at $\lambda=633$ nm and a methane transition at $\lambda=3.39$ μm used as references. This measurement provides a new optical frequency reference in the visible range.

1. Introduction

The knowledge of certain optical frequencies is important for metrology, spectroscopy and the determination of the fundamental constants. Unfortunately, such a measurement requires a frequency multiplication chain linked to the Cs clock and it is a rather complicated experiment [1]. For this reason, it is useful to have at one's disposition in the visible range accurate secondary frequency standards. So far, the most widely studied of these has been the iodine stabilized HeNe laser at $\lambda=633$ nm ($HeNe/I_2$). Its frequency has been measured at the National Bureau of Standards (NBS) in 1983 with an uncertainty of 1.6×10^{-10} [2] and, very recently, in Paris, at the Laboratoire Primaire des Temps et des Fréquences (L.P.T.F.), with a precision better than one part in 10^{11} [3]. Using this latest result, we have made a measurement of the Rydberg constant which takes advantage of the near coincidence (88 GHz) of the 2S–8S/D two-photon hydrogen frequencies with the frequency difference of two optical standards, the $HeNe/I_2$ at $\lambda=633$ nm and the methane stabilized HeNe laser ($HeNe/CH_4$) at $\lambda=3.39$ μm. The residual 88 GHz discrepancy has been measured in a preliminary step with a Fabry–Pérot interferometer [4], and more recently, by direct frequency measurements via a Schottky diode [5].

In this paper we report a frequency measurement of the hyperfine components of the $5S_{1/2}$–$5D_{3/2}$ two-photon transitions in rubidium. This experiment is very similar to the hydrogen one [4,5]. The frequencies of the $5S_{1/2}$–$5D_{3/2}$ and $5S_{1/2}$–$5D_{5/2}$ transitions of rubidium ($\lambda=777.98$ nm and 777.89 nm, respectively) lie even closer to the frequency difference of the $HeNe/CH_4$ and I_2 reference lasers; indeed, these residual differences are only about 5 GHz

[1] Laboratoire associé au CNRS URA 18.

and 50 GHz for the $5S_{1/2}$–$5D_{3/2}$ and $5S_{1/2}$–$5D_{5/2}$ transitions, respectively.

2. The 5S–5D two-photon transition in rubidium

The Doppler-free two-photon method was first applied to the spectroscopy of the 5S–nD transitions in rubidium by Kato and Stoicheff in 1976; in a first experiment they studied the range $n=11$–32 by detecting the fluorescence [6], and in a second step up to $n=124$ with a thermoionic detector [7]. These transitions, whose wavelengths are in the range $\lambda=594$–660 nm, have also been used to study for instance two-photon Ramsey fringes [8] or Rydberg levels in crossed electric and magnetic fields [9]. By comparison, the 5S–5D transitions ($\lambda=778$ nm) are much more intense because the laser frequency is close to resonance with the strong $5S_{1/2}$–$5P_{1/2}$ and $5S_{1/2}$–$5P_{3/2}$ lines at $\lambda=795$ nm and 780 nm. For this reason, the 5S–5D transition has been used to observe two-photon optical bistability [10].

Our experimental set-up is basically the same as that described in ref. [6]. We use a fused silica, sealed cell containing natural rubidium (consisting of 73% ^{85}Rb and 27% ^{87}Rb) with Brewster window ends. The cold finger of the cell is maintained at about 90 °C, corresponding to a pressure of 8×10^{-5} Torr. We send into the cell a laser beam from a home made cw titanium–sapphire laser [11]. This beam is retroreflected by a concave miror of 10 m curvature radius. In the cell the beam cross section, πw^2, is about 10 mm^2 and the one-way laser power 100 mW. The two-photon transition is detected by monitoring the fluorescence at $\lambda=420$ nm due to the radiative cascade 5D–6P–5S. This fluorescence is collected with a $f/0.5$ aspheric lens system, selected with a filter (Schott SFK 6) and detected with a photomultiplier (RCA 1P 28). The terrestrial magnetic field is compensated by a system of three Helmoltz coils. The titanium–sapphire laser is locked to a first Fabry–Pérot cavity, labelled FP, in order to reduce its frequency jitter to the 2 kHz level; the long-term stability is assured by the use of a second Fabry–Pérot cavity which is stabilized to a HeNe/I_2 standard laser. A description of this system can be found in refs. [11,12].

Figures 1a and 1b display the observed spectra for

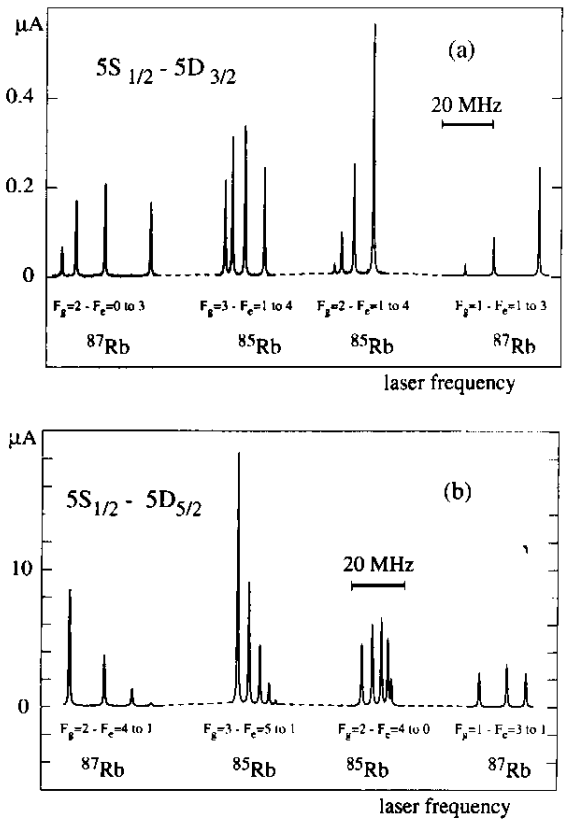

Fig. 1. Excitation spectra of the Doppler-free $5S_{1/2}$–$5D_{3/2}$ and $5S_{1/2}$–$5D_{5/2}$ two-photon transitions in rubidium (a) and (b), respectively). The vertical scale corresponds to the photomultiplier current with a voltage of 800 V.

the two fine structure transitions $5S_{1/2}$–$5D_{3/2}$ and $5S_{1/2}$–$5D_{5/2}$, respectively. For each spectrum, there are four groups of hyperfine components which correspond to the hyperfine structure of the $5S_{1/2}$ ground state of ^{85}Rb (nuclear spin $I=5/2$, total angular momentum $F_g=2$ and 3, $5S_{1/2}$ hyperfine structure: 3035.732 439 (5) MHz) and of ^{87}Rb (nuclear spin $I=3/2$, total angular momentum $F_g=1$ and 2, $5S_{1/2}$ hyperfine structure: 6834.682 614 (1) MHz) [13]. The structure of each group is due to the smaller hyperfine structure of the $5D_J$ states. In a two-photon transition between a $S_{1/2}$ and a D_J state, the two-photon transition operator is purely quadrupolar in nature [14] and the relative hyperfine line intensities are given by

$$(2F_g+1)(2F_e+1)\begin{Bmatrix} J & 2 & 1/2 \\ F_g & I & F_e \end{Bmatrix}^2/(2I+1)\,,$$

where F_e is the total angular momentum of the hyperfine excited state. These relative theoretical intensities are listed in tables 1 and 2 and are in very good agreement with the experimental ones. The $5S_{1/2}$–$5D_{5/2}$ transitions are found to be about twenty times stronger than the $5S_{1/2}$–$5D_{3/2}$ ones. This is due to the fact that, in the first case, the principal intermediate state involved in the calculation of the two-photon transition is the $5P_{3/2}$ state, which is only 35 cm^{-1} from resonance with the laser frequency, while, in the second case, this principal intermediate state is the $5P_{1/2}$ one which is 271 cm^{-1} from resonance. Using the oscillator strengths of the 5S–5P and 5P–5D transitions (1 and 3.44×10^{-3}, respectively) and the natural width of the 5D level (600 kHz) [15], we have calculated, for our experimental conditions ($\pi w^2=10$ mm^2 and $P=100$ mW), an excitation rate of 1.4 s^{-1} for the $5D_{3/2}$ state and 26 s^{-1} for the $5D_{5/2}$ state; these values are in good agreement with the observed intensity ratio.

Figure 2 shows the ^{87}Rb $5S_{1/2}(F_g=1)$–$5D_{3/2}$ ($F_e=3$) line with a low frequency excursion. Obviously, the signal to noise is very good (about 450). The observed linewidth, in terms of the laser frequency, is about 500 kHz, while the natural width is 300 kHz. This difference cannot be explained by the second order Doppler effect (about 6×10^{-13}, i.e. 225 Hz) nor by the finite transit time broadening (about 25 kHz for a beam waist of 1.8 mm). It is probably due to either imperfect mode matching of the two counterpropagating laser beams (this effect introduces a small first order Doppler effect) or to a residual magnetic field. Note however that neither of these two effects shifts the line provided that the atom velocity-distribution in the cell is isotropic and the polarisation of the laser beam linear.

3. Optical frequency measurement and reproducibility

In the case of the $5S_{1/2}$–$5D_{3/2}$ line, we have measured the absolute frequencies of each hyperfine component. We have employed the same method as in our hydrogen experiment [4]. Figure 3 shows the experimental set-up. The rubidium transitions are observed with a first-titanium sapphire laser labelled TiS1. The principle of the experiment is to compare the frequency of this TiS1 laser with the frequency difference between the HeNe/I_2 and HeNe/CH_4

Table 1
Frequencies of the hyperfine components of the $5S_{1/2}$–$5D_{3/2}$ transition in rubidium.

Hyperfine component	Relative intensity	Measured frequency
^{85}Rb		
$F_g=3\rightarrow F_e=1$	$7/60\approx11.7\%$	385 240 679 712.0 (5.0) kHz
$F_g=3\rightarrow F_e=2$	$1/6\approx16.7\%$	385 240 683 216.5 (5.0) kHz
$F_g=3\rightarrow F_e=3$	$7/40=17.5\%$	385 240 689 192.1 (5.0) kHz
$F_g=3\rightarrow F_e=4$	$1/8=12.5\%$	385 240 698 496.0 (5.0) kHz
$F_g=2\rightarrow F_e=1$	$1/120\approx0.8\%$	385 242 197 577.5 (5.0) kHz
$F_g=2\rightarrow F_e=2$	$1/24\approx4.2\%$	385 242 201 083.9 (5.0) kHz
$F_g=2\rightarrow F_e=3$	$7/60\approx11.7\%$	385 242 207 058.8 (5.0) kHz
$F_g=2\rightarrow F_e=4$	$1/4=25\%$	385 242 216 362.9 (5.0) kHz
^{87}Rb		
$F_g=2\rightarrow F_e=0$	$1/16\approx6.2\%$	385 240 094 977.7 (5.0) kHz
$F_g=2\rightarrow F_e=1$	$27/160\approx16.9\%$	385 240 101 727.6 (5.0) kHz
$F_g=2\rightarrow F_e=2$	$7/32\approx21.9\%$	385 240 115 692.6 (5.0) kHz
$F_g=2\rightarrow F_e=3$	$7/40=17.5\%$	385 240 137 803.8 (5.0) kHz
$F_g=1\rightarrow F_e=1$	$3/160\approx1.9\%$	385 243 519 070.2 (5.0) kHz
$F_g=1\rightarrow F_e=2$	$3/32\approx9.4\%$	385 243 533 031.8 (5.0) kHz
$F_g=1\rightarrow F_e=3$	$21/80\approx26.2\%$	385 243 555 144.5 (5.0) kHz

Table 2
Frequencies of the hyperfine components of the $5S_{1/2}$–$5D_{5/2}$ transition in rubidium.

Hyperfine component	Relative intensity	Measured frequency
^{85}Rb		
$F_g=3\rightarrow F_e=5$	$11/36\approx 30.6\%$	385 285 142 367.0 (8.0) kHz
$F_g=3\rightarrow F_e=4$	$1/6\approx 16.7\%$	385 285 147 084.9 (8.0) kHz
$F_g=3\rightarrow F_e=3$	$7/90\approx 7.8\%$	385 285 151 594.8 (8.0) kHz
$F_g=3\rightarrow F_e=2$	$1/36\approx 2.8\%$	385 285 155 397.6 (8.0) kHz
$F_g=3\rightarrow F_e=1$	$1/180\approx 0.6\%$	385 285 158 138.0 (13.0) kHz
$F_g=2\rightarrow F_e=4$	$1/12\approx 8.3\%$	385 286 664 961.9 (8.0) kHz
$F_g=2\rightarrow F_e=3$	$7/60\approx 11.7\%$	385 286 669 461.0 (8.0) kHz
$F_g=2\rightarrow F_e=2$	$1/9\approx 11.1\%$	385 286 673 254.3 (8.0) kHz
$F_g=2\rightarrow F_e=1$	$7/90\approx 7.8\%$	385 286 675 998 (10.0) kHz
$F_g=2\rightarrow F_e=0$	$1/36\approx 2.8\%$	385 286 677 451 (26.0) kHz
^{87}Rb		
$F_g=2\rightarrow F_e=4$	$3/8=37.5\%$	385 284 566 366.3 (8.0) kHz
$F_g=2\rightarrow F_e=3$	$7/40=17.5\%$	385 284 580 777.8 (8.0) kHz
$F_g=2\rightarrow F_e=2$	$1/16=6.25\%$	385 284 592 255.2 (8.0) kHz
$F_g=2\rightarrow F_e=1$	$1/80=1.25\%$	385 284 600 225.2 (8.0) kHz
$F_g=1\rightarrow F_e=3$	$7/60\approx 11.7\%$	385 287 998 122.2 (8.0) kHz
$F_g=1\rightarrow F_e=2$	$7/48\approx 14.6\%$	385 288 009 600.2 (8.0) kHz
$F_g=1\rightarrow F_e=1$	$9/80=11.25\%$	385 288 017 566.9 (8.0) kHz

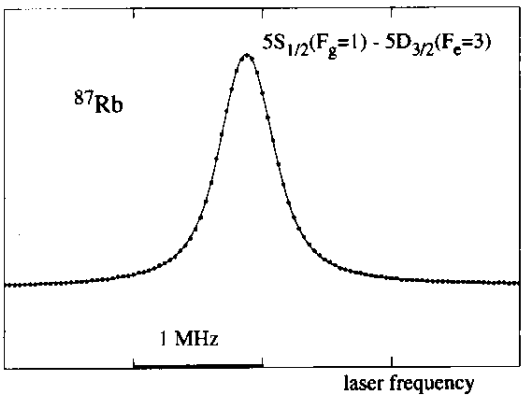

Fig. 2. Lineshape of the $5S_{1/2}$ ($F_g=1$)–$5D_{3/2}$ ($F_e=3$) hyperfine component in ^{87}Rb. The experimental points are fitted with a Voigt profile.

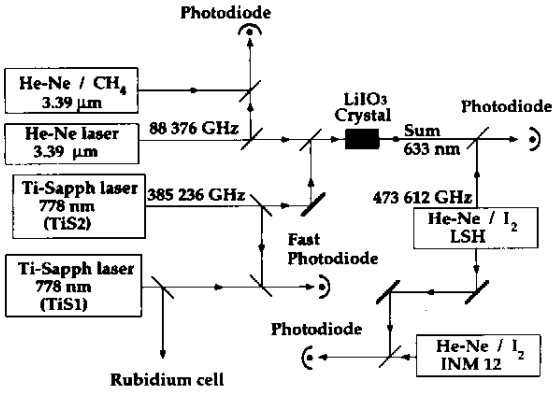

Fig. 3. Experimental set-up for the frequency comparison between the 5S–5D transitions in rubidium and the standard lasers.

standard lasers of respective frequency $\nu(I_2)$ and $\nu(CH_4)$. Our HeNe/I_2 reference laser, labelled INM12, has been measured recently at the LPTF with an uncertainty of 3.4 kHz [3]. The frequency of the R(127) 11–5 f hyperfine component is

$$\nu(I_2)=473\,612\,353\,586.9\ (3.4)\ \text{kHz}\ .$$

The HeNe/CH_4 standard belongs to the BIPM. Its frequency is known with an uncertainty of 1 kHz [16]

$$\nu(CH_4)=88\,376\,181\,602.6\ (1)\ \text{kHz}\ .$$

We use a second titanium sapphire laser (labelled TiS2) to synthesize the 633 nm radiation. The TiS2 laser and a second HeNe laser at $\lambda=3.39$ µm – fre-

quency locked to the HeNe/CH_4 reference laser – both are sent into a $LiIO_3$ crystal. With 400 mW from TiS2 and 20 mW from the 3.39 μm laser we obtain 100 nW at 633 nm. The frequency of this generated beam at 633 nm is compared with a second HeNe/I_2 laser (labelled LSH).

For the frequency measurement, the laser TiS1 is locked to a rubidium hyperfine component in a simple way. Its frequency is modulated at about 500 Hz (modulation width, 500 kHz peak to peak). The photomultiplier signal is analysed at the same modulation frequency with a lock-in amplifier which produces the error signal. We count simultaneously the beat frequency between the two HeNe/I_2 lasers, that between the two lasers at $\lambda = 3.39$ μm, that between the synthesized beam at $\lambda = 633$ nm and the HeNe/I_2 laser and finally that between the two titanium–sapphire lasers. The latter varies from 3 to 7 GHz depending upon which hyperfine component of the $5S_{1/2}$–$5D_{3/2}$ transition is used for stabilizing TiS1. The knowledge of $\nu(I_2)$ and $\nu(CH_4)$ as well as these beat frequencies yields the absolute frequency of the rubidium transition.

We have made a preliminary study of the stability and of the reproducibility of the titanium–sapphire laser locked to the ^{87}Rb $5S_{1/2}(F_g=1)$–$5D_{3/2}(F_e=3)$ line. The Allan standard deviation of the measured frequency varies from 7×10^{-12} for 1 s integration time to 7×10^{-13} for 100 s integration time. These values are similar to the ones determined for INM12 during the LPTF experiment [3]. This points out that our frequency measurement chain and our titanium–sapphire laser do not add significant frequency noise to that of INM12. From day to day, we have observed variation of a few kHz in the measured frequency, all the measurements (100 s integration time) lying in a total spread of 3 kHz. These values correspond typically to the reproducibility of the HeNe/I_2 laser.

The reproducibility of the TiS1 laser locked on the rubidium seems very good. The measured frequency is sensitive neither to change in the modulation width of TiS1, nor to a variation of the servo-loop gain. If the cell temnperature is lowered from 90 °C to 50 °C the two-photon signal is reduced by a factor 5.5, but the measured frequency does not change significantly (the variation being smaller than 300 Hz). We have also made measurements using another rubidiujm cell without significant effect (variation of the measured frequency of about 500 Hz). The only measurable effect is the light shift. Figure 4 illustrates the frequency change versus the light power. Under our typical experimental conditions ($P=100$ mW, $\pi w^2 \approx 10$ mm^2), the shift is only 2 kHz. This value is in fairly good agreement with our theoretical calculation which predicts, for the same conditions, a light shift of 2.4 kHz for the $5S_{1/2}$ level (the $5D_{3/2}$ light shift is about 30 times smaller).

4. Results

We have made absolute frequency measurements of all the hyperfine components of the $5S_{1/2}$–$5D_{3/2}$ transition. For the $5S_{1/2}$–$5D_{5/2}$ transition we were forced to use an interferometric technique similar to the one described in ref. [4] because, in this case, the difference is of about 50 GHz between the rubidium frequencies and the difference $\nu(I_2)-\nu(CH_4)$. These results, corrected for the light shift, are reported in tables 1 and 2 with the corresponding relative intensities. In the case of the $5S_{1/2}$–$5D_{3/2}$ transitions the 1 σ uncertainty is about 5 kHz. The main contribution is the uncertainty of both HeNe reference lasers. For $5S_{1/2}$–$5D_{5/2}$ transitions, the interferometric procedure introduces an additional contribution leading to a total uncertainty of about 8 kHz. In the case of the ^{85}Rb, the hyperfine structure of the $5D_{5/2}$ level is small and the overlapping

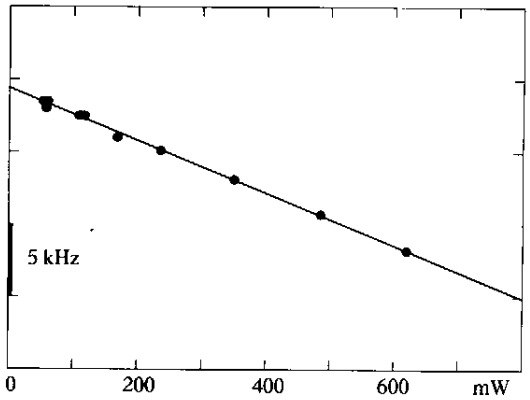

Fig. 4. Frequency shift of the two-photon line versus the light power.

Table 3
Hyperfine structure constants of the $5S_{1/2}$ and $5D_J$ level of rubidium.

^{85}Rb transition	$5S_{1/2}$–$5D_{3/2}$	$5S_{1/2}$–$5D_{5/2}$
$5S_{1/2}$ hyperfine structure	3035.7333 (7) MHz	3035.7332 (95) MHz
$5D_J$ magnetic dipole constant A	4.2221 (2) MHz	−2.1911 (12) MHz
$5D_J$ electric quadrupole constant B	1.9106 (8) MHz	2.6804 (200) MHz
Standard deviation of the fit	0.5 kHz	5.9 kHz
^{87}Rb transition	$5S_{1/2}$–$5D_{3/2}$	$5S_{1/2}$–$5D_{5/2}$
$5S_{1/2}$ hyperfine structure	6834.6823 (21) MHz	6834.6870 (17) MHz
$5D_J$ magnetic dipole constant A	14.5080 (6) MHz	−7.4923 (3) MHz
$5D_J$ electric quadrupole constant B	0.9320 (17) MHz	1.2713 (20) MHz
Standard deviation of the fit	1.33 kHz	1.09 kHz

of the low components is not negligible: for these components the total uncertainty may be 26 kHz. We have analyzed these data to deduce the hyperfine structure constants of the $5D_J$ levels. To reproduce the observed frequencies, for each isotope and fine structure transition, we have fitted the magnetic dipole constant A and the electric quadrupole constants B of the $5D_J$ levels, the $5S_{1/2}$ hyperfine splitting and the mean weighted position of the hyperfine components. Table 3 gives the results and the standard deviation σ between the experimental and the calculated position. The agreement between the theory and the experiment is very good (about 1 kHz), except for the $5S_{1/2}$–$5D_{5/2}$ transition of ^{85}Rb (6 kHz). The discrepancy in the latter case is attributed to the overlaping of the lines which complicates the line shape analysis. Our results for the $5S_{1/2}$ hyperfine splitting are also in agreement with the much more precise magnetic resonance measurement [13]. The largest discrepancy (4.4 kHz), observed for the $5S_{1/2}$–$5D_{5/2}$ transition of ^{87}Rb, may be explained by a laser frequency shift of 2.2 kHz during the measurement and gives an idea of the frequency reproducibility of the laser. The hyperfine structure constants of the $5D_J$ states also agree well with other, less precise, previous measurements [13]. We have also deduced the isotope shift of $5S_{1/2}$–$5D_{3/2}$ and $5S_{1/2}$–$5D_{5/2}$ transitions, 165.230 (2) MHz and 163.033 (6) MHz, respectively, in terms of the atomic frequency. These values are very similar to the ones obtained for the more excited levels in refs. [6,7].

5. Conclusion

We have measured the absolute frequencies of the hyperfine components of the $5S_{1/2}$–$5D_{3/2}$ two-photon transition in rubidium. In the most favourable case, the uncertainty of the determination (1.3×10^{-11}) is mainly due to the uncertainties of the standard lasers which have been used. This measurement provides a new optical frequency reference in the near infrared range at $\lambda=778$ nm. As the frequency reproducibility of this experiment seems very good, we plan to stabilize a diode laser to certain hyperfine components of these transitions. Our preliminary analysis shows that the frequency reproducibility of a rubidium stabilized diode laser should be better than one part in 10^{-11}.

Acknowledgements

The authors are indebted to B. Cagnac for many stimulating discussions during this experiment. They also thank A. Clairon and his co-workers for fruitful advice. This work is partially supported by the Bureau National de Métrologie and by the Direction des Recherches et Etudes Techniques.

References

[1] J. Vannier and C. Audouin, The quantum physics of atomic frequency standards (Adam Hilger, Bristol, 1989) p. 1502.

[2] D.A. Jennings, C.R. Pollock, F.R. Petersen, R.E. Drullinger, K.M. Evenson, J.S. Wells, J.L. Hall and H.P. Layer, Optics Lett. 11 (1983) 136.
[3] O. Acef, J.J. Zondy, M. Abed, D.G. Rovera, A.H. Gérard, A. Clairon, Ph. Laurent, Y. Millerioux and P. Juncar, Optics Comm. 97 (1992) 29.
[4] F. Nez, M.D. Plimmer, S. Bourzeix, L. Julien, F. Biraben, R. Felder, O. Acef, J.J. Zondy, P. Laurent, A. Clairon, M. Abed, Y. Millerioux and P. Juncar, Phys. Rev. Lett. 69 (1992) 2326.
[5] F. Nez, M.D. Plimmer, S. Bourzeix, L. Julien, F. Biraben, R. Felder, Y. Millerioux and P. De Natale, Proc. eleventh Intern. Conference on Laser Spectroscopy, eds. L.A. Bloomfield, T.F. Gallagher and D.J. Larson, American Institute of Physics Conference Proceedings series, to be published.
[6] Y. Kato and B.P. Stoicheff, J. Opt. Soc. Am. 66 (1976) 490.
[7] B.P. Stoicheff and E. Weinberger, Can. J. Phys. 57 (1979) 2143.
[8] S.A. Lee, J. Helmcke and J.L. Hall, Laser spectroscopy V, eds. K. Rothe and H. Walther (Springer, Berlin, 1979) p. 130.
[9] F. Penent, D. Delande, F. Biraben and J.C. Gay, Optics Comm. 49 (1984) 184.
[10] E. Giacobino, M. Devaud, F. Biraben and G. Grynberg, Phys. Rev. Lett. 45 (1980) 484.
[11] S. Bourzeix, M.D. Plimmer, F. Nez, L. Julien and F. Biraben, Optics Comm. 99 (1993) 89.
[12] J.C. Garreau, M. Allegrini, L. Julien and F. Biraben, J. Phys. France 51 (1990) 2263.
[13] E. Arimondo, M. Inguscio and P. Violino, Rev. Mod. Phys. 49 (1977) 31; and references therein.
[14] B. Cagnac, G. Grynberg and F. Biraben, J. Phys. France 34 (1973) 845.
[15] A. Lindgard and S.E. Nielsen, Atomic Data and Nuclear Data Tables 19 (1977) 606.
[16] Procès-verbaux CIPM, BIPM, 1991-1992, to be published.

High Resolution Spectroscopy of the Hydrogen Atom: Determination of the 1S Lamb Shift

S. Bourzeix, B. de Beauvoir, F. Nez, M. D. Plimmer, F. de Tomasi, L. Julien, and F. Biraben
Laboratoire Kastler Brossel, Ecole Normale Supérieure et Université Pierre et Marie Curie, Laboratoire associé au CNRS URA18, 4 place Jussieu, Tour 12 E01, 75252 Paris Cedex 05, France

D. N. Stacey
Clarendon Laboratory, Parks Road, Oxford OX1 3PU, United Kingdom
(Received 1 August 1995)

We have measured the 1S Lamb shift by comparing the frequencies of the $1S_{1/2}$-$3S_{1/2}$ and $2S_{1/2}$-$6S_{1/2}$ or $2S_{1/2}$-$6D_{5/2}$ two-photon transitions. Our result is 8172.798 (46) MHz. It is the most precise yet reported and is consistent with the larger existing proton radius measurement of $r_p = 0.862(12)$ fm.

PACS numbers: 32.30.Jc, 06.20.Jr, 12.20.Fv, 42.65.Ky

For some fifty years, quantum electrodynamics (QED) calculations have steadily improved for bound atomic systems and now give the energy levels of the hydrogen atom to an impressive accuracy, of order 10^{-11} [1]. The hydrogen level energy is conventionally expressed as the sum of three terms: The energy given by the Dirac equation for a particle with the reduced mass, the first relativistic correction due to the recoil of the proton, and the Lamb shift. The first two terms are exactly known, apart from the uncertainties in the physical constants involved (the Rydberg constant R_∞, the fine structure constant, and the electron-to-proton mass ratio). The Lamb shift contains all the other corrections, i.e., the QED corrections, the other relativistic corrections due to the proton recoil, and the effect of the proton charge distribution. Precise measurements of the Lamb shift are required to test QED calculations or, if we suppose these calculations exact, to determine the proton charge radius. This last point is important, because there are two inconsistent measurements of the proton radius, $r_p = 0.805(11)$ and $0.862(12)$ fm [2,3]. Further, precise values of the Lamb shifts are essential to deduce R_∞ from recent optical measurements of hydrogen frequencies [4,5].

The so-called 2S Lamb shift (in fact the difference of the $2S_{1/2}$ and $2P_{1/2}$ Lamb shifts) is deduced from radio-frequency measurements of the $2S_{1/2}$-$2P_{1/2}$ splitting, the first by Lamb and Retherford [6]. The precision is now limited by the 2P natural width (100 MHz) [7,8]. The 1S Lamb shift is 8 times larger but is much more difficult to measure, since the 1S level is isolated. Up to now, all measurements of the 1S Lamb shift have been obtained from the study of the 1S-2S two-photon transition by subtracting the 1S-2S Dirac and recoil energies from the 1S-2S experimental result [9–11]. This subtraction is made by comparing the 1S-2S frequency with 4 times the 2S-4S, 2S-4P, or 2S-4D frequencies. Here the main limitations to further accuracy are the natural widths of the $n = 4$ levels (700 kHz, 12.9, and 4.4 MHz for the S, P, and D levels, respectively) and the low probabilities of the 2S-4S/D two-photon transitions. Another possibility is to use higher 2S-nS/D transitions. In this paper we present a measurement of the 1S Lamb shift deduced from the comparison of the 1S-3S and 2S-6S/D frequencies, which are also in the ratio 4:1. The 2S-6S and 2S-6D transitions are narrower (300 kHz and 1.3 MHz, respectively) and stronger than the 2S-4S and 2S-4D. To exploit this advantage, uncertainty due to light shifts, greater for the two-photon transitions due to stray electric fields is also larger (by a factor of 17), but the effect in this case is negligible. The 1S-3S transition is much weaker than the 1S-2S (by a factor of 140 with a cw laser of 50 kHz bandwidth), and much broader, but this line is not the limiting factor. With this method, we have measured the Lamb shift with an uncertainty of 5.6 parts in 10^6.

Figure 1 shows the general scheme of our experiment. A home-made titanium-sapphire laser at 820 nm is used to excite the two-photon transitions, either the 2S-6S/D or, after two frequency doubling steps, the 1S-3S. The laser frequency is actively stabilized by locking to a cavity using an FM sideband method, and the jitter is reduced to the level of 5 kHz. The long term stability is guaranteed

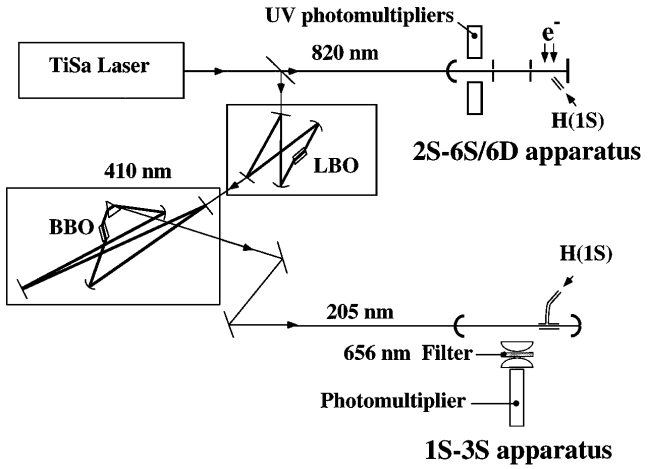

FIG. 1. Experimental setup for the frequency comparison between the 1S-3S and 2S-6S/D transitions.

 0031-9007/96/76(3)/384(4)$06.00

by the use of a second Fabry-Pérot reference cavity (FPR), which is frequently locked to an iodine stabilized He-Ne laser at 633 nm: the laser frequency is reproducible to 2 kHz day to day and to about 10 kHz over a year.

The 205 nm UV radiation is produced by two successive frequency doubling stages with two enhancement cavities. The first step, using a LBO crystal, has been described elsewhere [12] and provides up to 500 mW at 410 nm for a pump power of 2.3 W at 820 nm. The UV light is produced in a BBO crystal, 14 mm long, cut at the Brewster angle and placed inside a four-mirror astigmatically compensated ring cavity (BBO cavity). In the crystal the waist is 27 μm, and the UV light is extracted from the cavity using an intracavity prism. This second doubling step is far more challenging for several reasons. (i) The nonlinear coefficient d_{eff} is only 0.25 pm/V (for comparison, in the case of the $1S$-$2S$ transition, the generation of the 243 nm radiation involves a nonlinear coefficient d_{eff} of 1.39 pm/V). (ii) Rapid damage of the BBO crystal occurs during UV production, with a time constant of about 1 min, due probably to photochemical reactions on the faces of the crystal. However, we found that with the crystal inside a clean chamber filled with oxygen, the lifetime of a point on the crystal increases to about 15 min. (iii) After a few minutes, a counterpropagating wave at 410 nm begins to appear in the ring cavity, probably due to a photorefractive effect in the bulk of the BBO crystal. To reduce these effects, we have worked in a quasicontinuous regime where the UV intensity consists of 3 μs pulses at a frequency of 30 kHz. This is done by modulating the length of the BBO cavity so as to be resonant only some of the time. Under these conditions, despite the low duty cycle, the mean square power (which is involved in the probability of the two-photon transition) is higher than one can get by continuous locking. We obtain 1 mW peak power at 205 nm for several hours with the same point on the crystal. This modulation produces a frequency shift, the UV frequency being upshifted (downshifted) by about 125 kHz when the length of the BBO cavity decreases (increases).

To reduce transit time broadening the $1S$-$3S$ Doppler free two-photon signal is observed with an effusive atomic beam collinear with the UV beams. The atoms are produced from molecular hydrogen by a radio-frequency discharge linked to the vacuum apparatus by a 9 cm length of Teflon tube. After correction of the astigmatism, the UV beam emerging from the BBO crystal is mode matched to a third, linear, buildup cavity (two spherical mirrors with 25 cm radius of curvature) surrounding the atomic beam. Inside the cavity the beam waist is 50 μm and the UV power about 10 mW. The length of this cavity is locked to the UV frequency so that successive UV pulses have the same intensity inside the cavity. In these conditions, the frequency shifts of two successive UV pulses cancel and the residual frequency shift is estimated to be smaller than 3 kHz. The two-photon transition is detected by monitoring, through an interference filter, the $3S$-$2P$ fluorescence. The total background is about 160 counts s^{-1} and the $1S$-$3S$ signal 10 counts s^{-1} [Fig. 2(a)]. Each point in the figure corresponds to an acquisition time of about 1100 s. The experimental linewidth (1.7 MHz in terms of atomic frequency) is made up of the 1 MHz $3S$ natural width, the laser jitter (8 times 5 kHz), the transit time broadening (about 200 kHz), the second-order Doppler effect (about 100 kHz), and broadening due to the modulation of the UV light (about 500 kHz).

The $2S$-$6S/D$ apparatus is similar to the one used to measure the Rydberg constant [13,14]. The transitions are induced in a metastable atomic beam collinear with two counterpropagating laser beams. The atomic beam is produced by molecular dissociation followed by electron impact [15], and it is placed inside an enhancement cavity where the optical power can be as much as 130 W in each direction with a beam waist of 670 μm. To measure the metastable yield, an electric field quenches the $2S$ metastable atoms at the end of the atomic beam, and we detect the Lyman-α fluorescence. When the laser frequency is resonant with the $2S$-$6S/D$ transition, optical quenching of the metastable atoms occurs and we detect the corresponding decrease of the metastable beam intensity. In the recording shown in Fig. 2(b) the linewidth is about 2.5 MHz (in terms of atomic frequency). The $6D$ natural width is 1.3 MHz; the broadening is mainly due to the inhomogeneous light shift experienced by the atoms through the Gaussian profile of the laser beams. The light shift is also a major source of shift; we allow for it by recording the atomic signal for different laser intensities. For each recording, we fit a theoretical profile which takes into account the light shift and the saturation of the transition [13], enabling us to deduce the unperturbed position of the line.

We have made two series of measurements to compare, by means of the FPR cavity, the $1S$-$3S$ transition with the $2S_{1/2}$-$6D_{5/2}$ and $2S_{1/2}$-$6S_{1/2}$ transitions. For the first, we collected successively the data for the $2S$-$6D$ transition (1 day), the $1S$-$3S$ (3 days), and the $2S$-$6D$ once

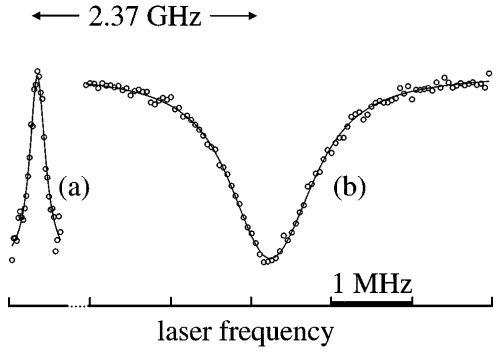

FIG. 2. Hydrogen two-photon spectra: (a) $1S(F = 1)$-$3S(F = 1)$ transition, (b) $2S_{1/2}(F = 1)$-$6D_{5/2}$ transition.

again (2 days). We used the same procedure to study the $2S_{1/2}$-$6S_{1/2}$ transition, but, due to its low intensity, the acquisition times were longer (4, 3, and 4 days, respectively). The results (i.e., the laser frequency splitting between the $1S$-$3S$ and $2S$-$6S/D$ lines), given in the first line of Table I, are multiplied by 8 to deduce the $1S$ Lamb shift (a factor of 4 for the two frequency doublings and 2 for the two-photon excitation). The quoted uncertainties (35 and 71 kHz for each measurement, one standard deviation) are mainly due to the uncertainties in the position of the $1S$-$3S$ line (19 and 24 kHz for each measurement) and of the $2S$-$6D$ or $2S$-$6S$ lines (28 and 66 kHz). We estimate the uncertainty due to a possible drift of the laser frequency during the experiment to be 8×1 kHz. The free spectral range of our FPR cavity is very precisely known by interferometry, the reference frequencies being the iodine stabilized He-Ne laser (633 nm) and the $2S$-$6D$ and $2S$-$8D$ hydrogen transitions (820 and 778 nm). The second-order Doppler effect is evaluated from the velocity distribution of the metastable atoms [4], and we estimate the shift of the $2S$-$6S/D$ line to be 37.8(1.9) kHz. Taking into account the electronic excitation of the metastable atoms, we can deduce the velocity distribution of the $1S$ atoms at the exit of the radio-frequency discharge. As the two discharges of the two atomic beams are of identical design, we can estimate the velocity distribution of the $1S$ atomic beam and calculate a second-order Doppler shift of 124(10) kHz for the $1S$-$3S$ transition. The Zeeman effect of the $2S$-$6S/D$ transitions is made negligible by means of a magnetic shield. For the $1S$-$3S$ transition, a residual magnetic field of 270 mG induces a quadratic Zeeman shift of about 1 kHz. A graphite coating of the two-vacuum apparatus reduces stray electric fields, and the residual Stark shifts are estimated to be smaller than 100 Hz. Finally, the light shift of the $1S$-$3S$ transition is also negligible (660 Hz at the center of the Gaussian beam).

The deduction of the $1S$ Lamb shift is detailed in Table I. After corrections for the hyperfine structure and the Dirac and relativistic recoil energies, we obtain the linear combination of Lamb shifts $L_{1S} - L_{3S} + 4L_{6S/D} - 4L_{2S}$. We have used the experimental value of the $2S_{1/2}$-$2P_{1/2}$ (the weighted mean value from Refs. [7,8]) and the theoretical values of the $2P$, $3S$, and $6S/D$ Lamb shifts. We have taken into account all the recent calculations of the high order terms following Ref. [1], particularly the two-loop QED corrections [16] and the more recent calculation of the $m/M\ (Z\alpha)^6$ term [17]. Using $r_p = 0.862$ fm, we obtain $L_{2P} = -12.8356(20)$ MHz, $L_{3S} = 311.403(2)$ MHz, $L_{6S} = 39.0859(3)$ MHz, and $L_{6D} = 0.1660(2)$ MHz. The two values obtained for the $1S$ Lamb shift are in good agreement and give a weighted mean value of 8172.798(46) MHz. This value, the most precise to date, is in good agreement with previous measurements (Table II) and with the theoretical value using the large proton radius [8172.802(40) MHz]. With the small proton radius, the disagreement is 2.3 standard deviations. If we assume the validity of the QED calculations, we can deduce a value of the proton radius $r_p = 0.861(20)$ fm.

In all these experiments, a large part of the uncertainty arises from the experimental value of the $2S$ Lamb shift. In the future, a way to avoid this limitation will be to use the $1/n^3$ scaling law of the Lamb shift. The quantity $L_{1S} - 8L_{2S}$ can be calculated very precisely, because all the terms varying exactly as $1/n^3$ (and particularly the effect of the size of the proton) disappear. For instance, from our experiment, we deduce the quantity $L_{1S} - 4L_{2S}$ [3992.768(34) MHz]. Using this result alone, together with the theoretical value of $L_{1S} - 8L_{2S}$ [$-187.236(11)$ MHz [19]], we obtain values of the $1S$ and $2S$ Lamb shifts [$L_{1S} = 8172.772(69)$ MHz and $L_{2S\text{-}2P} = 1057.837(9)$ MHz]. For the $2S$ Lamb shift, this result agrees very well with the microwave measurements [1057.845(9) MHz [7] and 1057.839(12) MHz [8]] but disagrees slightly with the indirect measurement of Pal'chikov, Sokolov, and Yakovlev [1057.8514(19) MHz [20]]. To exploit the potential of this approach, one needs very precise optical frequency measurements. For this reason, we intend to measure the optical frequency of the $1S$-$3S$ transition with respect to the cesium clock. The second-order Doppler effect, which is the major source of shift, will be canceled by the use of an appropriate

TABLE I. Determination of the $1S$ Lamb shift (frequency unit MHz).

	$2S_{1/2}$-$6D_{5/2}$	$2S_{1/2}$-$6S_{1/2}$
Laser frequency splitting	2370.1249(43)	2120.1714(88)
Laser frequency splitting $\times 8$	18 960.999(35)	16 961.371(19)
$2S$-$6S/D$ second-order Doppler effect	$4 \times 0.0378(19)$	$4 \times 0.0378(19)$
$1S$-$3S$ second-order Doppler effect	$-0.124(10)$	$-0.124(10)$
$1S$-$3S$ Zeeman effect	0.001	0.001
Hyperfine corrections	-164.6552	-170.9683
Dirac and recoil contributions	$-15\,114.3572$	$-12\,952.6568$
$L_{1S} - L_{3S} + 4(L_{6S/D} - L_{2S})$	3682.015(37)	3837.774(72)
$4(L_{2S} - L_{2P})$ (experiment)	4231.372(29)	4231.372(29)
$L_{3S} + 4L_{2P} - 4L_{6S/D}$ (theory)	259.3965(83)	103.7169(84)
$1S$ Lamb shift	8172.783(48)	8172.863(78)

TABLE II. Some recent measurements of the $1S$ Lamb shift and comparison with theory (MHz).

Transitions	$1S$ Lamb shift
$1S$-$2S$ and $2S$-$4S/D$ [a]	8172.820(110)
$1S$-$2S$ and $2S$-$8S/D$ [b]	8172.815(70)
$1S$-$2S$ and $2S$-$4S$ [c]	8172.860(60)
$1S$-$2S$ and $2S$-$4P$ [d]	8172.827(51)
This work	8172.798(46)
Theory ($r_p = 0.862$ fm)	8172.802(40)
Theory ($r_p = 0.805$ fm)	8172.653(40)

[a]Reference [18].
[b]Reference [4].
[c]Reference [10].
[d]Reference [11].

transverse magnetic field [21]. The comparison of different hydrogen optical frequencies (for example, $1S$-$3S$ and $2S$-$8S/D$) will reduce the uncertainty in the Lamb shift to a few parts in 10^6 and that in the Rydberg constant to a few parts in 10^{12}.

The authors are indebted to B. Cagnac for many stimulating discussions. They thank C. D. Thompson for assistance with this experiment and P. Indelicato for the communication of preliminary results for the calculation of the Lamb shifts of the excited levels. They thank also M. I. Eides, E. A. Hinds, K. Pachucki, and P. Mohr for communicating their results before publication. This work is partially supported by the Bureau National de Métrologie, by the Direction des Recherches et Etudes Techniques and by the European Community (SCIENCE cooperation Contract No. SC1*-CT92-0816 and network Contract No. CHRX-CT93-0105).

[1] See, for example, J. R. Sapirstein and D. R. Yennie, in *Quantum Electrodynamics*, edited by T. Kinoshita (World Scientific, Singapore, 1990); K. Pachucki *et al.*, in "Electron Theory and Quantum Electrodynamics–100 Years Later" (Plenum, New York, to be published); P. Mohr, in "Atomic, Molecular and Optical Physics Reference Book," edited by G. W. F. Drake (American Institute of Physics, New York, to be published).
[2] L. N. Hand, D. G. Miller, and R. Wilson, Rev. Mod. Phys. **35**, 335 (1963).
[3] G. G. Simon, C. Schmitt, F. Borkowski, and V. H. Walther, Nucl. Phys. **A333**, 381 (1980).
[4] F. Nez *et al.*, Europhys. Lett. **24**, 635 (1993).
[5] T. Andreae *et al.*, Phys. Rev. Lett. **69**, 1923 (1992).
[6] W. E. Lamb and R. C. Retherford, Phys. Rev. **72**, 241 (1947).
[7] S. R. Lundeen and F. M. Pipkin, Phys. Rev. Lett. **46**, 232 (1981).
[8] E. W. Hagley and F. M. Pipkin, Phys. Rev. Lett. **72**, 1172 (1994).
[9] M. G. Boshier *et al.*, Phys. Rev. A **40**, 6169 (1989).
[10] M. Weitz *et al.*, Phys. Rev. Lett. **72**, 328 (1994).
[11] D. J. Berkeland, E. A. Hinds, and M. G. Boshier, Phys. Rev. Lett. **75**, 2470 (1995).
[12] S. Bourzeix, M. D. Plimmer, F. Nez, L. Julien, and F. Biraben, Opt. Commun. **99**, 89 (1993).
[13] J. C. Garreau, M. Allegrini, L. Julien, and F. Biraben, J. Phys. **51**, 2263 (1990); **51**, 2275 (1990); **51**, 2293 (1990).
[14] F. Nez *et al.*, Phys. Rev. Lett. **69**, 2326 (1992).
[15] F. Biraben, J. C. Garreau, L. Julien, and M. Allegrini, Rev. Sci. Instrum. **61**, 1468 (1990).
[16] K. Pachucki, Phys. Rev. Lett. **72**, 3154 (1994).
[17] R. N. Fell, I. B. Khriplovich, A. I. Milstein, and A. S. Yelkhovsky, Phys. Lett. A **181**, 172 (1993); K. Pachucki and H. Grotch, Phys. Rev. A **51**, 1854 (1995).
[18] M. Weitz, F. Schmidt-Kaler, and T. W. Hänsch, Phys. Rev. Lett. **68**, 1120 (1992).
[19] S. G. Karshenboim, JETP **79**, 230 (1994); M. I. Eides and V. A. Shelyuto, Phys. Rev. A **52**, 954 (1995).
[20] V. G. Pal'chikov, Yu. L. Sokolov, and V. P. Yakovlev, Metrologia **21**, 99 (1985).
[21] F. Biraben, L. Julien, J. Plon, and F. Nez, Europhys. Lett. **15**, 831 (1991).

Absolute Frequency Measurement of the $2S$-$8S/D$ Transitions in Hydrogen and Deuterium: New Determination of the Rydberg Constant

B. de Beauvoir, F. Nez, L. Julien, B. Cagnac, and F. Biraben

Laboratoire Kastler Brossel, Ecole Normale Supérieure et Université Pierre et Marie Curie, Laboratoire associé au CNRS URA18, 4 place Jussieu, Tour 12 E01, 75252 Paris Cedex 05, France

D. Touahri, L. Hilico,* O. Acef, A. Clairon, and J. J. Zondy

Laboratoire Primaire du Temps et des Fréquences, Bureau National de Métrologie-Observatoire de Paris, 61 avenue de l'Observatoire, 75014 Paris, France

(Received 22 July 1996; revised manuscript received 2 December 1996)

We have performed a pure optical frequency measurement of the $2S$-$8S/D$ two-photon transitions in atomic hydrogen and deuterium. These frequencies are directly compared to a new frequency standard, a diode laser stabilized to a two-photon transition at 778 nm in rubidium. We deduce a new value for the Rydberg constant, $R_\infty = 109\,737.315\,685\,9(10)$ cm^{-1} with an uncertainty of 9×10^{-12}. From the isotope shift, we derive a precise value of the $2S$ Lamb shift in deuterium [$L_{2S\text{-}2P} = 1059.230(9)$ MHz] and the difference of the quadratic charge radii of deuteron and proton. [S0031-9007(96)02260-0]

PACS numbers: 31.30.Jv, 06.20.Jr, 21.10.Ft

Hydrogen is the simplest atom, and its properties have been calculated very precisely: quantum electrodynamics (QED) calculations have continuously improved to achieve an impressive accuracy, currently of order 10^{-11} [1]. At the same time, experimental measurements in hydrogen have been performed at a comparable level of precision to deduce the Rydberg constant and to test the QED calculations [2]. Recently, the interferometric measurements have been superseded by accurate optical frequency ones. These measurements need frequency-multiplication chains which link the measured frequency via intermediate standard lasers to the cesium clock. With a frequency chain starting from the methane-stabilized helium-neon laser, Hänsch and co-workers measured the frequency of the $1S$-$2S$ two-photon transition with an uncertainty of 1.8×10^{-11} [3]. In our group, we built a frequency chain linking the frequencies of the $2S$-$8S/D$ two-photon transitions to two standard lasers (the iodine-stabilized and the methane-stabilized helium-neon lasers) and reached a precision of 1.3×10^{-11} [4]. Here we present a new optical frequency measurement of the $2S$-$8S/D$ transitions in hydrogen and deuterium with a frequency-multiplication chain. The relative uncertainty is reduced to about 6×10^{-12} and provides a more precise value of the Rydberg constant. In deuterium, we give a precise determination of the $2S$ Lamb shift and, from the isotope shift, we obtain the difference of the squared proton and deuteron charge radii $r_d^2 - r_p^2$.

Our frequency chain connects indirectly hydrogen frequencies to the cesium clock (see Fig. 1). The experiment is carried out at two different laboratories, the *Laboratoire Primaire du Temps et des Fréquences* (LPTF) at the *Observatoire de Paris* and the *Laboratoire Kastler Brossel* (LKB) in the *Université Pierre et Marie Curie*, which are linked by two, 3 km long, optical fibers. The cornerstone of this chain is a new standard, namely a laser diode at 778 nm (i.e., $\nu = 385$ THz) stabilized to the $5S_{1/2}$-$5D_{5/2}$ two-photon transition of rubidium (LD/Rb laser) [5]. The laser diode is used in an extended cavity configuration, the rubidium cell is placed inside an enhancement cavity, and the transition is detected by monitoring the fluorescence from the radiative cascade $5D$-$6P$-$5S$. The main metrological features of the LD/Rb laser are a 4×10^{-13} short term stability for $1s$ integration time and a day-to-day repeatability of 400 Hz. Two such lasers are operational at LPTF and one at LKB. The frequencies of these lasers are compared between the two laboratories using the optical fibers. To check the frequency shift due to the fiber, we have used a titanium-sapphire laser with a frequency jitter reduced to the few kHz level. After a round trip of 6 km through the optical fibers, we have observed a maximum frequency shift of 3 Hz. This shift is completely negligible for our frequency measurements. The frequencies of the LD/Rb lasers have been measured at the LPTF with a frequency chain which connects the LD/Rb laser

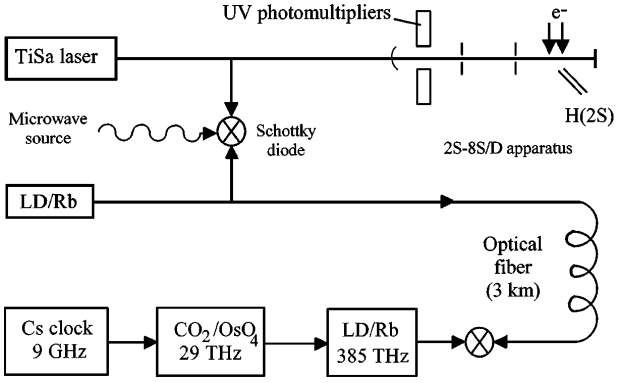

FIG. 1. Outline of the frequency chain between the $2S$-$8S/D$ hydrogen frequencies and the cesium clock.

 0031-9007/97/78(3)/440(4)$10.00

at 385 THz to a standard at 29 THz, which is a CO_2 laser stabilized to an osmium tetraoxyde line (CO_2/OsO_4). This standard had been previously measured with an uncertainty of 70 Hz [6]. The details of this frequency chain will be published shortly [7]. The frequency of the LD/Rb standard laser working at the LKB has been measured directly with respect to the CO_2/OsO_4 standard using the optical fiber and the frequency chain of the LPTF. Its frequency is

$$\nu_{\mathrm{Rb}}(\mathrm{LKB}) = 385\,285\,142\,370.5\ (1.0)\ \mathrm{kHz}\,.$$

The uncertainty is due to the CO_2/OsO_4 standard (13×70 Hz) and the day-to-day repeatability of the LD/Rb standard (about 400 Hz). Thanks to regular frequency comparisons between the LD/Rb standards, we have kept this precision throughout the measurements in hydrogen and deuterium (about four months).

The frequency comparison between the $2S$-$8S/D$ transitions and the LD/Rb standard is easy, thanks to the quasicoincidence between these frequencies (about 40 GHz in hydrogen and 144 GHz in deuterium). The LD/Rb laser and the titanium-sapphire laser (used for the observation of the hydrogen lines) are focused on a Schottky diode [8]. For the measurements in hydrogen, the Schottky diode is simultaneously irradiated with a microwave source at 13 GHz (48.4 GHz for deuterium) phase-locked to a low phase-noise quartz oscillator at 100 MHz. We detect the low-frequency beat note between the two optical frequencies and the third harmonic of the microwave source with a signal-to-noise ratio of 35 dB (resolution bandwidth of 300 kHz). A tracking oscillator is phase locked to this beat signal, and we count continuously this beat frequency. The frequency of the 100 MHz quartz oscillator has been continuously measured with respect to a high stability quartz oscillator at 10 MHz (stability of 2×10^{-9} during four months), which has been compared to a hydrogen maser several times. We estimate the uncertainty due to the Schottky diode frequency measurement to be about 15 Hz in hydrogen and 50 Hz in deuterium.

The hydrogen experiment has been described elsewhere [4,9]. The two-photon transition is induced with a highly stable titanium-sapphire laser. The frequency jitter is reduced to the level of 2 kHz by locking to a first cavity. The long term stability is obtained by a second reference cavity locked to an iodine stabilized He-Ne laser [10]. To reduce the collisional and transit time broadening, we use a metastable atomic beam collinear with the laser beams. The atomic beam is placed inside an enhancement cavity, where the optical power can be as much as 100 W in each direction with a beam waist of 660 μm. The laser-atom interaction region (56 cm long) is surrounded by a magnetic shield. To measure the metastable flux, we detect the Lyman-α fluorescence at the end of the beam, where an electric field quenches the metastable atoms. When the laser frequency is resonant with the $2S$-$8S/D$ transition, optical quenching of the metastable atoms occurs and we observe the corresponding decrease of the metastable yield (see Fig. 2). In this recording the linewidth is about 1.3 MHz (in terms of atomic frequency), including the natural width of the $8D$ level of 572 kHz. The broadening is mainly due to the inhomogenous light shift experienced by the atoms through the Gaussian profile of the laser beams. To evaluate the light shift, we record the atomic signal for different laser intensities and we extrapolate the line position to zero light power (Fig. 3). We have followed the same procedure as in Ref. [9]. For each recording, we fit a theoretical profile which takes into account the light shift and the saturation of the transition. Since our previous work, we have improved the calculation of the theoretical line shape: we have included the small hyperfine structure of the $8D$ levels (143 and 222 kHz for $8D_{5/2}$ and $8D_{3/2}$ in hydrogen), the photoionization of the excited levels, as well as the second-order Doppler shift. This effect is evaluated from the velocity distribution of the metastable atoms measured by monitoring the Doppler broadened $2S$-$6P$ transition at 410 nm with a collinear laser beam. We have also measured the population of the hyperfine levels of the $2S_{1/2}$ state (80% and 20% for the $F = 1$ and $F = 0$ levels in hydrogen), which are slightly different from the statistical weights (75% and 25%). Each fit gives both the experimental line center and the line position corrected for light shift and hyperfine structure of the $8D$ levels. An extrapolation of these data is given in Fig. 3. As we measure continuously the beat frequency between the titanium-sapphire laser and the LD/Rb standard laser, we deduce the absolute frequency of the line. Finally, from the linewidth of the $2S$-$15D$ transition, we find the stray electric field to be smaller than 3 mV/cm, corresponding to a Stark shift of about -400 Hz for the $8D_{5/2}$ level and 700 Hz for the $8S_{1/2}$. We have neglected these corrections in the data analysis.

We have studied three transitions in hydrogen and deuterium: $2S_{1/2}(F = 1 \text{ or } \frac{3}{2})$-$8S_{1/2}$, -$8D_{3/2}$, and -$8D_{5/2}$.

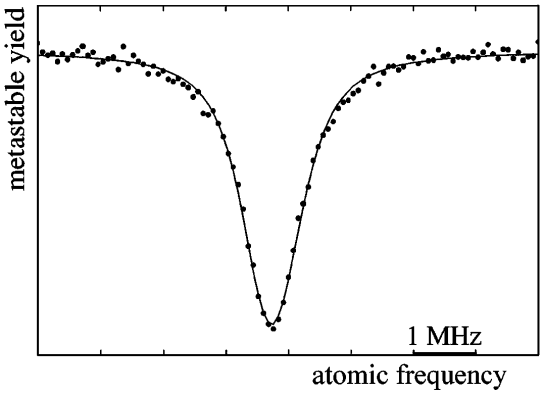

FIG. 2. Hydrogen two-photon spectra of the $2S_{1/2}(F = 1)$-$8S_{5/2}$ transition.

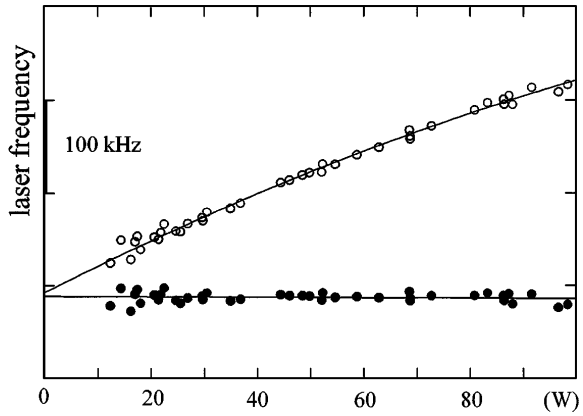

FIG. 3. Extrapolation of the line-center frequency (∘) and of the line position corrected for light-shift and $8D$ hyperfine structure (•) versus the light power in the case of the $2S_{1/2}$-$8D_{5/2}$ transition of deuterium.

In hydrogen, the $2S_{1/2}$-$8D_{5/2}$ transition was measured twice, at the beginning and at the end of the experiment. For each extrapolation we recorded the signal for about forty different light powers. Each signal is the average over ten scans during a 20-min run. We have tried to observe the line for very low light power. In this case we make the mean of several runs to improve the signal-to-noise ratio. In total we have performed 378 runs for data collection. Table I gives the measured frequencies after correction of the hyperfine structure of the S levels. The quoted uncertainties are only statistical. These experimental values can be intercompared using the theoretical value of the fine structure and of the Lamb shifts in the $n = 8$ levels. We have taken into account all the recent calculations of the high-order terms following Ref. [1]. Using $r_p = 0.862$ fm and $r_d = 2.115$ fm for the nucleus charge radii [11,12], the values of the Lamb shifts are $L_{8S_{1/2}} = 16.5008(3)$ MHz, $L_{8D_{3/2}} = -0.0607(2)$ MHz, and $L_{8D_{5/2}} = 0.0714(2)$ MHz [16.5223(3) MHz, −0.0607(2) MHz, and 0.0715(2) MHz, respectively, in deuterium]. We can thus deduce several independent values of the $2S_{1/2}$-$8D_{5/2}$ interval (see Table I). These values are in good agreement for both hydrogen and deuterium. The mean values are, respectively, 770 649 561 585.0(4.9) kHz and 770 859 252 851.5(4.4) kHz. The 4.9 and 4.4 kHz uncertainties (one standard deviation) come from the statistics, the frequency of the LD/Rb laser (2 kHz), the evaluation of the second-order Doppler effect (1 kHz), and the imperfections of the theoretical model (3 kHz).

In hydrogen, there have been several precise measurements of the $2S$ Lamb shift (in fact, the difference $L_{2S\text{-}2P}$ of $2S_{1/2}$ and $2P_{1/2}$ Lamb shifts) by microwave [13] or by optical spectroscopy [14]. This latter method used the $1/n^3$ scaling law of the Lamb shift [15]. Using the weighted mean value of these results [$L_{2S\text{-}2P} = 1057.8400(56)$ MHz] and the theoretical value of the Lamb shifts of the $2P$ and $8D$ levels [$L_{2P} = -12.8356(20)$ MHz], we can extract the Rydberg constant from the hydrogen $2S_{1/2}$-$8D_{5/2}$ interval. The result is $R_\infty = 109\,737.315\,685\,6(11)$ cm^{-1} with an uncertainty of 1 part in 10^{11}. This uncertainty arises mainly from the frequency measurement (6.4×10^{-12}), the Lamb shifts (7.7×10^{-12}), and the proton-to-electron mass ratio (1.3×10^{-12}) [16].

In deuterium, there exists no precise determination of the $2S$ Lamb shift, so we cannot deduce directly R_∞. On the other hand, using the value of R_∞ given above, we deduce the $2S$ Lamb shift $L_{2S\text{-}2P} = 1059.230(9)$ MHz. This value is in good agreement with a previous, less precise determination [1059.240(100) MHz [17]] but disagrees with the theoretical value [1059.210(7) MHz [12]] calculated with the deuteron charge distribution $r_d = 2.115$ fm. From another point of view, we can consider the isotope shift of the $2S$-$8D$ interval. This

TABLE I. Frequencies of he $2S$-$8S/D$ two-photon transitions.

Transition	Measured frequency (MHz)	$2S_{1/2}$-$8D_{5/2}$ deduced frequency (MHz)
Hydrogen		
$2S_{1/2}$-$8D_{5/2}$	770 649 561.5866 (58)	770 649 561.5866
$2S_{1/2}$-$8D_{3/2}$	770 649 504.4535 (66)	770 649 561.5826
$2S_{1/2}$-$8D_{1/2}$	770 649 350.0163 (75)	770 649 561.5784
$2S_{1/2}$-$8D_{5/2}$	770 649 561.5886 (54)	770 649 561.5886
Mean value of the $2S_{1/2}$-$8D_{5/2}$ measurements:		770 649 561.5850 (49)
Deuterium		
$2S_{1/2}$-$8D_{5/2}$	770 859 252.8523 (32)	770 859 252.8523
$2S_{1/2}$-$8D_{3/2}$	770 859 195.7044 (38)	770 859 252.8492
$2S_{1/2}$-$8D_{1/2}$	770 859 041.2511 (52)	770 859 252.8538
Mean value of the $2S_{1/2}$-$8D_{5/2}$ measurements:		770 859 252.8515 (44)

isotope shift is mainly a mass effect. Thanks to the precise determination of the mass ratios m_p/m_e and m_d/m_p, the uncertainty in the mass effect is only 0.6 kHz. As this isotope shift is very sensitive to the nuclear volume effect, we can calculate the difference of the quadratic charge radii of the deuteron and the proton. We obtain $r_d^2 - r_p^2 = 3.827(32)$ fm^2, in good agreement with the result of Weitz *et al.* deduced from the $1S$-$2S$ isotope shift [3.822(16) fm^2 [12]]. Using $r_p = 0.862$ fm, we deduce a value of the deuteron charge distribution $r_d = 2.138(9)$ fm.

If we use the $1/n^3$ scaling law of the Lamb shift [15], we can make another analysis of the measurements in deuterium. If we consider the frequencies $\nu_{1S\text{-}2S}$ and $\nu_{2S\text{-}8D}$ of the $1S$-$2S$ and $2S$-$8D$ intervals, we can form the linear combination $7\nu_{2S\text{-}8D}$-$\nu_{1S\text{-}2S}$. In this way, the theoretically well-known quantity L_{1S}-$8L_{2S}$ appears [15]. If we apply this method to the precise measurements of the $1S$-$2S$ [3,18] and $2S$-$8D$ deuterium frequencies, we obtain $R_\infty = 109\,737.315\,687\,1(22)$ cm^{-1}, in excellent agreement with the hydrogen determination. The weighted mean of the hydrogen and deuterium values is $R_\infty = 109\,737.315\,685\,9(10)$ cm^{-1}. This result, with a relative uncertainty of 9×10^{-12}, is the most precise available. It is in fair agreement with both our result of 1993 [$R_\infty = 109\,737.315\,683\,4(24)$ cm^{-1} [4]] and that of Hänsch and co-workers [$R_\infty = 109\,737.315\,684\,9(30)$ cm^{-1} [12]]. Finally, using the $1S$-$2S$ isotope shift [18], we can also calculate the isotope shift of the quantity $7\nu_{2S\text{-}8D}$-$\nu_{1S\text{-}2S}$, which is independent of the nuclear effects and mainly sensitive to the mass ratio m_p/m_e. In this way we derive a proton-to-electron mass ratio of $m_p/m_e = 1836.152\,68(10)$ in agreement with the far more precise value $m_p/m_e = 1836.152\,666\,5(40)$ obtained by van Dyck *et al.* [16].

To conclude, we have determined the Rydberg constant with an uncertainty of 9×10^{-12}. For the future, thanks to the $1/n^3$ scaling law of the Lamb shifts, the comparison of different optical frequencies provides a new method to reduce further the uncertainties in both the Rydberg constant and the Lamb shifts. In this paper, we have provided a demonstration of this method in the case of deuterium. To exploit the potential of this approach, one needs very precise optical frequency measurements. For this reason, we intend to measure the optical frequencies of the $2S$-$12S/D$ and $1S$-$3S$ transitions with respect to the cesium clock. The comparison of these measurements will reduce the uncertainty in the Rydberg constant to a few parts in 10^{12}.

The authors thank M. D. Plimmer for critical reading of the manuscript. This work is partially supported by the Bureau National de Métrologie and by the Direction des Recherches et Etudes Techniques.

*Permanent address: Laboratoire Kastler Brossel, UPMC, 4 Place Jussieu, 75252 Paris Cedex 05, France. Affiliated with Université d'Evry Val d'Essone, France.

[1] See, for example, J. R. Sapirstein and D. R. Yennie, in *Quantum Electrodynamics*, edited by T. Kinoshita (World Scientific, Singapore, 1990); K. Pachucki *et al.*, J. Phys. B **29**, 177 (1996).
[2] See, for example, B. Cagnac, M. D. Plimmer, L. Julien, and F. Biraben, Rep. Prog. Phys. **57**, 853 (1994).
[3] T. Andreae *et al.*, Phys. Rev. Lett. **69**, 1923 (1992).
[4] F. Nez *et al.*, Europhys. Lett. **24**, 635 (1993).
[5] Y. Millerioux *et al.*, Opt. Commun. **108**, 91 (1994).
[6] A. Clairon *et al.*, IEEE Trans. Instrum. Meas. **34**, 265 (1985); Metrologia **25**, 9 (1988).
[7] D. Touahri *et al.*, Opt. Commun. (to be published).
[8] O. Acef *et al.*, Opt. Commun. **109**, 428 (1994).
[9] J. C. Garreau, M. Allegrini, L. Julien, and F. Biraben, J. Phys. **51**, 2263 (1990); **51**, 2275 (1990); **51**, 2293 (1990).
[10] S. Bourzeix, M. D. Plimmer, F. Nez, L. Julien, and F. Biraben, Opt. Commun. **99**, 89 (1993).
[11] G. G. Simon, C. Schmitt, F. Borkowski, and V. H. Walther, Nucl. Phys. **A333**, 381 (1980).
[12] For the value of r_d, see an analysis by M. Weitz *et al.*, Phys. Rev. A **52**, 2664 (1995).
[13] S. R. Lundeen and F. M. Pipkin, Phys. Rev. Lett. **46**, 232 (1981); E. W. Hagley and F. M. Pipkin, Phys. Rev. Lett. **72**, 1172 (1994).
[14] S. Bourzeix *et al.*, Phys. Rev. Lett. **76**, 384 (1996).
[15] S. G. Karshenboim, J. Phys. B **29**, L31 (1996).
[16] D. L. Farnham, R. S. Van Dyck, and P. B. Schwinberg, Phys. Rev. Lett. **75**, 3598 (1995).
[17] B. L. Cosens, Phys. Rev. **173**, 49 (1968).
[18] F. Schmidt-Kaler, D. Leibfried, M. Weitz, and T. W. Hänsch, Phys. Rev. Lett. **70**, 2261 (1993).

Accurate Measurement of the 2^3S_1-3^3D_1 Two-Photon Transition Frequency in Helium: New Determination of the 2^3S_1 Lamb Shift

C. Dorrer,* F. Nez, B. de Beauvoir, L. Julien, and F. Biraben

Laboratoire Kastler Brossel, Ecole Normale Supérieure et Université Pierre et Marie Curie, Laboratoire associé au CNRS URA18, 4 Place Jussieu, Tour 12 E01, 75252 Paris Cedex 05, France

(Received 10 February 1997)

We have performed a precise measurement of the 2^3S_1-3^3D_1 two-photon transition frequency in ^{4}He at 762 nm. The 2^3S_1-3^3D_1 frequency is 786 823 850.002(56) MHz, with a relative uncertainty of 7.1×10^{-11}. The deduced 2^3S_1 Lamb shift is 4057.276(60) MHz. This result, the most accurate at the present time, reduces the uncertainty in the 2^3S_1 Lamb shift by 1 order of magnitude and is 100 times more precise than the theoretical prediction [4062.3(8.0) MHz]. [S0031-9007(97)03086-X]

PACS numbers: 32.30.Jc, 12.20.Fv, 31.30.Jv

In simple atomic systems, calculations, as well as experimental measurements, have reached an impressive accuracy. The hydrogen atom is the most significant case. Its properties have been calculated very precisely, with a relative accuracy of order 10^{-11} [1,2], and, at the same time, experimental measurements have been performed at the same level of precision [3–6]. Because it is the simplest multielectron atom, atomic helium plays an important role. The helium level energy is conventionally expressed as the sum of three terms: the nonrelativistic energy, the lowest order relativistic correction, and the Lamb shift, which includes the quantum electrodynamics corrections (QED) and the high order relativistic terms. As the theoretical uncertainties of the first two terms are well below the experimental accuracy [7], precise measurements in helium provide an important test of QED calculations. Thanks to a better evaluation of the Bethe logarithm for the $1S$ and $2S$ states [8], the theoretical uncertainties are now 180 MHz for the $1S$ state and 8 MHz for the $2S$ and $2P$ states [9]. For the D states, the theoretical uncertainties are much smaller, for instance, 20 kHz for the $3D$ states. Consequently, it is possible to use the D states as points of reference in the interpretation of the spectroscopic results. For example, very precise measurements of $2S$-nD transitions in helium provide accurate determination of the 2^1S and 2^3S Lamb shifts.

Helium has been studied experimentally for many years. Optical spectroscopy involving the ground state is very difficult since the lowest excited level lies about 20 eV above it. Recently, a beautiful experiment has been performed in Amsterdam, by Hogervorst *et al.* who have measured the frequency of the 1^1S-2^1P transition in both ^{4}He and ^{3}He at 58.4 nm [10]. The 1^1S Lamb shift, in agreement with the theoretical one, was deduced with a relative uncertainty of 4.2×10^{-3}. Most other spectroscopic studies use the 2^1S and 2^3S metastable states as lower level [11–18]. For instance, the combination of the Lamb shifts involved in the 2^3S-2^3P transition has been measured by an interferometric method with a relative uncertainty of 1.3×10^{-5} [12]. In Florence, the group of Inguscio has realized the first pure frequency measurement of an optical transition in helium and deduced the 2^3S Lamb shift with an accuracy of 790 kHz [13]. The 2^3S-n^3D two-photon transitions were extensively studied during the 1980's [16,17] and, more recently, the 2^1S-n^1D transitions (with n in the range 7–20) were investigated at Yale [18]. In this Letter, we report a very precise measurement of the 2^3S_1-3^3D_1 two-photon transition at 762 nm in ^{4}He and we deduce an improved value for the 2^3S_1 Lamb shift.

The heart of our measurement apparatus is a very stable Fabry-Pérot reference cavity, labeled FPR. It consists of a 50 cm zerodur rod and two silver coated mirrors, one flat and one spherical (60 cm curvature radius). The finesse is about 100 at 760 nm. The FPR cavity is scanned with a piezoelectric translator and locked to an iodine stabilized helium-neon laser (He-Ne/I_2) at 633 nm. The 762 nm radiation used for the two-photon excitation in helium is provided by a homemade titanium sapphire laser (TiSa) described in Ref. [19]. This laser is actively stabilized on a second cavity by the sideband technique, the frequency jitter being reduced below 10 kHz. The laser is then locked on a fringe of the FPR cavity. This second servo loop transfers the long term stability of the He-Ne/I_2 standard to the TiSa laser. The laser frequency scanning is made with an acoustooptic modulator placed between the FPR cavity and the laser. The FPR cavity is also used to determine the TiSa frequency. Frequency measurements with a Fabry-Pérot cavity are difficult, owing to the reflective and Fresnel phase shifts. The reflective phase shift is influenced by the mirror coatings and is wavelength dependent. To eliminate this effect, a first method is to change the length of the Fabry-Pérot cavity. We used this technique in our group in 1989 to measure precisely some hydrogen frequencies, but this method is long and difficult to implement [20]. In the present experiment, the length of the FPR cavity was fixed and we simply used the FPR cavity to make a linear interpolation between two, very

 0031-9007/97/78(19)/3658(4)$10.00

well known reference frequencies. The first is provided by a new frequency standard, a laser diode stabilized on the $5S$-$5D$ two-photon transition of rubidium at 778 nm, whose frequency has been measured recently with an uncertainty of only 2 kHz [21]. The second reference frequency is the $2S_{1/2}$-$10D_{5/2}$ two-photon transition in deuterium at 760 nm. We have chosen this transition because it lies close to the 2^3S-3^3D transition in helium (about 2 nm). Taking advantage of our apparatus used for the Rydberg constant measurement [3,20], we have made several recordings of this line. Using the recent experimental value of the $2S_{1/2}$-$8D_{5/2}$ two-photon frequency in deuterium [3], and the theoretical value of the $8D_{5/2}$-$10D_{5/2}$ splitting, we are able to know the frequency of the closest FPR fringe with an uncertainty of 10 kHz. To evaluate the effect of the reflective phase shift, we have used a third reference frequency, the 633 nm radiation of the He-Ne/I_2 laser. Immediately after the helium experiment, we have measured the frequency of our He-Ne/I_2 standard with an uncertainty of 4 kHz, using the same scheme as described in Ref. [22]. If we simulate the effect of the reflective phase shift by a slight, linear variation of the FPR free spectral range versus the frequency, we can make a quadratic interpolation between these three reference frequencies. The result, for the FPR fringe close to the helium line, differs from the linear interpolation by only 0.8 kHz. Consequently, the variation of the reflective phase shift between the two reference frequencies at 760 and 778 nm is negligible. This is due to the fact that we use silver coated mirrors which are very broad band. Finally, we estimate the uncertainty on the frequency of the FPR fringe used to stabilize the TiSa laser close to the helium line at 10 kHz. In addition, we have to take into account the accuracy of the servo loop of the TiSa laser on the FPR fringe, which is also estimated to be 10 kHz.

The apparatus used for the helium experiment is the following. The cell is a sphere (6 cm in diameter) with Brewster windows. A large spherical cell is necessary to avoid quenching of the metastable state on the wall. The cell is filled with ^{4}He gas. A radio-frequency discharge, at 14 MHz, populates the 2^3S_1 metastable states. The Earth's magnetic field is compensated by a system of three Helmoltz coils. To enhance the optical power seen by the atoms and to obtain two counterpropagating waves, the cell is placed in a built-up cavity formed by two spherical mirrors (77 and 104 mm curvature radius, 150 mm apart). This cavity maintained in resonance with the TiSa laser using a lock-in amplifier. The two-photon transition is detected by monitoring the 3^3D_1-2^3P fluorescence at 587 nm which is collected with a large lens (150 mm of diameter and 100 mm of focal length) and detected with a photomultiplier. To avoid parasitic light due to the discharge, the discharge is pulsed at 10 kHz and detection carried out in the afterglow regime. The data acquisition is driven by a computer. The radio frequency is switched on only during 5 μs, then we look at the photomultiplier signal for 40 μs starting 40 μs later. This signal is sent in an integrator which is read once every second by the computer. In addition, this delay reduces the effect of parasitic electric field produced by the discharge: no significant frequency shift was observed when the radio-frequency power was varied by a factor of 2. Ten scans on the line are combined to obtain the signal shown in Fig. 1.

To study the pressure shift, we filled the cell with seven different gas pressures, in the range 0.05–0.5 Torr. For each pressure, the two-photon transition was recorded for various optical powers (typically ten different one-way powers from 9 to 26 W inside the cavity). A theoretical line shape is fitted on each experimental signal (see Fig. 1). We employ a convolution of a Lorentzian line shape, which takes into account the natural width and the pressure broadening, and of a double exponential curve, which describes the broadening due to the finite transit time [23]. The parameters of the fit are the parameters of the Lorentzian shape. The fit provides the width of the Lorentzian shape and the frequency of the experimental line. For each pressure, linear extrapolations of these data versus the light power give the width of the Lorentzian shape and the frequency of the 2^3S_1-3^3D_1 transition without light shift. In a second step, we make linear extrapolations versus pressure [see Figs. 2(a) and 2(b)]. Figure 2(a) shows the pressure broadening of the line which is evaluated to be 35.6(1.7) MHz/Torr. The width for zero pressure is 11.33(19) MHz, in very good agreement with the natural width of the 3D level (11.25 MHz [9]). On the other hand, the pressure shift is small [0.4(3) MHz/Torr]. The extrapolation of Fig. 2(b) gives the frequency of the line corrected for the light and pressure shifts. This frequency is also

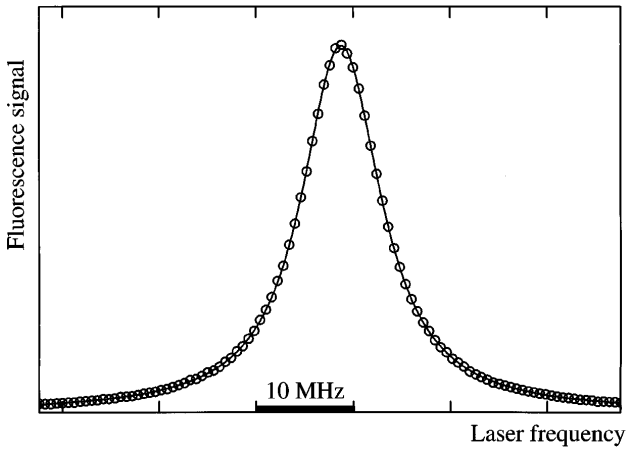

FIG. 1. Line shape of the 2^3S_1-3^3D_1 two-photon transition in ^{4}He. Optical power inside the Fabry-Pérot cavity is 11 W in each direction; the pressure in the cell is 0.151 Torr. The experimental points are fitted with a theoretical curve which takes into account the natural width, the pressure broadening, and the transit time broadening.

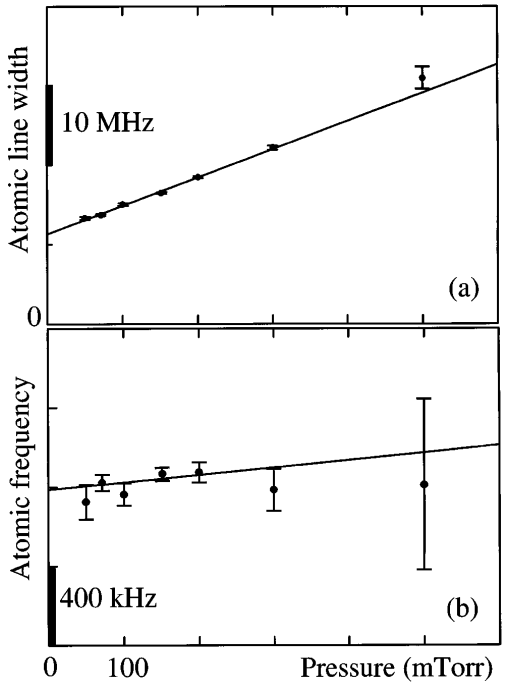

FIG. 2. Extrapolations of the Lorentzian width (a) and of the line position (b) versus the pressure.

shifted by the second order Doppler effect. At 300 K, the correction to the atomic frequency is about 8.1 kHz. Finally, the frequency of the 2^3S_1-3^3D_1 transition in ^{4}He is 786 823 850.002(56) MHz. This uncertainty arises from the interferometric measurement (28 kHz) and the statistics of the extrapolations (in optical power and pressure) of the line center (48 kHz). This result is in good agreement with a previous measurement of the 2^3S_1-3^3D_3 transition [786 822 451(13) MHz [16]] using the theoretical value of the 3^3D_1-3^3D_3 fine structure splitting [1 400.455(24) MHz] given in Ref. [7].

Using the theoretical value of the 3^3D_1 ionization energy [366 018 892.857(20) MHz from Refs. [7,9] after correction of the recent value of the Rydberg constant [3]], we obtain the ionization energy of the 2^3S_1 level. By subtracting the nonrelativistic energy, the first relativistic corrections and the finite nuclear size correction calculated in Ref. [7] for the 2^3S_1 state [1 152 846 800.135(3) MHz after correction for the Rydberg constant], we can deduce the 2^3S_1 Lamb shift. We obtain the value $L(2^3S_1) = 4057.276(60)$ MHz. The uncertainty is essentially due to the experimental determination of the two-photon frequency. Contributions to this uncertainty are listed in Table I. Our precision surpasses by more than 2 orders of magnitude that of the theoretical prediction [4062.3(8.0) MHz]. This result should stimulate new developments on the theoretical side. We compare our result to previous measurements in Fig. 3, where we have extracted the Lamb shift values from other measurements by using the theoretical predictions and the conservative uncertainties given in Ref. [9]. Our result, 10 times more precise, is in very good agreement with the latest measurement made by Inguscio *et al.* [4057.61(79) MHz] [13]. Our measurement is also in good agreement with the precise result deduced from the 2^3S_1-2^3P_0 and 2^3P_0-3^3D_1 measurements [4056.7(9) MHz] [12,17].

TABLE I. Uncertainty budget of the Lamb shift determination.

Frequency determination (experimental)	56 kHz
Lamb shift of the 3^3D_1 level (theoretical)	20 kHz
Nuclear size	3 kHz
Uncertainty in Rydberg constant	8 kHz
Overall uncertainty	60 kHz

We can also combine our measurement with various measurements starting from the 2^3S_1 state to eliminate the uncertainty due to the 2^3S_1 Lamb shift and so get an accurate determination of the Lamb shift of the higher level. These results are presented in Table II. There is good agreement with the theoretical predictions, which are given with uncertainties from Ref. [9].

In conclusion, we have measured the frequency of 2^3S_1-3^3D_1 transition in ^{4}He with an uncertainty of 7.1×10^{-11}. The deduced 2^3S_1 Lamb shift is the most precise determination at the present time. The comparison between different precise measurements gives access to accurate values of other Lamb shifts. To complete these

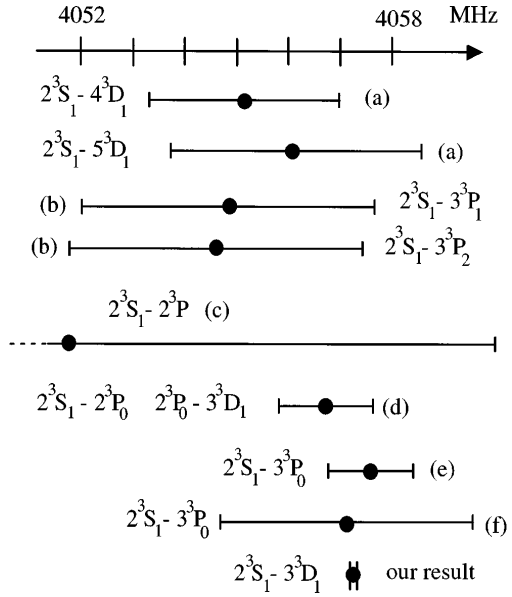

FIG. 3. Comparison of 2^3S_1 Lamb shift deduced from our result and recent high precision measurements in ^{4}He with the theoretical calculations from Ref. [9]: (a) Ref. [17], (b) Ref. [11], (c) Ref. [12], (d) Refs. [12,17], (f) Ref. [13]. (e) corresponds to Ref. [13] using the theoretical values from Ref. [7].

TABLE II. Comparison with other transitions.

2^3S_1-3^3D_1 combined with	Deduced Lamb shift	Theoretical predictions[e]
2^3S_1-3^3P_1[a]	$L(3^3P_1) = -357.3(1.5)$ MHz	$L(3^3P_1) = -359.7(2.4)$ MHz
2^3S_1-3^3P_2[a]	$L(3^3P_2) = -356.6(1.5)$ MHz	$L(3^3P_2) = -359.7(2.4)$ MHz
2^3S_1-3^3P_0[b]	$L(3^3P_0) = -359.51(20)$ MHz	$L(3^3P_0) = -359.7(2.4)$ MHz
2^3S_1-4^3D_1[c]	$L(4^3D_1) = -10.1(1.8)$ MHz	$L(4^3D_1) = -7.887(10)$ MHz
2^3S_1-5^3D_1[c]	$L(5^3D_1) = -5.4(2.4)$ MHz	$L(5^3D_1) = -4.224(6)$ MHz
2^3S_1-2^3P[d]	$L(2^3P) = -1253.9(1)$ MHz	$L(2^3P) = -1259.5(8.0)$ MHz

[a]Ref. [11].
[b]Ref. [13].
[c]Ref. [17].
[d]Ref. [12].
[e]Ref. [9].

data, we plan to make a pure frequency measurement of the 2^3S_1-4^3D_1 two photon transition in ^{4}He thanks to the coincidence between the excitation laser frequency and that of the $HeNe/I_2$ standard (the frequency difference is only $\Delta\nu = 112$ GHz). The same technique frequency scheme could also be applied to measure the 2^1S_0-16^1D transition in ^{4}He ($\Delta\nu \approx 130$ GHz).

The authors thank M. Inguscio for stimulating discussions, P. Indelicato for much theoretical advice, and M. D. Plimmer for a critical reading of the manuscript. This work is partially supported by the Bureau National de Métrologie.

*Present address: Laboratoire d'Optique Appliquée, CNRS URA 1406, ENSTA-Ecole Polytechnique, 91120 Palaiseau, France.

[1] K. Pachucki *et al.*, J. Phys. B **29**, 177 (1996).
[2] S. G. Karshenboim, J. Phys. B **29**, L31 (1996).
[3] B. de Beauvoir *et al.*, Phys. Rev. Lett. **78**, 440 (1997).
[4] M. Weitz *et al.*, Phys. Rev. A **52**, 2664 (1995).
[5] D. J. Berkeland, E. A. Hinds, and M. B. Boshier, Phys. Rev. Lett. **75**, 2470 (1995).
[6] S. Bourzeix *et al.*, Phys. Rev. Lett. **76**, 384 (1996).
[7] G. W. F. Drake, *Long Range Casimir Forces: Theory and Recent Experiments on Atomic Systems*, edited by F. S. Levin and D. A. Micha (Plenum, New York, 1993).
[8] J. D. Baker *et al.*, Bull. Am. Phys. Soc. **38**, 1127 (1993).
[9] G. W. F. Drake in *Atomic, Molecular & Optical Physics Handbook*, edited by G. W. F. Drake (AIP, New York, 1996). In this reference, the theoretical uncertainties are more conservative than in Ref. [7].
[10] K. S. E. Eikema, W. Ubachs, W. Vassen, and W. Hogervorst, Phys. Rev. Lett. **76**, 1216 (1996).
[11] C. S. Adams, E. Riis, A. I. Ferguson, and W. R. C. Rowley, Phys. Rev. A **45**, 2667 (1992).
[12] D. Shiner, R. Dixson, and P. Zhao, Phys. Rev. Lett. **72**, 1802 (1994).
[13] F. S. Pavone, F. Marin, P. De Natale, M. Inguscio, and F. Biraben, Phys. Rev. Lett. **73**, 42 (1994). This value is deduced by using the theoretical calculations from Ref. [7]. With the new calculations from Ref. [9], the uncertainty increases and this result becomes 4057.1(2.4) MHz. These two values are shown in Fig. 3.
[14] D. Shiner, R. Dixson, and V. Vedantham, Phys. Rev. Lett. **74**, 3553 (1995).
[15] F. Marin *et al.*, Z. Phys. D **32**, 285 (1995).
[16] E. Giacobino and F. Biraben, J. Phys. B **15**, L385 (1982).
[17] L. Hlousek, S. A. Lee, and W. M. Fairbank, Phys. Rev. Lett. **50**, 328 (1983).
[18] W. Litchen, D. Shiner, and Zhi-Xiang Zhou, Phys. Rev. A **43**, 1663 (1991).
[19] S. Bourzeix, M. D. Plimmer, F. Nez, L. Julien, and F. Biraben, Opt. Commun. **99**, 89 (1993).
[20] J. C. Garreau, M. Allegrini, L. Julien, and F. Biraben, J. Phys. (Paris) **51**, 2263 (1990); **51**, 2275 (1990); **51**, 2293 (1990).
[21] D. Touahri *et al.*, Opt. Commun. **133**, 471 (1997).
[22] F. Nez, F. Biraben, R. Felder, and Y. Millerioux, Opt. Commun. **102**, 432 (1993).
[23] C. Bordé, C. R. Hebd. Séan. Acad. Sci. **282**, B341 (1976); F. Biraben, M. Bassini, and B. Cagnac, J. Phys. (Paris) **40**, 445 (1979).

Optical Frequency Measurement of the $2S$-$12D$ Transitions in Hydrogen and Deuterium: Rydberg Constant and Lamb Shift Determinations

C. Schwob, L. Jozefowski, B. de Beauvoir, L. Hilico,* F. Nez, L. Julien, and F. Biraben
Laboratoire Kastler Brossel, Ecole Normale Supérieure et Université Pierre et Marie Curie, Laboratoire associé au CNRS UMR 8552, 4 place Jussieu, Tour 12 E01, 75252 Paris Cedex 05, France

O. Acef and A. Clairon
Laboratoire Primaire du Temps et des Fréquences, Bureau National de Métrologie-Observatoire de Paris, 61 avenue de l'Observatoire, 75014 Paris, France
(Received 22 December 1998)

We have performed a pure optical frequency measurement of the $2S$-$12D$ two-photon transitions in atomic hydrogen and deuterium. From a complete analysis taking into account this result and all other precise measurements (by ourselves and other authors), we deduce optimized values for the Rydberg constant, $R_\infty = 109\,737.315\,685\,16(84)\ \mathrm{cm}^{-1}$ (relative uncertainty of 7.7×10^{-12}) and for the $1S$ and $2S$ Lamb shifts $L_{1S} = 8172.837(22)$ MHz and $L_{2S\text{-}2P} = 1057.8446(29)$ MHz [respectively, $L_{1S} = 8183.966(22)$ MHz, and $L_{2S\text{-}2P} = 1059.2337(29)$ MHz for deuterium]. These are now the most accurate values available. [S0031-9007(99)09458-2]

PACS numbers: 06.20.Jr, 21.10.Ft, 31.30.Jv

For many years, Doppler free two-photon spectroscopy has been applied to the hydrogen atom in order to test quantum electrodynamics calculations and to improve the precision of the Rydberg constant R_∞ [1]. Recently, the uncertainty of the measurements has been reduced to a level below 10^{-11} thanks to optical frequency-multiplication chains, which link the measured frequency via intermediate standard lasers to the caesium clock. With such a chain, Hänsch and co-workers have taken advantage of the small natural width of the $1S$-$2S$ two-photon transition (1.3 Hz) to measure this frequency with an uncertainty of 3.4×10^{-13} [2]. In our group, we have made absolute frequency measurements of the $2S$-$8S/D$ transitions with an accuracy better than 8×10^{-12} [3]. In this last case, the precision was limited by the line shape analysis which becomes complicated by a large broadening (up to 1 MHz) due to the inhomogeneous light shift. The comparison of the $1S$-$2S$ and $2S$-$8S/D$ measurements has provided very precise determinations of R_∞ and of the Lamb shift [2,3]. Nevertheless, in order to confirm our $2S$-$8S/D$ frequency measurements, we have built a new chain to measure the frequencies of another transition, that is the $2S$-$12D$ transition. This transition yields complementary information to our study of the $2S$-nS/nD transitions, because it is very sensitive to stray electric fields (the shift due to the quadratic Stark effect varies as n^7), and so such a measurement is a stringent test of Stark corrections to the Rydberg levels. In this Letter, we present these new results and make a complete analysis of the optical frequency measurements to determine the best values for R_∞ and the Lamb shifts.

Our new frequency chain uses two standard lasers, a laser diode stabilized on the $5S$-$5D$ two-photon transition of rubidium (LD/Rb laser, $\lambda = 778$ nm, $\nu = 385$ THz) and a CO_2 laser stabilized to an osmium tetraoxyde line (labeled CO_2/OsO_4, $\lambda \approx 10\ \mu$m, $\nu \approx 29$ THz). In 1996, the frequencies of three LD/Rb lasers, one in the Laboratoire Kastler Brossel (LKB) and two in the Laboratoire Primaire du Temps et des Fréquences (LPTF), were measured with a frequency chain which connected the LD/Rb laser to the CO_2/OsO_4 standard [4]. More recently, the frequency measurement of this CO_2/OsO_4 standard has been remade with respect to the Cs clock with an uncertainty of 20 Hz (i.e., a relative uncertainty of 7×10^{-13}) [5]. This last measurement corrects the previous one of the CO_2/OsO_4 standard by -87 Hz. With this correction, the frequency of the LD/Rb standard laser working at the LKB is 385 285 142 369.4(1.0) kHz. We have kept a conservative uncertainty of 1 kHz which takes into account the day-to-day repeatability and the long term stability of the LD/Rb standard and the accuracy of the CO_2/OsO_4 standard (13×20 Hz).

The frequency gap between the $2S$-$12D$ lines ($\lambda \approx 750$ nm, $\nu \approx 399.5$ THz) and the LD/Rb standard is almost equal to half of the CO_2/OsO_4 standard frequency. We have built an optical frequency divider to reduce this frequency by a factor of 2 [2,6]. The different parts of the experiment are carried out simultaneously at the LKB and LBTF (see Fig. 1). The two laboratories are linked by two, 3 km long, optical fibers which are used, via a phase coherent chain, to transfer the CO_2/OsO_4 frequency reference from LPTF to LKB. The frequency shift introduced by these optical fibers is at most 3 Hz [7]. We use an auxiliary laser at 809 nm ($\nu \approx 370.5$ THz) and the laser frequencies satisfy the equations,

$$\nu(2S\text{-}12D) + \nu(809) = 2\nu_{\mathrm{Rb}},$$
$$\nu(2S\text{-}12D) - \nu(809) = \nu(\mathrm{CO_2}).$$

 0031-9007/99/82(25)/4960(4)$15.00

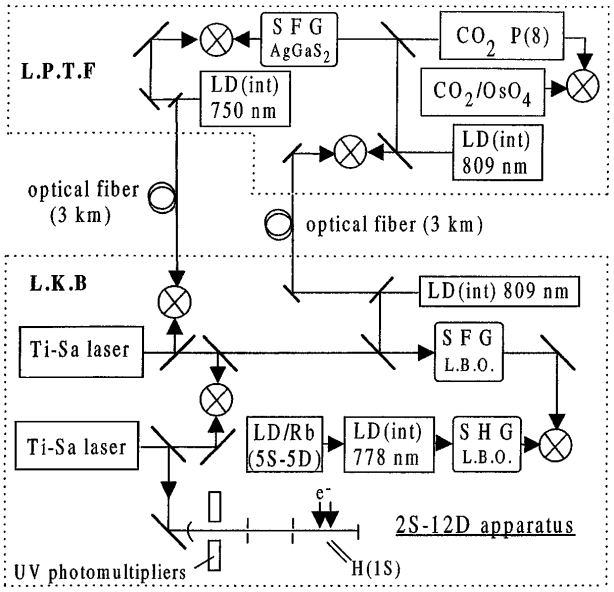

FIG. 1. Outline of the frequency chain between the $2S$-$12D$ hydrogen frequencies and the LD/Rb and CO_2/OsO_4 standards. The details are explained in the text.

A laser diode (power of 50 mW) is injected by the LD/Rb standard at 778 nm and frequency doubled in a LiB_3O_5 (LBO) crystal placed in a ring cavity. The generated UV beam is frequency compared to the frequency sum (made also in an LBO crystal) of the 750 and 809 nm radiations produced by a first titanium-sapphire laser (about 300 mW) and a laser diode (about 30 mW). One part of the 809 nm radiation is sent via one fiber to the LPTF. There, a 809 nm local laser diode is phase locked on the LKB one. A frequency sum of this 809 nm laser diode and of an intermediate CO_2 laser in an $AgGaS_2$ crystal generates a wave at 750 nm. This wave is used to phase lock a laser diode at 750 nm which is sent back to the LKB by the second fiber. In such a way, the two equations are simultaneously satisfied and all the frequency counting is performed in the LKB. A second titanium-sapphire laser induces the two-photon transitions. For the hydrogen measurements, the CO_2 intermediate laser uses the $P(8)$ line [respectively, CO_2 $R(4)$ line for deuterium], and the residual frequency difference between the two titanium-sapphire lasers is about 2.5 GHz (respectively, 41.3 GHz for deuterium). These frequency beat notes are detected with a photodiode or a Schottky diode.

The hydrogen experiment has been described elsewhere [3,8]. To reduce the collisional and transit time broadening, the two-photon transitions are induced in a metastable atomic beam collinear with the laser beams. We use a highly stable titanium-sapphire laser with a frequency jitter and a long term stability of a few kHz [9]. Thanks to an enhancement cavity surrounding the atomic beam, the optical power can be as much as 50 W in each direction with a beam waist of 646 μm. At the end of the atomic beam, an electric field quenches the metastable atoms and we detect the Lyman-α fluorescence to measure the metastable yield. As the excited $12D$ states decay preferentially to the $1S$ ground state in a proportion of 95%, the optical excitation can be detected via the corresponding decrease of the $2S$ beam intensity. The acquisition and analysis of the experimental data follow the same procedure as in Ref. [8]. To evaluate the light shift, which is the major source of shift and broadening, we record the atomic signal for different laser intensities, and we extrapolate the line position to zero light power. For each recording, a theoretical profile is fitted to the experimental curve. This theoretical line shape takes into account the light shift, the saturation of the transition, the small hyperfine structure of the $12D$ levels, the photoionization, the small deviation of the atomic trajectories due to the light forces, as well as the second-order Doppler shift. The velocity distribution is measured by monitoring the Doppler shifted $2S$-$6P$ transition. Each fit gives both the experimental line center and the line position corrected for light shift and hyperfine structure of the $12D$ level. As we measure continuously the various beat frequencies of our frequency chain, we can deduce the absolute frequency of the line. Finally, the result is corrected for the shift due to black-body radiation (2.1 kHz for the $12D$ levels at 330 K [10]) and for the Stark shift due to stray electric fields. To evaluate these fields, we have studied the $2S$-$20D$ transitions. In this case, the broadening due to the linear Stark effect is large (it varies as n^2) and, from the line shape of the $2S$-$20D$ transitions, we deduce a mean value of the stray electric fields of 2.0 (1.0) mV/cm. A careful analysis of the Stark effect, including the mixing of the quasidegenerate levels ($D_{5/2}$-$F_{5/2}$ and $D_{3/2}$-$P_{3/2}$), gives a Stark shift of -2.1 (1.2) kHz and -6.0 (4.9) kHz for the $12D_{5/2}$ and $12D_{3/2}$ levels.

We have studied the $2S_{1/2}(F = 1 \text{ or } 3/2)$-$12D_{5/2}$ and $2S_{1/2}(F = 1 \text{ or } 3/2)$-$12D_{3/2}$ transitions in hydrogen and deuterium. For each transition, the atomic signal is recorded for at least 50 light powers, and, in total, we have used 237 runs (20 min long) for data collection. The measured frequencies (after correction of the hyperfine structures) are reported in Table I. The quoted uncertainties are due only to the statistics. The two experimental results for the $12D_{5/2}$ and $12D_{3/2}$ levels can be compared by taking into account the theoretical value of the fine structure and the Lamb shift of the $12D$ levels. Following recent calculations of the Bethe logarithm [11], these Lamb shifts are $L_{12D_{3/2}} = -17.6(2)$ kHz and $L_{12D_{5/2}} = 21.5(2)$ kHz in hydrogen and deuterium. Finally, we obtain two independent values of the $2S_{1/2}$-$12D_{5/2}$ interval (see Table I) which are in fair agreement for hydrogen and deuterium. The average values are, respectively, 799 191 727 402.8(6.7) kHz and 799 409 184 967.6(6.5) kHz. These uncertainties (1 standard deviation) are due to the statistical error, the

TABLE I. Frequencies of the $2S$-$12D$ two-photon transitions.

Transition	Measured frequency (MHz)	$2S_{1/2}$-$12D_{5/2}$ Deduced frequency (MHz)
Hydrogen		
$2/S_{1/2}$-$12D_{5/2}$	799 191 727.4037 (47)	799 191 727.4037
$2S_{1/2}$-$12D_{3/2}$	799 191 710.4727 (62)	799 191 727.3999
Mean value of the $2S_{1/2}$-$12D_{5/2}$ measurements:		799 191 727.4028 (67)
Deuterium		
$2/S_{1/2}$-$12D_{5/2}$	799 409 184.9668 (45)	799 409 184.9668
$2S_{1/2}$-$12D_{3/2}$	799 409 168.0380 (44)	799 409 184.9698
Mean value of the $2S_{1/2}$-$12D_{5/2}$ measurements:		799 409 184.9676 (65)

Stark effect (2.1 kHz), the second-order Doppler effect (1 kHz), the stability and the measurement of the LD/Rb standard laser (2 kHz), and the imperfections of the theoretical model (4.5 kHz). These measurements are slightly less precise than our previous ones of the $2S$-$8S/D$ transitions [3,12], because of the smaller signal-to-noise ratio and the larger quadratic Stark effect.

Table II gives the values of the Rydberg constant deduced from different transitions by several methods. It is convenient to express an energy level in hydrogen as the sum of two terms: the first, given by the Dirac equation and by the first relativistic correction due to the recoil of the proton, is known exactly, apart from the uncertainties in the physical constants involved (mainly R_∞). The second term is the Lamb shift, which contains all the other corrections, i.e., the QED corrections, the other relativistic corrections, and the effect of the proton charge distribution. Consequently, to extract R_∞ from the accurate measurements one needs to know the Lamb shifts. For this analysis, the theoretical values of the Lamb shifts are sufficiently precise, except for those of the $1S$ and $2S$ levels. In hydrogen, there have been several precise determinations of the $2S_{1/2}$-$2P_{1/2}$ splitting by microwave spectroscopy [13] and by the anisotropy method [14]. Using the mean value of these results [$L_{2S\text{-}2P} = 1057.8454(65)$ MHz], we can deduce from our $2S_{1/2}$-$12D_{5/2}$ determination a value of the Rydberg constant $R_\infty = 109\,737.315\,684\,5(13)$ cm^{-1}. The uncertainty (1.2×10^{-11}) comes from the frequency measurement (8.4×10^{-12}), the $2S$ Lamb shift (8.1×10^{-12}), and the proton-to-electron mass ratio (1.3×10^{-12}) [15]. To compare our present result with our earlier one [3], Table II gives the Rydberg constant value deduced from the $2S$-$8D$ measurement with the same procedure. These two values are in acceptable agreement (they differ by about 1 standard deviation). Although slightly less precise, our new result confirms our previous one and shows that the correction due to the quadratic Stark effect is well analyzed (this correction is 17 times larger for the $12D$ than for the $8D$ levels). Table II gives the average of these two results with an uncertainty of 10^{-11}. This result is the most precise if we do not make theoretical assumptions concerning the $1S$ and $2S$ Lamb shifts.

The other methods to determine R_∞ use the $1/n^3$ scaling law of the Lamb shift which gives the theoretical value of the linear combination of the Lamb shifts

TABLE II. Determination of the Rydberg constant R_∞.

Method and transitions involved	$(R_\infty - 109737)$ cm^{-1}
Determination of R_∞ from the $2S$-nD and $2S$-$2P$ measurements	
$2S$-$12D$ and $2S$-$2P$ in hydrogen	0.315 6845 (13)
$2S$-$8D$ and $2S$-$2P$ in hydrogen	0.315 6858 (13)
$2S$-$12D$, $2S$-$8D$, and $2S$-$2P$ in hydrogen	0.315 6852 (11)
Determination of R_∞ without the $2S$-nS/D measurements	
$1S$-$2S$, $2S$-$2P$, and $1/n^3$ law in hydrogen	0.315 6854 (20)
Determination of R_∞ from linear combination of optical frequencies measurements	
$2S$-$12D$, $1S$-$2S$, and $1/n^3$ law in hydrogen	0.315 6838 (17)
$2S$-$12D$, $1S$-$2S$, and $1/n^3$ law in deuterium	0.315 6838 (16)
$2S$-$12D$, $1S$-$2S$, and $1/n^3$ law in hydrogen and deuterium	0.315 6838 (13)
$2S$-$8D$, $1S$-$2S$, and $1/n^3$ law in hydrogen and deuterium	0.315 6861 (12)
$2S$-$8D$, $2S$-$12D$, $1S$-$2S$, and $1/n^3$ law in hydrogen and deuterium	0.315 685 0 (10)
General least squares adjustment in hydrogen and deuterium	0.315 685 16 (84)

L_{1S}-$8L_{2S}$ [16]. Using this relation and the measurements of the $2S$ Lamb shift, it is possible to extract a value of R_∞ from the very precise measurement of the $1S$-$2S$ transition [2]. The result, independent of our $2S$-nD measurements, is given in the second part of Table II and agrees perfectly with the value deduced from the $2S$-nD frequencies.

Finally, in the third part of Table II, we give the values of R_∞ obtained from the linear combination of several optical frequencies. For example, if we consider the frequencies $\nu_{1S\text{-}2S}$ and $\nu_{2S\text{-}12D}$ of the $1S$-$2S$ and $2S$-$12D$ intervals, we can form the linear combination $7\nu_{2S\text{-}12D}$-$\nu_{1S\text{-}2S}$, where the theoretically well-known quantity L_{1S}-$8L_{2S}$ appears. This method is independent of the microwave measurements of the $2S$ Lamb shift and is relevant for both hydrogen and deuterium. If we consider the $1S$-$2S$ and $2S$-$12D$ transitions, the values obtained for hydrogen and deuterium are in excellent agreement (see Table II). With a least squares procedure, it is possible to apply this method to several transitions. If we use all the precise optical frequency measurements in hydrogen and deuterium (transitions $1S$-$2S$, $2S$-$8D$, and $2S$-$12D$), we obtain a value of R_∞ more precise than the previous ones. This method also provides very accurate determination of the $1S$ and $2S$ Lamb shifts, $L_{1S} = 8172.834(26)$ MHz and $L_{2S\text{-}2P} = 1057.8442(34)$ MHz [respectively, 8183.963(26) MHz and 1059.2333(34) MHz for deuterium]. This result for the $2S$ Lamb shift is independent and more precise than the direct determinations made by microwave spectroscopy.

To make an average of these various determinations of R_∞, we have performed a least squares adjustment which takes into account the measurements of the $2S$ Lamb shift [13,14], the optical frequency measurements of the $1S$-$2S$ [2], $2S$-$8D$ [3], and $2S$-$12D$ transitions in hydrogen and deuterium, and also the measurements of the $1S$ Lamb shift made by frequency comparison of the $1S$-$2S$ and $2S$-$4S/P/D$ transitions [17,18] or of the $1S$-$3S$ and $2S$-$6S/D$ ones [19]. We obtain the values $R_\infty = 109\,737.315\,685\,16(84)$ cm^{-1}, $L_{1S} = 8172.837(22)$ MHz, and $L_{2S\text{-}2P} = 1057.8446(29)$ MHz [respectively, 8183.966(22) MHz and 1059.2337(29) MHz for deuterium]. These values, which take into account all the most recent results, are the most precise to date. The $1S$ Lamb shift value is in poor agreement with the more recent calculation in hydrogen [$L_{1S} = 8172.731(40)$ MHz with the proton radius $r_p = 0.862(12)$ fm [20]]. Assuming the validity of these QED calculations, we deduce $r_p = 0.900(16)$ fm.

To conclude, we have made an optical frequency measurement of the $2S$-$12D$ transition in hydrogen and deuterium. This result confirms our previous work on the $2S$-$8S/D$ transitions and, furthermore, we have reduced the uncertainty in the Rydberg constant to less than 7.7×10^{-12}. We present also an exhaustive analysis of the most accurate measurements in hydrogen and deuterium which shows that the optical frequency measurements have superseded the microwave determination of the $2S$ Lamb shift. The precision is now limited by the uncertainties of the $2S$-nD frequencies.

The authors are indebted to B. Cagnac for many stimulating discussions, and they thank M. D. Plimmer for critical reading of the manuscript. This work is partially supported by the Bureau National de Métrologie.

*Affiliated with Université d'Evry Val d'Essonne, France.

[1] See, for example, B. Cagnac, M. D. Plimmer, L. Julien, and F. Biraben, Rep. Prog. Phys. **57**, 853 (1994).
[2] Th. Udem *et al.*, Phys. Rev. Lett. **79**, 2646 (1997); A. Huber *et al.*, Phys. Rev. Lett. **80**, 468 (1998).
[3] B. de Beauvoir *et al.*, Phys. Rev. Lett. **78**, 440 (1997).
[4] D. Touahri *et al.*, Opt. Commun. **133**, 471 (1997).
[5] G. D. Rovera and O. Acef, IEEE Trans. Instrum. Meas. (to be published).
[6] H. R. Telle, D. Meschede, and T. W. Hänsch, Opt. Lett. **15**, 532 (1990).
[7] B. de Beauvoir *et al.*, Eur. Phys. J. D **1**, 227 (1998).
[8] J. C. Garreau, M. Allegrini, L. Julien, and F. Biraben, J. Phys. (Paris) **51**, 2263 (1990); **51**, 2275 (1990); **51**, 2293 (1990).
[9] S. Bourzeix, M. D. Plimmer, F. Nez, L. Julien, and F. Biraben, Opt. Commun. **99**, 89 (1993).
[10] J. W. Farley and W. H. Wing, Phys. Rev. A **23**, 2397 (1981).
[11] G. W. F. Drake and R. A. Swainson, Phys. Rev. A **41**, 1243 (1990).
[12] We have remade the analysis of our $2S$-$8S/D$ measurements to take into account the improvements of the theoretical line shapes and the corrections due to the standard laser, the black-body radiation, and the Stark effect. With the same more conservative uncertainties, the results are $\nu(2S_{1/2}\text{-}8D_{5/2}) = 770\,649\,561\,581.1(5.9)$ kHz and $\nu(2S_{1/2}\text{-}8D_{5/2}) = 770\,859\,252\,848.3(5.5)$ kHz for hydrogen and deuterium.
[13] S. R. Lundeen and F. M. Pipkin, Phys. Rev. Lett. **46**, 232 (1981); E. W. Hagley and F. M. Pipkin, Phys. Rev. Lett. **72**, 1172 (1994); U. Jentschura and K. Pachucki, Phys. Rev. A **54**, 1853 (1996).
[14] A. van Wijngaarden, F. Holuj, and G. W. F. Drake, Can. J. Phys. **76**, 95 (1998).
[15] D. L. Farnham, R. S. Van Dyck, and P. B. Schwinberg, Phys. Rev. Lett. **75**, 3598 (1995).
[16] S. G. Karshenboim, Z. Phys. D **39**, 109 (1997).
[17] M. Weitz *et al.*, Phys. Rev. Lett. **72**, 328 (1994).
[18] D. J. Berkeland, E. A. Hinds, and M. G. Boshier, Phys. Rev. Lett. **75**, 2470 (1995).
[19] S. Bourzeix *et al.*, Phys. Rev. Lett. **76**, 384 (1996).
[20] S. Mallampalli and J. Sapirstein, Phys. Rev. Lett. **80**, 5297 (1998).

Eur. Phys. J. D **12**, 61–93 (2000)

THE EUROPEAN PHYSICAL JOURNAL D

EDP Sciences

Metrology of the hydrogen and deuterium atoms: Determination of the Rydberg constant and Lamb shifts

B. de Beauvoir[1], C. Schwob[1], O. Acef[2], L. Jozefowski[1], L. Hilico[1,a], F. Nez[1], L. Julien[1], A. Clairon[2], and F. Biraben[1,b]

[1] Laboratoire Kastler Brossel, École Normale Supérieure et Université Pierre et Marie Curie[c], 4 place Jussieu, 75252 Paris Cedex 05, France

[2] Laboratoire Primaire du Temps et des Fréquences, Bureau National de Métrologie-Observatoire de Paris, 61 avenue de l'Observatoire, 75014 Paris, France

Received 9 March 2000

Abstract. We present a detailed description of several experiments which have been previously reported in several letters: the determination of the 1S Lamb shift in hydrogen by a comparison of the frequencies of the 1S–3S and 2S–6S or 2S–6D two-photon transitions, and the measurement of the 2S–8S/D and 2S–12D optical frequencies. Following a complete study of the lineshape of the two-photon transitions, we provide the updated values of these frequencies which have been used in the 1998 adjustment of the fundamental constants. From an analysis taking into account these results and several other precise measurements by other authors, we show that the optical frequency measurements have superseded the microwave determination of the 2S Lamb shift and we deduce optimized values for the Rydberg constant, $R_\infty = 109\,737.315\,685\,50(84)$ cm^{-1} (relative uncertainty of 7.7×10^{-12}) and for the 1S and 2S Lamb shifts $L(1S) = 8\,172.840(22)$ MHz and $L(2S–2P) = 1\,057.8450(29)$ MHz (respectively, 8 183.970(22) MHz and 1 059.2341(29) MHz for deuterium). These are now the most accurate values available.

PACS. 06.20.Jr Determination of fundamental constants – 21.10.Ft Charge distribution – 31.30.Jv Relativistic and quantum electrodynamic effects in atoms and molecules

1 Introduction

Over the past two decades the absolute measurement of wavelengths or frequencies of hydrogen has been continuously improved with the aim of determining the Rydberg constant and testing quantum electrodynamics calculations. With the interferometric measurements, the relative accuracy was in the range of one part in 10^{10}. A review of these results is provided in reference [1]. Recently, the interferometric measurements have been superseded by accurate optical frequency ones. The latter make use of frequency-multiplication chains which link the measured frequency, *via* intermediate standard lasers, to the caesium clock. With this method, Hänsch and collaborators have measured the optical frequency of the 1S–2S two-photon transition with an accuracy better than 3.4×10^{-13} [2,3]. In our group, we have studied the 2S–nS and 2S–nD two-photon transitions. In 1993, we measured the optical frequencies of the $2S_{1/2}$–$8S_{1/2}$, $2S_{1/2}$–$8D_{3/2}$ and $2S_{1/2}$–$8D_{5/2}$ transitions in hydrogen with a frequency chain using two standard lasers (the iodine stabilized and the methane stabilized helium-neon lasers) and obtained a precision in the range of 10^{-11} [4,5]. In 1996, we remade these measurements in hydrogen and deuterium with an accuracy better than one part in 10^{11} [6]. We used a new frequency chain with a new standard laser, namely a diode laser at 778 nm stabilized on the 5S–5D two-photon transition of rubidium (LD/Rb laser). The frequency of this standard was measured with a frequency chain at the *Laboratoire Primaire du Temps et des Fréquences* (LPTF) [7]. More recently, in order to check these 2S–8S/D frequency measurements, we have built a new chain to measure the frequencies of the 2S–12D transitions in hydrogen and deuterium [8]. In parallel, we have taken advantage of our experimental setup on the 2S–nS/D transitions to deduce the Lamb shift of the 1S level *via* a comparison of the frequencies of the 1S–3S and 2S–6S/D transitions [9].

The aim of this paper is to relate in detail these experiments. Section 2 describes our apparatus for the observation of the 2S–nS and 2S–nD transitions, which is the corner stone of our hydrogen experiments. The Doppler free two-photon transitions, in the range 750–820 nm, are induced by a highly stable titanium-sapphire laser. To reduce the transit time broadening, we use an atomic beam colinear with the laser beam. Section 3 is devoted to the line shape analysis of the 2S–nS/D transitions. We follow

[a] Affiliated with Université d'Évry Val d'Essonne, France.

[b] e-mail: biraben@spectro.jussieu.fr

[c] Laboratoire associé au CNRS, UMR 8552.

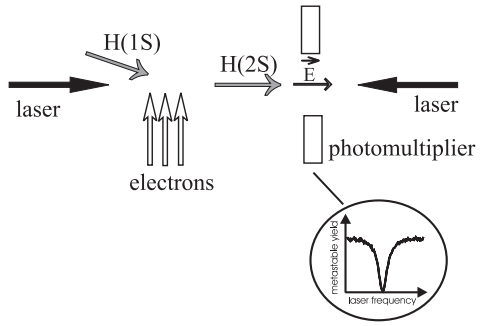

Fig. 1. Experimental geometry of laser and atom beams to observe the 2S–nS and 2S–nD two-photon transitions. When the laser frequency is scanned over the resonance, we observe a decrease of the metastable yield (see the inset).

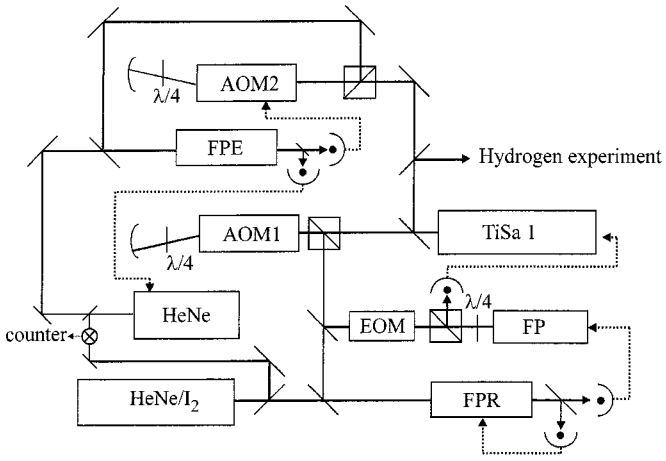

Fig. 2. Experimental setup for the frequency stabilisation of the titanium-sapphire laser. The explanations are given in the text (TiSa1: titanium-sapphire laser, HeNe/I_2: iodine stabilized helium-neon laser, He–Ne: auxiliary helium-neon laser, AOM1 and AOM2: acousto-optic modulators, EOM: electro-optic modulator, FP, FPR and FPE: Fabry-Perot cavities).

the same procedure as in our previous work [10–12]. We calculate the two-photon transition probability for a single atom and average over all the possible trajectories. In our recent calculations, we have taken into account the small hyperfine structure of the D levels, photoionisation effects, the small deviation of the atomic trajectories due to the light forces, as well as the second-order Doppler effect. We present the data analysis procedure and calculate the corrections due to stray electric fields. The optical frequency measurements are presented in Section 4. We describe the rubidium optical frequency standard and the various frequency chains used to measure the 2S–8S/D and 2S–12D transitions. Finally, we give the up-to-date results, which take into account the best line shape analysis and the most recent measurements of the optical frequency standards. The comparison of the 1S–3S and 2S–6S/D frequencies is described in Section 5. Finally, in Section 6, we analyse all these results to deduce the Rydberg constant and the Lamb shifts of the 1S and 2S levels. We show that the optical frequency measurements have superseded the radiofrequency measurements of the 2S Lamb shift and, using a least squares procedure which takes into account all the precise measurements in hydrogen and deuterium, we deduce a value of the Rydberg constant with a relative uncertainty of 7.7×10^{-12}.

2 Spectroscopy of the 2S–nS and 2S–nD transitions

2.1 Method

The principle of the experiment has been described previously [10]. The experimental geometry is illustrated in Figure 1. A metastable atomic beam is formed by electronic excitation of a 1S hydrogen atomic beam. Due to the inelastic collision with the electron, the atomic trajectory is deviated by an angle of about 20°. We use this deviation to make colinear, after the collision, the 2S atomic beam with the laser beams. At the end of the atomic beam we monitor the metastable yield: an electric field quenches the metastable state and we detect the Lyman-α fluorescence. When the laser frequency is in resonance with the 2S–nS/D transition, the atoms in the nS or nD states undergo a radiative cascade towards the 1S state in a proportion of about 95%. It occurs an optical quenching of the metastable level before the detection region and the optical excitation can be detected *via* the corresponding decrease of the 2S beam intensity (see Fig. 1).

2.2 Laser source

To induce the optical excitation, we use a home-made titanium-sapphire laser which has been described previously [13]. With a pump power of 13 W (from a Spectra-Physics 2030 argon ion laser), the single frequency output power is about 2 W at 800 nm. For some experiments [4,5, 8], we use a second titanium-sapphire laser with the same pump laser and the available power is reduced to about 1 W. For the high-resolution hydrogen spectroscopy, we require a narrow laser bandwidth and a good long term frequency stability. The frequency stabilisation set-up is shown in Figure 2. The short term and long term stability are assured with two Fabry-Perot cavities, labelled FP and FPR respectively. The principle of this stabilisation arrangement is to lock the titanium-sapphire laser on the FP cavity, the FP cavity to the FPR cavity and, finally, the FPR cavity to an iodine stabilized helium-neon laser. A secondary laser beam from the titanium-sapphire laser is splitted after a double pass through an acousto-optic modulator (model 3200 from Crystal Technology at 200 MHz, labelled AOM1 in Fig. 2) and sent on the FP and FPR cavities. The FP cavity (free spectral range 600 MHz and finesse of about 400) is placed in a robust vacuum box (wall thickness of 2 cm) and carefully isolated from the external vibrations[13]. To reduce the frequency jitter, the laser is locked, in a first step, on the FP cavity. We use an FM sideband method [14]: the laser beam sent in the FP cavity is phase modulated at about

15 MHz with an electro-optic modulator (Gsänger PM25, labelled EOM in Fig. 2). From the modulation detected on the beam reflected by the FP cavity, we extract an error signal which controls the piezoelectric and electro-optic transducers monitoring the length of the laser cavity. Thanks to this servo-loop, the frequency jitter is reduced from 500 kHz (free running laser) to about 2 kHz [13].

The long term stability is guaranteed by the reference Fabry-Perot cavity FPR. This cavity is very stable. It consists of a 50 cm long zerodur spacer and two silver coated mirrors, one flat and one spherical (60 cm curvature radius). Its finesse is about 75 at 633 nm and 120 at 800 nm. A piezoelectric transducer (PZT) moves the flat mirror thanks to a mechanical construction (made in fused silica) which avoid the rotation of the mirror (the principle is to deform a parallelogram) [15]. This cavity is also placed in a vacuum box with the same design that for the FP cavity. To obtain the long term stability, the FPR cavity is irradiated simultaneously by an iodine stabilized helium-neon laser and a part of the titanium-sapphire laser (after the double pass in the acousto-optic modulator). A first servo-loop locks the FPR length to the helium-neon wavelength (we use the 10 kHz frequency modulation of the helium-neon laser). As the zerodur spacer is very stable, we have always used, since ten years, the same fringes of the FPR cavity (1 580 868 or 1 580 869 following the PZT voltage). The length of the FPR cavity is also modulated (frequency of about 4.2 kHz). This modulation is detected on the transmission of the titanium-sapphire laser and a second servo-loop locks the length of the FP cavity to the FPR cavity. To scan the laser frequency, we sweep the frequency of the radiofrequency wave which drives the acousto-optic modulator. With this arrangement, the lengths of the two FP and FPR cavities are fixed and the commutation time of the laser frequency is only limited by the bandwidth of the first servo-loop on the FP cavity (about 50 kHz). An other advantage of this system with two cavities is that the accuracy is given by the servo-loop on the FPR cavity. This accuracy is better than the accuracy of the first servo-loop on the FP cavity for two reasons: (i) the modulation of the FPR cavity is small (about 10% of the cavity bandwidth) and the error signal is less perturbated by the transverse modes of the FPR cavity which appear when the laser beam is not perfectly mode matched on the cavity, (ii) the transmission signal of the cavity is an Airy function which has approximatively a symmetric Lorentzian profile. It is not the case for the servo-loop on the FP cavity which is made with the reflected beam by the cavity. In this case, the profile of the resonance of the cavity can be dissymetric because of the losses of the mirrors (it is the sum of an absorption and a dispersion shapes due to the phase shift between the first reflection on the input mirror and the beam which comes out of the cavity) [15].

Thanks to our optical frequency measurements (see Sect. 4), we have tested the metrological features of this laser system. For instance, we have very often measured the optical frequency of the fringe 1 286 174 of the FPR cavity which is close to the 2S–8S/D two-photon transition

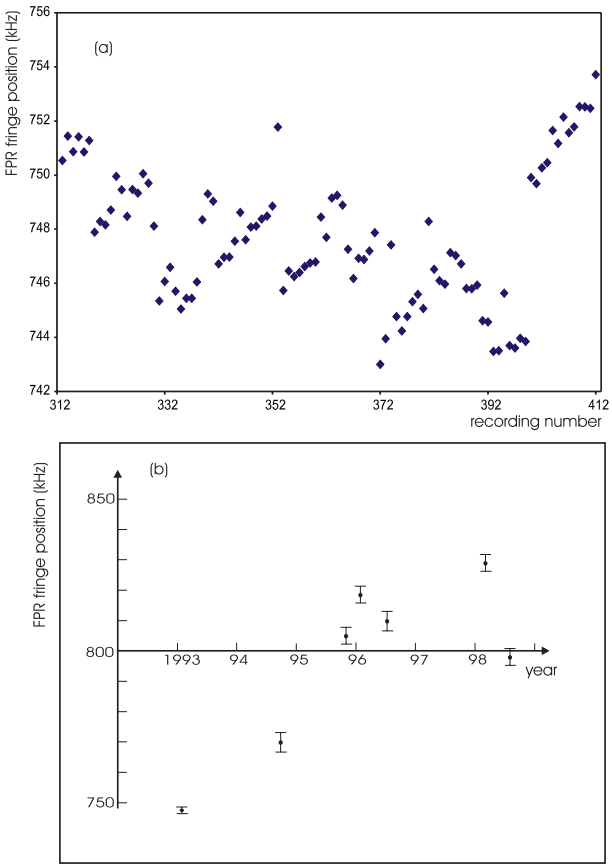

Fig. 3. Absolute frequency of the fringe 1 286 174 of the FPR cavity when the fringe 1 580 868 is locked to the d line of the iodine stabilized He–Ne laser. The values are in kHz and we have subtracted 385 325 GHz. (a) Measurements made in 1993: each point is the value obtained during a 20 minutes recording of the 2S–8S/D transitions in hydrogen. The measurements were made during about two weeks. The mean value is 385 325 000 747.7(2.5) kHz. (b) Drift of the fringe frequency on the period 1993–1998.

in hydrogen. The results are reported in Figures 3a and 3b. Figure 3a shows a series of measurements made in 1993 [5]. Each point is the mean of a 20 minutes recording (see Sect. 2.3). The standard deviation of these data is about 2.5 kHz, *i.e.* a day-to-day stability of 7×10^{-12}. Figure 3b shows the results since several years. During five years, we have observed a frequency drift of about 100 kHz which is perhaps due to an aging of the silver coating.

We use also several other interferometers to control the wavelength of the laser: a lambdameter (typical accuracy 10^{-3} nm), a 3 cm Fabry-Perot cavity (placed in a vacuum box and scanned by pressure variation) and an other, 50 cm long, Fabry-Perot cavity (labelled FPE in Fig. 2). This cavity has the same design that the FPR cavity, except that there is no PZT. To know the length of the FPE cavity, an auxiliary He–Ne laser is locked on a fringe of this cavity and we measure the beat frequency between the two He–Ne lasers. Simultaneously, a secondary beam of the titanium-sapphire laser is sent on the FPE cavity after a double pass in an acousto-optic modulator (labelled AOM2 in Fig. 2). The frequency of this AOM

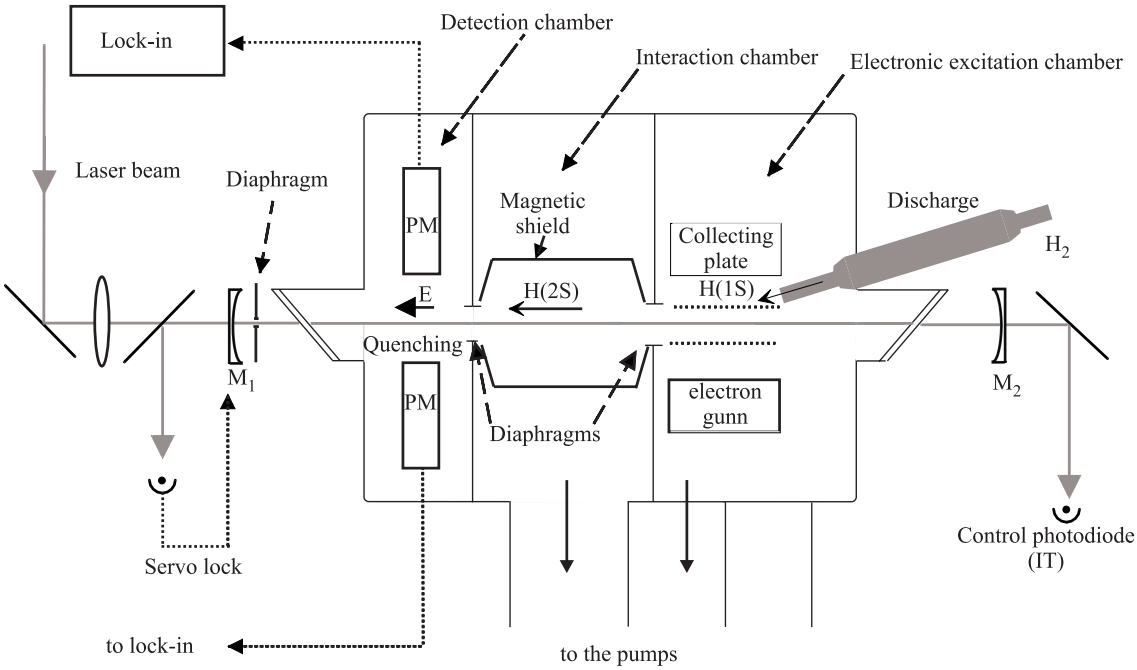

Fig. 4. The metastable hydrogen atomic beam. The three vacuum chambers are not sketched with the same scale: following the laser beams axis, the sizes of the electronic excitation chamber, interaction chamber and detection chamber are respectively 10 cm, 56 cm and 7 cm. M1 and M2: mirrors of the enhancement cavity, PM: photomultiplier.

is locked in order that the transmitted beam is in resonance with the FPE cavity. By this way, we can know the frequencies of the fringes of the FPE cavity with respect to the ones of the FPR cavity. As the free spectral range of the two cavities are slightly different (299.590 MHz and 299.700 MHz for the FPR and FPE cavity respectively), there is a Vernier effect between the two cavities: the relative positions of the fringes of the two cavities are similar every about 2700 fringes (*i.e.* 1.6 nm in terms of wavelength) and, from these measurements, we can deduce the numbers of the fringes of the FPR and FPE cavities with a typical uncertainty of one fringe.

2.3 The metastable hydrogen atomic beam

2.3.1 The atomic beam apparatus

Our metastable atomic beam is sketched in Figure 4. It is very similar to a first apparatus described in reference [16]. The metastable atomic beam is produced in two steps: molecular hydrogen is dissociated in a water cooled Pyrex tube by a radiofrequency discharge (about 26 MHz). An atomic beam flows through a Teflon nozzle and effuses into a first vacuum chamber, which is evacuated by an oil diffusion pump (Alcatel 6250, pumping speed of 2 500 l/s) to a pressure of about 10^{-4} mbar. Thereafter ground state atoms are excited to the 2S metastable state by electronic bombardment (in an equipotential region to prevent the quenching of the metastable atoms, see details in Ref. [16]). The optical excitation takes place in the second vacuum chamber, where the metastable atomic beam is delimited by two holes, 7 mm in diameter, 56 cm apart (this metastable atomic beam makes an angle of 20° with the 1S atomic beam). To evacuate this chamber, we use a cryogenic pump (CTI-Cryogenics CT8, pumping speed of 2 000 l/s for hydrogen) and the running pressure is typically 10^{-6} mbar. In our first experiments [4,5,9], the ambient magnetic field was reduced to less than 20 mG by three pairs of coils. More recently [6,8], we have placed a magnetic shield in the second vacuum chamber (see Fig. 4). To reduce the stray electric fields, the walls of the chamber and the magnetic shield are painted with Aquadag, a conductive colloidal graphite suspension in an ammonia solution. This chamber is also permanently heated to 330 K to prevent the formation of any insulating deposits on the walls and the magnetic shield. From the line shape analysis of the 2S–nD transitions (n in the range 15–20), which are very sensitive to the stray electric fields, we have deduced that this painting reduces the stray electric fields from several tens of millivolts per centimetre to about 3 mV/cm (see Sect. 3). To preserve this property, the Aquadag paint is renewed approximatively about once a year. The metastable atoms are detected in the third vacuum chamber, which is simply evacuated through the 7 mm hole between the two vacuum chambers. An applied electric field quenches the 2S state and two photomultipliers (Hamamatsu R1459) detect the Lyman-α fluorescence. The two photomultiplier windows are 1 cm apart around the quenching region, and the detection solid angle is: $\Omega/4\pi \simeq 60\%$. To detect the photomultiplier signal, the quenching voltage is square-wave modulated at about 1.45 kHz and we use a lock-in amplifier (ATNE ADS2). From the photomultiplier current, we estimate the

metastable beam intensity to be at best 2×10^7 atoms/s (4×10^7 for deuterium). Nevertheless, we work usually with a metastable yield of about 8×10^6 atoms/s, regime where the signal-to-noise ratio is better.

To maximise the excitation rate for the 2S–nS/D two-photon transitions, the whole metastable atomic beam is placed inside an enhancement cavity whose optical axis is in coincidence with the atomic beam. This cavity is formed by two mirrors, 101 cm apart, one flat (high reflector) and the other concave (4 m curvature radius, transmission of about 1.1%). With this geometry, the beam waist is about 660 μm. To reduce the perturbations due to the vibrations of the cryogenic pump, this cavity is mounted on a small granite bench ($220\times20\times13$ cm^3) which is carefully isolated from the vacuum apparatus. The two mirrors are mounted on piezoelectric transducers and the length of the cavity is locked to the laser wavelength by monitoring the reflected beam polarisation [17]. In this servo-loop, the rapid length fluctuations are corrected by a small PZT acting on the flat mirror, which is of a small size (8 mm in diameter, 4 mm thick). Inside the cavity, the optical power can be as much as 100 W in each direction. This light intensity is controlled with a photodiode which measures the small intensity transmitted by the high reflector.

2.3.2 Velocity distribution of the metastable atoms

A precise knowledge of the velocity distribution of the atoms is necessary to calculate the line shapes of the two-photon lines and to deduce the corrections due to the second order Doppler effect. We have measured this velocity distribution by observing the Doppler broadened 2S–6P transition at 410 nm with a collinear laser beam. This laser source is obtained from the titanium-sapphire laser by a frequency doubling in an LBO crystal (see Ref. [13] and Sect. 5). For this measurement, we remove the concave mirror of the enhancement cavity. The beam at 410 nm (typical power of 100 mW) is sent along the metastable beam and a fraction of the laser beam (about 30%) is reflected by the flat mirror of the enhancement cavity, so that the atoms see two counterpropagating waves. Usually, the measurements are made with two different beam waists, one matched to the diameter of the metastable beam (7 mm), the other more focused (about 2 mm) and we have observed that the results are not sensitive to the beam waist. For the detection, the quenching voltage in the third vacuum chamber is applied continuously and the laser beam is chopped at about 120 Hz. At this frequency, the duration of the square-modulation of the light (4 ms) is long with respect to the atomic transit time through the second vacuum chamber (190 μs for an atom at 3 km/s), so that only the very slow atoms (velocity of about 70 m/s) are not detected with this method. The laser frequency is scanned by locking the titanium-sapphire on the successive fringes of the FPR cavity. A typical recording is shown in Figure 5. The signal is split into two peaks, separated by 19 GHz, which are due to the two counterpropagating waves at 410 nm. In a first rough analysis, this separation $\Delta\nu$ corresponds to a beam velocity $c\Delta\nu/2\nu_0$ of

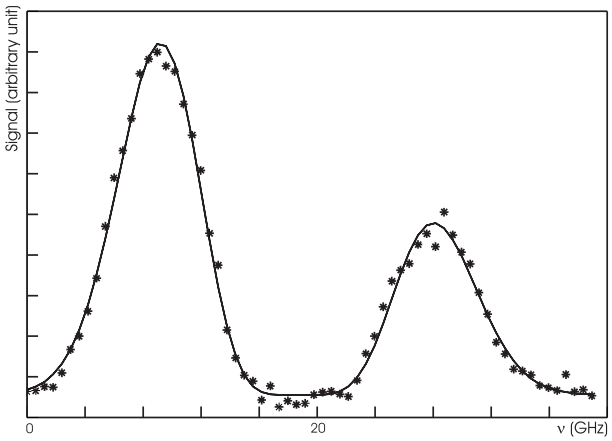

Fig. 5. Doppler broadened profile of the 2S–6P transition at 410 nm (the frequency is two times the frequency of the titanium-sapphire laser at 820 nm).

3.9 km/s (c is the velocity of light and ν_0 the frequency of the 2S–6P transition). The maximum signal is about 10% of the total metastable yield. Because of the long interaction time between the atom and the laser beam, there is a large saturation and the velocity classes are broadened to about 360 MHz, when the natural width of the 6P level is 3.9 MHz.

Due to the electronic excitation of the metastable atoms, the velocity distribution $f(v)$ in the beam should vary as $v^4 \exp(-v^2/2\sigma^2)$, where σ is related to the mass M of the atom and the temperature as $\sigma = \sqrt{kT/M}$[16]. In our case, we have observed that the velocity distribution can be more narrow and we have fitted the data with a velocity distribution of the form:

$$f(v) \sim v^n \exp(-v^2/2\sigma^2) \tag{1}$$

where n is an integer which can be different from 4. With this distribution, the second order Doppler shift $\delta_{\rm D}$ of a transition of frequency $\nu_{\rm trans}$ is, in a simple model (see Ref. [11]):

$$\delta_{\rm D} = -\frac{n}{2}\left(\frac{\sigma}{c}\right)^2 \nu_{\rm trans}. \tag{2}$$

In our first papers [4,5,9], we used simply the equation (2) to determine the second order Doppler shift. In our more recent work [6,8], the velocity distribution is directly included in the line shape calculation of the 2S–nS/D transitions (see Sect. 3).

If we suppose that the light intensity is uniform along an atomic trajectory, the shape $F(\nu)$ of the Doppler broadened 2S–6P line is:

$$F(\nu) \sim \int_0^\infty f(v) H(v,\nu) \mathrm{d}v \tag{3}$$

$$H(v,\nu) = 1 - \exp\left\{-\frac{1}{v}\left[I_+ L\left(\nu - \nu_0\left(1 + v/c\right)\right) + I_- L\left(\nu - \nu_0\left(1 - v/c\right)\right)\right]\right\} \tag{4}$$

Table 1. Velocity distribution of the hydrogen and deuterium atomic beam.

date	n	σ (m/s)	v_{Max} (m/s)	$\delta_{2\mathrm{S}-8\mathrm{D}}$ (kHz)
hydrogen				
1988 [11,16]	4	1525 (10)	3050 (20)	−39.9 (1.0)
1992 [4]	5	1385 (30)	3100 (70)	−41.0 (2.0)
1993 [5]	5	1406 (33)	3144 (75)	−42.4 (2.0)
1996 [6]	5	1814 (13)	4056 (29)	−70.6 (1.0)
1997 [8]	6	1614 (11)	3953 (27)	−67.0 (1.0)
deuterium				
1988 [11,16]	4	983 (10)	1966 (20)	−16.6 (1.0)
1997 [6]	7	995 (10)	2633 (26)	−29.7 (1.0)
1998 [8]	6	1044 (10)	2557 (24)	−26.3 (1.0)

where I_+ and I_- are proportional to the intensity of the two travelling waves and $L(\nu)$ is the Lorentzian profile of the 2S–6P transition. In this equation, we have neglected the fine and the hyperfine structures of the 2S and 6P levels (the largest is the 6P fine structure $\Delta\nu_0 \sim 400$ MHz). A simple model shows that this approximation leads to, for the second order Doppler shift, a relative error of $(\Delta\nu_0/\Delta\nu)^2 \simeq 5\times10^{-4}$ (*i.e.* an error of about 40 Hz for the frequencies of the 2S–nS/D transitions). The function $H(v,\nu)$ describes the two velocity classes which are excited by the two travelling waves. Because of the saturation of 2S–6P transition, the width of these velocity classes varies as $1/\sqrt{v}$. Consequently the function $H(v,\nu)$ can be approximated by two square functions of v at the velocities $v_0 = \pm c(\nu-\nu_0)/\nu_0$, with a height of unity and a width proportional to $1/\sqrt{|v_0|}$. With these approximations, the shape $F(\nu)$ becomes:

$$F(\nu) = A(\nu-\nu_0)^{n-1/2}\exp\left[-(\nu-\nu_0)^2/2\sigma_\nu^2\right] \quad \text{if} \quad \nu>\nu_0 \quad (5)$$

$$F(\nu) = B(\nu_0-\nu)^{n-1/2}\exp\left[-(\nu-\nu_0)^2/2\sigma_\nu^2\right] \quad \text{if} \quad \nu<\nu_0 \quad (6)$$

where A and B are two adjustable constants and $\sigma_\nu = \nu_0\sigma/c$. From the fit of the profile $F(\nu)$ to the experimental data, we deduce the integer n and the parameter σ which describe the velocity distribution.

The results for the measurements made since 1988 are given in Table 1 where we also show the most probable velocity $v_{\mathrm{Max}} = \sqrt{n}\sigma$ and the second order Doppler shift $\delta_{2\mathrm{S}-8\mathrm{D}}$ of the 2S–8D transition (Eq. (2)). We can make two comments: (i) during the period 1988–1993, the typical velocity of the hydrogen beam was very stable, v_{Max} being around 3.1 km/s. By contrast, in the experiments made since 1996, the atoms have been distinctly more rapid, with a velocity of about 4 km/s. This velocity increase appeared after an accidental contamination of the vacuum apparatus by the oil of the diffusion pump. After this pollution, the beam velocity was less reproducible and, in spite of our careful cleaning of the vacuum system, we have never been able to obtain the original characteristics of the atomic beam. This effect is probably due to the destruction of the slow atoms by the stray electric fields which are more important in the first vacuum chamber since this contamination. (ii) On the other hand, the ratio between the hydrogen and deuterium velocities is very stable with a value of 1.55. This value is slightly different from the $\sqrt{2}$ factor to be expected for a thermal beam. This fact can be explained by the deviation due to the electronic excitation of the 2S level. For deuterium, the mean deviation is only 14° and the 20° angle of our atomic beam apparatus selects the slow deuterium atoms.

2.4 Data acquisition

The experiment is driven by a microcomputer which commands the frequency of the titanium-sapphire laser (through the synthesizer which drives the AOM1), performs the acquisition of the atomic signal and records several other parameters of the experiment: the signal of the photodiode which monitors the light intensity inside the enhancement cavity, the frequency of the beat note between the two He–Ne lasers, the modulation frequency of the AOM2 and several other frequency measurements used to determine the optical frequency of the laser (see Sect. 4). The atomic spectrum is divided in 101 frequency points. For each point, the duration of the measurement is 1 s (the signal of the lock-in amplifier which detects the atomic signal is acquired 10 times every 100 ms with a time constant of 100 ms) and there is a dead time of about 300 ms for the acquisition procedure by the computer and the shift of the laser frequency. To reduce the effect of the low drift of the metastable yield, the sweep of the line is not regular: the 101 points are obtained by 10 scans of the line in the following order:

0	10	20	30...80	90	100
99	89	79	69...19	9	
8	18	28	38...88	98	
...					
91	81	71	61...11	1	

Finally, the laser frequency is scanned ten times across the atomic resonance during a 22 minutes run. After an average of these 10 scans, the relative noise of the metastable yield is about 0.3%.

Figure 6 shows a typical signal obtained in the case of the $2\mathrm{S}_{1/2}(F=1)$–$8\mathrm{D}_{5/2}$ transition of hydrogen. In this recording, the decrease of the metastable intensity is 13% and the linewidth 1.13 MHz (in terms of atomic frequency). By comparison with the natural width of the 8D level (572 kHz), there is a large broadening which is mainly due to the inhomogeneous light shift experienced by the atoms through the Gaussian profile of the laser beams. To evaluate this effect, we record the signal for several laser intensities and we made an extrapolation

Table 2. Some features of the observed transitions.

transition	number of runs	amplitude of a scan	width variation	maximum amplitude
hydrogen				
$2S_{1/2}(F=1)$–$6D_{5/2}$ [9]	49	10 MHz	1.8 MHz to 3.4 MHz	19.7%
$2S_{1/2}(F=1)$–$6S_{1/2}$ [9]	91	4 MHz	400 kHz to 1.2 MHz	5.7%
$2S_{1/2}(F=1)$–$8D_{5/2}$ [5]	20	8 MHz	900 kHz to 2.1 MHz	18.6%
$2S_{1/2}(F=1)$–$8D_{3/2}$ [5]	24	8 MHz	900 kHz to 1.9 MHz	16.0%
$2S_{1/2}(F=1)$–$8S_{1/2}$ [5]	47	4 MHz	330 kHz to 800 kHz	5.1%
$2S_{1/2}(F=1)$–$8D_{5/2}$ [6]	90	8 or 12 MHz	750 kHz to 2.0 MHz	21.7%
$2S_{1/2}(F=1)$–$8D_{3/2}$ [6]	53	8 or 12 MHz	800 kHz to 1.6 MHz	18.5%
$2S_{1/2}(F=1)$–$8S_{1/2}$ [6]	77	2.8 or 4 MHz	300 kHz to 950 kHz	6.7%
$2S_{1/2}(F=1)$–$12D_{5/2}$ [8]	78	3.6 MHz	300 kHz to 600 kHz	8.7%
$2S_{1/2}(F=1)$–$12D_{3/2}$ [8]	62	3.6 MHz	300 kHz to 600 kHz	6.7%
deuterium				
$2S_{1/2}(F=3/2)$–$8D_{5/2}$ [6]	41	8 or 12 MHz	750 kHz to 2.2 MHz	19.8%
$2S_{1/2}(F=3/2)$–$8D_{3/2}$ [6]	49	8 or 12 MHz	700 kHz to 2.0 MHz	19.5%
$2S_{1/2}(F=3/2)$–$8S_{1/2}$ [6]	47	2.8 or 4 MHz	250 kHz to 1.0 MHz	7.3%
$2S_{1/2}(F=3/2)$–$12D_{5/2}$ [8]	44	3.6 MHz	300 kHz to 650 kHz	9.1%
$2S_{1/2}(F=3/2)$–$12D_{3/2}$ [8]	54	3.2 MHz	350 kHz to 650 kHz	8.3%

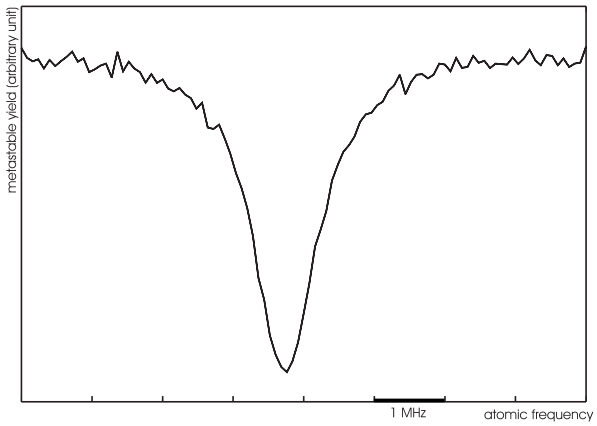

Fig. 6. Typical two-photon transition signal, recorded as a decrease of the metastable beam intensity. Example of the $2S_{1/2}(F=1)$–$8D_{5/2}$ transition of hydrogen: the decrease of the metastable yield is 13%.

to zero light power. Consequently, the data acquisition takes 3 or 4 days for each atomic transition. Table 2 gives some details for the measurements which have been made during the period 1993–1998 [5,6,8,9]. For each transition, we indicate the number of the runs used for the extrapolation, the amplitude of the frequency scan (in terms of atomic frequency), the range of variation of the line width with the light power and the maximum amplitude of the observed signal.

3 Line shape analysis

3.1 Expression for the line shape

Figure 7 shows an atomic trajectory in the laser-atom interaction region (the second vacuum chamber). In this region, the collisions are negligible and the atomic trajectories are straight lines passing through the two diaphragms (the small deviation of the atomic trajectory due to the forces induced by the light shifts will be studied below). The calculation procedure is the following. In a first step, we calculate for each trajectory the destruction probability of the metastable atom when it crosses the laser beam. Then we make an average over all the possible trajectories.

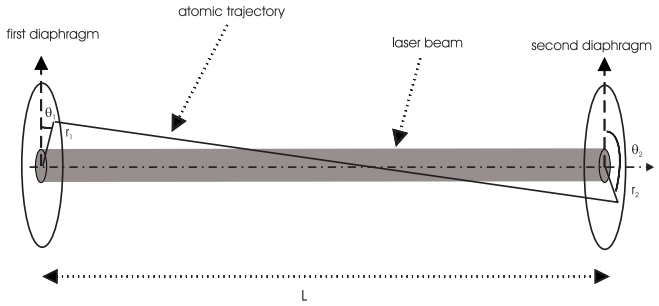

Fig. 7. Schematic view of an atom trajectory in the laser-atom interaction region.

3.1.1 Two-photon excitation rate

The two-photon transition probability Γ_g between two states $|g\rangle$ and $|e\rangle$ (energies E_g and E_e) is given by [11,18]:

$$\Gamma_g = \frac{n^2\omega^2}{\varepsilon_0^2\hbar^2}\left|\sum_r \frac{\langle e|\,\mathbf{d}\cdot\varepsilon\,|r\rangle\,\langle r|\,\mathbf{d}\cdot\varepsilon\,|g\rangle}{\omega-\omega_{rg}}\right|^2 \times \frac{\Gamma_e}{(2\omega-\omega_{eg})^2+(\Gamma_e/2)^2} \quad (7)$$

$$\Gamma_g = \left(\frac{4\pi a_0^2}{mc^2\alpha}\right)^2 \sum_e \frac{\left|\langle e\left|Q_{\rm tp}\right|g\rangle\right|^2 \Gamma_e \left(1+c_{\rm io}I\right) I^2}{\left[2\omega - \left(\omega_{eg}\left(1-v^2/c^2\right)+c_{\rm ls}I\right)\right]^2 + \left[\Gamma_e\left(1+c_{\rm io}I\right)/2\right]^2 \left(1+c_{\rm sat}I^2\right)} \tag{10}$$

Table 3. 2S–nS/D two-photon transition amplitude $\langle e\left|Q_{\rm tp}\right|g\rangle$ and natural width of the excited level.

transitions	$\langle e\left\|Q_{\rm tp}\right\|g\rangle$ (a.u.)	$\Gamma_e/2\pi$
2S–6S	−14.711	297 kHz
2S–8S	−14.921	144 kHz
2S–6D	−133.16	1.337 MHz
2S–8D	−92.937	572 kHz
2S–12D	−55.033	172 kHz
2S–15D	−40.677	88.7 kHz
2S–20D	−27.187	19.0 kHz

where n is the number of photons per unit volume for each counterpropagating wave, ω the laser frequency, ε the polarisation, $\omega_{ij} = (E_i - E_j)/\hbar$, $\mathbf{d}$ the electric dipole moment operator and Γ_e the natural width of the excited state (we suppose that the natural width of the state $|g\rangle$ is negligible). The summation is made over all the possible states $|r\rangle$ (including the continuum). We introduce the two-photon operator $Q_{\rm tp}$. In our experiment, the polarisation of the laser beam is linear (because of the Brewster windows of the vacuum apparatus placed in the enhancement cavity). For a polarisation along the z-axis, $Q_{\rm tp}$ is given in atomic units ($\hbar = \alpha c = m = 1$) by:

$$Q_{\rm tp} = \sum_r \frac{z\left|r\right\rangle\left\langle r\right|z}{\omega - \omega_{rg}}\,. \tag{8}$$

With this notation, equation (7) becomes:

$$\Gamma_g = \left(\frac{4\pi a_0^2}{mc^2\alpha}\right)^2 \frac{\left|\langle e\left|Q_{\rm tp}\right|g\rangle\right|^2 \Gamma_e I^2}{\left(2\omega-\omega_{eg}\right)^2 + \left(\Gamma_e/2\right)^2} \tag{9}$$

where I is the power density of the light ($I = n\hbar\omega/c$), a_0 the Bohr radius, α the fine structure constant and m the electron mass. For the transitions studied in this paper, Table 3 gives the values of the matrix element $\langle e\left|Q_{\rm tp}\right|g\rangle$ (calculated in Ref. [11]) for an atom without electronic and nuclear spin, and the natural width of the excited level.

In the calculation of the line shape of the 2S–nS/D transitions, we have taken into account the fine and hyperfine structures of the S and D levels, the light shift, the second order Doppler effect, the photoionisation of the upper level and the saturation of the two-photon transition. The states $|g\rangle$ and $|e\rangle$ are the magnetic hyperfine sublevels $|F_g m_F\rangle$ and $|F_e m_F\rangle$ (F_i is the total angular momentum of the state $|i\rangle$, $|i\rangle = |g\rangle$ or $|e\rangle$). We have the selection rule $\Delta m_F = 0$. Then the two-photon transition probability becomes:

see equation (10) above.

The coefficients $c_{\rm ls}$, $c_{\rm io}$ and $c_{\rm sat}$ describe the light shift, the photoionisation, and the saturation of the two-photon transition.

Following the notations of reference [11], the light shift coefficient is given by:

$$c_{\rm ls} = \left(\frac{4\pi a_0^2}{mc^2\alpha}\right)\left(\beta_e - \beta_g\right)$$

where β_i are the matrix elements of the light shift operator $Q_{\rm ls}$. We have:

$$Q_{\rm ls} = \sum_r \left[\frac{z\left|r\right\rangle\left\langle r\right|z}{\omega_{ir}+\omega} + \frac{z\left|r\right\rangle\left\langle r\right|z}{\omega_{ir}-\omega}\right] \qquad \text{(atomic units)}. \tag{11}$$

The light shift operator is the sum of a scalar operator $Q_{\rm ls}^0$ and of an operator of rank 2 $Q_{\rm ls}^2$. For the state $|i\rangle = |nLJFm_F\rangle$ (n principal quantum number, L and J orbital and electronic momenta), straightforward algebra gives:

$$\begin{aligned}\langle i\left|Q_{\rm ls}\right|i\rangle = {} & \frac{\langle nL\left\|Q_{\rm ls}^0\right\|nL\rangle}{\sqrt{2L+1}} \\ & + (-1)^{F-m_F}\begin{pmatrix} F & 2 & F \\ -m_F & 0 & m_F\end{pmatrix}\langle JF\left\|Q_{\rm ls}^2\right\|JF\rangle\end{aligned} \tag{12}$$

where:

$$\begin{aligned}\langle JF\left\|Q_{\rm ls}^2\right\|JF\rangle = {} & (-1)^{F+I+2J+L+S}\left(2F+1\right)\left(2J+1\right) \\ & \times \begin{Bmatrix} J & 2 & J \\ F & I & F\end{Bmatrix}\begin{Bmatrix} L & 2 & L \\ J & S & J\end{Bmatrix}\langle nL\left\|Q_{\rm ls}^2\right\|nL\rangle.\end{aligned}$$

The calculation of the matrix elements $\langle nL\left\|Q_{\rm ls}^k\right\|nL\rangle$ and ionisation coefficient $c_{\rm io}$ has been made with a method using Sturmian functions [19] (the coefficient $c_{\rm io}$ can be also obtained with the Fermi's golden rule, see Refs. [11,20, 21]). Table 4 gives the values of these parameters. The effect of the ionisation is not entirely negligible. For example, for a laser beam of 100 W with a waist of 660 μm, the ionisation rate of the 8S level is, at the center of the beam, 1.5×10^5 s^{-1}, *i.e.*, because of this ionisation probability, the width of the 8S level increases by 24 kHz. The saturation coefficient $c_{\rm sat}$ can be obtained by using an effective Hamiltonian [22]. Its expression is:

$$c_{\rm sat} = 8\left(\frac{4\pi a_0^2}{mc^2\alpha}\right)^2 \frac{\left|\langle e\left|Q_{\rm tp}\right|g\rangle\right|^2}{\Gamma_e^2}\,. \tag{13}$$

Table 4. Light shift and ionisation coefficients for the 2S–nS or 2S–nD transitions studied in this paper (expressed in atomic units).

transitions	$\langle nL_g \left\|Q^0_{\rm ls}\right\| nL_g\rangle$ (a.u.)	$\langle nL_e \left\|Q^0_{\rm ls}\right\| nL_e\rangle$ (a.u.)	$\langle nL_e \left\|Q^2_{\rm ls}\right\| nL_e\rangle$ (a.u.)	ionisation coefficient $c_{\rm io}$ ($\mathrm{m^2W^{-1}}$)
2S–6S	−290.96	324.42	0	1.536×10^{-9}
2S–8S	−355.31	291.35	0	1.144×10^{-9}
2S–6D	−290.96	727.20	34.99	2.315×10^{-10}
2S–8D	−355.31	648.51	19.19	1.805×10^{-10}
2S–12D	−428.53	603.94	6.78	1.517×10^{-10}

Table 5. Data for the calculation of the $2S(F=1)$–$8D_{5/2}$ two-photon line shape.

transition	F_e	hyperfine shift	$a_{\rm hfs}$ weight of the F_e level	β_{2S} (a.u.)	β_{F_e} (a.u.)
hydrogen					
$2S_{1/2}(F=1)$–$8D_{5/2}$	2	−82.3 kHz	2/9	−355.31	288.19
	3	59.4 kHz	7/9	−355.31	286.88
deuterium					
$2S_{1/2}(F=3/2)$–$8D_{5/2}$	3/2	−25.6 kHz	1/15	−355.31	290.02
	5/2	−7.3 kHz	4/15	−355.31	289.16
	7/2	18.3 kHz	2/3	−355.31	287.22

This effect is also not negligible: with the same laser beam parameters as above, the value of $c_{\rm sat}I^2$ is about 0.1 for the $2S_{1/2}$–$8D_{5/2}$ transition.

In the case of the 2S–nS transition, the two-photon operator is scalar and we have the selection rules $\Delta F = 0$, $\Delta m_F = 0$. In equation (10) the summation over the states $|e\rangle$ is reduced to a single term and, for the two-photon matrix element, we have $\langle nL_eJ_eFm_F| Q_{\rm tp} |2L_gJ_gFm_F\rangle = \langle nL_em_L| Q_{\rm tp} |2L_gm_L\rangle$. For the 2S–$n$D transition, the two-photon operator is quadrupolar and, in equation (10), we have to make the sum, for each m_F value, on all the states $|F_em_F\rangle$. Nevertheless, as the quadrupolar term of the light shift is very small (see Tab. 4), we have used the mean values (with respect to the magnetic quantum number m_F) of the light shift coefficient $c_{\rm ls}$ (given by Eq. (12)) and of the intensities of the hyperfine components. With these approximations, the two-photon transition probability Γ_g does not depend on m_F. The summation in equation (10) is made over the F_e quantum number and the two-photon fine and hyperfine intensities are given by:

$$|\langle nL_eJ_eFm_F| Q_{\rm tp} |2L_gJ_gFm_F\rangle|^2 = a_{\rm fs}a_{\rm hfs} |\langle nL_em_L| Q_{\rm tp} |2L_gm_L\rangle|^2 . \quad (14)$$

The matrix elements $\langle nL_em_L| Q_{\rm tp} |2L_gm_L\rangle$ have been given in Table 3. The coefficient $a_{\rm fs}$ takes into account the fine structure of the D level. It is proportional to the degeneracy $2J_e + 1$ (0.4 and 0.6 for the $D_{3/2}$ and $D_{5/2}$ levels). The coefficient $a_{\rm hfs}$ describes the intensity of the hyperfine components and is proportional to [12]:

$$(2F_e+1) \left\{ \begin{array}{ccc} J_e & J_g & 2 \\ F_g & F_e & I \end{array} \right\}^2 .$$

As an example, Table 5 gives the numerical values used in equation (10) for the $2S(F=1)$–$8D_{5/2}$ transition. The hyperfine splittings are calculated with the Fermi's formula [20].

3.1.2 Destruction probability of the metastable atoms

We consider an atomic trajectory between two points (r_1, θ_1) and (r_2, θ_2) on the diaphragms which delimit the metastable beam (see Fig. 7). If the laser beam is aligned with the x-axis, the laser intensity varies along the atomic trajectory as:

$$I(x,\rho) = I_0 \left(\frac{w_0}{w(x)}\right)^2 \exp\left[-2\left(\frac{\rho}{w(x)}\right)^2\right] \quad (15)$$

where x is the coordinate along the laser beam, ρ the radial distance to the laser beam axis, $w(x)$ the radius of the laser beam. Along the atomic trajectory, ρ is a function $\rho(x)$ and, if we assume that the transit time of the atom through the laser beam is long with respect to the life time $1/\Gamma_e$ of the excited level, the two-photon transition probability Γ_g becomes a function of x. The probability that the atom undergoes a transition during this trajectory is:

$$P(r_1,\theta_1,r_2,\theta_2) = 1 - \exp - \int_0^L \frac{\Gamma_g(x)\mathrm{d}x}{v_x} \quad (16)$$

Table 6. Two-photon cascade probability R_n from the nS or nD levels to the 2S metastable state.

level	6S	6D	8S	8D	12D	15D	20D
R_n	0.0740	0.0463	0.0815	0.0513	0.0548	0.0558	0.0567

Table 7. Partition of the probability R_n between the two hyperfine levels of the metastable state when the two-photon excitation is made from the $2S_{1/2}(F = 1)$ hyperfine sublevel ($F = 3/2$ for deuterium).

upper level	$nS_{1/2}$	$nD_{3/2}$	$nD_{5/2}$
hydrogen			
p_0	$(4/27)R_n$	$(32/135)R_n$	$(2/15)R_n$
p_1	$(23/27)R_n$	$(103/135)R_n$	$(13/15)R_n$
deuterium			
$p_{1/2}$	$(16/81)R_n$	$(128/405)R_n$	$(8/45)R_n$
$p_{3/2}$	$(65/81)R_n$	$(277/405)R_n$	$(37/45)R_n$

where v_x is the component of the atom velocity along the x axis and L the distance between the two diaphragms. We have to correct this expression to take into account the hyperfine structure and the repopulation of the 2S level.

(i) *Hyperfine structure of the metastable state.* In our experiment, we resolve the hyperfine structure of the metastable state and we have studied the most intense transitions starting from the $2S_{1/2}(F = 1)$ hyperfine level ($2S_{1/2}(F = 3/2)$ for deuterium). As we detect all the metastable atoms we have to multiply the equation (16) by a coefficient $C_{\rm hfs}$ which describes the population of the two hyperfine levels. By observing some transitions starting from the $2S_{1/2}(F = 0)$ hyperfine level ($2S_{1/2}(F = 1/2)$ for deuterium), we have measured these populations:

$$C_{\rm hfs}(F = 1) = 80\% \qquad \text{in hydrogen,}$$

$$C_{\rm hfs}(F = 3/2) = 67.6\% \qquad \text{in deuterium.}$$

These values are slightly different from the statistical weights (3/4 and 2/3 respectively). This effect is probably due to a larger quenching of the $2S_{1/2}(F = 0)$ ($2S_{1/2}(F = 1/2)$ in deuterium) which is closer to the $2P_{1/2}$ level and more sensitive to the stray electric fields.

(ii) *Repopulation of the metastable state.* When an atom is excited to the nS or nD level, it can undergo a radiative cascade towards the $2S_{1/2}$ level with the probability $R_n = p_0 + p_1$ ($p_{1/2} + p_{3/2}$ for deuterium), where the probabilities p_0 and p_1 ($p_{1/2}$ and $p_{3/2}$ for deuterium) are correlated to the two $2S_{1/2}(F = 0)$ and $2S_{1/2}(F = 1)$ levels (respectively $F = 1/2$ and $F = 3/2$ for deuterium). These probabilities have been calculated taking into account only the two photon cascades [11]. The values relevant to this paper are given in Tables 6 and 7.

Finally, after solving the rate equations which describe the evolution of the populations of the two hyperfine sublevels, we obtain the destruction probability of a metastable atom at the end of its trajectory:

$$P'(r_1, \theta_1, r_2, \theta_2) = C_{\rm hfs}\left(1 - \frac{p_0}{1 - p_1}\right) \times \left[1 - \exp -\frac{1}{v_x}\int_0^L (1 - p_1)\, \Gamma_g(x) {\rm d}x\right]. \quad (17)$$

For deuterium, we have to replace in equation (17) the probabilities p_0 and p_1 by $p_{1/2}$ and $p_{3/2}$. The first factor describes the optical pumping from the $F = 1$ hyperfine sublevel to the $F = 0$ one. The factor $1 - p_1$ in the integral describes the inefficiency of the two-photon excitation when the atom comes back to the initial $F = 1$ hyperfine sublevel.

Up to now, we have supposed that the atomic trajectories were straight lines. Let us consider the effect of the force due to the light shift of the metastable state. As the 2S state is down shifted (see Tab. 4), the atom is attracted towards the axis of the laser beam by a force $F_\rho(x, \rho)$ (we neglect the component of this force along the x-axis):

$$F_\rho(x, \rho) = -\hbar\beta_g \left(\frac{4\pi a_0^2}{mc^2\alpha}\right) \frac{\partial}{\partial\rho} I(x, \rho).$$

The acceleration due to this force is considerable. For example, for a laser beam of 100 W with a waist of 660 μm, the maximum radial acceleration is about 350 m/s^2. Nevertheless, because of the small transit time of the atom through the second vacuum chamber (typically 190 μs), the deviation from a straight trajectory is small, about a few micrometres. Even so, in the case of the 2S–nD transitions, which give the most accurate results, we have included this effect for the line shape calculation. The atomic trajectory is calculated step by step to determine the function $\rho(x)$ which is used to obtain the intensity $I(x, \rho)$ (Eq. (15)) and the two-photon transition probability $\Gamma_g(x)$ (Eq. (10)).

3.1.3 Summation on the atomic trajectories and velocities

The last step of this calculation is to make a summation of equation (17) over all velocities and all possible trajectories. We have studied the velocity distribution $f(v)$ in Section 2 and these functions are given in Table 1. On the other hand, we do not know the exact distribution of the atomic trajectories. Because of the recoil of the atom involved by the electronic excitation of the 2S state, there is a large dispersion in the direction of the metastable atoms. For this reason, we can suppose a uniform distribution for the points (r_2, θ_2) at the end of the atomic beam. This is not the case however at the beginning of the beam. The distribution of the metastable atoms can depend on the

spatial distribution of the 1S hydrogen atoms, the electron density or the quenching stray electric fields. Our approach has been to simulate the spatial distribution of the points (r_1, θ_1) by a uniform one on a virtual diaphragm centered on the real diaphragm at the beginning of the beam but with a smaller radius R_1. In this case the line shape $L(\omega)$ is given by:

$$L(\omega) = \frac{4}{\pi R_1^2 R_2^2} \int_0^\infty f(v)\mathrm{d}v \int_0^{R_1} r_1 \mathrm{d}r_1 \int_0^{R_2} r_2 \mathrm{d}r_2 \times \int_0^\pi \mathrm{d}\theta_2 P'(r_1, \theta_1, r_2, \theta_2). \quad (18)$$

We have supposed that we have a cylindrical symmetry and that the laser beam is well aligned with respect to the atomic beam. R_2 is the radius of the real diaphragm at the end of the atomic beam ($R_2 = 3.5$ mm). As explained below, the radius R_1 is determined during the analysis of the experimental curves to obtain a correct evaluation of the light shift. A typical value is $R_1 = 2$ mm.

3.1.4 Other broadening and shifting effects

In the above analysis, we have neglected several other effects which can broaden or shift the line. The Stark effect produced by the stray electric fields, which can induce a significant shift, will be studied subsequently. The other effects are the following.

(i) *Laser line width.* The jitter of our laser is about 2 kHz (see Sect. 2) corresponding to a line broadening of 4 kHz in terms of atomic frequency.

(ii) *Finite transit time.* Though the metastable atomic beam and the laser beam are colinear, the broadening due to the finite transit time of the atoms through the laser beam is not entirely negligible. For an atomic trajectory making an angle θ with the laser beam, the line broadening is $2v \sin\theta\sqrt{\ln 2}/\pi w$ [23]. In the case of the largest possible angle θ (about 0.6°), this broadening is 32 kHz for a velocity of 4 km/s and a waist of 660 μm.

(iii) *Residual magnetic field.* As the atomic beam is placed in a magnetic shield, the residual magnetic field is about 1 mG. For the 2S–nS transitions, the Zeeman splittings of the 2S and nS levels are similar. Because of the selection rules $\Delta F = 0$, $\Delta m_F = 0$, there is no broadening. In the case of the 2S–nD transition, the broadening due to the Zeeman effect can be about 10 kHz, but there is no shift if the laser polarisation is linear.

(iv) *Black body radiation.* The black body radiation induces transitions between the different hydrogen energy levels. Consequently, there is a depopulation of each level of the two-photon transition, *i.e.* a broadening of the line, and a shift. These effects are studied in detail in reference [24] for a temperature of 300 K. In our experiment, the magnetic shield which surrounds the atomic beam is heated at about 330 K.

Table 8. Broadening and shift due to the black body radiation.

transition	broadening	shift
2S–6S	1.2(0.1) kHz	−360(90) Hz
2S–6D	1.7(0.2) kHz	−430(105) Hz
2S–8S	4.4(0.4) kHz	520(130) Hz
2S–8D	5.5(0.5) kHz	650(160) Hz
2S–12D	7.1(0.7) kHz	2.1(0.5) kHz

If we assume an uncertainty of 30 K to take into account the inhomogeneity of the heating, we obtain the broadenings and shifts given in Table 8. Using the data of reference [24], we have supposed that the broadening varies as the temperature T and the shift as $T^{2.7}$.

3.2 Analysis of the data

3.2.1 Fit procedure

The aim of this analysis is to determine very precisely, with respect to our very stable FPR cavity, the transition frequency, corrected for the light shift, the second order Doppler effect and the nD hyperfine structure. As the two-photon transitions are observed by measuring the decrease of the metastable yield, we can calibrate this decrease with respect to the intensity of the metastable beam when the laser is off resonance. The principle of the adjustement procedure is hence the following: from the amplitude of this decrease we deduce the optical power and, consequently, the light shift.

In practice the theoretical curves given by equation (18) are adjusted to fit the experimental data. As the numerical calculations of the theoretical line shape are long (there is a quintuple integration), we calculate a set of theoretical curves for several laser powers P ($P = \pi w_0^2 I_0/2$) from 5 W to 150 W with a step of 5 W, and as a function of 301 atomic frequency points. The frequency steps are adjusted to the line width (50 kHz for the 2S–6D and 2S–8D transitions, 25 kHz for the 2S–12D and 20 kHz for the 2S–6S and 2S–8S). We obtain the curves $L(\omega, P)$. Then we make two convolutions: a first convolution following ω by a Gaussian curve of width Δ_ω which takes into account the broadening effects which are not included in the line shape, and a second convolution following P by an other Gaussian curve of width Δ_P which describes the fluctuations of the light power seen by the atoms. The width Δ_P is deduced, for each recording, from the light intensity measurements obtained using the enhancement cavity by a photodiode. Finally, the four parameters of the adjustment are the metastable yield when the laser is off resonance, the light power P, the frequency of the atomic transition CLP (without the light shift, the second order Doppler effect and the hyperfine structure of the D level) and the Gaussian broadening Δ_ω. During the adjustement, we make an interpolation, quadratically for the power and linearly for the frequencies.

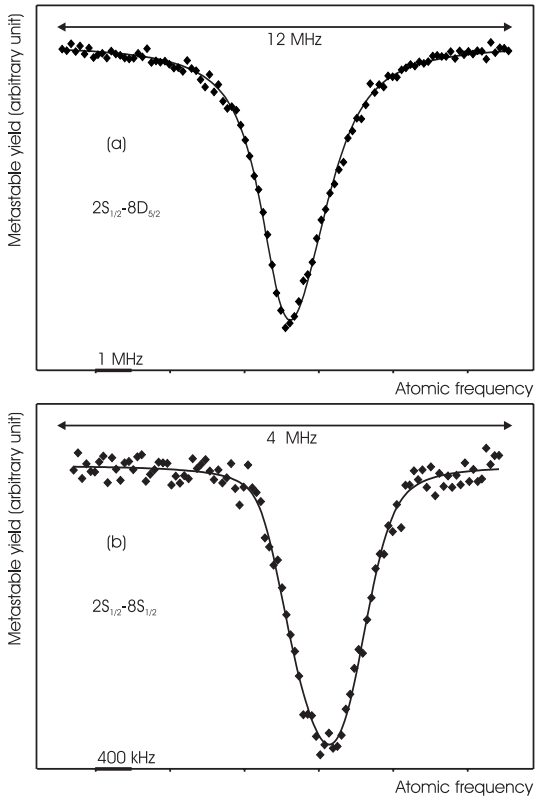

Fig. 8. Fit of the experimental line profile with the theoretical one. (a) $2S_{1/2}(F = 3/2)$–$8D_{5/2}$ transition in deuterium. (b) $2S_{1/2}(F = 3/2)$–$8S_{1/2}(F = 3/2)$ transition in deuterium. The light powers deduced from the fits are respectively 90.6(2.2) W and 96.2(2.6) W and the decreases of the metastable yield 18% and 6%.

Figures 8a and 8b show two examples of adjustements in the case of the $2S_{1/2}$–$8D_{5/2}$ and $2S_{1/2}$–$8S_{1/2}$ transitions of deuterium. The asymmetry of the experimental recordings, which appears for both transitions, but with different signs, is well reproduced by the theoretical profiles. For the $2S_{1/2}$–$8S_{1/2}$ transition, this asymmetry is related to the quadratic dependence with $I(x, \rho)$ of the atomic excitation rate at any point in the beam, since the light shift is linear with $I(x, \rho)$. Thus, the more shifted contributions to the signal are also the more intense. In the case of the $2S_{1/2}$–$8D_{5/2}$ transition, there is a very large saturation of the two-photon excitation probability. This saturation reduces the weight of the more shifted contributions to the signal, so that the sign of the asymmetry is reversed. In both cases, experimental and theoretical profiles are in excellent agreement.

3.2.2 Extrapolation versus the light power

The most crucial point of our analysis is the determination of the optical power seen by the atoms. A first test is to compare the fitted power P with the signal IT given by the photodiode placed after the enhancement cavity (see Fig. 9). There is a good agreement between these

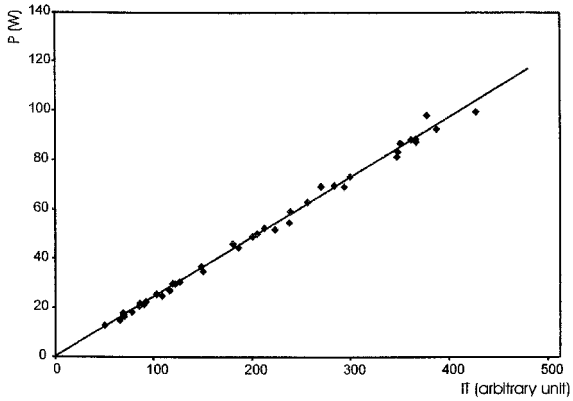

Fig. 9. Fitted power P *versus* the photodiode signal IT for the $2S_{1/2}(F = 3/2)$–$8D_{5/2}$ transition in deuterium (40 recordings).

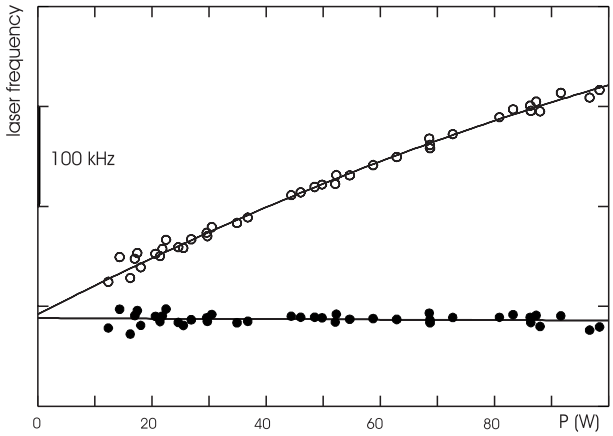

Fig. 10. Extrapolation of the half maximum center (○) and of the line position corrected for the light-shift, second-order Doppler effect and 8D hyperfine structure (●) *versus* the light power P in the case of the $2S_{1/2}(F = 3/2)$–$8D_{5/2}$ transition of deuterium.

data which lie in a linear ratio. We use the slope of this straight line P/IT as a parameter to control the optical alignment of the experiment: the slope P/IT is maximised to obtain the best matching between the laser beams and the atomic beam. The slope P/IT is also determined by the distribution of the atomic trajectories. For example, if we increase the radius R_1 of the first diaphragm, the theoretical curves exhibit a smaller decrease of the metastable yield, and, consequently, the fitting procedure gives a larger light power P. To determine the correct value for R_1, we study the shift of the line position *versus* the laser power. For each record, the adjustment procedure gives us the corrected line position CLP and the half-maximum center of the line HMC. Figure 10 shows a typical extrapolation of the HMC and CLP data *versus* the light power. Because of the saturation of the two-photon transition probability, the variation of HMC is not exactly linear with P. The shift of the line is about 400 kHz for a power of 100 W. On the other hand, there is no variation of the corrected line position. This result has been obtained by varying the radius R_1 to eliminate

Table 9. Calculation of the position of the line in the case of the $2S_{1/2}$–$8D_{3/2}$ transition in hydrogen. The extrapolated values are the absolute frequencies given in terms of laser frequency (*i.e.* $CLP/2$). Here we have indicated only the last digits and the real value is obtained by adding 385 324 GHz.

distribution of the trajectories	$R_1 = 1.8$ mm	$R_1 = 2$ mm
slope of the straight line P/IT (arb. units)	0.224	0.246
extrapolation of CLP *versus* P (MHz)	730.029 80	730.030 72
uncertainty (kHz)	3.27	3.23
extrapolation of CLP *versus* IT (MHz)	730.030 35	730.031 05
uncertainty (kHz)	3.21	3.20
mean of the extrapolation *versus* P and IT (MHz)	730.030 07	730.030 88
uncertainty (kHz)	3.24	3.20
slope of the straight line CLP *versus* P (MHz/W)	9×10^{-5}	-8×10^{-5}
final position of the line (MHz)	730.030 5(33)	
(interpolated position for a slope null)		
interpolated value for P/IT (arb. units)	0.236	
interpolated value for R_1	1.9 mm	

the variations of CLP with P. In practice, to obtain the position of the line, we use the following procedure: we make the mean of the linear extrapolations of CLP *versus* P and IT for two values of R_1 (for example 1.8 and 2 mm) and we interpolate these data to null the slope of the straight line $CLP(P)$. The details of this method are illustrated in Table 9 in the case of the $2S_{1/2}$–$8D_{3/2}$ transition in hydrogen. For this extrapolation, we have used the absolute frequency measurement described in Section 4 and the corrected line position CLP is not related to the FPR cavity but is an absolute frequency.

The uncertainties given in this table are only statistical. For each recording, the adjustement procedure gives an uncertainty for CLP which is deduced from the disagreement between the experimental and the theoretical curves. The linear extrapolation is made with a weighted least squares method. We calculate an *a priori* uncertainty σ_1 given by the propagation of the uncertainties of each record through the least squares calculations. This uncertainty does not depend on the dispersion of the points (CLP, P) with respect to a straight line. Next we calculate an *a posteriori* uncertainty σ_2 which takes into account this dispersion and is given by:

$$\sigma_2 = \sigma_1 t_{1\sigma} \sqrt{\frac{\chi^2}{n-2}}$$

where n is the number of recordings involved in the extrapolation and χ^2 the weighted least squares sum. The coefficient $t_{1\sigma}$ is estimated from the Student's t-distribution to obtain one standard deviation (*i.e.* $A\,(t_{1\sigma}|\,n-2) = 0.683$). Finally, we choose whichever value σ_1 and σ_2 which is largest.

We can test the consistency of our analysis by comparing, for several transitions, the interpolated values of P/IT and R_1 which correspond to the elimination of the variation of CLP with P. For example, the data obtained during the measurements of the 2S–8S/D transitions [6] are given in Table 10. The dispersion of the values of P/IT, which is not negligible, is probably due to the variation of the optical alignment of the experiment. We have also estimated directly this ratio from the light power transmitted by the enhancement cavity and the transmission of the end mirror of this cavity. We obtain the value $P = 0.259 \times IT$ with a typical uncertainty of 5%. This result is in acceptable agreement with the values given in Table 10. The same table also shows that the spatial distribution of the trajectories is more concentrated for deuterium (R_1 is smaller than for hydrogen). This is probably due to the larger quenching probability of the metastable deuterium atoms which are slower: the equipotential region where the metastable atoms are produced is reduced.

Table 10. Values of the slope of the straight line P *versus* IT and of the radius R_1 of the first diaphragm which correspond to the best determination of the light shift.

transition	R_1 (mm)	P/IT (arb. units)
hydrogen		
$2S_{1/2}$–$8D_{5/2}$	1.80	0.230
$2S_{1/2}$–$8D_{3/2}$	1.91	0.236
$2S_{1/2}$–$8S_{1/2}$	1.89	0.259
$2S_{1/2}$–$8D_{5/2}$	2.00	0.262
deuterium		
$2S_{1/2}$–$8D_{5/2}$	1.73	0.225
$2S_{1/2}$–$8D_{3/2}$	1.75	0.225
$2S_{1/2}$–$8S_{1/2}$	1.82	0.257

Some examples of the line width variations with the light power are shown in Figures 11a–11c in the case of the $2S_{1/2}$–$8S_{1/2}$, $2S_{1/2}$–$8D_{5/2}$ and $2S_{1/2}$–$12D_{5/2}$ transitions. The widths (full width at half maximum in terms of atomic frequency) deduced from the theoretical curves $L(\omega, P)$ correspond to the solid curves. We observe that the experimental widths are larger than the theoretical

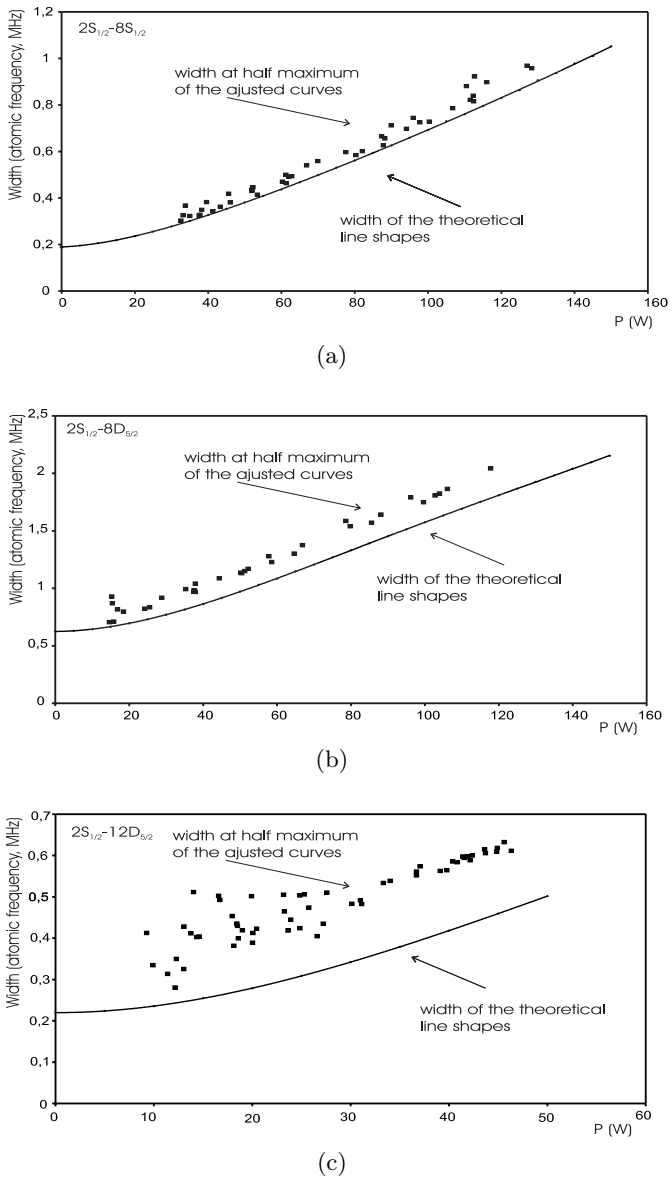

Fig. 11. Variation of the line width (full width at the half maximum in terms of atomic frequency) *versus* the light power P. (a) $2S_{1/2}(F = 1)$–$8S_{1/2}(F = 1)$ transition of hydrogen. (b) $2S_{1/2}(F = 1)$–$8D_{5/2}$ transition of hydrogen. (c) $2S_{1/2}(F = 1)$–$12D_{5/2}$ transition of hydrogen.

ones, especially for the 2S–nD transitions. These differences can be explained by the various effects which are not taken into account in the theoretical line shapes: the frequency jitter of the laser, the finite transit time, the residual Zeeman effect (for the 2S–nD transitions), black body radiation, the fluctuations of the light intensity seen by the atoms or the Stark effect due to stray electric fields.

Finally, to take into account the imperfections of our theoretical analysis, we introduce another uncertainty divided in two parts. (i) An uncertainty related to the optical alignment of the experiment. We have made a simulation of a bad alignment between the atomic beam and the laser beam [25] and we estimate this uncertainty to 4 kHz (in terms of atomic frequency). We consider that these uncertainties are correlated for a given series of extrapolations (for example the transitions 2S–8S/D in hydrogen, which are made in a relatively short time), but uncorrelated for the hydrogen and deuterium measurements and for the transitions with different principal quantum numbers. (ii) A theoretical uncertainty, common to all the measurements, which takes into account the possible incompleteness of our theoretical calculation. We have estimated this uncertainty from our results with different theoretical line shapes. For example, when we modified the theoretical calculations to include the ionisation of the upper level, the deviation of the atomic trajectories, or to reduce the step of the set of theoretical curves $L(\omega, P)$ from 10 W to 5 W, the shifts of the $2S_{1/2}$–$8D_{5/2}$ extrapolation in hydrogen were successively −640 Hz, 280 Hz and 1.4 kHz (in terms of atomic frequency). Finally, we have assumed that the effects neglected have the same order of magnitude and adopted a value of 2 kHz for this theoretical uncertainty.

3.3 Stark effect

3.3.1 Theoretical background

In our experiment, the stray electric fields are reduced to a few mV/cm thanks to the Aquadag coating. Nevertheless, as the matrix element of the Stark Hamiltonian $V_S = -\mathbf{d} \cdot \mathbf{E}$ ($\mathbf{E}$ is the electric field) varies with the principal quantum number as n^2, this small electric field can shift and broaden the lines, mainly for the 2S–12D transitions. The Stark coupling between the states $|nLJFm_F\rangle$ and $|nL'J'F'm'_F\rangle$ induces a quadratic Stark effect if $J \neq J'$ and a linear Stark effect if $J = J'$ which vary as n^7 and n^2 respectively. For instance, if we consider the energy levels for $n = 8$ (see Figs. 12a–12b), the quadratic Stark shift of the $8D_{5/2}$ level is due to the interaction with the $8P_{3/2}$ and $8F_{7/2}$ levels when the linear Stark effect is due to the mixing between the $8D_{5/2}$ and $8F_{5/2}$ levels. A straightforward second order calculation gives the quadratic Stark shift. As the anisotropic part of the quadratic Stark shift is small (7.6% and 1.8% for the $8D_{5/2}$ and $12D_{5/2}$ levels), we have considered only the scalar part of this shift (*i.e.* the mean shift for the m_F sublevels) which does not depend on the quantum number F. Table 11 gives the results for $n = 8$ and $n = 12$.

The linear Stark shift is more difficult to analyse. For example, the $8D_{5/2}$ and $8F_{5/2}$ hyperfine levels are mixed (see Fig. 12b) and these structures are smaller than the natural widths of the 8D and 8F levels (572 kHz and 285 kHz respectively). Consequently, in the experiment, we are not able to resolve these structures and we observe together the $8D_{5/2}$ and $8F_{5/2}$ levels. Nevertheless, to a first approximation, the shift of the line is null. If we assume that the effect of the electric field on the initial state g of the transition is negligible, the position ω_{tr}

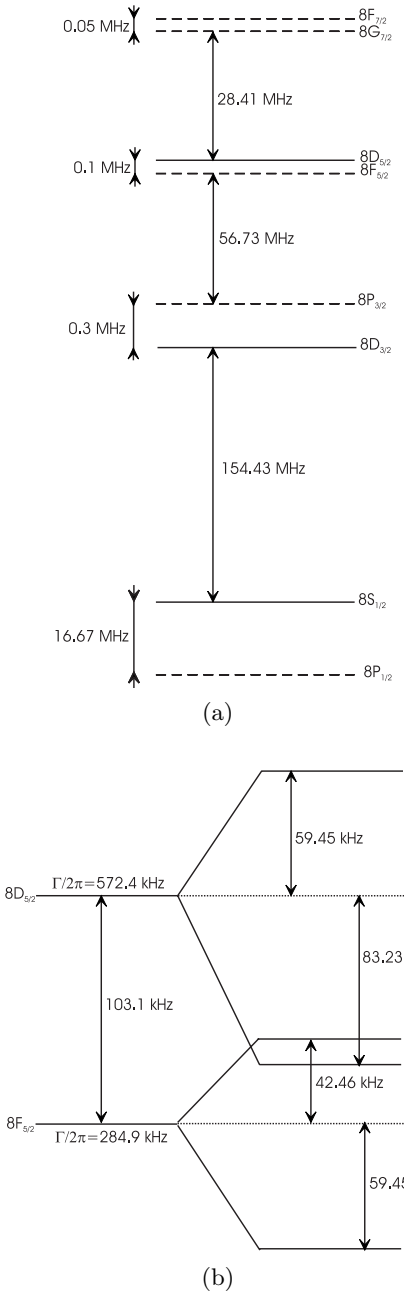

Fig. 12. (a) Fine structure and Lamb shifts of the 8S, 8P, 8D and 8F levels. The solid line corresponds to the levels which are excited with a two-photon transition from the metastable state. (b) Hyperfine structure of the $8D_{5/2}$ and $8F_{5/2}$ levels in hydrogen.

of the transition is:

$$\omega_{\rm tr} = \frac{\sum_i |\langle g| Q_{\rm tp} |\Psi_i\rangle|^2 \omega_i}{\sum_i |\langle g| Q_{\rm tp} |\Psi_i\rangle|^2} \tag{19}$$

where $Q_{\rm tp}$ is the two-photon operator (Eq. (8)), Ψ_i the eigenvectors with the energies $\hbar\omega_i$ of the Hamiltonian $H_0 + V_{\rm S}$ (H_0 being the Hamiltonian without electric field, $\hbar\omega_g$ the zero energy). Then we can write:

$$\omega_{tr} = \frac{\langle g| Q_{\rm tp}(H_0 + V_{\rm S}) P_e Q_{\rm tp}^+ |g\rangle}{\hbar \langle g| Q_{\rm tp} P_e Q_{\rm tp}^+ |g\rangle} \,. \tag{20}$$

We have introduced the projector on the subspace of the excited states $P_e = \sum_i |\Psi_i\rangle \langle\Psi_i|$. Then, because of parity conservation ($Q_{\rm tp}$ and $V_{\rm S}$ are respectively even and odd), we have $\langle g| Q_{\rm tp} V_{\rm S} P_e Q_{\rm tp}^+ |g\rangle = 0$ and the barycentre of the line does not depend on the electric field.

In our case, which is far more complicated, there are several limitations to the validity of this argument.

(i) Equation (19) does not take into account the strong saturation of the two-photon transition which modifies the weights of each component i.
(ii) We ignore the different natural widths of the upper states.
(iii) The adjustement procedure gives a line position which is not necessarily the barycentre of the line. For these reasons, we present now a line shape calculation taking into account the linear Stark effect.

Table 11. Coefficients of the quadratic Stark shift for some $n = 8$ and $n = 12$ levels.

level	quadratic Stark shift (MHz $V^{-2}cm^2$)
$8S_{1/2}$	77.69
$8P_{3/2}$	−39.11
$8D_{3/2}$	−36.29
$8D_{5/2}$	−53.59
$8F_{5/2}$	−45.28
$12P_{3/2}$	−698.10
$12D_{3/2}$	−684.87
$12D_{5/2}$	−1029.44
$12F_{5/2}$	−965.73

3.3.2 Line shape in presence of an electric field

The aim of this calculation is to consider simultaneously the natural width and the Stark coupling. The initial state g is coupled to a set of p states e (for instance the 12 sublevels $8D_{5/2}(F, m_F)$) by the optical excitation. The states e are mixed with the p states f (for instance the 12 sublevels $8F_{5/2}(F, m_F)$) by the Stark Hamiltonian $V_{\rm S}$. The evolution of the density operator ρ is:

$$\frac{{\rm d}\rho}{{\rm d}t} = \frac{1}{{\rm i}\hbar} \left[(H_0 + V_{\rm L} + V_{\rm S}), \rho \right] + \Gamma\rho \tag{21}$$

where the operators $V_{\rm L}$ and Γ describe the two-photon excitation and the spontaneous emission. We make the rotating wave approximation and we introduce the two-photon Rabi frequencies Ω_e:

$$\langle e| V_{\rm L} |g\rangle = \frac{\Omega_e}{2} \exp(-2{\rm i}\omega t),$$
$$\Omega_e = \frac{8\pi a_0^2 |\langle e| Q_{\rm tp} |g\rangle| I}{mc^2\alpha} \,. \tag{22}$$

If we assume that $\Omega_e \ll \Gamma_e$, we can neglect the populations and coherences $\rho_{ee'}$, $\rho_{ff'}$ or ρ_{ef} of the upper levels. In the rotating frame, we replace the density operator by an operator σ with $\sigma_{gg} = \rho_{gg}$, $\sigma_{eg} = \rho_{eg}\exp(2\mathrm{i}\omega t)$ and $\sigma_{ge} = \rho_{ge}\exp(-2\mathrm{i}\omega t)$ and we introduce the frequency detunings $\Delta_e = 2\omega - \omega_e$ and $\Delta_f = 2\omega - \omega_f$. In this way, we obtain from equation (21) a set of equations:

$$\frac{\mathrm{d}\sigma_{gg}}{\mathrm{d}t} = -\frac{\mathrm{i}}{2}\sum_e \Omega_e\left(\sigma_{eg} - \sigma_{ge}\right), \tag{23}$$

$$\frac{\mathrm{d}\sigma_{eg}}{\mathrm{d}t} = \left(\mathrm{i}\Delta_e - \frac{\Gamma_e}{2}\right)\sigma_{eg} - \mathrm{i}\frac{\Omega_e}{2}\sigma_{gg} - \frac{\mathrm{i}}{\hbar}\sum_f V_{ef}\sigma_{fg} \qquad (p \text{ equations}), \tag{24}$$

$$\frac{\mathrm{d}\sigma_{fg}}{\mathrm{d}t} = \left(\mathrm{i}\Delta_f - \frac{\Gamma_f}{2}\right)\sigma_{fg} - \frac{\mathrm{i}}{\hbar}\sum_e V_{fe}\sigma_{eg} \quad (p \text{ equations}). \tag{25}$$

We have introduced the matrix elements $V_{fe} = \langle f|\, V_\mathrm{S}\,|e\rangle$. Then we assume that the optical coherences σ_{eg} and σ_{fg} follow adiabatically the population σ_{gg}, *i.e.* that:

$$\frac{\mathrm{d}\sigma_{eg}}{\mathrm{d}t} = 0 \qquad \text{and} \qquad \frac{\mathrm{d}\sigma_{fg}}{\mathrm{d}t} = 0.$$

With these hypotheses, the equations (24, 25) become:

$$\left(\mathrm{i}\Delta_e - \frac{\Gamma_e}{2}\right)\sigma_{eg} + \sum_{e',f}\frac{V_{ef}V_{fe'}}{\hbar^2\left(\mathrm{i}\Delta_f - \Gamma_f/2\right)}\sigma_{e'g} = \mathrm{i}\frac{\Omega_e}{2}\sigma_{gg} \qquad (p \text{ equations}). \tag{26}$$

We obtain a set of p equations with p unknowns σ_{eg}. If we introduce the column vectors $[\sigma_{eg}]$ and $[\Omega_e/2]$, the set of equations (26) becomes:

$$A\left[\sigma_{eg}\right] = \mathrm{i}\left[\frac{\Omega_e}{2}\right]\sigma_{gg}$$

where the matrix elements of the $p \times p$ operator A are the coefficients of the set of equations (26). With these notations, the equation (23) becomes:

$$\frac{\mathrm{d}\sigma_{gg}}{\mathrm{d}t} = 2\,\mathrm{Re}\left[\frac{\Omega_e}{2}\right]^T A^{-1}\left[\frac{\Omega_e}{2}\right]\sigma_{gg}. \tag{27}$$

This equation describes the evolution of the population σ_{gg} and, finally, the two-photon transition probability Γ_g is:

$$\Gamma_g = -2\,\mathrm{Re}\left[\frac{\Omega_e}{2}\right]^T A^{-1}\left[\frac{\Omega_e}{2}\right]. \tag{28}$$

This equation is the equivalent, in the case of the Stark mixing, of equation (9). The two-photon probability is proportional to I^2 and we can separate the frequency and intensity variations:

$$\Gamma_g = I^2\gamma_g(\omega)$$

where $\gamma_g(\omega)$ describes the line profile. Afterwards we include the light shifts, but we neglect the photoionisation and the saturation of the two-photon transition probability. Strictly speaking, we should replace each atomic frequency ω_i ($i = g$, e or f) by $\omega_i - c_\mathrm{ls}(i)I$, where the light shift coefficient depends on the state i. In actual fact, to reduce the calculation time, we assume that all the states e and f have the same light shift coefficient c_ls. This is justified for two reasons: (i) the anisotropy of the light shift is small (see Tab. 4); (ii) the light shift coefficients of the levels nP, nD and nF are all very similar. For instance, the light shift coefficients β_e of the states 8P($m_L = 0$), 8D($m_L = 0$) and 8F($m_L = 0$) are respectively 287.78, 285.43 and 281.1 (in atomic units). With this approximation, when we include the light shift, the transition probability becomes:

$$\Gamma_g = I^2\gamma_g(\omega - \frac{1}{2}c_\mathrm{ls}I). \tag{29}$$

This equation replaces equation (10). Then we follow the procedure described in Section 3.1 (Eqs. (16–18)). However,we have not summed over the velocity distribution in equation (18) but used instead the mean velocity v_m [11]:

$$1/v_m = \langle 1/v\rangle = \frac{\displaystyle\int_0^\infty \frac{f(v)}{v}\mathrm{d}v}{\displaystyle\int_0^\infty f(v)\mathrm{d}v}$$

where $f(v)$ is the velocity distribution (Eq. (1)).

In reality, we do not know the orientation of the stray electric fields. Consequently, we have made the line shape calculation for an electric field either parallel or perpendicular to the laser polarisation to obtain the line shapes $L_\parallel(\omega, P, E)$ and $L_\perp(\omega, P, E)$ ($E = |\mathbf{E}|$). Moreover we have to consider the case of each hyperfine sublevel m_F of the $2\mathrm{S}_{1/2}(F = 1)$ level ($2\mathrm{S}_{1/2}(F = 3/2)$ for deuterium). Finally, we evaluate the mean of these different profiles:

$$L(\omega, P, E) = \frac{1}{2F+1}\sum_{m_F}\left[\frac{1}{3}L_{\parallel,m_F}(\omega, P, E) + \frac{2}{3}L_{\perp,m_F}(\omega, P, E)\right].$$

Figure 13 shows an example of this line shape in the case of the $2\mathrm{S}_{1/2}(F{=}3/2)$–$20\mathrm{D}_J$ transition in deuterium for a light power of 20 W and several electric fields (in this calculation we have neglected the quadratic Stark effect between the $J = 3/2$ and $J = 5/2$ levels). For an electric field of 5 mV/cm, the linear Stark structure appears clearly and we see that the $n\mathrm{D}_{3/2}$ level is more sensitive to an electric field than the $n\mathrm{D}_{5/2}$.

3.3.3 Corrections due to the Stark effect

As the linear Stark effect varies as n^2, we can estimate the residual electric fields from the widths of the transitions to higher nD levels. During the measurements

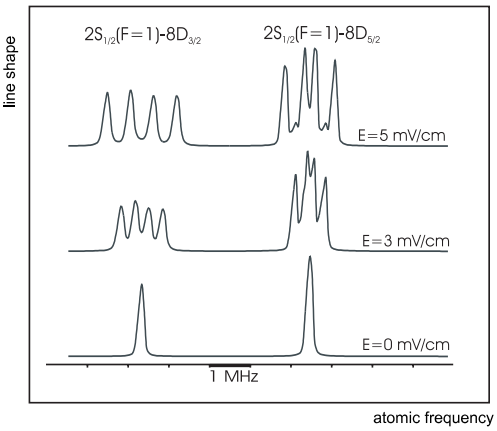

Fig. 13. Stark splitting of the $2S_{1/2}(F = 3/2)$–$20D_{3/2}$ and –$20D_{5/2}$ transitions for several electric fields.

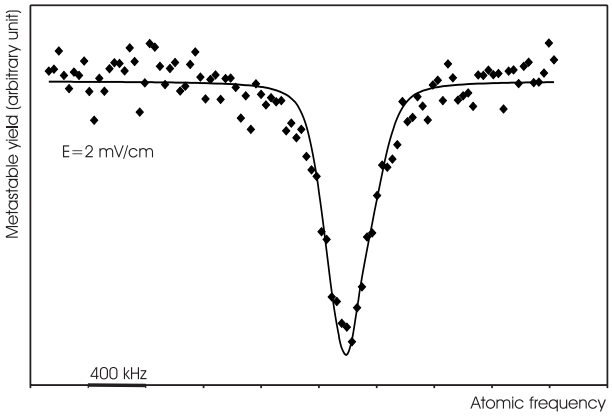

Fig. 14. Fit of the $2S_{1/2}(F = 3/2)$–$15D_{3/2}$ two-photon transition in deuterium. The theoretical curve (solid) is calculated with an electric field of 2 mV/cm.

of the 2S–8S/D frequencies [5,6], we have made several recordings of the $2S_{1/2}$–$15D_J$ transition. For the 2S–12D measurements [8], we have also observed the $2S_{1/2}$–$20D_J$ lines. To determine the electric field, we adjust the profile $L(\omega, P, E)$ to the experimental data for several values of the electric field E. We use the procedure described in Section 3.2, but without the Gaussian broadening ($\Delta_\omega = 0$). Two examples are given in Figures 14 and 15. For the $2S_{1/2}$–$15D_{3/2}$ transition (Fig. 14), the best fit is obtained for an electric field of about 2 mV/cm. Figure 15 shows the fit of the $2S_{1/2}$–$20D_J$ with an electric field of 3 mV/cm. In this case we see the structure of the theoretical curve (in the experiment, we have in fact a distribution of the amplitude E), but the experimental lines are narrower than the theoretical ones. Finally, we can estimate the residual electric field E_R to be 2.5(1.0) mV/cm during the 2S–8S/D measurements [6] and 2.0(1.0) mV/cm for the 2S–12D ones [8].

The calculation of the quadratic Stark effect is straightforward (see Tab. 11). To evaluate the corrections due to the linear Stark effect, we have fitted all the experimental curves $2S_{1/2}$–$8D_J$ and $2S_{1/2}$–$12D_J$ with the theoretical profiles $L(\omega, P, E)$ for the electric field $E = 0$ and $E = E_R$ (for the calculation of $L(\omega, P, E)$ we have used $R_1 = 2$ mm). Then, we make the difference between the two extrapolated values of CLP (obtained for $E = 0$ and $E = E_R$) to obtain the shift due to the linear Stark effect. These corrections are given in Table 12. We can make two comments.

(i) Contrary to the result of equation (20), the shift due to the linear Stark effect is not zero: the $nD_{5/2}$ level is shifted up, and the $nD_{3/2}$ shifted down. We have the following explanation. Schematically, as the $nD_{5/2}$ level is above the $nF_{5/2}$, the mixing of the two levels divides the two-photon line in two components, a large component above the $nD_{5/2}$ level and a small component below the $nF_{5/2}$ level. Following equation (20), the barycentre of these two components is not shifted. If we take into account the saturation of the two-photon transition, the large component is reduced more than the small component and the barycentre should be down shifted. In fact we observe a shift of opposite sign: the adjustment procedure does not give the barycentre of the line, but rather makes the fit to the main component, which is up shifted. The explanation is similar for the $nD_{3/2}$ level but with the signs reversed.

(ii) The total shift is larger for the $nD_{3/2}$ level than for the $nD_{5/2}$, because the quadratic and the linear Stark shift have the same signs in the former case and opposite signs in the latter. This result is important for the 2S–12D transitions: the correction and the uncertainty due to the Stark effect are significant for the $2S_{1/2}$–$12D_{3/2}$ transition and smaller for the $2S_{1/2}$–$12D_{5/2}$ one (see Tab. 12).

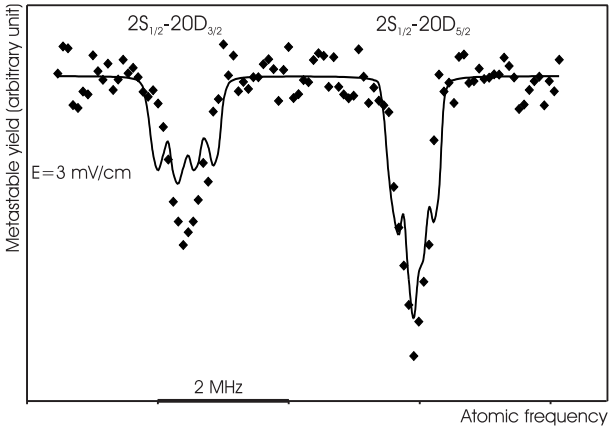

Fig. 15. Fit of the experimental $2S_{1/2}(F = 3/2)$–$20D_{3/2}$ and –$20D_{5/2}$ profiles in deuterium. The theoretical curve (solid) is calculated with an electric field of 3 mV/cm. For the $2S_{1/2}(F = 3/2)$–$20D_{3/2}$ transition, the experimental curve is narrower than the theoretical one.

Table 12. Corrections due to the Stark effect for the 2S–8S/D and 2S–12D transitions (the quadratic Stark corrections are similar for hydrogen and deuterium).

transition	E_R (mV/cm)	quadratic Stark effect (kHz)	linear Stark effect (kHz)	total shift (kHz)
$2S_{1/2}$–$8S_{1/2}$	2.5(1.0)	0.56(40)		0.56(40)
hydrogen				
$2S_{1/2}$–$8D_{3/2}$	2.5(1.0)	−0.27(19)	−0.24(14)	−0.51(33)
$2S_{1/2}$–$8D_{5/2}$	2.5(1.0)	−0.36(25)	0.54(38)	0.18(13)
deuterium				
$2S_{1/2}$–$8D_{3/2}$	2.5(1.0)	−0.27(19)	−0.59(43)	−0.86(62)
$2S_{1/2}$–$8D_{5/2}$	2.5(1.0)	−0.36(25)	0.38(26)	0.02(1)
hydrogen				
$2S_{1/2}$–$12D_{3/2}$	2.0(1.0)	−3.4(2.8)	−2.6(2.1)	−6.0(4.9)
$2S_{1/2}$–$12D_{5/2}$	2.0(1.0)	−5.0(4.0)	2.9(2.8)	−2.1(1.2)
deuterium				
$2S_{1/2}$–$12D_{3/2}$	2.0(1.0)	−3.4(2.8)	−2.7(2.6)	−6.1(5.4)
$2S_{1/2}$–$12D_{5/2}$	2.0(1.0)	−5.0(4.5)	3.9(3.6)	1.1(1.0)

4 Optical frequency measurements

4.1 The rubidium frequency standard

4.1.1 Experimental arrangement and metrological properties

The cornerstone of our optical frequency measurements is a new standard, namely a laser diode at 778 nm (*i.e.* a frequency ν of 385 THz) stabilized to the $5S_{1/2}$–$5D_{5/2}$ two-photon transition of rubidium (LD/Rb laser). This standard has been described previously elsewhere [7,26,27]. The AlGaAs laser diode is used in an extended cavity configuration to obtain a typical spectral width of 100 kHz. The rubidium cell (temperature of 90 °C and pressure of about 8×10^{-5} torr) is placed in an enhancement cavity (30 cm long with a beam waist of 420 μm) in order to define well the two counterpropagating Gaussian beams and eliminate completely the first order Doppler effect. The optical isolation between the laser and the cavity is provided by a Faraday isolator (isolation of 60 dB) and an acousto-optic modulator (AOM) in a double-pass configuration. To control the light shift, we stabilize with the AOM the intensity of the beam transmitted by the cavity to a reference value I_R. The two-photon transition is monitored *via* the fluorescence at 420 nm due to the cascade 5D–6P–5S. The frequency lock of this system is made with two servo-loops. The laser frequency is modulated at 100 kHz with a peak-to-peak amplitude of 300 kHz. A first error signal is extracted from the intensity of the transmitted beam by the cavity to lock the cavity length to the laser wavelength. We then detect the modulation of the fluorescence signal to lock the laser frequency to the two-photon transition of rubidium.

Three identical systems have been built, two at the LPTF (labelled L_1 and L_2) and a third in *Laboratoire Kastler Brossel* (labelled KB). As the two laboratories are linked by two, 3 km long, optical fibers, we can compare the frequencies of the three systems. To check the frequency shift due to the fiber, we have used our highly stabilized titanium-sapphire laser. After a round trip of 6 km through the fibers, we have observed a maximum frequency shift of 3 Hz [28]. This shift is completely negligible for our frequency measurements. From these frequency comparisons, we have determined precisely the light shift of each system (−7.32 kHz for the KB system with the intensity reference value I_R). The main metrological features of the LD/Rb laser are a frequency stability (Allan variance) of about $4\times10^{-13}\tau^{-1/2}$ per laser over 1000 s and a day-to-day repeatability of 400 Hz.

4.1.2 Optical frequency measurement

The frequencies of the three LD/Rb lasers stabilized on the $5S_{1/2}(F{=}3)$–$5D_{5/2}(F{=}5)$ two-photon transition of ^{85}Rb were measured in 1996 at the LPTF with a frequency chain. This frequency chain connects the LD/Rb laser at 385 THz to a standard at 29 THz, namely a CO_2 laser stabilized to an osmium tetraoxyde line (CO_2/OsO_4) [7]. This standard had been previously measured in 1985 with respect to the Cs clock with an uncertainty of 70 Hz (ν = 29 096 274 952 340 (70) Hz) [29,30]. The optical frequencies of the three LD/Rb systems have been found to lie very close to each other (the maximum difference was 1.1 kHz) and the measured frequency of the system working at LKB was, after correction for the light shift:

$$\nu_{KB} = 385\ 285\ 142\ 377.82\ \text{kHz} \qquad (30)$$

with an uncertainty of 1 kHz. This uncertainty was due to the CO_2 laser (13×70 Hz) and the day-to-day repeatability of the LD/Rb standard (400 Hz).

To keep this precision, we have made several frequency comparisons between the L_1, L_2 and KB systems. In 1998, for instance, we have measured the frequency difference $\nu_{KB} - \nu_{L_1}$ and $\nu_{KB} - \nu_{L_2}$. If we suppose that there was no drift of the frequencies ν_{L_1} or ν_{L_2} between 1996 and

1998, we can deduce two values for the frequency of the KB system:

$$\nu_{\mathrm{KB}}(\mathrm{L}_1) = 385\ 285\ 142\ 377.53\ \mathrm{kHz},$$

$$\nu_{\mathrm{KB}}(\mathrm{L}_2) = 385\ 285\ 142\ 378.32\ \mathrm{kHz}.$$

These values are very close to that of the 1996 measurement (Eq. (30)) so we estimate the frequency shift of the KB system to be smaller than 500 Hz.

In 1998, the measurement of the CO_2/OsO_4 standard with respect to the Cs clock was remade with an uncertainty of 20 Hz (*i.e.* a relative uncertainty of 7×10^{-13}) [31]. This measurement corrects the previous one by −88 Hz. With this correction, the frequency of the LD/Rb standard of LKB becomes:

$$\nu_{\mathrm{KB}} = 385\ 285\ 142\ 376.68\ \mathrm{kHz}.$$

Finally, if we take into account the light shift, the frequency $\nu_{\mathrm{KB}}(I_{\mathrm{R}})$ of the LD/Rb standard of LKB working with the reference intensity I_{R} is:

$$\nu_{\mathrm{KB}}(I_{\mathrm{R}}) = 385\ 285\ 142\ 369.4\ (1.0)\ \mathrm{kHz}. \qquad (31)$$

It is this value which has been used for the analysis of the 2S–8S/D and 2S–12D measurements. We have kept a conservative uncertainty of 1 kHz which takes into account the day-to-day repeatability (400 Hz), the long term stability of the LD/Rb standard (500 Hz) and the accuracy of the CO_2/OsO_4 standard (13×20 Hz).

4.2 Optical frequency measurements of the 2S–8S and 2S–8D transitions

4.2.1 The first measurement of the 2S–8S and 2S–8D transitions

In 1993 we carried out a first optical frequency measurement of the 2S–8S and 2S–8D two-photon transitions [5,32]. The principle of this measurement was the near coincidence between the 2S–8S/D frequencies and the frequency difference of two standard lasers, the iodine stabilized (He–Ne/I_2) and the methane stabilized (He–Ne/CH_4) helium-neon lasers (frequencies ν_f and $\nu_{\mathrm{CH_4}}$ respectively):

$$\nu(2\mathrm{S}{-}8\mathrm{S/D}) = \nu_f - \nu_{\mathrm{CH_4}} + \Delta_1$$

where the residual frequency difference Δ_1 is about 89 GHz. After a short description of our experimental scheme, we present an up-to-date analysis of the data which takes into account the recent improvements of the line shape calculations and some optical frequency measurements made subsequently with the LD/Rb standard.

Figure 16 shows the experimental set-up. We use two titanium-sapphire lasers labelled TiS1 and TiS2 which are frequency shifted by about Δ_1. We observe the two-photon transition in hydrogen with the first titanium-sapphire laser. As the power of the He–Ne/CH_4 laser is only 100 μW, we use a more powerful (about 15 mW) auxiliary He–Ne laser at 3.39 μm, which is frequency locked to the He–Ne/CH_4 standard laser. Then the second titanium-sapphire laser and the auxiliary He–Ne laser are mixed in a $LiIO_3$ crystal to generate a radiation at 633 nm. This light is heterodyned with that of the He–Ne/I_2 standard laser. Finally, the frequency difference Δ_1 between the two titanium-sapphire lasers is measured with a Schottky diode which is simultaneously illuminated by the two titanium-sapphire lasers and a Gunn diode at 89 GHz. From the frequency Δ_1 and that of the beat notes at 3.39 μm and 633 nm, we deduce the optical frequency of the TiS1 laser. The details of these frequency measurements are given in references [5,15].

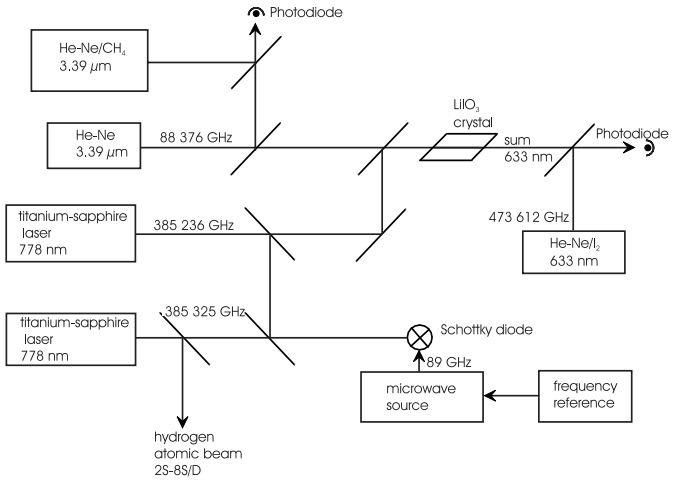

Fig. 16. Experimental set-up for the frequency comparison between the 2S–8S/D transitions in hydrogen and the methane stabilized and iodine stabilized standard lasers.

The He–Ne/CH_4 standard laser was the laser VB-BIPM from the *Bureau International des Poids et Mesures*. Its frequency is known from previous measurements with an uncertainty of 1 kHz:

$$\nu_{\mathrm{CH_4}} = 88\,376\,181\,602.6\,(1.0)\ \mathrm{kHz}.$$

The He–Ne/I_2 standard laser was the laser INM12 from the *Institut National de Métrologie*. In 1992, the frequency ν_f of INM12 laser (locked on the f hyperfine component of the $^{127}I_2$ R11-5 iodine line) was measured in the LPTF with respect to the CO_2/OsO_4 standard [33]. The measured frequency was:

$$\nu_f = 473\ 612\ 353\ 586.9(3.4)\ \mathrm{kHz}. \qquad (32)$$

In 1993 we used these frequency values to determine the hydrogen frequencies. Today, we can use a more reliable value of the frequency ν_f of the INM12 laser. First, in 1993, promptly after the hydrogen measurements, we measured the frequency $\nu_{\mathrm{Rb}}(5\mathrm{S}_{1/2}{-}5\mathrm{D}_{3/2})$ of the $5\mathrm{S}_{1/2}{-}5\mathrm{D}_{3/2}$ two-photon transition of rubidium with the same frequency chain [34]. Indeed, we have a similar coincidence:

$$\nu_{\mathrm{Rb}}(5\mathrm{S}_{1/2}{-}5\mathrm{D}_{3/2}) = \nu_f - \nu_{\mathrm{CH_4}} + \Delta_2 \qquad (33)$$

Table 13. Experimental determination of the 2S–8S/D transition frequencies from our 1993 measurements (all values in MHz).

transition	$2S_{1/2}$–$8S_{1/2}$	$2S_{1/2}$–$8D_{3/2}$	$2S_{1/2}$–$8D_{5/2}$
1993 analysis [5]	770 649 306.3195	770 649 460.0438	770 649 517.1844
updated analysis	770 649 306.3187	770 649 460.0467	770 649 517.1887
correction of ν_f	0.0070	0.0070	0.0070
$2S_{1/2}$ hyperfine shift	44.3892	44.3892	44.3892
$8S_{1/2}$ hyperfine shift	−0.6936		
$\nu(2S_{1/2}$–$8S_{1/2}/8D_J)$	770 649 350.0213	770 649 504.4429	770 649 561.5849
$8S_{1/2}/8D_{3/2}$–$8D_{5/2}$ splitting	211.5621	57.1291	
$\nu(2S_{1/2}$–$8D_{5/2}) - 770\,649\,000$	561.5834 (143)	561.572 (131)	561.5849 (123)
mean value		770 649 561.580 (11)	

but in this case the residual frequency Δ_2 is only 4 to 7 GHz. For instance, for the $5S_{1/2}(F = 1)$–$5D_{3/2}(F = 3)$ hyperfine component in ^{87}Rb, we have measured $\Delta_2 = 7\,383\,160.2\,(2.0)$ kHz. Afterwards, the fine structure $5D_{3/2}$–$5D_{5/2}$ in rubidium was measured at the LPTF [35]. The frequency difference between the ^{85}Rb $5S_{1/2}(F = 3)$–$5D_{5/2}(F = 5)$ (*i.e.* the frequency of the LD/Rb standard) and ^{87}Rb $5S_{1/2}(F = 1)$–$5D_{3/2}(F = 3)$ hyperfine components was measured to be 41 587 229.1 (2.0) kHz. Finally, if we take into account the frequency measurement of the LD/Rb standard, we can deduce the frequency $\nu_{\rm Rb}(5S_{1/2}$–$5D_{3/2})$ and use equation (33) to obtain the frequency ν_f of the He–Ne/I_2 INM12 standard. The result is:

$$\nu_f = 473\ 612\ 353\ 590.4(3.5)\ \text{kHz}. \qquad (34)$$

We have used the mean value of the three LD/Rb standard lasers L_1, L_2 and KB corrected for the recent measurement of the CO_2/OsO_4 standard [7,31] (*i.e.* $\nu(\text{LD/Rb}) = 385\,285\,142\,377.1\,(2.0)$ kHz). The obtained ν_f value is up shifted (3.5 kHz) with respect to the 1992 measurement (Eq. (32)). Though the uncertainties are similar, the value given by equation (34) seems the most reliable because of the very good reproducibility of the two-photon rubidium lines.

In 1993, we measured the three $2S_{1/2}$–$8S_{1/2}$, $2S_{1/2}$–$8D_{3/2}$ and $2S_{1/2}$–$8D_{5/2}$ two-photon transitions in hydrogen (see Tab. 2). We have remade the analysis of the data with the line shape calculations presented in Section 3. The hyperfine structure of the 8D levels, the photoionisation of the excited level, the saturation of the two-photon transition as well as the second order Doppler effect are included in the theoretical profile. The details of this analysis are given in Table 13. We recall the results of our first analysis made in 1993 (first row of the table). The results, given in terms of atomic frequency, are corrected for the second order Doppler effect and the hyperfine structure of the D levels (we have detected an error in the reference [5]: the correction due to the second order Doppler effect is not 40.2 kHz, but rather 42.4 kHz, as indicated in Tab. 1). These values can be directly compared with those of our up-to-date analysis (second row of the table). The result is similar for the $2S_{1/2}$–$8S_{1/2}$ transition, but is upshifted by about 3 kHz for the $2S_{1/2}$–$8D_J$ ones. After the correction of the He–Ne/I_2 frequency (see Eqs. (32, 34)) and of the hyperfine structure of the S levels, we obtain the $2S_{1/2}$–$8S_{1/2}$ and $2S_{1/2}$–$8D_J$ splittings (for this analysis we neglect the Stark effect and the shift due to the black body radiation). For the $2S_{1/2}$ hyperfine structure, we use the value of reference [36]. We deduce the $8S_{1/2}$ hyperfine structure with a simple $1/n^3$ scaling law, because at this level of precision the relativistic corrections in $(Z\alpha)^2$ are negligible. The three experimental values of the $2S_{1/2}$–$8S_{1/2}$ and $2S_{1/2}$–$8D_J$ splittings can be intercompared using the theoretical values of the fine structure and of the Lamb shifts in the $n = 8$ levels. Table 14 gives the theoretical Lamb shifts useful in this paper. We have taken into account the more precise values of the Bethe logarithms [37] and all the recent calculations of the high-order terms following the references [38–40]. For the nuclear charge radii in hydrogen and deuterium, we have used $r_{\rm p} = 0.862$ fm and $r_{\rm d} = 2.115$ fm [41,42]. This enables us to deduce three independent values for the $2S_{1/2}$–$8D_{5/2}$ splitting which are in good mutual agreement (see Tab. 13). The quoted uncertainties come from the statistics, the second-order Doppler effect (2 kHz), the optical alignment and the theoretical line shape (4 kHz and 2 kHz respectively, see Sect. 3.2) and the He–Ne/I_2 standard laser (2×3.5 kHz, see Eq. (34)). Finally, the mean value is:

$$\nu(2S_{1/2}-8D_{5/2}) = 770\,649\,561.580\,(11)\ \text{MHz}.$$

Table 14. Theoretical Lamb shifts in hydrogen and deuterium.

level	hydrogen (MHz)	deuterium (MHz)
$3S_{1/2}$	311.4040 (20)	311.8106 (20)
$6S_{1/2}$	39.0860 (3)	39.1368 (3)
$6D_{5/2}$	0.1660 (2)	0.1662 (2)
$8S_{1/2}$	16.5008 (3)	16.5222 (3)
$8D_{3/2}$	−0.0607 (2)	−0.0607 (2)
$8D_{5/2}$	0.0714 (2)	0.0715 (2)
$12D_{3/2}$	−0.0176 (2)	−0.0176 (2)
$12D_{5/2}$	0.0215 (2)	0.0215 (2)

Table 15. Experimental determination of the 2S–8S/D transition frequencies from the measurements made in hydrogen with the rubidium standard. All the values are in MHz and we have subtracted a frequency ν_0 of 770 649 GHz. The values in bold-faced type are the ones used in the 1998 CODATA adjustment of the fundamental constants [44].

transition in hydrogen	$2S_{1/2}$–$8S_{1/2}$	$2S_{1/2}$–$8D_{3/2}$	$2S_{1/2}$–$8D_{5/2}$
result of the extrapolation $-\nu_0$	306.3175 (70)	460.0609 (66)	517.1958 (40)
stark effect	−0.0006 (4)	0.0005 (3)	−0.0002 (1)
black body radiation	−0.0005 (1)	−0.0006 (2)	−0.0006 (2)
$2S_{1/2}$ hyperfine shift	44.3892	44.3892	44.3892
$8S_{1/2}$ hyperfine shift	−0.6936		
$\nu(2S_{1/2}$–$8S_{1/2}/8D_J)-\nu_0$	**350.0120 (86)**	**504.4500 (83)**	**561.5842 (64)**
$8S_{1/2}/8D_{3/2}$–$8D_{5/2}$ splitting	211.5621	57.1291	
$\nu(2S_{1/2}$–$8D_{5/2})-\nu_0$	561.5741 (86)	561.5791 (83)	561.5842 (64)
mean value and χ^2	770 649 561.5811 (59)		$\chi^2 = 1.69$

By comparison with the published value in 1993 ($\nu(2S_{1/2}$–$8D_{5/2}) = 770\,649\,561.567$ (10) MHz [5]), there is a difference of 13 kHz due to the error in the calculation of the second-order Doppler effect (2.2 kHz), the frequency of the He–Ne/I_2 standard laser (7 kHz), the improvements of the theoretical line shape (2.6 kHz) and the more precise Bethe logarithms (1.2 kHz).

4.2.2 The 1996 measurement using the rubidium standard

To take advantage of the very good long term stability of the LD/Rb standard laser, we have remade the optical frequency measurements of the 2S–8S and 2S–8D transitions in hydrogen and deuterium [6,25]. In this case, the link between the hydrogen frequencies and the standard laser is straightforward. We have:

$$\nu(2S{-}8S/D) = \nu(LD/Rb) + \Delta_3$$

where the residual difference Δ_3 is about 40 GHz in hydrogen and 144 GHz in deuterium. To measure this frequency difference, we focus on a Schottky diode the titanium-sapphire laser (used for the observation of the hydrogen lines) and the LD/Rb standard laser. The Schottky diode is simultaneously irradiated by a microwave source at 13 GHz for hydrogen and 48.4 GHz for deuterium. We detect the low frequency beat note between the two optical radiations and the third harmonic of the microwave. Typically, the signal-to-noise ratio is 35 dB with a resolution bandwidth of 300 kHz. A tracking oscillator is phase locked to this beat note, and we count continuously this frequency. The 13 GHz source is the 130th harmonic of a very stable quartz oscillator at 100 MHz (we use a step recovery diode, a YIG filter and a 35 dB amplifier). For deuterium, this microwave source is shifted to 12.1 GHz (on the 121th harmonic of the 100 MHz quartz). Then, a Gunn diode at 48.4 GHz is phase locked on the fourth harmonic of the 12.1 GHz source. The frequency of the 100 MHz quartz oscillator is continuously compared to a high stability quartz oscillator at 10 MHz (stability of 4×10^{-9} during four months), which has been measured with a hydrogen maser several times. Finally, the uncertainty on the Schottky diode measurement is about 15 Hz in hydrogen and 50 Hz in deuterium.

We have measured the three $2S_{1/2}$–$8S_{1/2}$, $2S_{1/2}$–$8D_{3/2}$ and $2S_{1/2}$–$8D_{5/2}$ two-photon transitions in hydrogen and deuterium (see Tab. 2). In hydrogen, the $2S_{1/2}$–$8D_{5/2}$ frequency was measured twice, at the beginning and at the end of the experiment. The analysis of the results is made in Tables 15 and 16. We use the same procedure than for the 1993 results, but we include the corrections due to the Stark effect and the black body radiation (see Tabs. 12 and 8). In deuterium, we have used the $2S_{1/2}$ hyperfine structure given in reference [43]. In addition to the uncertainties quoted in the Tables, the final uncertainties take into account the second-order Doppler effect (1 kHz), the measurement and the long term stability of the LD/Rb standard laser (2 kHz), the optical alignment and the theoretical line shape (4 kHz and 2 kHz respectively, see Sect. 3.2). The three transition frequencies in hydrogen and deuterium, in bold-faced type in the tables, were used in the 1998 CODATA adjustment of the fundamental constants [44]. As in Table 13, we use the theoretical values of the fine structure between the $8D_{5/2}$ level and the $8S_{1/2}$ or $8D_{3/2}$ ones to obtain three independent values of the $2S_{1/2}$–$8D_{5/2}$ interval. These values are in good agreement with each other, especially these for deuterium. The comparison with the results of 1993 in hydrogen (see Tab. 13) shows an improvement of the accuracy by about a factor 2 and a perfect agreement between the mean values of the $2S_{1/2}$–$8D_{5/2}$ frequencies. The results given in the Tables 15 and 16 are slightly different from the ones published previously [6] (for the mean values, −3.9 kHz and −3.2 kHz in hydrogen and deuterium). These differences are due to the new measurement of the CO_2/OsO_4 laser (−2.3 kHz), the corrections due to the Stark effect and the black body radiation (about −0.6 kHz) and some improvements of the theoretical line shape. With respect to reference [6], the uncertainties are also more conservative.

4.3 Optical frequencies measurements of the 2S–12D transitions

In order to test the measurements of the 2S–8S and 2S–8D transitions, we have built a new frequency chain to measure the frequencies of the 2S–12D intervals [8,45].

Table 16. Experimental determination of the 2S–8S/D transition frequencies from the measurements made in deuterium with the rubidium standard. All the values are in MHz and we have subtracted a frequency ν_0 of 770 859 GHz. The values in bold-faced type are the ones used in the 1998 CODATA adjustment of the fundamental constants [44].

transition in deuterium	$2S_{1/2}$–$8S_{1/2}$	$2S_{1/2}$–$8D_{3/2}$	$2S_{1/2}$–$8D_{5/2}$
result of the extrapolation $-\nu_0$	27.8184 (47)	182.0600 (38)	239.2086 (32)
stark effect	−0.0006 (4)	0.0009 (6)	$\simeq 0$
black body radiation	−0.0005 (1)	−0.0006 (2)	−0.0006 (2)
$2S_{1/2}$ hyperfine shift	13.6415	13.6415	13.6415
$8S_{1/2}$ hyperfine shift	−0.2131		
$\nu(2S_{1/2}$–$8S_{1/2}/8D_J)-\nu_0$	**41.2457 (69)**	**195.7018 (63)**	**252.8495 (59)**
$8S_{1/2}/8D_{3/2}$–$8D_{5/2}$ splitting	211.6027	57.1448	
$\nu(2S_{1/2}$–$8D_{5/2})-\nu_0$	252.8484 (69)	252.8466 (63)	252.8495 (59)
mean value and χ^2	770 859 252.8483 (55)		$\chi^2 = 0.34$

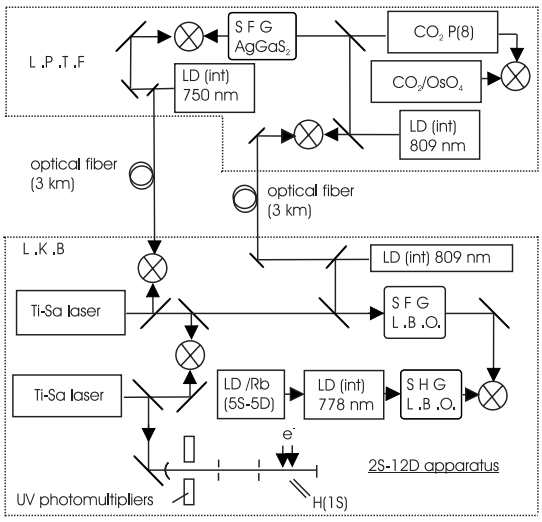

Fig. 17. Outline of the frequency chain between the 2S–12D hydrogen frequencies and the LD/Rb and CO_2/OsO_4 standards. The details are explained in the text (Ti-Sa: titanium sapphire laser, LD/Rb: rubidium stabilized laser diode, LD(int): intermediate laser diode, CO_2/OsO_4: osmium tetraoxyde stabilized CO_2 laser, SHG: second harmonic generation, SFG: sum frequency generation).

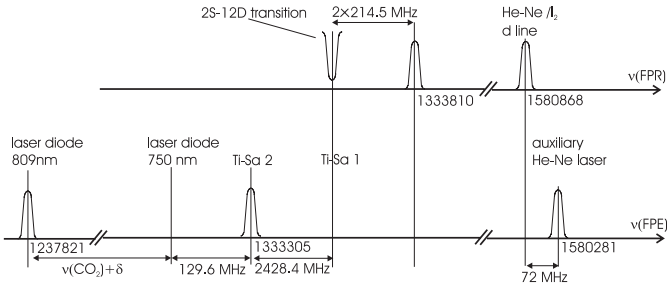

Fig. 18. Example of the position of the laser frequencies with respect to the FPR and FPE cavities during the measurements of the 2S–12D transitions. The fringe 1 580 868 of the FPR cavity is locked on the d line of the He–Ne/I_2 standard laser. The first titanium sapphire laser (Ti-Sa1) is locked on the fringe 1 333 810 of the FPR cavity with an offset of 2×214.5 MHz. The 809 nm laser diode, the second titanium sapphire laser (Ti-Sa2) and the auxiliary He–Ne laser are respectively locked on the fringes 1 237 821, 1 333 305 and 1 580 281. The laser diode at 750 nm is frequency shifted by $\nu(CO_2)+\delta$ with respect to the one at 809 nm.

This transition yields complementary information, because the 12D levels are very sensitive to the stray electric fields (the quadratic Stark shift varies as n^7, see Sect. 3.3), and so such a measurement provides a stringent test of Stark corrections to the Rydberg levels.

4.3.1 The experimental scheme

The frequency difference between the 2S–12D transitions ($\lambda \approx 750$ nm, $\nu \approx 399.5$ THz) and the LD/Rb standard laser is about 14.2 THz, *i.e.* the half of the frequency of the CO_2/OsO_4 standard. To bisect this frequency we use an optical divider [2,46]. The frequency chain (see Fig. 17) is split between the LPTF and the LKB: the two optical fibers are used to transfer the CO_2/OsO_4 standard from the LPTF to the LKB, where we observe the hydrogen transitions. This chain includes an auxiliary source at 809 nm ($\nu \approx 370.5$ THz) such that the laser frequencies satisfy the equations:

$$\nu(2S{-}12D) + \nu(809) = 2\nu(LD/Rb),$$
$$\nu(2S{-}12D) - \nu(809) = \nu(CO_2).$$

The first equation is realized at the LKB while the second one is carried out at the LPTF. For this experiment we use two-titanium-sapphire lasers. Figure 18 shows an example of the positions of the laser frequencies with respect to the FPR and FPE cavities in the case of the $2S_{1/2}$–$12D_{5/2}$ transition in hydrogen. We observe the hydrogen transitions with a first titanium-sapphire laser (TiS1). It is locked on the fringe 1 333 810 of the FPR cavity with a frequency shift due to the AOM1 (see Fig. 2). The source at 809 nm (a laser diode in an extended cavity configuration with a power of about 30 mW) and the second titanium-sapphire laser (TiS2) are frequency modulated

Table 17. Experimental determination of the 2S–12D transition frequencies in hydrogen. All the values are in MHz and we have subtracted a frequency ν_0 of 799 191 GHz. The values in bold-faced type are the ones used in the 1998 CODATA adjustment of the fundamental constants [44].

transition in hydrogen	$2S_{1/2}$–$12D_{3/2}$	$2S_{1/2}$–$12D_{5/2}$
result of the extrapolation $-\nu_0$	666.0796 (62)	683.0145 (47)
stark effect	0.0060 (49)	0.0021 (12)
black body radiation	−0.0021 (5)	−0.0021 (5)
$2S_{1/2}$ hyperfine shift	44.3892	44.3892
$\nu(2S_{1/2}$–$12D_J)-\nu_0$	**710.4727 (93)**	**727.4037 (70)**
$12D_{3/2}$–$12D_{5/2}$ splitting	16.9272	
$\nu(2S_{1/2}$–$12D_{5/2})-\nu_0$	727.3999 (93)	727.4037 (70)
mean value ($\chi^2 = 0.26$)	799 191 727.4028 (67)	

and locked on the fringes 1 237 821 and 1 333 305 of the FPE cavity. A laser diode (power of 50 mW) is injected by the LD/Rb standard and frequency doubled in a LiB_3O_5 crystal (LBO) placed in a ring cavity. This cavity is similar to the one described in reference [13]. We obtain about 10 μW in the UV. At the same time, the TiS2 laser (about 300 mW) and the source at 809 nm are summed in an other LBO crystal to obtain a second UV beam. A tracking oscillator is phase locked on the beat note between the two UV beams (frequency δ_1). A part of the 809 nm source is sent *via* one fiber to the LPTF. There, a 809 nm local laser diode is phase locked to the one at LKB. A frequency sum of this 809 nm laser diode and of an intermediate CO_2 laser in an $AgGaS_2$ crystal produces a wave at 750 nm. This wave is used to phase lock, with a frequency shift δ, a laser diode at 750 nm which is sent back to the LKB by the second optical fiber. This 750 nm laser diode is frequency shifted by $\nu(CO_2) + \delta$ with respect to the one at 809 nm. Then we use a second tracking oscillator to count the beat note (frequency δ_2) between the 750 nm laser diode and the TiS2 laser. Finally, we measure the frequency δ_3 between the two titanium-sapphire lasers. For the hydrogen measurements, the CO_2 auxiliary laser uses the P(8) line (CO_2 R(4) line for deuterium) and the frequency δ_3 is about 2.4 GHz (41.3 GHz in deuterium). The frequency δ_3 is mixed with two times the frequency which drives the AOM1, in order to eliminate the variation of the measured frequency when we scan the TiS1 frequency to observe the hydrogen lines. The 2.4 GHz frequency beat notes is detected with a fast photodiode. For deuterium, we measure the 41.3 GHz frequency with a Schottky diode. As for the hydrogen measurements of the 2S–8S/D transitions (see Sect. 4.2.2), the Schottky diode is irradiated with the two titanium-sapphire lasers and a microwave source at 13.9 GHz and we detect the beat note between the TiS1 and TiS2 lasers and the third harmonic of this microwave radiation (for this measurement we use also a tracking oscillator). Then, from the frequencies δ_1, δ_2 and δ_3, we can deduce the frequency ν(TiS1) of the TiS1 laser. Specifically, we have:

$$\nu(\mathrm{TiS1}) = \nu(\mathrm{LD/Rb}) + \frac{1}{2}\left(\nu(\mathrm{CO_2}) + \delta + \delta_1 + \delta_2\right) + \delta_3.$$

The advantage of this scheme is that all the frequency counting is performed at the LKB.

4.3.2 Results and uncertainties

We have measured the two $2S_{1/2}(F{=}1 \text{ or } 3/2)$–$12D_{3/2}$ and $2S_{1/2}(F{=}1 \text{ or } 3/2)$–$12D_{5/2}$ two-photon transitions in hydrogen and deuterium. We have not studied the $2S_{1/2}$–$12S_{1/2}$ transition because of the low signal-to-noise ratio. For each transition, the signal is recorded for about 50 light powers (see Table 2). The extrapolated frequencies and the analysis of the data are shown in Tables 17 and 18.

For these transitions, the corrections due to the black body radiation and to the Stark effect are not negligible (several kHz), especially the Stark correction of the $2S_{1/2}$–$12D_{3/2}$ (6 kHz). In Tables 17 and 18, these transition frequencies are corrected for the hyperfine structure and compared by taking into account the theoretical value of the fine structure $12D_{3/2}$–$12D_{5/2}$. We obtain two independent values of the $2S_{1/2}$–$12D_{5/2}$ interval which are in good agreement for hydrogen and deuterium. As for the 2S–8S/D results, the final uncertainty takes into account the second order Doppler effect (1 kHz), the accuracy of the LD/Rb standard (2 kHz) and the uncertainties due to the alignment and the theoretical line shape (4 kHz and 2 kHz). Ultimately, these measurements are slightly less precise than those for the 2S–8S/D transitions, owing to the smaller signal-to-noise ratio and the larger Stark shifts.

5 Comparison of the 1S–3S and 2S–6S/D transitions

In this experiment our purpose is the determination of the 1S Lamb shift. This Lamb shift is difficult to measure, because the 1S level is isolated. Up to this experiment, all the measurements of the 1S Lamb shift have been obtained from the study of the 1S–2S two-photon transition by subtracting the 1S–2S Dirac and recoil energies from the experimental value of the 1S–2S interval [47,48]. In the most recent experiments [49,50], this subtraction is made

Table 18. Experimental determination of the 2S–12D transition frequencies in deuterium. All the values are in MHz and we have subtracted a frequency ν_0 of 799 409 GHz. The values in bold-faced type are the ones used in the 1998 CODATA adjustment of the fundamental constants [44].

transition in deuterium	$2S_{1/2}$–$12D_{3/2}$	$2S_{1/2}$–$12D_{5/2}$
result of the extrapolation $-\nu_0$	154.3925 (44)	171.3263 (45)
stark effect	0.0061 (54)	0.0011 (10)
black body radiation	−0.0021 (5)	−0.0021 (5)
$2S_{1/2}$ hyperfine shift	13.6415	13.6415
$\nu(2S_{1/2}$–$12D_J)-\nu_0$	**168.0380 (86)**	**184.9668 (68)**
$12D_{3/2}$–$12D_{5/2}$ splitting	16.9318	
$\nu(2S_{1/2}$–$12D_{5/2})-\nu_0$	184.9698 (86)	184.9668 (68)
mean value ($\chi^2 = 0.28$)	799 409 184.9676 (65)	

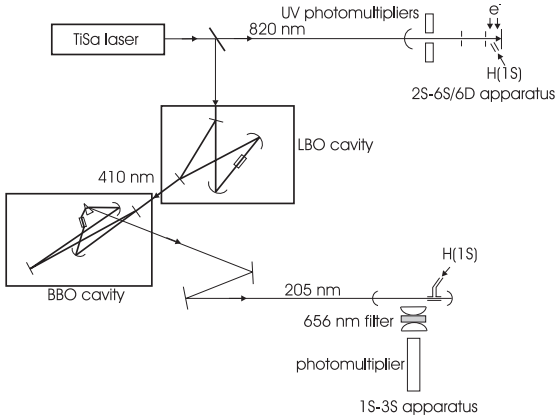

Fig. 19. Experimental setup for the frequency comparison between the 1S–3S and 2S–6S/D transitions (TiSa: titanium sapphire laser, LBO: lithium tri-borate crystal, BBO: β-barium borate crystal).

in a simple way by comparison of the 1S–2S frequency with four times the 2S–4S, 2S–4P or 2S–4D frequencies. Indeed, in the Bohr model, these frequencies lie exactly in a ratio 4:1, and the deviation from this factor is mainly due to the Lamb shifts which vary as $1/n^3$. The principle of our measurement is similar, except that we compare the 1S–3S and 2S–6S/D frequencies, which, for the same reason, are also in a ratio 4:1. This experiment has been described briefly elsewhere [9]. Here we provide some additional details and an updated analysis of the results.

5.1 The 1S–3S transition

Figure 19 shows the general scheme of the experiment. The same titanium-sapphire laser is used to observe, alternately, the 2S–6S or 2S–6D transitions at 820 nm and the 1S–3S transition at 205 nm. The 2S–6S/D apparatus is the one described in Section 2. The UV radiation at 205 nm is obtained from two successive doubling stages with a LBO crystal and a β-barium borate crystal (BBO). Both steps have been described elsewhere [13,51]. Each crystal is placed in an enhancement ring cavity. The first frequency doubling produces up to 500 mW at 410 nm for a pump power of 2.3 W at 820 nm. The second harmonic generation at 205 nm is far more challenging. To avoid rapid degradation of the faces of the BBO crystal, the second enhancement cavity is placed inside a clean chamber filled with oxygen. Moreover, the length of this enhancement cavity is modulated (modulation frequency of 15 kHz) so as to be resonant only some of the time. We work in an intermediate regime in which the UV intensity consists of 3 μs pulses at a frequency of 30 kHz. This method prevents the generation, in the ring cavity, of a counterpropagating wave at 410 nm, probably due to a photorefractive effect in the BBO crystal. This modulation produces a frequency shift, the UV frequency being upshifted (downshifted) by about 120 kHz when the length of the BBO cavity decreases (increases). In this regime, a UV power of about 1 mW (peak power) can be obtained for several hours using the same point of the crystal.

To observe the 1S–3S transition, we use a second atomic beam. Atomic hydrogen is produced by a radiofrequency discharge similar to the one described in Section 2.3.1. The discharge is off-axis with respect to the atomic beam, and linked to the vacuum chamber by a 9 cm length of Teflon tube. The atomic hydrogen flows through a Teflon nozzle (3 cm long, 3 mm in diameter) into the vacuum chamber which is evacuated by an oil diffusion pump (Alcatel 6250). Under running conditions, the pressures in the discharge tube and the vacuum chamber are 0.4 mbar and 9×10^{-5} mbar respectively. With the method described in reference [52], we have measured the angular width of the profile of the effusive atomic beam to be about 8° (full width at the half maximum). By comparison with a previous version of the experiment where the discharge was on the axis of the atomic beam (there was only the Teflon nozzle), we have also found that the atomic flux is reduced by about a factor 4. This effect shows that the recombination of the hydrogen atoms in the Teflon tube is significant. The atomic beam is carefully delimited by two diaphragms (diameter of 2 mm and 3 mm successively) to eliminate the stray light coming from the hydrogen discharge. The atomic beam is also placed inside a linear

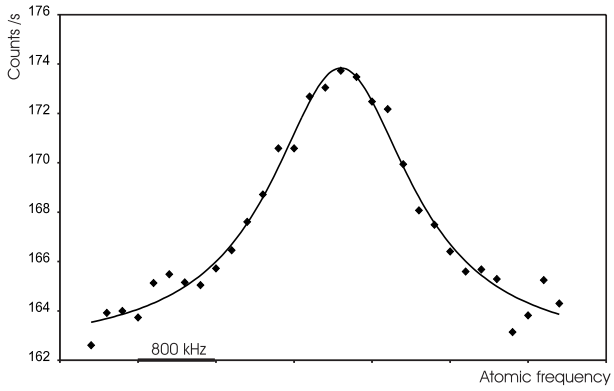

Fig. 20. Spectrum of the $1S_{1/2}(F = 1)$–$3S_{1/2}(F = 1)$ transition detected by Balmer-α fluorescence. The total acquisition time is about 14 hours. The signal is fitted with a Lorentzian curve (solid).

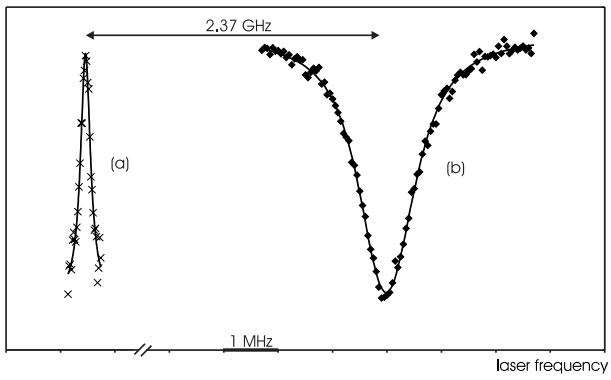

Fig. 21. Hydrogen two-photon spectra. (a) $1S_{1/2}(F = 1)$–$3S_{1/2}(F = 1)$ transition. (b) $2S_{1/2}(F = 1)$–$6D_{5/2}$ transition. The two signals are shifted by about 2.37 GHz in terms of laser frequency at 820 nm.

buildup cavity formed by two spherical mirrors (radius of curvature 25 cm). The UV beam emerging from the BBO crystal is corrected for astigmatism with a spherical lens (focal length 87 mm) and a cylindrical lens (focal length 290 mm) and mode matched into the cavity with two more lenses. Inside the cavity, the UV power is typically 10 mW and the UV beam is focused at a distance of 12 cm from the Teflon nozzle with a waist of about 48 μm. At this distance, we estimate the density of hydrogen atoms to be about 3×10^{10} atoms/cm^3. The two cavity mirrors are mounted on PZT stacks and the length of the cavity is locked to the UV frequency so that successive UV pulses have the same intensity inside the cavity. In these conditions, the frequency shifts of two successive UV pulses cancel each other and the residual frequency shift is estimated to be less than 3 kHz. The two-photon transition is detected by monitoring the Balmer-α fluorescence due to the radiative decay 3S–2P. This fluorescence is collected with a spherical mirror and a $f/0.5$ aspheric lens system, selected with an interference filter and detected with a cooled photomultiplier (EMI 9658R).

The data acquisition is similar to the one described in Section 2.4. Each scan is divided in 31 frequency points. For each point, the photomultiplier signal is counted during 1 s and we make 10 scans of the line to achieve a 7 minute run. As the signal-to-noise ratio is small, we take the mean of several runs to obtain an observable signal. Figure 20 shows the mean of 102 runs. The total background is about 160 counts/s and the 1S–3S signal 10 counts/s. In Figure 20, the signal is fitted with a Lorentzian curve. The observed line width (1.7 MHz in terms of atomic frequency) is mainly due to the natural width of the 3S level (1 MHz), transit time broadening (200 kHz) and broadening due to the modulation of the UV light (about 500 kHz). We can compare the signal amplitude with a theoretical estimate. The two-photon transition probability Γ_g is given by equation (9). As the value of the matrix element $\langle 3S\,|Q_{\rm tp}|\,1S\rangle$ of the two-photon operator is 2.14 in atomic units [53], we obtain for a UV power of 10 mW: $\Gamma_g = 2\times10^{-2}$ s^{-1}. If we take into account the effective linewidth (1.7 MHz), the atomic density in front of the photomultiplier (3×10^{10} atoms/cm^3), the observation length (12 mm because of the transmission of the interference filter), the detection solid angle ($\Omega/4\pi = 0.24$), the transmission of the detection optics (about 66%), the photomultiplier quantum efficiency (8%), the population of the $F = 1$ hyperfine level (3/4) and the modulation of the UV light (reduction of the excitation time by a factor 0.066), we estimate the signal to be about 20 counts/s. This value is in fair agreement with the experiment if we consider the uncertainties in the UV power and the atomic density.

5.2 Comparison of the 1S–3S and 2S–6S/D frequencies

We have compared the $1S_{1/2}$–$3S_{1/2}$ frequencies with those of the $2S_{1/2}$–$6D_{5/2}$ and $2S_{1/2}$–$6S_{1/2}$ transitions. To do this, we have measured alternately the 1S–3S and 2S–6S/D line positions with respect to the fringes 1 219 477 (transition $1S_{1/2}$–$3S_{1/2}$) and 1 219 485 (transition $2S_{1/2}$–$6D_{5/2}$) or 1 219 484 (transition $2S_{1/2}$–$6S_{1/2}$) of our very stable FPR cavity. For the first comparison, we collected the data for the $2S_{1/2}$–$6D_{5/2}$ transition (1 day), the $1S_{1/2}$–$3S_{1/2}$ (3 days), then $2S_{1/2}$–$6D_{5/2}$ once again (2 days). The procedure was similar for the $2S_{1/2}$–$6S_{1/2}$ transition, but, because of its lower intensity, longer acquisition times were required (4, 3 and 4 days respectively). Figure 21 shows, on the same frequency scale, the recordings of the $1S_{1/2}$–$3S_{1/2}$ and $2S_{1/2}$–$6D_{5/2}$ lines. As the 2S–6S/D linewidth is larger than the 1S–3S one, the accuracy is mainly limited by the uncertainty in the 2S–6S/D line positions.

The results are given in Table 19. For the 2S–6S/D transitions, we have used our updated analysis of the data: the second-order Doppler effect and the 6D hyperfine structure are included in the theoretical line shape. The quoted uncertainties of the second row of the table (8.8 kHz and 20 kHz for each measurement) are mainly due to the uncertainties in the positions of the 1S–3S line

Table 19. Comparison between the $1S_{1/2}$–$3S_{1/2}$ and $2S_{1/2}$–$6D_{5/2}/6S_{1/2}$ frequencies. All the values are in MHz. The values in bold-faced type are the ones used in the 1998 CODATA adjustment of the fundamental constants [44].

comparison with	$2S_{1/2}$–$6D_{5/2}$	$2S_{1/2}$–$6S_{1/2}$
laser frequency splitting	2370.1140 (44)	2120.188 (10)
laser frequency splitting ×2	4740.2280 (88)	4240.377 (20)
1S–3S second-order Doppler effect	−0.0310 (25)	−0.0310 (25)
hyperfine structure corrections	−41.0981	−42.7421
ν(2S–6S/D) − ν(1S–3S)/4	**4699.099 (11)**	**4197.604 (21)**
$6S_{1/2}$–$6D_{5/2}$ splitting		501.5051
$\nu(2S_{1/2}–6D_{5/2}) - \nu$(1S–3S)/4	4699.099 (11)	4699.109 (21)
mean value	4699.1006 (98)	

(4.7 kHz and 6 kHz for each measurement) and of the 2S–6D or 2S–6S lines (7.1 kHz and 19 kHz). For the 1S atomic beam, the velocity distribution is that of a thermal beam, *i.e.* $f(v) \sim v^3 \exp\left(-v^2/2\sigma^2\right)$ and the second-order Doppler shift of the 1S–3S line is $-3/2(\sigma/c)^2\nu_{1S-3S}$ (see Eq. (2)). The analysis of the features of the metastable atomic beam shows that the heating due to the discharge is typically 30 K. As the two discharges of the two atomic beams are of identical design, we can assume that the temperature of the beam is in the range 280–330 K and we obtain a second-order Doppler shift of −124(10) kHz for the 1S–3S transition in terms of atomic frequency, *i.e.* −31.0(2.5) kHz for the comparison with the 2S–6S/D frequencies. Because of the 1S and 3S hyperfine structures, there is a quadratic Zeeman effect of the $F = 1, m_F = 0$ sublevels. For the 1S–3S line this effect introduces a mean shift of 11.9 kHz/G^2 (in terms of atomic frequency). In our experiment, the Earth's magnetic field is about 260 mG and the Zeeman shift of the 1S–3S transition 800 Hz. We have neglected this effect and several other small effects: the shifts due to the black body radiation (see Tab. 8), the residual Stark shifts (smaller than 300 Hz for the 2S–6S/D transition) and the light shift of the 1S–3S transition. For this transition, the light shift coefficients β_i (see Eq. (11)) are −6.445 and 20.926 (atomic units) for the 1S and 3S level respectively [19]. With a UV power of 10 mW, the light shift is about 740 Hz for an atom at the center of the laser beam. As previously, the final uncertainties (11 kHz and 21 kHz for the two measurements, see Tab. 19) take into account the uncertainty of the second-order Doppler effect of the 2S–6S/D lines (2 kHz), and the uncertainties due to the alignment and the theoretical line shape (4 kHz and 2 kHz).

Finally, if we use the theoretical value of the $6S_{1/2}$–$6D_{5/2}$ splitting, we can compare the two measurements. We obtain two independent values of the frequency difference $\nu(2S_{1/2}–6D_{5/2}) - \nu$(1S−3S)/4 which are in fair agreement. By comparison with the results published previously [9], these values are shifted by 6 kHz and −3.7 kHz for the $2S_{1/2}$–$6D_{5/2}$ and $2S_{1/2}$–$6S_{1/2}$ measurements because of the new theoretical line shape. Finally we obtain an uncertainty of 9.8 kHz for the difference $\nu(2S_{1/2}–6D_{5/2}) - \nu$(1S−3S)/4.

6 Determination of the Rydberg constant and Lamb shifts

6.1 Method and analysis of the data

6.1.1 Theoretical background

The aim of this section is to extract from our measurements the values of Rydberg constant and Lamb shifts. More details of the theory of atomic hydrogen can be found in the review articles [38–40]. The hydrogen level energy is conventionally expressed as the sum of three terms: the energy given by the Dirac equation for a particle with the reduced mass, the first relativistic correction due to the recoil of the proton, and the Lamb shift. The energy $E_{\rm H}(nLJ)$ of the level $|nLJ\rangle$ of hydrogen is:

$$E_{\rm H}(nLJ) = d_{\rm H}(nLJ)hcR_\infty + r_{\rm H}(n)hcR_\infty + hL_{\rm H}(nLJ) \quad (35)$$

where $d_{\rm H}(nLJ)hcR_\infty$ and $r_{\rm H}(nLJ)hcR_\infty$ describe the Dirac and recoil energies. The coefficients $d_{\rm H}(nLJ)$ and $r_{\rm H}(n)$ can be expressed exactly as a function of the fine structure constant α and the electron to proton mass ratio $m_{\rm e}/m_{\rm p}$. Moreover, the coefficient $r_{\rm H}(n)$ does not depend on the quantum numbers L and J [20]. The Lamb shift $L_{\rm H}(nLJ)$ is expressed in terms of frequency. It contains all the theoretical corrections, *i.e.* the QED corrections, the other relativistic corrections due to the proton recoil and the effect of the proton charge distribution. For deuterium, the energy $E_{\rm D}(nLJ)$ is given by a similar equation with the subscripts D. Equation (35) shows that, to extract the Rydberg constant from our measurements, we need to know the Lamb shifts. For the upper levels of the transitions, we can use the theoretical values of the Lamb shift (see Tab. 14), because the theoretical uncertainties (only a few hundred hertz) are far smaller than those of our measurements (typically 6 kHz). On the other hand, for the 1S and 2S levels, this is not the case. The one-loop QED corrections are now calculated with an accuracy of 1 Hz [54]. By contrast, for the calculations of the higher order terms, the QED uncertainties are typically 5 kHz and 40 kHz for the 2S and 1S levels [55–57]. Moreover, the disagreement between the two determinations

of the charge radius of the proton ($r_p = 0.805(11)$ fm [58] and $r_p = 0.862(12)$ fm [41]) corresponds to a difference of 18 kHz and 149 kHz respectively for the 2S and 1S Lamb shifts. Consequently, in our data analysis, we shall consider that the 1S and 2S Lamb shifts are unknowns to be determined by the experiment. Nevertheless, since several terms of the Lamb shift calculations vary with the principal quantum number exactly as $1/n^3$ (for instance the effect of the charge distribution of the nucleus), the deviation from this scaling law as been calculated precisely by Karshenboim [59]. For the 1S and 2S levels of hydrogen and deuterium the results are:

$$L_H(1S_{1/2}) - 8L_H(2S_{1/2}) = -187.232(5)\ \text{MHz} \quad (36)$$

$$L_D(1S_{1/2}) - 8L_D(2S_{1/2}) = -187.225(5)\ \text{MHz} \quad (37)$$

as one might expect, there are similar equations for the other $n\mathrm{S}_{1/2}$ levels.

6.1.2 Experimental data

To determine the Rydberg constant and the Lamb shifts, we use the mean values of the frequencies $\nu_A(2S_{1/2}–nD_{5/2})$ (A = H or D and n = 8 or 12) and of the frequency difference $\nu_H(2S_{1/2}–6D_{5/2}) - \nu_H(1S_{1/2}–3S_{1/2})/4$ which are given at the end of the Tables 15–19. We have introduced the subscripts H and D to distinguish the hydrogen and deuterium cases. If we define the coefficient $a_A(2S_{1/2}–nD_{5/2}) = d_A(nD_{5/2}) + r_A(nD_{5/2}) - d_A(2S_{1/2}) - r_A(2S_{1/2})$ we deduce from our experimental results five equations:

$$\nu_A(2S_{1/2}–nD_{5/2}) = a_A(2S_{1/2}–nD_{5/2})cR_\infty + L_A(nD_{5/2}) - L_A(2S_{1/2}) \quad \text{(4 equations)}. \quad (38)$$

And we obtain from the 1S–3S and 2S–6S/D comparison:

$$\nu_H(2S_{1/2}–6D_{5/2}) - \frac{1}{4}\nu_H(1S_{1/2}–3S_{1/2}) = \left[a_H(2S_{1/2}–6D_{5/2}) - \frac{1}{4}a_H(1S_{1/2}–3S_{1/2})\right] cR_\infty + L_H(6D_{5/2}) - L_H(2S_{1/2}) - \frac{1}{4}\left(L_H(3S_{1/2}) - L_H(1S_{1/2})\right). \quad (39)$$

We will use also several other precise measurements in hydrogen and deuterium, at first the measurements of the 2S Lamb shift in hydrogen. This Lamb shift (in fact the difference between the $2S_{1/2}$ and $2P_{1/2}$ Lamb shifts) is deduced from radiofrequency measurements of the $2P_{1/2}$–$2S_{1/2}$ splitting, the first by Lamb and Retherford [60]. The most precise direct determination of this splitting is the one by Lundeen and Pipkin (1 057.845(9) MHz [61]). We have also used two other indirect determinations deduced from the $2S_{1/2}$–$2P_{3/2}$ splitting (1 057.842(12) MHz [62,63]) and obtained by the anisotropy method (1 057.852(15) MHz [64]). From the weighted mean value of these three results (1 057.8454(65) MHz) and the theoretical value of the $2P_{1/2}$ Lamb shift (−12.835 99(8) MHz [63]) we deduce the $2S_{1/2}$ Lamb shift:

$$L_H(2S_{1/2}) = 1\,045.009\,4(65)\ \text{MHz}. \quad (40)$$

We have not taken into account the determination of Pal'chikov *et al.* (1 057.8514(19) MHz [65]) who measured in fact the ratio between the $2S_{1/2}$ Lamb shift and the natural width of the $2P_{1/2}$ level. Since there is an ongoing discussion about the theoretical value of this natural width [66,67], we have not used this result.

The frequency and the isotope shift of the 1S–2S transition have been measured very accurately by Hänsch and coworkers [2,3]. Their results provide us with equations:

$$\nu_H(1S_{1/2}–2S_{1/2}) = a_H(1S_{1/2}–2S_{1/2})cR_\infty + L_H(2S_{1/2}) - L_H(1S_{1/2}), \quad (41)$$

$$\nu_D(1S_{1/2}–2S_{1/2}) - \nu_H(1S_{1/2}–2S_{1/2}) = \left[a_D(1S_{1/2}–2S_{1/2}) - a_H(1S_{1/2}–2S_{1/2})\right] cR_\infty + L_D(2S_{1/2}) - L_H(2S_{1/2}) - L_D(1S_{1/2}) + L_H(1S_{1/2}). \quad (42)$$

Lastly, we will use also the measurements of the $1S_{1/2}$ Lamb shift made by comparison of the 1S–2S frequency with the 2S–4S/D frequencies [42,49] or with the 2S–4P frequencies [50]. If we use the theoretical values of the Lamb shifts for the $n = 4$ levels, the analysis of these data gives two experimental values of the linear combination of the Lamb shifts:

$$L_H(1S_{1/2}) - 5L_H(2S_{1/2}) = 2\,947.831(37)\ \text{MHz} \quad (1S–2S \text{ and } 2S–4S/D \text{ comparison}), \quad (43)$$

$$L_H(1S_{1/2}) - 5L_H(2S_{1/2}) = 2\,947.787(34)\ \text{MHz} \quad (1S–2S \text{ and } 2S–4P \text{ comparison}). \quad (44)$$

These two measurements are in fair agreement with each other.

To conclude, we obtain a set of 12 equations where the 5 unknowns are the Rydberg constant and the Lamb shifts of the 1S and 2S levels in hydrogen and deuterium: 2 theoretical equations (36, 37), 5 equations given by our experimental results (38, 39) and 5 equations which resume the accurate measurements made in hydrogen or deuterium by several other groups (40–44). This set of equations give us the possibility, with least squares procedures, to extract the Rydberg constant and the Lamb shifts by different ways. We present several approaches below. For these calculations, we use the value of the fine structure constant given by the last adjustment of the fundamental constants $\alpha^{-1} = 137.035\,999\,76(50)$ [44]. This choice is justified because, in this adjustment, the hydrogen measurements have no significant influence on the determination of the fine structure constant. For the proton-to-electron and deuteron-to-proton mass ratios, we use the values taken from references [68,69]: $m_p/m_e = 1\,836.152\,666\,5(40)$ and $m_d/m_p = 1.999\,007\,501\,3(14)$.

Table 20. Determination of the Rydberg constant.

method and transitions involved	equations	$(R_\infty - 109\,737)$ cm^{-1}
determination of R_∞ from the 2S–nD and 2S–2P measurements		
2S–2P and 2S–8S/D in hydrogen	(38, 40)	0.315 6861(13)
2S–2P and 2S–12D in hydrogen	(38, 40)	0.315 6848(13)
2S–2P, 2S–8S/D and 2S–12D in hydrogen	(38, 40)	0.315 6855(11)
determination of R_∞ from linear combination of optical frequencies measurements		
2S–8S/D, 1S–2S and $1/n^3$ law in hydrogen	(36, 38, 41)	0.315 6865(16)
2S–12D, 1S–2S and $1/n^3$ law in hydrogen	(36, 38, 41)	0.315 6842(17)
2S–8S/D, 2S–12D, 1S–2S and $1/n^3$ law in hydrogen	(36, 38, 41)	0.315 6854(13)
2S–8S/D, 2S–12D, 1S–2S and $1/n^3$ law in deuterium	(37, 38, 41, 42)	0.315 6854(12)
2S–8S/D, 2S–12D, 1S–2S and $1/n^3$ law in hydrogen and deuterium	(36–38, 41, 42)	0.315 6854(10)
general least squares adjustment in hydrogen and deuterium		
2S–2P, 2S–8S/D, 2S–12D, 1S–2S and $1/n^3$ law	(36–44)	0.315 685 50(84)

6.2 Rydberg constant

We can extract the Rydberg constant from only our results by considering the $8D_{5/2}$–$12D_{5/2}$ splitting, which is obtained by difference between our $2S_{1/2}$–$8D_{5/2}$ and $2S_{1/2}$–$12D_{5/2}$ measurements. Nevertheless, since this splitting is small (about 30 THz), the relative accuracy of this method is only 2×10^{-10}. A first precise method is to use the experimental determination of the $2S_{1/2}$ Lamb shift in hydrogen (Eq. (40)). The first part of Table 20 gives the values of the Rydberg constant deduced from our $2S_{1/2}$–$8D_{5/2}$ and $2S_{1/2}$–$12D_{5/2}$ measurements in hydrogen. These two values have a similar precision and are in an acceptable agreement (they differ by about 1 standard deviation). This agreement shows that the corrections due to the Stark effect are well analyzed (these corrections are about 10 times larger for the 12D than for the 8D levels, see Tab. 12). Table 20 gives the average of these results ($R_\infty = 109\,737.315\,685\,5(11)$ cm^{-1}). The relative uncertainty (about 10^{-11}) comes from the optical frequency measurements (6.1×10^{-12}), the $2S_{1/2}$ Lamb shift (8.3×10^{-12}) and the proton-to-electron mass ratio (1.2×10^{-12}). The uncertainty due to the fine structure constant is negligible (1.3×10^{-13}). This result is the most precise if we make no theoretical assumptions concerning the $1S_{1/2}$ and the $2S_{1/2}$ Lamb shifts. Unfortunately, this method is not appropriate for deuterium, because, for this isotope, no comparably accurate determination of the $2S_{1/2}$ Lamb shift has been performed.

If we use the $1/n^3$ scaling law for the Lamb shifts (Eqs. (36, 37)), we can form the linear combination of the $1S_{1/2}$–$2S_{1/2}$ and $2S_{1/2}$–$nD_{5/2}$ frequencies:

$$7\nu_{\rm H}(2S_{1/2}-nD_{5/2}) - \nu_{\rm H}(1S_{1/2}-2S_{1/2}).$$

In this way, we can eliminate from the equations (38, 41) the Lamb shift combination $L_{\rm H}(1S_{1/2}) - 8L_{\rm H}(2S_{1/2})$ (Eq. (36)) and we deduce the Rydberg constant without the microwave measurements of the $2S_{1/2}$ Lamb shift. Moreover, this method is applicable to both hydrogen and deuterium. The results are given in the second part of Table 20. The values obtained for hydrogen and deuterium are in perfect agreement. If we use all the precise optical frequency measurements in hydrogen and deuterium (transitions $1S_{1/2}$–$2S_{1/2}$, $2S_{1/2}$–$8D_{5/2}$ and $2S_{1/2}$–$12D_{5/2}$), we obtain a value of R_∞ more precise than the previous ones ($R_\infty = 109\,737.315\,685\,4(10)$ cm^{-1}). This value is also in perfect agreement with the one deduced *via* the measurements of the $2S_{1/2}$ Lamb shift.

To make an average of these different determinations of R_∞, we have performed a least squares adjustement which takes into account all the precise measurements described by the equations (36–44): the measurements of the $2S_{1/2}$ Lamb shift, the optical frequency measurements of the 1S–2S and 2S–nD transitions in hydrogen and deuterium, and also the measurements of the 1S Lamb shift which will be described in Section 6.3. This result ($R_\infty = 109\,737.315\,685\,50(84)$ cm^{-1}) is similar to the one of the 1998 adjustment of the fundamental constant [44], with a relative uncertainty of 7.7×10^{-12}. By comparison with the 1986 adjustment [70], the uncertainty is reduced by a factor of about 150. Figure 22 compares the recent determinations of the Rydberg constant and shows the different steps of this improvement since 1986.

The values of Table 20 are slightly different from the ones published previously [8], because for the fine structure constant α we had used the value of the 1986 CODATA adjustment, which differs from the new value by about 7.5×10^{-8} [70]. To obtain these results, we have chosen to leave out our first determination of the $2S_{1/2}$–$8D_{5/2}$ frequency (see Tab. 13), because this measurement has no significant bearing upon the final result: if we included this value, the uncertainty in R_∞ would be reduced to only 83×10^{-8} cm^{-1}.

6.3 Lamb shifts

We can deduce the $1S_{1/2}$ Lamb shift from the comparison of the $1S_{1/2}$–$3S_{1/2}$ and $2S_{1/2}$–$6D_{5/2}$ frequencies

Table 21. Determination of the $1S_{1/2}$ Lamb shift in hydrogen.

method and transitions involved	equations	$L_H(1S_{1/2})$ (MHz)
comparison of transition frequencies lying in a ratio 4:1		
2S–2P, 1S–3S and 2S–6S/D	(39, 40)	8 172.825(47)
2S–2P, 1S–2S and 2S–4S/D	(43, 40)	8 172.878(51)
2S–2P, 1S–2S and 2S–4P	(44, 40)	8 172.834(48)
comparison of the 1S–2S and 2S–nD frequencies using the $2S_{1/2}$ Lamb shift		
2S–2P, 1S–2S and 2S–8S/D	(38, 40, 41)	8 172.854(33)
2S–2P, 1S–2S and 2S–12D	(38, 40, 41)	8 172.825(34)
2S–2P, 1S–2S, 2S–8S/D and 2S–12D	(38, 40, 41)	8 172.840(31)
comparison of the 1S–2S and 2S–nD frequencies using the $1/n^3$ scaling law		
2S–8S/D, 2S–12D, 1S–2S and $1/n^3$ law in hydrogen	(36, 38, 41)	8 172.837(32)
2S–8S/D, 2S–12D, 1S–2S and $1/n^3$ law in hydrogen and deuterium	(36–38, 41, 42)	8 172.837(26)
general least squares adjustment in hydrogen and deuterium		
2S–2P, 2S–8S/D, 2S–12D, 1S–2S and $1/n^3$ law	(36–44)	8 172.840(22)
theory $r_p = 0.862(12)$ fm [56]		8 172.731(40)
theory $r_p = 0.805(11)$ fm [56]		8 172.582(40)

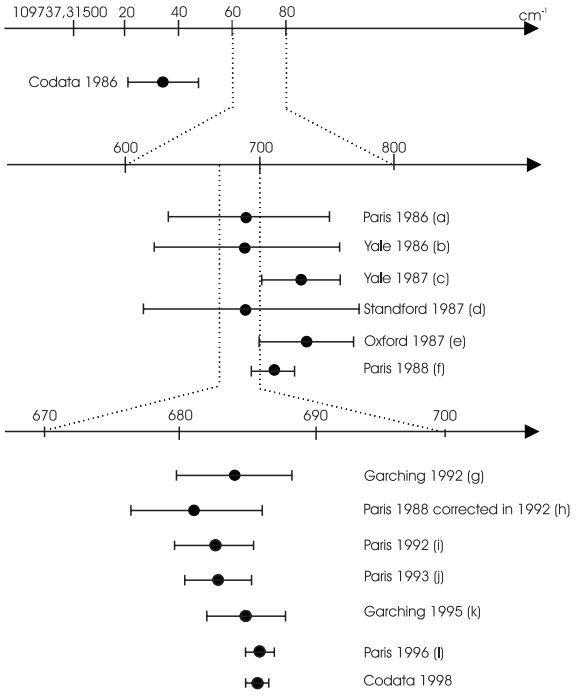

Fig. 22. Comparison of various determinations of the Rydberg constant since the 1986 adjustment of the fundamental constants; Codata 1986 [70], a [71], b [72], c [73], d [74], e [48], f [75], g [76], h: reference [75] corrected for the new measurement of the He–Ne/I_2 standard laser [33], i [4], j [5], k [42], l [6], Codata 1998 [44].

(see Eq. (39)). The value of the term $[a_H(2S_{1/2}-6D_{5/2}) - a_H(1S_{1/2}-3S_{1/2})/4]cR_\infty$ is 3 778.5887 MHz. If we use the theoretical values of the $2S_{1/2}$ and $6D_{5/2}$ Lamb shift, we obtain the linear combination of the $1S_{1/2}$ and $2S_{1/2}$ Lamb shifts:

$$L_H(1S_{1/2}) - 4L_H(2S_{1/2}) = 3\,992.787(39) \text{ MHz}. \quad (45)$$

Finally, thanks to the experimental value of the $2S_{1/2}$ Lamb shift (Eq. (40)) we deduce the value $L_H(1S_{1/2}) = 8\,172.825(47)$ MHz. This value differs from the one published previously by 27 kHz. This is due to a different value of the $2S_{1/2}$ Lamb shift (10 kHz) and to our new theoretical line shape (17 kHz). This result is compared in the first part of Table 21 with the determinations obtained by comparison of the 1S–2S and 2S–4S/D or 2S–4P frequencies (Eqs. (43, 44); with respect to references [42, 50], these two values are updated by taking into account the different values of the $2S_{1/2}$ Lamb shift and of the fine structure constant). The three results have a similar precision and are in good agreement.

Another way to obtain the $1S_{1/2}$ Lamb shift is to use the precise optical frequency measurements of the $1S_{1/2}$–$2S_{1/2}$ and $2S_{1/2}$–$nD_{5/2}$ transitions. A first method uses the experimental value of the $2S_{1/2}$ Lamb shift (Eq. (40)) to extract R_∞ from the $2S_{1/2}$–$nD_{5/2}$ splitting (see the first part of Tab. 20). Then the $1S_{1/2}$ Lamb shift is deduced from the $1S_{1/2}$–$2S_{1/2}$ frequency. The results are given in the second part of Table 21. The final result ($L_H(1S_{1/2}) = 8\,172.840(31)$ MHz) is more precise than the precedent ones because of the very high accuracy of the optical frequency measurements. The 31 kHz uncertainty is due to the optical frequency measurements (15 kHz) and, mainly, to the measurement of the $2S_{1/2}$ Lamb shift (27 kHz). In a second method, we can avoid this limitation by using the $1/n^3$ scaling law of the Lamb shift. The values obtained by this way are slightly more precise (see the third part of Tab. 21). Moreover, this method provides the $2S_{1/2}$ Lamb shift and is reliable in the case of deuterium. Finally, we give the result of the general

Table 22. Determination of the $1S_{1/2}$ Lamb shift in deuterium.

method and transitions involved	equations	$L_D(1S_{1/2})$ (MHz)
comparison of transition frequencies lying in a ratio 4:1		
1S–2S, 2S–4S/D and theoretical value of $L_D(2S_{1/2})$ [42]		8 183.807(78)
comparison of the 1S–2S and 2S–nD frequencies using the $1/n^3$ scaling law		
2S–8S/D, 2S–12D, 1S–2S and $1/n^3$ law in deuterium	(37, 38, 41, 42)	8 183.968(31)
2S–8S/D, 2S–12D, 1S–2S and $1/n^3$ law in hydrogen and deuterium	(36–38, 41, 42)	8 183.967(26)
general least squares adjustment in hydrogen and deuterium		
2S–2P, 2S–8S/D, 2S–12D, 1S–2S and $1/n^3$ law	(36–44)	8 183.970(22)

Table 23. Determination of the $2S_{1/2}$ Lamb shift in hydrogen.

method and transitions involved	equations	$\nu_H(2S_{1/2}-2P_{1/2})$ (MHz)
direct measurement of the $2S_{1/2}$–$2P_{1/2}$ splitting		
$2S_{1/2}$–$2P_{1/2}$, Newton *et al.* [77]		1 057.862(20)
$2S_{1/2}$–$2P_{1/2}$, Lundeen *et al.* [61]		1 057.845(9)
$2S_{1/2}$–$2P_{3/2}$, Hagley *et al.* [62,63]		1 057.842(12)
2S–2P, Wijngaarden et al. [64]		1 057.852(15)
comparison of transition frequencies lying in a ratio 4:1		
1S–3S, 2S–6S/D and $1/n^3$ scaling law	(36, 39)	1 057.841(10)
1S–2S, 2S–4S/D and $1/n^3$ scaling law	(36, 43)	1 057.857(12)
1S–2S, 2S–4P and $1/n^3$ scaling law	(36, 44)	1 057.842(11)
comparison of the 1S–2S and 2S–nD frequencies using the $1/n^3$ scaling law		
2S–8S/D, 2S–12D, 1S–2S and $1/n^3$ law in hydrogen	(36, 38, 41)	1 057.8446(42)
2S–8S/D, 2S–12D, 1S–2S and $1/n^3$ law in hydrogen and deuterium	(36–38, 41, 42)	1 057.8447(34)
general least squares adjustment in hydrogen and deuterium		
2S–2P, 2S–8S/D, 2S–12D, 1S–2S and $1/n^3$ law	(36–44)	1 057.8450(29)
theory $r_p = 0.862(12)$ fm [56]		1 057.836(6)
theory $r_p = 0.805(11)$ fm [56]		1 057.812(6)

adjustment ($L_H(1S_{1/2}) = 8\,172.840(22)$ MHz) with a relative uncertainty of 2.7×10^{-6}.

Table 22 gives the results for the $1S_{1/2}$ Lamb shift in deuterium. First, we recall the value of reference [42] which was obtained by comparison of the 1S–2S and 2S–4S/D frequencies, but which used the theoretical value of the $2S_{1/2}$ Lamb shift. Afterwards, we give the results of the comparison of the 1S–2S and 2S–nD frequencies and we conclude with the general least square adjustment in hydrogen and deuterium. This last value ($L_D(1S_{1/2}) = 8\,183.970(22)$ MHz) has the same uncertainty as that for hydrogen.

Several values of the $2S_{1/2}$ Lamb shift in hydrogen and deuterium are given in Tables 23 and 24. The first part of these tables displays the determinations deduced from the 2S–2P splitting by microwave spectroscopy or by level crossing or anisotropy methods [61,62,64,77,78]. For hydrogen, the combination of the equations (43, 44, 45) with the $1/n^3$ scaling law of the Lamb shift (Eq. (36)) yields three determinations of the $2S_{1/2}$ Lamb shift (second part of Tab. 23) with a precision equivalent to that of the direct measurements. For deuterium, a first value of the $2S_{1/2}$ Lamb shift is deduced from the isotope shift of the $2S_{1/2}$–$8D_{5/2}$ and $2S_{1/2}$–$12D_{5/2}$ transitions. These isotope shifts are mainly a mass effect. Thanks to the precise determination of the mass ratios m_p/m_e and m_d/m_p, the uncertainty in the mass effect is only 0.5 kHz. Then, from these isotope shifts, we deduce the difference between the $2S_{1/2}$ Lamb shift in deuterium and hydrogen. By using the experimental value of the $2S_{1/2}$ Lamb shift in hydrogen, we obtain finally the $2S_{1/2}$ Lamb shift in deuterium (second part of Tab. 24). To obtain the $2S_{1/2}$–$2P_{1/2}$ splitting, we use the theoretical value of the $2P_{1/2}$ Lamb shift ($L_D(2P_{1/2}) = -12.8350(3)$ MHz). These results are in very good agreement with the first measurement of Cosens [78].

Next we give the values deduced from the 1S–2S and 2S–nD optical frequency measurements. These results for the $2S_{1/2}$ Lamb shift ($L_H(2S_{1/2}) = 1\,057.8447(34)$ MHz and $L_D(2S_{1/2}) = 1\,059.2338(34)$ MHz) are independent and more precise than the direct determinations made by microwave spectroscopy. Lastly, we make

Table 24. Determination of the $2S_{1/2}$ Lamb shift in deuterium.

method and transitions involved	equations	$\nu_D(2S_{1/2}-2P_{1/2})$ (MHz)
direct measurement of the $2S_{1/2}$–$2P_{1/2}$ splitting		
$2S_{1/2}$–$2P_{1/2}$, Cosens [78]		1 059.240(33)
determination from the $2S_{1/2}$–$nD_{5/2}$ isotope shift		
2S–2P in H and 2S–8S/D in H and D	(38, 40)	1 059.234(10)
2S–2P in H and 2S–12D in H and D	(38, 40)	1 059.235(11)
2S–2P in H, 2S–8S/D and 2S–12D in H and D	(38, 40)	1 059.234(8)
comparison of the 1S–2S and 2S–nD frequencies using the $1/n^3$ scaling law		
2S–8S/D, 2S–12D, 1S–2S and $1/n^3$ law in deuterium	(37, 38, 41, 42)	1 059.234(4)
2S–8S/D, 2S–12D, 1S–2S and $1/n^3$ law in hydrogen and deuterium	(36–38, 41, 42)	1 059.2338(34)
general least squares adjustment in hydrogen and deuterium		
2S–2P, 2S–8S/D, 2S–12D, 1S–2S and $1/n^3$ law	(36–44)	1 059.2341(29)

an average of all these determinations: the results ($L_H(2S_{1/2})$ = 1 057.8450(29) MHz and $L_D(2S_{1/2})$ = 1 059.2341(29) MHz), with an uncertainty of 2.9 kHz, are the most precise to date.

For hydrogen, we compare the values of the $1S_{1/2}$ and $2S_{1/2}$ Lamb shift with theory [56] (see Tabs. 21 and 23). There is a large discrepancy, which varies from 2.4 to 5.6 standard deviations according to which value of the proton charge radius one adopts (r_p = 0.862(12) fm [41] or r_p = 0.805(11) fm [58]). This discrepancy is perhaps due to the calculation of the two-loop corrections [57]. Conversely, if we believe the calculations of the reference [56], we can deduce the radius of the proton charge distribution r_p = 0.901(16) fm.

6.4 Proton-to-electron mass ratio

In a first approximation, the isotope shift of an optical transition is proportional to $(m_e/m_p)(1 - m_p/m_d)cR_\infty$. Since the deuteron-to-proton mass ratio is known with a high accuracy (relative uncertainty of 7×10^{-10}), we could deduce the proton-to-electron mass ratio from the value of the isotope shift. In actual fact, this method is not reliable, because the corrections due to the charge distribution of the proton and deuteron are not well known. To avoid this difficulty, we consider the isotope shift Δ_{H-D} on the linear frequency combination $7\nu(2S_{1/2}-nD_{5/2}) - \nu(1S_{1/2}-2S_{1/2})$, where the Lamb shifts are eliminated using equations (36, 37). From the measurements of the $1S_{1/2}$–$2S_{1/2}$, $2S_{1/2}$–$8D_{5/2}$ and $2S_{1/2}$–$12D_{5/2}$ frequencies, we deduce the values:

$$\Delta_{H-D}(n = 8) = 796\,844.536(50) \text{ MHz}$$

$$\Delta_{H-D}(n = 12) = 851\,208.619(59) \text{ MHz}$$

where the uncertainties are mainly due to the measurements of the $2S_{1/2}$–$nD_{5/2}$ frequencies.

To sum up, we can obtain two independent values of the proton-to-electron mass ratio which are given in Table 25. The weighted mean value is m_p/m_e = 1 836.152 667(85) with a relative uncertainty of 4.6×10^{-8}. This value is in perfect agreement with the far more precise determination of Farnham *et al.* [68], and also with other previous measurements [12,79,80] (see Tab. 25).

Table 25. Determination of the proton-to-electron mass ratio.

	m_p/m_e	relative uncertainty
van Dyck *et al.* [79]	1 836.152 701(37)	2×10^{-8}
Garreau *et al.* [12]	1 836.152 59(24)	1.3×10^{-7}
Gabrielse *et al.* [80]	1 836.152 680(88)	4.8×10^{-8}
Farnham *et al.* [68]	1 836.152 6665(40)	2.2×10^{-9}
this work		
$\Delta_{H-D}(n = 8)$	1 836.152 668(115)	6.3×10^{-8}
$\Delta_{H-D}(n = 12)$	1 836.152 666(128)	7×10^{-8}
weighted mean	1 836.152 667(85)	4.6×10^{-8}

7 Conclusion

Thanks to a detailed analysis of the lineshapes of the 2S–nS/D transitions, we have obtained more reliable values of the $1S_{1/2}$ Lamb shift and of the $2S_{1/2}$–$nS_{1/2}$, –nD_J frequencies. These results have been analyzed with a least squares procedure, by taking into account several precise measurements from other groups. If we do not use the $1/n^3$ scaling law for the Lamb shift, the relative uncertainties in the Rydberg constant and the $1S_{1/2}$ Lamb shift are 10^{-11} and 3.8×10^{-6} respectively. In this case, the accuracy is limited mainly by the uncertainty in the $2S_{1/2}$ Lamb shift. To avoid this problem, we make theoretical assumptions concerning the Lamb shift. By using the $1/n^3$ scaling law between the $1S_{1/2}$ and $2S_{1/2}$ Lamb shifts, the very precise optical frequency measurements reduce the uncertainties to 9.1×10^{-12} and 3.2×10^{-6} for R_∞ and the Lamb shifts. By this means, we obtain a value of the $2S_{1/2}$ Lamb shift which is about 2.6 times more precise than the direct microwave measurement. Moreover, the same method can

be applied to deuterium. Finally, we average these different results to reduce the uncertainties in R_∞ and in the Lamb shifts to 7.7×10^{-12} and 2.7×10^{-6}. The precision is now limited by the uncertainties in the 2S–nS/D frequencies, which, in our experiment, are mainly due to the light shifts. To obtain more accurate values of these frequencies, a first possibility is to use ultracold hydrogen to increase the interaction time and decrease the light shifts [81]. In our group, we intend to measure the optical frequency of the 1S–3S transition. In this case, as the number of atoms in the 1S atomic beam is about 10^8 times larger than in the metastable atomic beam, we can observe the transition with a very small light power and, consequently, with negligible light shifts. For this experiment, we plan to compensate the second-order Doppler effect using a magnetic field perpendicular to the atomic beam [82]. As a last word, we note that a new determination of the proton radius r_p is highly desirable. The future measurement of r_p, being prepared at the Paul Scherrer Institute by spectroscopy of muonic hydrogen, should provide the opportunity to test even further the theoretical calculations of the Lamb shift [83].

The authors thank S. Bourzeix, M.D. Plimmer, F. de Tomasi and D.N. Stacey for their essential contribution to the first step of the 1S–3S experiment. They are indebted to B. Cagnac for many stimulating discussions as well as his constant interest in these projects. They thank also M. Pinard for fruitful discussions on the calculation of the theoretical line shape and D. Delande for his help in the use of the Sturmian functions and the calculation of several matrix elements of the two-photon and light shift operators. Finally, they thank again M.D. Plimmer for critical reading of manuscript. This work was partially supported by the Bureau National de Métrologie, by the Direction des Recherches et Études Techniques and by the European Community (SCIENCE cooperation Contract No. SCI*-CT92-0816 and network Contract No. CHRX-CT93-0105).

References

1. B. Cagnac, M.D. Plimmer, L. Julien, F. Biraben, Rep. Prog. Phys. **57**, 853 (1994).
2. Th. Udem, H. Huber, B. Gross, J. Reichert, M. Prevedelli, M. Weitz, T.W. Hänsch, Phys. Rev. Lett. **79**, 2646 (1997); note added in proof: a more accurate result has been recently published: J. Reichert, M. Niering, R. Holwarth, M. Weitz, Th. Udem, T.W. Hänsch, Phys. Rev. Lett. **84**, 3232 (2000).
3. A. Huber, Th. Udem, B. Gross, J. Reichert, M. Kourogi, K. Pachucki, M. Weitz, T.W. Hänsch, Phys. Rev. Lett. **80**, 468 (1998).
4. F. Nez, M.D. Plimmer, S. Bourzeix, L. Julien, F. Biraben, R. Felder, O. Acef, J.J. Zondy, P. Laurent, A. Clairon, M. Abed, Y. Millerioux, P. Juncar, Phys. Rev. Lett. **69**, 2326 (1992).
5. F. Nez, M.D. Plimmer, S. Bourzeix, L. Julien, F. Biraben, R. Felder, Y. Millerioux, P. de Natale, Europhys. Lett. **24**, 635 (1993).
6. B. de Beauvoir, F. Nez, L. Julien, B. Cagnac, F. Biraben, D. Touahri, L. Hilico, O. Acef, A. Clairon, J.J. Zondy, Phys. Rev. Lett. **78**, 440 (1997).
7. D. Touahri, O. Acef, A. Clairon, J.J. Zondy, R. Felder, L. Hilico, B. de Beauvoir, F. Biraben, F. Nez, Opt. Commun. **133**, 471 (1997).
8. C. Schwob, L. Jozefowski, B. de Beauvoir, L. Hilico, F. Nez, L. Julien, F. Biraben, O. Acef, A. Clairon, Phys. Rev. Lett. **82**, 4960 (1999).
9. S. Bourzeix, B. de Beauvoir, F. Nez, M.D. Plimmer, F. de Tomasi, L. Julien, F. Biraben, D.N. Stacey, Phys. Rev. Lett. 76, 384 (1996).
10. J.C. Garreau, M. Allegrini, L. Julien, F. Biraben, J. Phys. France **51**, 2263 (1990).
11. J.C. Garreau, M. Allegrini, L. Julien, F. Biraben, J. Phys. France **51**, 2275 (1990).
12. J.C. Garreau, M. Allegrini, L. Julien, F. Biraben, J. Phys. France **51**, 2293 (1990).
13. S. Bourzeix, M.D. Plimmer, F. Nez, L. Julien, F. Biraben, Opt. Commun. **99**, 89 (1993).
14. R.W.P. Drever, J.L. Hall, F.V. Kowalski, J. Hough, G.M. Ford, A.J. Munley, H. Ward, Appl. Phys. B **31**, 97 (1983).
15. F. Nez, Thèse de doctorat de l'université Pierre et Marie Curie, Paris, 1993.
16. F. Biraben, J.C. Garreau, L. Julien, M. Allegrini, Rev. Sci. Instrum. **61**, 1468 (1990).
17. T.W. Hänsch, B. Couillaud, Opt. Commun. **41**, 441 (1980).
18. B. Cagnac, G. Grynberg, F. Biraben, J. Phys. France **34**, 845 (1973).
19. D. Delande, private communication.
20. H.A. Bethe, E.E. Salpeter, in *Quantum mechanics of one- and two-electron atoms* (Springer-Verlag, Berlin, 1957).
21. W.J. Karzas, R. Latter, Astrophys. J. Suppl. Ser. **6**, 167 (1961).
22. G. Grynberg, B. Cagnac, F. Biraben, in *Coherent Nonlinear Optics*, edited by M.S. Feld, V.S. Letokhov (Springer-Verlag, 1980).
23. F. Biraben, M. Bassini, B. Cagnac, J. Phys. France **40**, 445 (1979).
24. J.W. Farley, W.H. Wing, Phys. Rev. A **23**, 2397 (1981).
25. B. de Beauvoir, Thèse de doctorat de l'université Pierre et Marie Curie, Paris, 1996.
26. Y Millerioux, D. Touahri, L. Hilico, A. Clairon, R. Felder, F. Biraben, B. de Beauvoir, Opt. Commun. **103**, 91 (1994).
27. L. Hilico, R. Felder, D. Touahri, O. Acef, A. Clairon, F. Biraben, Eur. Phys. J. AP **4**, 219 (1998).
28. B. de Beauvoir, F. Nez, L. Hilico, L. Julien, F. Biraben, B. Cagnac, J.J. Zondy, D. Touahri, O. Acef, A. Clairon, Eur. Phys. J. D **1**, 227 (1998).
29. A. Clairon, B. Dahmani, A. Filimon, J. Rutman, IEEE Trans. Inst. Meas. **IM34**, 265 (1985).
30. A. Clairon, B. Dahmani, O. Acef, M. Granveaud, Y.S. Domnin, S.B. Pouchkine, V.M. Tatarenkov, R. Felder, Metrologia **25**, 9 (1988).
31. G.D. Rovera, O. Acef, IEEE Trans. Inst. Meas. **48,** 571 (1999).
32. F. Nez, M.D. Plimmer, S. Bourzeix, L. Julien, F. Biraben, R. Felder, Y. Millerioux, P. de Natale, IEEE Trans. Inst. Meas. **44,** 568 (1995).
33. O. Acef, J.J. Zondy, M. Abed, G.D. Rovera, A.H. Gerard, A. Clairon, P. Laurent, Y. Millerioux, P. Juncar, Opt. Commun. **97**, 29 (1993).
34. F. Nez, F. Biraben, R. Felder, Y. Millerioux, Opt. Commun. **102**, 432 (1993).

35. R. Felder, D. Touahri, O. Acef, L. Hilico, J.J. Zondy, A. Clairon, B. de Beauvoir, F. Biraben, F. Nez, L. Julien, Y. Millerioux, Proc. SPIE **2378**, 52 (1995).
36. J.W. Heberle, H.A. Reich, P. Kusch, Phys. Rev. **101**, 612 (1956).
37. G.W.F. Drake, R.A. Swainson, Phys. Rev. A **41**, 1243 (1990).
38. J.R. Sapirstein, D.R. Yennie, in *Quantum Electrodynamics*, edited by T. Kinoshita (World Scientific, Singapore, 1990).
39. P.J. Mohr, in *Atomic, Molecular and Optical Physics Handbook*, edited by G.W.F. Drake (AIP, New-York, 1996).
40. K. Pachucki, D. Leibfreid, M. Weitz, A. Huber, W. Köning, T.W. Hänsch, J. Phys. B **29**, 177 (1996).
41. G.G. Simon, C. Schmitt, F. Borkovski, V.H. Walther, Nucl. Phys. A **333**, 381 (1980).
42. M. Weitz, A. Huber, F. Schmidt-Kaler, D. Leibfreid, W. Vassen, C. Zimmermann, K. Pachucki, T.W. Hänsch, L. Julien, F. Biraben, Phys. Rev. A **52**, 2664 (1995).
43. H.A. Reich, J.W. Heberle, P. Kusch, Phys. Rev. **104**, 1585 (1956).
44. P.J. Mohr, B.N. Taylor, Rev. Mod. Phys. **72** (to be published, 2000).
45. C. Schwob, L. Jozefowski, O. Acef, L. Hilico, B. de Beauvoir, F. Nez, L. Julien, A. Clairon, F. Biraben, IEEE Trans. Inst. Meas. **48**, 178 (1999).
46. H.R. Telle, D. Meschede, T.W. Hänsch, Opt. Lett. **15**, 532 (1990).
47. T.W. Hänsch, S.A. Lee, R. Wallenstein, C. Wieman, Phys. Rev. Lett. **34**, 307 (1975)
48. M.G. Boshier, P.E.G. Baird, C.J. Foot, E.A. Hinds, M.D. Plimmer, D.N. Stacey, J.B. Swan, D.A. Tate, D.M. Warrington, G.K. Woodgate, Nature **330**, 463 (1987); Phys. Rev. A **40**, 6169 (1989).
49. M. Weitz, A. Huber, F. Schmidt-Kaler, D. Leibfreid, T.W. Hänsch, Phys. Rev. Lett. **72**, 328 (1994).
50. D.J. Berkeland, E.A. Hinds, M.G. Boshier, Phys. Rev. Lett. **75**, 2470 (1995).
51. S. Bourzeix, B. de Beauvoir, F. Nez, F. de Tomasi, L. Julien, F. Biraben, Opt. Commun. **133**, 239 (1997).
52. K.C. Harvey, C. Fehrenbach, Rev. Sci. Instrum. **54**, 1117 (1983).
53. Y. Gontier, M. Trahin, Phys. Lett. A **36**, 463 (1971).
54. U.D. Jentschura, P.J. Mohr, G. Soff, Phys. Rev. Lett. **82**, 53 (1999).
55. K. Pachucki, Phys. Rev. Lett. **72**, 3154 (1994).
56. S. Mallampalli, J. Sapirstein, Phys. Rev. Lett. **80**, 5297 (1998).
57. I. Goidenko, L. Labzowsky, A. Nefiodov, G. Plunien, G. Soff, Phys. Rev. Lett. **83**, 2312 (1999).
58. L.N. Hand, D.J. Miller, R. Wilson, Rev. Mod. Phys. **35**, 335 (1963).
59. S.G. Karshenboim, J. Phys. B **29**, L29 (1996); Z. Phys. D **39**, 109 (1997).
60. W.E. Lamb, R.C. Retherford, Phys. Rev. **72**, 241 (1947).
61. S.R. Lundeen, F.M. Pipkin, Phys. Rev. Lett. **46**, 232 (1981).
62. E.W. Hagley, F.M. Pipkin, Phys. Rev. Lett. **72**, 1172 (1994).
63. U. Jentschura, K. Pachucki, Phys. Rev. A **54**, 1853 (1996).
64. A. van Wijngaarden, F. Holuj, G.F.W. Drake, Can. J. Phys. **76**, 95 (1998).
65. V.G. Pal'chikov, Y.L. Sokolov, V.P. Yakovlev, Metrologia **21**, 99 (1985); Phys. Scripta **55**, 33 (1997).
66. V.G. Pal'chikov, Y.L. Sokolov, V.P. Yakovlev, Sov. Phys. JETP Lett. **38**, 419 (1983).
67. S.G. Karshenboim, Sov. Phys. JETP **79**, 230 (1994).
68. D.L. Farnham, R.S. van Dyck Jr, P.B. Schwinberg, Phys. Rev. Lett. **75**, 3598 (1995).
69. G. Audi, A.H. Wapstra, Nucl. Phys. A **565**, 1 (1993).
70. E.R. Cohen, B.N. Taylor, Rev. Mod. Phys. **59**, 1121 (1987).
71. F. Biraben, J.C. Garreau, L. Julien, Europhys. Lett. **2**, 925 (1986).
72. P. Zhao, W. Lichten, H.P. Layer, J.C. Bergquist, Phys. Rev. A **34**, 5138 (1986).
73. P. Zhao, W. Lichten, H.P. Layer, J.C. Bergquist, Phys. Rev. Lett. **58**, 1293 (1987).
74. D.H. Mc Intyre, R.G. Beausoleil, C.J. Foot, E.A. Hildum, B. Couillaud, T.W. Hänsch, Phys. Rev. A **39**, 4591 (1989).
75. F. Biraben, J.C. Garreau, L. Julien, M. Allegrini, Phys. Rev. Lett. **62**, 621 (1989).
76. T. Andreae, W. Köning, R. Wynands, D. Leibfried, F. Schmidt-Kaler, C. Zimmermann, D. Meschede, T.W. Hänsch, Phys. Rev. Lett. **69**, 1923 (1992).
77. G. Newton, D.A. Andrews, P.J. Unsworth, Philos. Trans. R. Soc. Lond. **290**, 373 (1979).
78. B.L. Cosens, Phys. Rev. **173**, 49 (1968).
79. R.S. van Dyck, F.L. Moore, D.L. Farnham, P.B. Schwinberg, Bull. Am. Phys. Soc. **31**, 244 (1986).
80. G. Gabrielse, X. Fei, L.A. Orozco, R.L. Tjoelker, J. Haas, H. Kalinowsky, T.A. Trainor, W. Kells, Phys. Rev. Lett. **65**, 1317 (1990).
81. C.L. Cesar, D.G. Fried, T.C. Killian, A.D. Polcyn, J.C. Sandberg, I.A. Yu, T.J. Greytak, D. Kleppner, J.M. Doyle, Phys. Rev. Lett. **77**, 255 (1996).
82. F. Biraben, L. Julien, J. Plon, F. Nez, Europhys. Lett. **15**, 831 (1991).
83. D. Taqqu, F. Biraben, C.A.N. Conde, T.W. Hänsch, F.J. Hartmann, P. Hauser, P. Indelicato, P. Knowles, F. Kottmann, F. Mulhauser, C. Petitjean, R. Pohl, P. Rabinowitz, R. Rosenfelder, J.M.F. Santos, W. Schott, L.M. Simons, J. Veloso, Hyperfine Interact. **119**, 311 (1999).

Observation of a Motional Stark Effect to Determine the Second-Order Doppler Effect

G. Hagel, R. Battesti, F. Nez, L. Julien, and F. Biraben

Laboratoire Kastler Brossel, Département de Physique de l'Ecole Normale Supérieure, Université Pierre et Marie Curie, 4 Place Jussieu, 75252 Paris Cedex 05, France

(Received 12 April 2002; published 23 October 2002)

The high resolution two-photon spectroscopy of hydrogen is often limited by the second-order Doppler effect. To determine this effect, we apply a magnetic field perpendicular to the atomic beam. This field induces a quadratic motional Stark shift proportional, as the second-order Doppler effect, to $\mathbf{v}^2$ ($\mathbf{v}$ atomic velocity). For some magnetic field, these two effects are opposite and the total shift due to the atomic velocity is reduced. We present the first observation of this effect for the $1S$-$3S$ transition in hydrogen.

DOI: 10.1103/PhysRevLett.89.203001 PACS numbers: 32.60.+i

High resolution spectroscopy of hydrogen has been continuously improved since the first laser experiments in the 1970s. Recently, thanks to an optical frequency comb, the frequency of the $1S$-$2S$ two-photon transition has been linked to a Cs atomic fountain clock to achieve an unprecedented precision of 2×10^{-14} [1]. Nevertheless, this outstanding experiment does not conclude the metrology of hydrogen, because, in hydrogen, the analysis of the results requires at least the precise measurement of two transitions. Indeed, in a simple way, the hydrogen level energy can be expressed as the sum of two terms: the first one, given by the Dirac equation and by the first relativistic correction due to the proton recoil, is exactly known, apart from the uncertainties in the physical constants involved (the Rydberg constant, the fine structure constant, and the electron-to-proton mass ratio). The second term is the Lamb shift, which contains all the other corrections, i.e., the QED corrections, the other relativistic corrections due to the proton recoil, and the effect of the proton charge distribution. The extraction of these two contributions needs together the measurement of at least two optical transitions, and a theoretical assumption on the variation of the Lamb shifts with the principal quantum number n. The Lamb shift is important for the S levels and varies approximatively as $1/n^3$. The deviation to this scaling law has been calculated by Karshenboïm [2]. At the present time, the most precise determinations of the Rydberg constant and the Lamb shift are deduced from the measurements of the $1S$-$2S$ transition in the group of Hänsch in Garching [1] and of the $2S$-nD transitions ($n = 8$ and 12) in our group in Paris [3–5]. The precision in R_∞ is now limited by the uncertainties in the second transition, which, in the Paris experiment, are mainly due to the light shifts. To obtain more accurate values of these frequencies, a first possibility is to use ultracold hydrogen to increase the interaction time and decrease the light shifts [6,7]. In Paris, we intend to measure the optical frequency of the $1S$-$3S$ transition. In this case, as the number of atoms in a $1S$ atomic beam is about 10^8 times larger than in a metastable atomic beam, we can observe the transition with a very small light power and, consequently, with negligible light shifts. A limitation of this experiment will be the second-order Doppler effect, which induces a redshift of $-\mathbf{v}^2/2c^2$ ($\mathbf{v}$ atomic velocity, c speed of light). In this Letter, we present the first demonstration of a new method to determine the second-order Doppler shift. The basic idea is similar to the one of Ref. [8] which proposed to compensate the first-order Doppler effect by a $\mathbf{v}$ dependent light shift. Here, we produce a $\mathbf{v}^2$ dependent Stark shift which is added or subtracted to the second-order Doppler effect.

This method is convenient for the $1S$-nS (or $2S$-nS) two-photon transition in hydrogen. We consider the case where these transitions are excited in an atomic beam. The principle, proposed in Ref. [9], is to apply a transverse magnetic field $\mathbf{B}$ with respect to the direction of the atomic beam [see Fig. 1(a)]. This magnetic field produces a motional electric field which induces a quadratic Stark shift proportional, as the second-order Doppler effect, to $\mathbf{v}^2$. From the observation of this effect, we can deduce the second-order Doppler effect. In fact, the first effect of this magnetic field is a Zeeman splitting [see Fig. 1(b) for the $1S$-$3S$ transition]. The line between the hyperfine levels $1S(F = 1)$ and $1S(F = 1)$ is split in three lines (we have the selection rule $\Delta m_F = 0$) following the m_F values (-1, 0, and 1). Practically, the shift of the $m_F = \pm 1$ components is very small, because, in a first approximation, the Landé factor is the same for the $1S$ and $3S$ levels. Following a relativistic calculation, the Landé factor g_J of the $1S$ and $3S$ levels is, respectively, 2.002 284 and 2.002 315 [10]. This difference induces, for a field of 200 G, a residual Zeeman shift of ± 4.3 kHz. There is also a diamagnetic shift of about 809 Hz for the same magnetic field. On the other hand, the $m_F = 0$ component is shifted, because the Zeeman effect is not the same for the $1S(F = 1, m_F = 0)$ and $3S(F = 1, m_F = 0)$ sublevels. For 200 G, this shift is about 200 MHz.

The second effect of this magnetic field is to produce a motional electric field $\mathbf{E} = \mathbf{v} \times \mathbf{B}$ which induces a

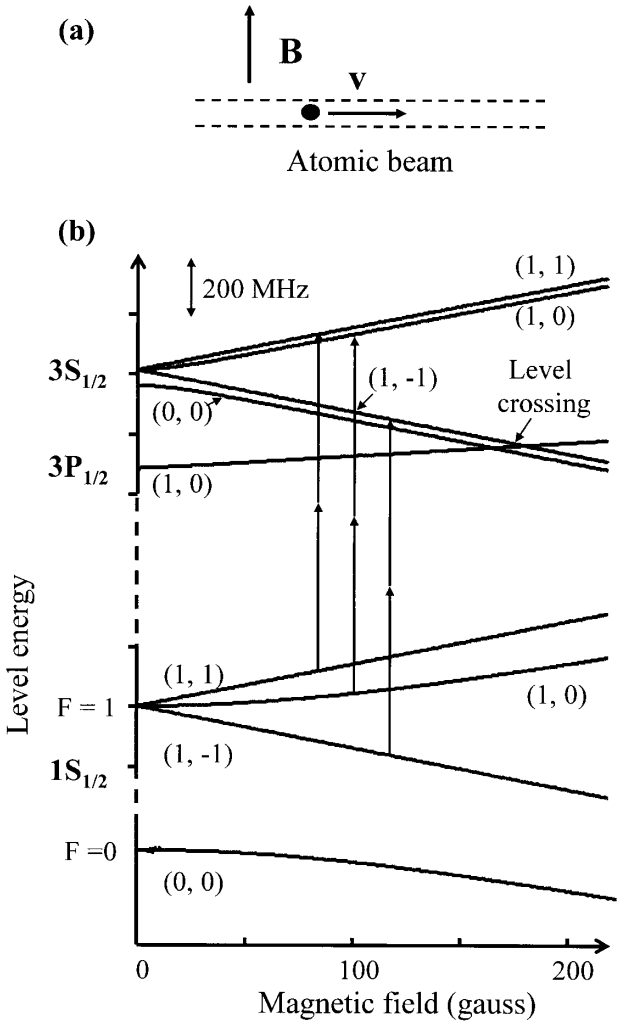

FIG. 1. (a) Experimental geometry; the atomic beam is placed in a transverse magnetic field **B** which induces a transverse electric field $\mathbf{v} \times \mathbf{B}$. (b) Zeeman's diagram of the $1S$-$3S$ transition in hydrogen. The levels are labeled by the quantum numbers (F, m_F). The $1S$-$3S(F = 1)$ line is split in three components following $m_F = 0, \pm 1$. The motional Stark effect is important, for the $1S$-$3S(F = 1, m_F = -1)$ component, around the crossing between the $3S_{1/2}(F = 1, m_F = -1)$ and $3P_{1/2}(F = 1, m_F = 0)$ levels.

coupling with the $3P_{1/2}$ and $3P_{3/2}$ levels. In the limit of a high magnetic field, the electronic and nuclear spins are decoupled. For example, in this case, the $3S_{1/2}(F = 1, m_F = -1)$ is mainly coupled to the $3P_{1/2}(F = 1, m_F = 0)$, $3P_{3/2}(F = 2, m_F = 0)$ and $3P_{3/2}(F = 2, m_F = -2)$ sublevels. This kind of motional Stark mixing is well known and, for instance, was used by Lamb and Retherford to polarize a metastable atomic beam [11]. Here, we consider the quadratic Stark effect due to this motional electric field. This shift, proportional to $\mathbf{v}^2$, is very small but is observable in the case of the $m_F = \pm 1$ line components, because the Zeeman shift of these components is negligible. In particular, this effect is important around the level crossing between the $3S_{1/2}(F = 1, m_F = -1)$ and $3P_{1/2}(F = 1, m_F = 0)$ Zeeman sublevels, which appears for a magnetic field of about 180 G [see Fig. 1(b)].

To calculate the line shape in the presence of this motional electric field, we follow the procedure described in Ref. [5]. The initial state g [the levels $1S(F = 1, m_F = \pm 1)$] is coupled by the two-photon excitation to an excited state e [here the levels $3S(F = 1, m_F = \pm 1)$]. This state e is mixed by the Stark Hamiltonian V_S with several f states (the Zeeman sublevels of the $3P_{1/2}$ and $3P_{3/2}$ states). We make the rotating wave approximation and we assume that the two-photon Rabi frequency Ω is small with respect to the natural width Γ_e and Γ_f of the excited levels ($\Omega \ll \Gamma_e, \Gamma_f$). With these hypotheses, the two-photon transition probability Γ_g is given by

$$\Gamma_g = -2\mathrm{Re}\frac{\Omega^2}{4}\left[\left(i\Delta_e - \frac{\Gamma_e}{2}\right) + \frac{1}{\hbar^2}\sum_f \frac{|V_{ef}|^2}{(i\Delta_f - \frac{\Gamma_f}{2})}\right]^{-1} \tag{1}$$

where Δ_e and Δ_f are the detunings between the laser frequency and the atomic frequencies (for instance, ω and ω_{ge} being the laser and atomic frequencies, $\Delta_e = 2\omega - \omega_{ge}$), and V_{ef} is the matrix element $\langle e|V_S|f\rangle$. In the case where the Stark coupling V_{ef} is small with respect to Γ_f, this profile presents a narrow resonance which has approximately a Lorentzian shape with a width of about $\Gamma_e/2\pi$. According to Eq. (1), Fig. 2 shows, for an atom at 3 km/s, the shifts of the $1S$-$3S(F = 1, m_F = \pm 1)$ transitions around the level crossing at 180 G. Because of the second-order Doppler effect, the line position without magnetic field (dashed line) is shifted by -146 kHz. With respect to this reference, the shift of the $1S$-$3S(F = 1, m_F = +1)$ line [curve (a)] is small (about 10 kHz), because the $3S(F = 1, m_F = +1)$ level is far from the $3P_{1/2}$ and $3P_{3/2}$ levels. On the other hand, the shift of the $1S$-$3S(F = 1, m_F = -1)$ line [curve (b)] is important around the level crossing. It has a dispersion shape and is larger than the second-order Doppler effect. Moreover, there are two values of the magnetic field (points A and B) where the second-order Doppler effect is exactly compensated by this motional Stark effect. For these values, the position of the line is independent of the atomic velocity, because the second-order Doppler effect and the motional Stark effect vary together as $\mathbf{v}^2$. Unfortunately, this effect cannot be used directly, because the $1S$-$3S(F = 1, m_F = \pm 1)$ lines are not separated (the motional Stark effect is small with respect to the $3S$ natural width $\Gamma_e/2\pi \simeq 1$ MHz). Curve (c) shows the barycenter of these two lines (defined as the center at the half maximum). Though reduced by a factor of 2, the dispersion amplitude is about 230 kHz, and the compensation of the second-order Doppler effect is still 73% for a magnetic field of 170 G. Our goal is to observe this effect to deduce the second-order Doppler effect.

The experimental setup to observe the $1S$-$3S$ transition has been described elsewhere [5,12]. The main difficulty of this experiment is the production of the excitation

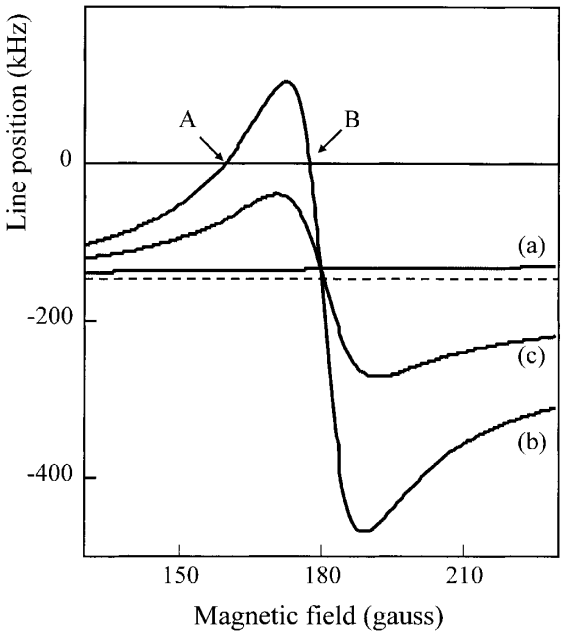

FIG. 2. Motional Stark effect of the $1S$-$3S$ transition versus the magnetic field (calculation for an atom at a velocity of 3 km/s). Zero: line position for an atom at rest; dashed line: line position without magnetic field. Curves (*a*) and (*b*): line position of the $1S$-$3S(F = 1, m_F = +1)$ and $1S$-$3S(F = 1, m_F = -1)$ components. In A and B, the second-order Doppler effect of the $1S$-$3S(F = 1, m_F = -1)$ component is exactly compensated by the motional Stark effect. Curve (*c*): global motional Stark effect for the two components $1S$-$3S(F = 1, m_F = \pm 1)$.

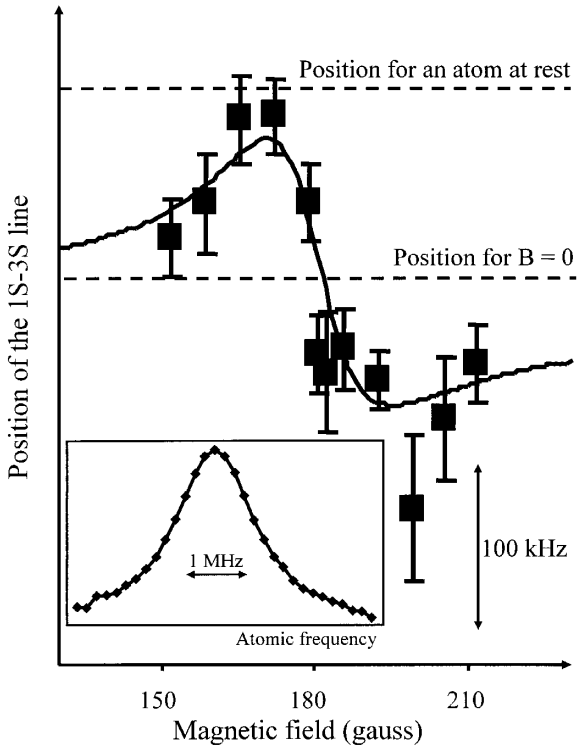

FIG. 3. Motional Stark effect of the $1S$-$3S(F = 1, m_F = \pm 1)$ components; experiment (■) and best fit of the theoretical calculations (solid line). In the inset, hydrogen two-photon spectra of the $1S$-$3S$ transition.

wavelength in the UV, at 205 nm. We use a titanium-sapphire laser at 820 nm, with two frequency doubling stages by a LBO (lithium tri-borate) and a BBO (beta-barium borate) crystal [13,14]. The $1S$-$3S$ transition is produced in a horizontal thermal $1S$ atomic beam colinear with the UV beams. The atoms are obtained from molecular hydrogen by a radio frequency discharge. To increase the UV intensity, the atomic beam is placed inside a linear buildup cavity. Inside the cavity, the UV power is at best 10 mW and is focused with a waist of 48 μm. To detect the $1S$-$3S$ excitation, we monitor the Balmer-α fluorescence due to the radiative decay $3S$-$2P$. The size of the detection region is 1.3 cm. Since our first experiment [12], we have modified the detection system and improved the signal to noise ratio by a factor of 15. The inset of Fig. 3 shows an example $1S$-$3S$ recording. The signal amplitude is about 100 counts/s and the experimental linewidth is 1.6 MHz (in terms of atomic frequency). The main contributions to the width are the $3S$ natural width (1 MHz) and a frequency broadening due to an overmodulation of the length of the enhancement cavity which surrounds the BBO crystal [14]. The statistical uncertainty on the line position is now 8 kHz (in terms of atomic frequency) for an acquisition time of 1 h, i.e., a relative uncertainty of 2.7×10^{-12}. Two water cooled coils, approximately in Helmoltz configuration, produce a vertical magnetic field up to 220 G. In the detection region, the field homogeneity is about 10^{-3}. This field is calibrated by measuring the Zeeman shift of the $1S$-$3S(F = 1, m_F = 0)$ component. As the motional Stark effect is small (about 10 kHz in terms of laser frequency at 820 nm), the titanium-sapphire laser is actively stabilized. The laser frequency is locked to a first Fabry-Perot cavity to reduce its frequency jitter to a level of a few kHz. The long term stability is assured by a second Fabry-Perot cavity which transfers the stability of a standard (either an iodine stabilized He-Ne laser, or a rubidium stabilized diode laser at 778 nm [15]) to the titanium-sapphire laser. With this setup, described in Ref. [5], the absolute laser frequency stability is about 3 kHz (24 kHz in terms of atomic frequency, because of the two doubling stages and the two-photon excitation).

To observe the motional Stark effect, we precisely measure the position of the $1S$-$3S(F = 1, m_F = \pm 1)$ components. To reduce the effect of the laser frequency drift, we alternate the measurements with and without the magnetic field, the line position for $\mathbf{B} = 0$ being the frequency reference. The results are reported in Fig. 3. In this figure, each point corresponds to a typical acquisition time of 2 h. The motional stark shift has effectively a dispersion shape around the level crossing. At the extrema, this shift is about 100 kHz, i.e., 10% of the $3S$ natural width. To deduce the velocity distribution and the

second-order Doppler shift, we have adjusted these data with a theoretical curve (solid line in Fig. 3). This calculation is more complete than Eq. (1). As the energy splitting between the $1S(F = 1, m_F = \pm 1)$ sublevels is, for a magnetic field of 200 G, about 10^4 times smaller than the thermal energy, we suppose that the populations of these levels are equal. We make the exact diagonalization of the Zeeman Hamiltonian. To obtain the $1S$-$3S$ line shape, we calculate the Balmer-α florescence from together the $3S$ level and the $3P$ level (because of the Stark coupling, there is an excitation of the $3P$ level which contributes to the experimental signal). Moreover, we make the summation on the atomic velocity distribution and, in the line shape, we take into account the second-order Doppler effect. The atomic velocity distribution of a hydrogen beam produced by a radio frequency discharge dissociator has been studied by Jaduszliwer *et al.* [16]. In our experimental conditions (dissociator pressure in the range of 0.4 T), we can assume that this distribution is close to the Maxwellian form $v^3 \exp -v^2/2\sigma^2$ (for a thermal atomic beam, $\sigma = \sqrt{kT/M}$, T temperature, M atomic mass). The theoretical curve in Fig. 3 is adjusted on the experimental data by varying σ. The best fit gives $\sigma = 1.55(11)$ km/s and a beam temperature of 290 K. From these results, we can deduce a value of the second-order Doppler effect $\delta = -116(17)$ kHz. This value is in agreement with the estimation made previously [$\delta = -124(10)$ kHz] [5,12]. The dependence of this analysis with the atomic velocity distribution is slight. For instance, with a speed distribution of the form $v^4 \exp -v^2/2\sigma^2$, we obtain $\delta = -112(13)$ kHz.

Although the uncertainty of this determination of δ is large with respect to our goal (our purpose is to measure the $1S$-$3S$ frequency with an accuracy of 1 kHz, i.e., a relative uncertainty of 3.4×10^{-13}), this method is promising for two reasons. (i) The measurement of the motional Stark effect can be easily improved by making absolute frequency measurements of the line position. Indeed, the drift of the laser frequency during the acquisition time induces a large part of the noise in Fig. 3. With the new techniques using a femtosecond frequency comb [17], the laser frequency will be measured with a precision better than 10^{-13}. Then, the measurement of the motional Stark effect will be made quickly and more precisely. (ii) We plan to use the partial compensation of the second-order Doppler effect around 170 G. For an absolute frequency measurement made for this magnetic field, the shift due to the velocity of the atoms is reduced by about a factor of 4. With the data of Fig. 3, we deduce a velocity correction of only $-30(5)$ kHz, corresponding to a relative uncertainty of 1.7×10^{-12} for a $1S$-$3S$ measurement. In the future, the procedure will be to measure the optical frequency of the line for the two extrema of the dispersion curve of Fig. 3, and for a zero magnetic field. From these data, we will be able to deduce together the second-order Doppler effect and the exact position of the $1S$-$3S$ transition.

To conclude, we have deduced the second-order Doppler effect from the observation of a motional Stark effect. Moreover, there is a partial compensation between the second-order Doppler effect and the motional Stark shift which reduces the shifts due to the atomic velocity. This method is easier to be implemented than the cooling of a hydrogen atomic beam or the production of ultracold hydrogen in a trap. Thanks to this method, we plan to measure the absolute frequency of the $1S$-$3S$ transition with an uncertainty of 1 kHz and to reduce the uncertainty in the $1S$ Lamb shift to 11 kHz, and that in the Rydberg constant to 4×10^{-12}.

The Laboratoire Kastler Brossel is a laboratory of the Ecole Normale Supérieure and the Université Pierre et Marie Curie, Unité Mixte de Recherche du CNRS (UMR8552). This work was partially supported by the Bureau National de Métrologie.

[1] M. Niering *et al.*, Phys. Rev. Lett. **84**, 5496 (2000).
[2] S. G. Karshenboïm, J. Phys. B **29**, L29 (1996); Z. Phys. D **39**, 109 (1997).
[3] B. de Beauvoir, F. Nez, L. Julien, B. Cagnac, F. Biraben, D. Touahri, L. Hilico, O. Acef, A. Clairon, and J. J. Zondy, Phys. Rev. Lett. **78**, 440 (1997).
[4] C. Schwob, L. Jozefowski, B. de Beauvoir, L. Hilico, F. Nez, L. Julien, F. Biraben, O. Acef, and A. Clairon, Phys. Rev. Lett. **82**, 4960 (1999).
[5] B. de Beauvoir, C. Schwob, O. Acef, J.-J. Zondy, L. Jozefowski, L. Hilico, F. Nez, L. Julien, A. Clairon, and F. Biraben, Eur. Phys. J. D **12**, 61–93 (2000).
[6] C. L. Cesar, D. G. Fried, T. C. Killian, A. D. Polcyn, J. C. Sandberg, I. A. Yu, T. J. Greytak, D. Kleppner, and J. M. Doyle, Phys. Rev. Lett. **77**, 255 (1996).
[7] L. Willmann and D. Kleppner, in *The Hydrogen Atom, Precision Physics of Simple Atomic Systems*, edited by S. G. Karshenboïm, F. S. Pavone, G. F. Bassani, M. Inguscio, and T. W. Hänsch, Lecture Notes in Physics Vol. 570 (Springer, Berlin, New York, 2001), pp. 42–56.
[8] S. Reynaud, M. Himbert, J. Dalibard, J. Dupont-Roc, and C. Cohen-Tannoudji, Opt. Commun. **42**, 39 (1982).
[9] F. Biraben, L. Julien, J. Plon, and F. Nez, Europhys. Lett. **15**, 831 (1991).
[10] P. Indelicato (private communication).
[11] W. E. Lamb, Jr. and R. C. Retherford, Phys. Rev. **79**, 549 (1950).
[12] S. Bourzeix, B. de Beauvoir, F. Nez, M. D. Plimmer, F. de Tomasi, L. Julien, F. Biraben, and D. N. Stacey, Phys. Rev. Lett. **76**, 384 (1996).
[13] S. Bourzeix, M. D. Plimmer, F. Nez, L. Julien, and F. Biraben, Opt. Commun. **99**, 89–94 (1993).
[14] S. Bourzeix, B. de Beauvoir, F. Nez, F. de Tomasi, L. Julien, and F. Biraben, Opt. Commun. **133**, 239 (1997).
[15] D. Touahri, O. Acef, A. Clairon, J. J. Zondy, R. Felder, L. Hilico, B. de Beauvoir, F. Biraben, and F. Nez, Opt. Commun. **133**, 471 (1997).
[16] B. Jaduszliwer and Y. C. Chan, Rev. Sci. Instrum. **65**, 2028 (1994).
[17] S. A. Diddams *et al.*, Phys. Rev. Lett. **84**, 5102 (2000).

Bloch Oscillations of Ultracold Atoms: A Tool for a Metrological Determination of h/m_{Rb}

Rémy Battesti,[1] Pierre Cladé,[1] Saïda Guellati-Khélifa,[2] Catherine Schwob,[1] Benoît Grémaud,[1] François Nez,[1] Lucile Julien,[1] and François Biraben[1]

[1]*Laboratoire Kastler Brossel, Ecole Normale Supérieure, CNRS-UMR 8552, UPMC, 4 place Jussieu, 75252 Paris Cedex 05, France*
[2]*BNM-INM, Conservatoire National des Arts et Métiers, 292 rue Saint Martin, 75141 Paris Cedex 03, France*

(Received 17 November 2003; published 22 June 2004)

We use Bloch oscillations in a horizontal moving standing wave to transfer a large number of photon recoils to atoms with a high efficiency (99.5% per cycle). By measuring the photon recoil of ^{87}Rb, using velocity-selective Raman transitions to select a subrecoil velocity class and to measure the final accelerated velocity class, we have determined h/m_{Rb} with a relative precision of 0.4 ppm. To exploit the high momentum transfer efficiency of our method, we are developing a vertical standing wave setup. This will allow us to measure h/m_{Rb} better than 10^{-8} and hence the fine structure constant α with an uncertainty close to the most accurate value coming from the $(g-2)$ determination.

DOI: 10.1103/PhysRevLett.92.253001 PACS numbers: 32.80.Pj, 06.20.Jr, 32.80.Qk, 42.50.Vk

In the past 20 years, atom manipulation using laser light has led to the emergence of many powerful techniques [1]. In particular, it is now possible to observe and measure elementary processes between light and atoms, such as a coherent momentum transfer (absorption and emission of a single photon). Furthermore, by increasing the interrogation time, laser cooling leads to an improvement of more than 2 orders of magnitude in both stability and accuracy in many fields of high precision measurements [2,3]. These advances allow us to measure precisely the recoil velocity v_r of the atom absorbing or emitting a photon ($v_r = \hbar k/m$, where k is the wave vector of the photon absorbed by the atom of mass m). Such a measurement yields a determination of h/m which can be used to infer a value for the fine structure constant α via [4]

$$\alpha^2 = \frac{2R_\infty}{c}\frac{M}{M_e}\frac{h}{m}. \tag{1}$$

M and m are, respectively, the mass of test particle in atomic and SI units. In this expression several terms are known with a very small uncertainty: 8×10^{-12} for the Rydberg constant R_∞ [5,6] and 7×10^{-10} for the electron mass M_e [7,8]. A recent measurement using Penning trap single ion spectrometry allows a determination of M_{Rb} with an uncertainty less than 2×10^{-10} [9]. In short, the determination of α using this formula is now limited by the uncertainty in the ratio h/m [4].

The fine structure constant can be deduced from experiments related to different branches of physics (QED, solid state physics,...) [10–15]. Many of these measurements lead to determinations of α with a relative uncertainty on the order of 10^{-8} but their total dispersion exceeds 10^{-7} [16]. In order to test the validity of these different measurements, a new accurate determination of α is highly desirable.

The recoil of an atom when it absorbs a photon was first observed in the recoil-induced spectral doubling of the CH_4 saturated absorption peaks [17]. Since then, almost all recent measurements of the recoil velocity have been based on atomic interferometry [18] using stimulated Raman transitions between two hyperfine ground state levels [19,21]. The precision of these experiments is increased by giving additional photon recoils to the different interferometer paths. In this process, the efficiency of the recoil transfer is a crucial parameter. Recently, the Chu group at Stanford, using a coherent adiabatic transfer technique [20] and high intensity Raman pulses, has achieved an efficiency of 94%, allowing a total momentum transfer of 120 recoils, and hence an absolute accuracy of 7.4 parts per 1×10^9 in α [21]. Pritchard and colleagues had developed another tool for a determination of h/m_{Na}, using a Bose-Einstein condensate as a bright subrecoil atom source in the "contrast interferometry" technique [22]. This experiment seems, presently, to be limited by the low momentum transfers.

In this Letter we investigate the phenomena of Bloch oscillations of atoms driven by a constant inertial force in a periodic optical potential [23]. This method is based on stimulated Raman transitions, induced by counterpropagating laser beams, involving only one hyperfine level in order to modify the atomic momentum, thus leaving the internal state unchanged. The atoms are coherently accelerated using a frequency-chirped standing wave. In order to compensate the Doppler effect, the frequency difference between the two beams is increased linearly. Consequently, the atoms are resonant with the beams periodically. This leads to a succession of rapid adiabatic passages between momentum states differing by $2\hbar k$ ($2v_r$ in terms of velocity). As explained above, the final accuracy is determined by the number of additional recoils, which strongly depends on the efficiency population transfer between momentum states. In our experiment, we achieve an efficiency of 99.5% per Bloch oscillation;

which may provide a great opportunity for high precision measurement of the recoil shift.

The details of the experiment have been described previously [24]. The setup for the laser cooling uses a magneto-optical trap (MOT) in a rubidium vapor cell. After a few seconds, the MOT is loaded and then the magnetic field is switched off, leaving the atoms to equilibrate in an optical molasses, at a temperature of about 3 μK. The sequence then involves three steps (see Fig. 1): first, we select a narrow subrecoil velocity class with a well-defined mean initial velocity using a Raman velocity-selective π pulse [25]. Next, we transfer $2N$ photon recoils by a coherent acceleration of atoms (Bloch oscillations). Finally, we measure the final velocity class, using another Raman velocity-selective π pulse.

For the initial selection and the final measurement, the two Raman beams are generated by two master oscillatory power amplifiers (MOPAs) injected by two grating-stabilized extended-cavity laser diodes (ECLs). One of the two diodes is frequency stabilized on a highly stable Zerodur Fabry-Perot cavity (ZFPC). This cavity was calibrated using different optical references, allowing a determination of the laser frequency with an accuracy better than 10 MHz (3×10^{-8}). A heterodyne signal and a frequency chain around the rubidium hyperfine splitting (6.8 GHz) are used to phase lock the second ECL to the first one. All auxiliary sources in the frequency chain are referenced to the same stable 10 MHz quartz oscillator. To

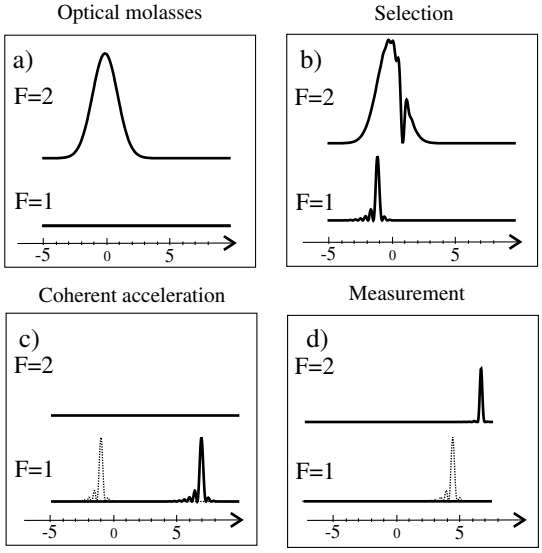

FIG. 1. Evolution of the velocity distribution (in v_r unit) during the experiment: (a) Initial velocity distribution; the atoms are in $5^2S_{1/2}$, $|F = 2, m_F = 0\rangle$ state. (b) Subrecoil selection; the atoms are transferred from $5^2S_{1/2}$, $|F = 2, m_F = 0\rangle$ to $5^2S_{1/2}$, $|F = 1, m_F = 0\rangle$. (c) Coherent acceleration for $N = 4$ Bloch oscillations; the atoms are in $5^2S_{1/2}$, $|F = 1, m_F = 0\rangle$. (d) Measurement of the final velocity class; the atoms are transferred from $5^2S_{1/2}$, $|F = 1, m_F = 0\rangle$ to $5^2S_{1/2}$, $|F = 2, m_F = 0\rangle$.

reduce spontaneous emission and light shift, the ECLs are detuned by about 340 GHz from the D2 line. The MOPA beams are sent through two 80 MHz acousto-optic modulators for timing and intensity control. Their radio frequencies are also referenced to the 10 MHz quartz oscillator. The two beams are coupled in an optical fiber; they have linear orthogonal polarizations, and their intensities are actively stabilized.

In order to perform the selection phase, we use a square Raman pulse with a frequency initially fixed at δ_{select}. For a detuning of 340 GHz and an intensity of 120 mW/cm^2, the π condition is achieved using a $T = 1.7$ ms pulse. Such a pulse transfers atoms from state $5^2S_{1/2}$, $|F = 2, m_F = 0\rangle$ to $5^2S_{1/2}$, $|F = 1, m_F = 0\rangle$, with a velocity dispersion of about $v_r/30$ centered around $(\lambda\delta_{\text{select}}/2) - v_r$ where λ is the laser wavelength. In this horizontal geometry, the width of the transferred velocity class, which is proportional to $1/T$, is limited only by the fall of the atoms through the lasers beams. The value of T represents a good compromise between resolution (the width of the selected velocity distribution) and the signal-to-noise ratio (proportional to the number of selected atoms).

After the Raman selection process, a beam resonant with $5^2S_{1/2}$, $F = 2$ to $5^2P_{3/2}$, $F = 3$ cycling transition pushes away atoms remaining in the state $F = 2$. The selected atoms are then exposed to two counterpropagating beams generated by a Ti:sapphire laser whose frequency is also stabilized to the ZFPC. This laser beam is split in two, each beam passing through an acousto-optic modulator to control its frequency. In order to perform a coherent acceleration, we vary the frequency difference between the two Bloch beams linearly with time: $\Delta\nu(t) = 2at/\lambda$ where a is the effective acceleration. The two beams are superimposed onto the horizontal optical axis of the selection Raman beams using the same optical fibers. The two Bloch beams have the same linear polarization, equal intensity (160 mW for each beam), and are red detuned by 100 GHz from the $5^2S_{1/2}$ to $5^2P_{3/2}$ resonance line. The duration of the acceleration process is typically 4.4 ms. The optical potential is adiabatically turned on in about 300 μs.

In the case where the constant inertial force seen by the atoms is weak enough, all the selected atoms are accelerated. In a Bloch oscillation scheme, this is equivalent to avoiding interband transitions. This condition may be expressed in the weak binding limit [26] by

$$\pi \frac{d\Delta\nu(t)}{dt} \ll \left(\frac{U_0}{2\hbar}\right)^2, \tag{2}$$

where U_0 is the depth of the potential induced by the light shift due to the standing wave. In this limit, the interband transition rate per Bloch period is given by a Landau-Zener formula $R = e^{(-a_c/a)}$ where a_c is the critical acceleration, proportional to $(U_0/E_r)^2$ (E_r is the recoil energy) [23]. In our experiment U_0 is about $11E_r$ and atoms

acceleration is 133 ms^{-2}, leading to a theoretical efficiency of 99.9% per oscillation.

After the acceleration process we perform the final velocity measurement using another Raman π pulse, whose frequency is $\delta_{\mathrm{measure}}$. Population transfer from the hyperfine state $F = 1$ to the hyperfine state $F = 2$ due to the second Raman pulse is maximal when $2\pi(\delta_{\mathrm{select}} - \delta_{\mathrm{measure}}) = 2N(\mathbf{k}_1 - \mathbf{k}_2) \cdot \mathbf{k}_{\mathrm{Bloch}} \hbar / m_{\mathrm{Rb}}$, where $\mathbf{k}_1$, $\mathbf{k}_2$, and $\mathbf{k}_{\mathrm{Bloch}}$ are, respectively, the wave vectors of the Raman and Bloch beams. The populations ($F = 1$ and $F = 2$) are measured separately by using the one-dimensional time of flight technique developed for atomic clocks and depicted in [27]. The detection zone is 15 cm below the center of the trap (Fig. 2). To avoid the horizontal motion of the atoms, and in order for the atoms to reach the detection zone, a symmetric acceleration-deceleration scheme is used: instead of selecting atoms at rest, we first accelerate them to $2N v_r$, using N Bloch oscillations. We then make the three step sequence: selection, coherent deceleration (N Bloch oscillations), and measurement, according to Fig. 1.

Figure. 2(b) shows a typical time of flight signal for $F = 2$ (left peak) and $F = 1$ (right peak) when the second Raman frequency is centered at the top of the final velocity distribution. In this figure, we present the signal for $N = 0$ and for $N = 40$ Bloch oscillations. Comparing the number of atoms between the two situations, we demonstrate that the losses during the Bloch acceleration for $N = 40$ are less than 20%, corresponding to a transfer efficiency of about 99.5% per oscillation. These losses are not due to the spontaneous emission, which is evaluated to 0.1% per oscillation, but probably to the residual horizontal displacement of the atoms (about 5 mm) after the acceleration-deceleration process.

To reduce systematic errors, we perform an alternate and symmetric recoil transfer in both horizontal opposite directions. We determine the recoil frequency by a differential measurement of the center of the two final velocity distributions. Figure 3 shows a typical scan of final velocity distribution for $N = 50$ Bloch oscillations for both directions. Each of the 400 data points corresponds to a single cycle (cooling, selection, acceleration of $2N v_r$, and measure). From a data analysis of 200 points (10 min) we can split the final velocity distribution with an uncertainty of $v_r/5000$. Hence, the relative uncertainty of the measurement of v_r is 1.5×10^{-6}.

Figure 4 shows, chronologically, 43 determinations of h/m_{Rb} using such measurements, compared to the expected value of h/m_{Rb}, using the CODATA 98 value of α. The mean value lies 6.1×10^{-7} above the expected value with a relative uncertainty of 4.2×10^{-7}.

We have estimated errors from wave front curvature (1.3 ppb), differential light shift (80 ppb), Zeeman effect (57 ppb), and laser frequencies (52 ppb). They are an order

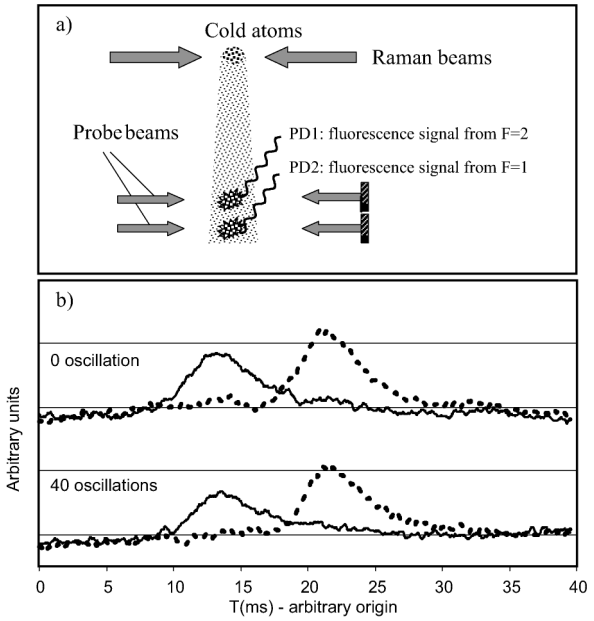

FIG. 2. (a) Experimental scheme. (b) Time of flight signal for $N = 0$ and $N = 40$ Bloch oscillations. The dashed line corresponds to the signal for the $F = 1$ atoms and the solid line for the $F = 2$ atoms, which are transferred from the hyperfine state $F = 1$ by the second Raman pulse. After 40 Bloch oscillations the time of flight signal remains almost unchanged, emphasizing thus the high efficiency transfer of our experiment. The analysis of these signals gives the number of atoms in each hyperfine state.

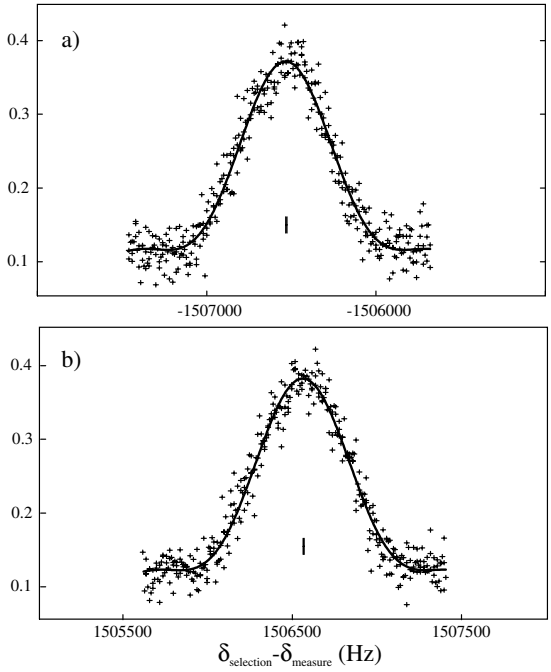

FIG. 3. Final velocity distribution for 50 Bloch oscillations, in both directions: (a) around $2N v_r$ and (b) around $-2N v_r$. The center of the final velocity distribution can be located with an uncertainty of 3 Hz. The photon recoil frequency deduced from these two measurements is 15066.690(23) Hz.

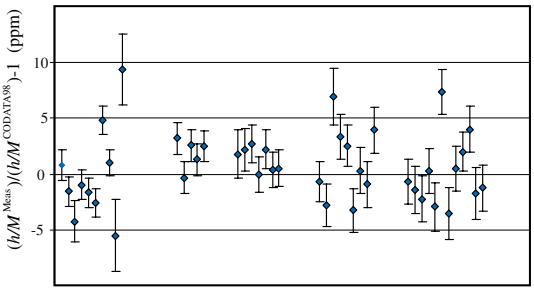

FIG. 4 (color online). Chronological display of the data taken for $N = 50$ Bloch oscillations in both directions. The mean deviation from the expected value is $6.1(4.2) \times 10^{-7}$, with $\chi^2 = 99$.

of magnitude lower compared to this disagreement. We believe that this disagreement and the dispersion of the results ($\chi^2 = 99$ for 43 measurements) can be explained by the systematic variations of the initial velocity distribution of the cold cloud and the phase fluctuation of the Raman beams. These effects have not yet been quantified.

In conclusion, we have demonstrated that coherent acceleration using Bloch oscillations is a powerful method to transfer a large number of additional photon recoils to atoms. In the horizontal scheme, the number of momentum recoil transfers is limited by the fall of atoms. In order to take advantage of the high transfer efficiency of the Bloch oscillation technique, we plan to build a setup with vertical Bloch and Raman beams. In this case, the number of additional recoils will be limited by the transverse motion, and we can increase the π pulse duration in order to select a narrower velocity class. Moreover, due to the gravitational acceleration g, the vertical motion is more complicated and this geometry provides scope for two different experiments: either the atoms are accelerated by a moving standing wave as in the horizontal scheme, or they are placed in a pure standing wave. In this case, the atoms oscillate around the same position at the frequency $mg/2\hbar k$ [24]. Furthermore, there is no significant displacement of the atom between the velocity selection and measurement, and, thus, several systematic effects are reduced. On the other hand, a precise determination of the local gravity field is required to fully exploit this technique. Finally, we expect to increase the number of transferred recoils up to $N = 500$, to obtain a determination of v_r with an uncertainty better than 10^{-8}, leading to a determination of α with an uncertainty of about 5 ppb, close to the more accurate value deduced from $(g - 2)$ [11,12,16]

We thank A. Clairon, C. Salomon, and J. Dalibard for valuable discussions. This experiment is supported in part by the Bureau National de Métrologie (Contract No. 993009) and by the Région Ile de France (Contract No. SESAME E1220).

[1] S. Chu, C. Cohen-Tannoudji, and W. D. Phillips, Rev. Mod. Phys. **70**, 685–741 (1998).
[2] G. Santarelli *et al.*, Phys. Rev. Lett. **82**, 4619 (1999).
[3] C.W. Oates, K. R. Vogel, and J. L. Hall, Phys. Rev. Lett. **76**, 2866 (1996).
[4] B. N. Taylor, Metrologia **31**, 181 (1994).
[5] C. Schwob, L. Jozefowski, B. de Beauvoir, L. Hilico, F. Nez, L. Julien, F. Biraben, O. Acef, and A. Clairon, Phys. Rev. Lett. **82**, 4960 (1999).
[6] Th. Udem, A. Huber, B. Gross, J. Reichert, M. Prevedelli, M. Weitz, and T.W. Hänsch, Phys. Rev. Lett. **79**, 2646 (1997).
[7] D. L. Farnham, R. S. Van Dyck, and P. B. Schwinberg, Phys. Rev. Lett. **75**, 3598 (1995).
[8] T. Beier *et al.*, Phys. Rev. Lett. **88**, 011603 (2002).
[9] M. P. Bradley, J.V. Porto, S. Rainville, J. K. Thompson, and D. E. Pritchard, Phys. Rev. Lett. **83**, 4510 (1999).
[10] W. Liu *et al.*, Phys. Rev. Lett. **82**, 711 (1999).
[11] T. Kinoshita, IEEE Trans. Instrum. Meas. **46**, 108 (1997).
[12] R. S. Van Dyck, P. B. Schwinberg, and H. G. Dehmelt, Phys. Rev. Lett. **59**, 26 (1987).
[13] E. Krüger, W. Nistler, and W. Weirauch, Metrologia **36**, 147 (1999).
[14] J. Q. Shields, R. F. Dziuba, and H. P. Layer, IEEE Trans. Instrum. Meas. **38**, 249 (1989).
[15] A. M. Jeffery, R. E. Elmquist, L. H. Lee, J. Q. Shields, and R. F. Dziuba, IEEE Trans. Instrum. Meas. **46**, 264 (1997).
[16] P. Mohr and B. Taylor, CODATA recommended values of the fundamental constants: 1998, Rev. Mod. Phys. **72**, 351 (2000).
[17] J. L. Hall, C. J. Bordé, and K. Uehara, Phys. Rev. Lett. **37**, 1339 (1976).
[18] C. J. Bordé, Phys. Lett. A **140**, 10 (1989).
[19] B. Young, M. Kasevich, and S. Chu, *Atom Interferometry*, edited by P. R. Berman (Academic, New York, 1997), p. 363.
[20] M. Weitz, B. C. Young, and S. Chu, Phys. Rev. Lett. **73**, 2563 (1994).
[21] A. Wicht, J. M. Hensley, E. Sarajlic, and S. Chu, in *Proceedings of the 6th Symposium on Frequency Standards and Metrology*, edited by P. Gill (World Scientific, Singapore, 2001), pp. 193–212.
[22] S. Gupta, K. Dieckmann, Z. Hadzibabic, and D. E. Pritchard, Phys. Rev. Lett. **89**, 140401 (2002).
[23] M. Ben Dahan, E. Peik, J. Reichel, Y. Castin, and C. Salomon, Phys. Rev. Lett. **76**, 4508 (1996).
[24] R. Battesti, P. Cladé, S. Guellati-Khélifa, C. Schwob, B. Grémaud, F. Nez, L. Julien, and F. Biraben, J. Opt. B **5**, S178-S182 (2003).
[25] M. Kasevich, D. S. Weiss, E. Riis, K. Moler, S. Kasapi, and S. Chu, Phys. Rev. Lett. **66**, 2297 (1991).
[26] E. Peik, M. Ben Dahan, I. Bouchoule, Y. Castin, and C. Salomon, Phys. Rev. A **55**, 2989 (1997).
[27] A. Clairon, P. Laurent, G. Santarelli, S. Ghezali, S. N. Lea, and M. Bahoura, IEEE Trans. Instrum. Meas. **44**, 128 (1995).

The muonic hydrogen Lamb shift experiment

R. Pohl, A. Antognini, F.D. Amaro, F. Biraben, J.M.R. Cardoso, C.A.N. Conde, A. Dax, S. Dhawan, L.M.P. Fernandes, T.W. Hänsch, F.J. Hartmann, V.W. Hughes, O. Huot, P. Indelicato, L. Julien, P.E. Knowles, F. Kottmann, Y.-W. Liu, L. Ludhova, C.M.B. Monteiro, F. Mulhauser, F. Nez, P. Rabinowitz, J.M.F. dos Santos, L.A. Schaller, C. Schwob, D. Taqqu, and J.F.C.A. Veloso

Abstract: The charge radius of the proton, the simplest nucleus, is known from electron scattering experiments only with a surprisingly low precision of about 2%. The poor knowledge of the proton charge radius restricts tests of bound–state QED to the precision level of about 6×10^{-6}, although the experimental data themselves (1S-Lamb shift in hydrogen) have reached a precision of 2×10^{-6}. The determination of the proton charge radius with an accuracy of 10^{-3} is the main goal of our experiment, opening a way to check bound–state QED predictions to a level of 10^{-7}. The principle is to measure the $2S - 2P$ energy difference in muonic hydrogen (μ^-p) by infrared laser spectroscopy. First data were taken in the 2nd half of 2003. Muons from our unique very low energy muon beam are stopped at a rate of ~ 100 s^{-1} in 0.6 mbar H_2 gas where the lifetime of the formed $\mu p(2S)$ atoms is about 1.3 μs. An incoming muon triggers a pulsed multi–stage laser system which delivers ~ 0.2 mJ at $\lambda \approx 6$ μm. Following the laser excitation $\mu p(2S) \rightarrow \mu p(2P)$ we observe the 1.9 keV x-rays from $2P - 1S$ transitions using large area avalanche photodiodes. The resonance frequency, and hence the Lamb shift and the proton radius, is determined by measuring the intensity of these x-rays as a functin of the laser wavelength. A broad range of laser frequencies was scanned in 2003 and the analysis is currently under way.

PACS Nos.: 36.10.Dr, 14.20.Dh, 42.62.Fi

Received xxx, 2004. Accepted yyy, 2004.

R. Pohl, A. Antognini, and T.W. Hänsch. Max–Planck–Institut für Quantenoptik, DE–85748 Garching, Germany
F.D. Amaro, J.M.R. Cardoso, C.A.N. Conde, L.M.P. Fernandes, C.M.B. Monteiro, J.M.F. dos Santos, and J.F.C.A. Veloso. Departamento de Fisica, Universidade de Coimbra, PT–3000 Coimbra, Portugal
F. Biraben, P. Indelicato, L. Julien, F. Nez, and C. Schwob. Laboratoire Kastler Brossel, FR–75252 Paris CEDEX 05, France
A. Dax, S. Dhawan, and V.W. Hughes. Physics Department, Yale University, New Haven, CT 06520–8121, USA
F.J. Hartmann. Physik–Department, Technische Universität München, DE–85747 Garching, Germany
O. Huot, P.E. Knowles, L. Ludhova, F. Mulhauser, and L.A. Schaller. Département de Physique de l'Université, CH–1700 Fribourg, Switzerland
F. Kottmann. Institut für Teilchenphysik, ETH–Hönggerberg, CH–8093 Zürich, Switzerland
Y.-W. Liu. Department of Physics, National Tsing Hua University, Hsinchu 300, Taiwan
P. Rabinowitz. Department of Chemistry, Princeton University, Princeton, NJ 08544–1009, USA
D. Taqqu. Paul Scherrer Institute, CH–5232 Villigen PSI, Switzerland

 DOI: 10.1139/Z*xx-xxx*

Résumé : French version of abstract (supplied by CJP)

[Traduit par la rédaction]

1. Introduction

The steady progress in the measurement of the Lamb shift in hydrogen and hydrogen–like atoms stimulated improvements of the methods of its calculation in the framework of bound–state quantum electrodynamics, and vice versa [1, 2]. It is now mainly the uncertainty of the proton charge radius r_p which limits the comparison of theory with experiment. Knowledge of r_p which does not depend on this theory comes from electron scattering experiments. A recent reanalysis of all available scattering data, considering also Coulomb corrections [3], results in a value of $r_p = 0.895(18)$ fm [4], i.e. the relative uncertainty is 2%. A determination of the proton radius with 10^{-3} relative accuracy is possible by measuring the $2S$ Lamb shift in muonic hydrogen (μp). The μp Lamb shift, $\Delta E_{2P-2S} \approx 0.2$ eV, is dominated by vacuum polarization which shifts the $2S$ binding energy towards more negative values. The μp fine- and hyperfine splittings are an order of magnitude smaller than the Lamb shift. The relative contribution of the proton size to ΔE_{2P-2S} is as much as 2%, two orders of magnitude more than for normal hydrogen. Measuring the μp Lamb shift and combining it with precision hydrogen spectroscopy will ultimately lead to a test of bound–state QED approaching the level of 10^{-7}.

Precise calculations of ΔE_{2P-2S} are available for a few years now [2, 5, 6]. They include contributions on the level of some ppm, like three–loop vacuum polarization (0.008 meV) [7] and hadronic vacuum polarization (0.011 meV) [8]. Relatively large uncertainties come from yet uncalculated light–by–light scattering terms, as discussed in ref. [9], but a calculation of these terms seems to be feasible as it was done, e.g., for muonic helium [10]. The $2S$-hyperfine splitting was recently investigated by Martynenko [11], reducing the uncertainty due to the proton structure (Zemach correction) to 0.008 meV for the $2S$-hfs which corresponds to only 0.002 meV for our $2S - 2P$ transition. Disregarding terms which depend on the proton radius, the calculated ΔE_{2P-2S}-value will finally be limited to the 10-20 ppm precision level by the uncertainty of the proton polarization shift (0.013 meV [12], 0.012 ± 0.002 meV [6], 0.017 ± 0.004 meV [13], 0.016 meV [14]).

An experiment is going on at the Paul Scherrer Institute (PSI), Switzerland, to determine the $2S$ Lamb shift in muonic hydrogen [15]. Our aim is to measure the energy difference $\Delta E(2\,^5P_{3/2} - 2\,^3S_{1/2})$ by laser spectroscopy ($\lambda \approx 6\,\mu$m) to a precision of 30 ppm (10% of the natural line width which is given by the $2P$-lifetime) and to deduce the proton charge radius with 10^{-3} relative accuracy, 20 times more precise than presently known. The various parts of the apparatus were taken into operation in 2002 and further improved in summer 2003. Data were taken towards the end of 2003 with the whole setup in operation, including the 6 μm laser system. A search for the $2S - 2P$ resonance line at various laser wavelengths was performed.

The principle of the experiment is to stop negative muons in H_2 gas where highly excited μp atoms are formed. Most of them deexcite quickly to the ground state, but $\sim 1\%$ form long–lived μp_{2S} atoms [16]. A short laser pulse with a wavelength tunable around $\lambda \approx 6\,\mu$m (corresponding to ΔE_{2P-2S}) is sent to a mirror cavity surrounding the target gas volume, about $1\,\mu$s after the muon stop. A resonance curve will be obtained by measuring at different laser wavelengths the number of $2P - 1S$ transitions (1.9 keV x-rays) which occur in time–coincidence with the laser pulse[1].

The metastability of μp_{2S} atoms at low gas pressures was investigated in a previous experiment [16]. A component of μp_{1S} atoms with kinetic energies as high as 900 eV was measured. It originates from resonant molecule formation from the $2S$-state and subsequent autodissociation [17]

$$\mu p(2S) + H_2 \rightarrow \{[(pp\mu)^+]^* pee\}^* \rightarrow \mu p(1S) + p + \ldots + 1.9\,\mathrm{keV}\,. \qquad (1)$$

[1] The $2P$-lifetime $\tau_{2P} = 8.6$ ps is negligibly short.

This collisional quenching process puts serious requirements on both the muon beam and the laser system. The fastest laser response time, i.e. delay time between muon stop and laser pulse, we can currently achieve with conventional laser technology is $\sim 1.5\,\mu$s. This means we have to work at a H_2 gas pressure as low as 0.6 hPa (at room temperature), where the $2S$-lifetime[2] is about 1.3 μs. Such a low target gas pressure makes it difficult to stop muons efficiently in the small volume of a laser enhancement cavity. A new muon beam was therefore developed at PSI.

The experimental setup is described in some detail in the following chapter 2, where we also present some raw data. The laser system is discussed in chapter 3, chapter 4 explains how the laser frequency is measured. The enhancement cavity is presented in chapter 5, and some conclusions are given in chapter 6.

2. Experimental setup

The essential parts of the apparatus are the muon beam line, the x-ray detectors, and the laser system. A new low–energy negative–muon beam line at PSI yields an order of magnitude more muon stops in a small low–density gas volume than a conventional muon beam line. Large area avalanche photo–diodes (LAAPD) are used as x-ray detectors for the 2 keV Lyman transitions of the μp atoms. A multistage excimer–dye–Ti:sapphire–Raman laser system provides laser pulses at 6 μm wavelength. A mirror–cavity surrounding the muon stop volume enhances the $2S - 2P$ transition probability.

The new beam line consists of the cyclotron trap for the production of low energy muons [18], the muon extraction channel (a curved solenoid) for the transport and the selection of these muons [15], and a 1 m long solenoid with the gas target and two transmission detectors for the muons. Fig. 1 shows the main components inside the solenoid. Two stacks of ultra–thin carbon foils ($d = 4$ μg/cm^2) are the key element of a fast detector for keV-muons [19]. The few electrons released by a muon crossing the carbon foils are accelerated in the electric field of the stacks and detected by plastic scintillators read out by photo–multiplier tubes (PM_1, PM_2). The $\vec{E} \times \vec{B}$ separator shifts the slow muons by about 10 mm downwards whereas the faster electrons nearly follow the magnetic field lines. The measured detection efficiencies are 87% for Stack 1 and 42% for Stack 2. A beam collimator restricts the beam size to 5×15 mm^2. The rate of muons detected in a time–of–flight coincidence corresponding to kinetic energies of 3-6 keV is 300 s^{-1}. These muons provide a trigger signal for the pulsed laser and the data acquisition system.

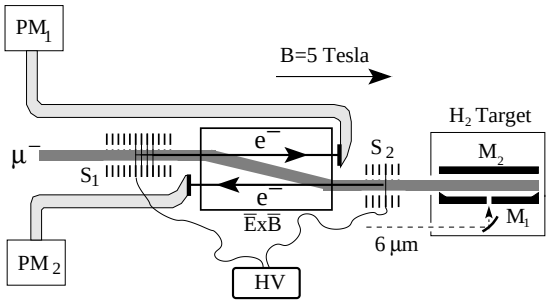

Fig. 1. Schematic view of the central part of the apparatus. The setup is mounted inside a solenoid providing an axial magnetic field of 5 Tesla, and is kept at high vacuum. The muons enter from the left and cross two stacks of ultra–thin carbon foils, S_1 and S_2, which act together with PM_1 and PM_2 as a muon detector. The $\vec{E} \times \vec{B}$ filter separates μ^- from e^-. The gas target is filled with 0.6 hPa H_2 gas. The 6 μm laser light enters the vacuum vessel and the gas target and reaches the multi–pass mirror cavity (M_1, M_2) through a hole in M_1.

[2] This was measured [16] using the time distributions of 900 eV-μp_{1S} atoms created by reaction (1).

The muon stop volume has to be as small as possible in order to match the requirements of high laser–induced $2S - 2P$ transition probability and large solid angle for the x-ray detectors. The gas target with x-ray detectors and mirror cavity (see Fig. 1) is therefore mounted in a superconducting solenoid (1 m long, 20 cm inner diameter, $B = 5$ Tesla), which keeps the transverse muon beam size to the value given by the beam collimator. The gas target has windows for the muon beam (30 nm thick Formvar foils supported by 15 μm thick wires), for the x-ray detectors (1.5 μm polypropylene foils), and a CaF_2 window for the entrance of the infrared laser beam. The target cell has to be relatively long in beam direction since the corresponding muon stop distribution extends over more than 20 cm. Using suitably shaped mirrors for the multi–pass cavity a volume of $7 \times 15 \times 170\,\mathrm{mm}^3$ is irradiated by the 6 μm laser light with good homogeneity.

Large area avalanche photodiodes (LAAPD) are used as x-ray detectors. With a depletion depth exceeding 10 μm and a very thin dead layer they achieve efficient and fast detection of 1-5 keV x-rays [20, 21]. They are insensitive to magnetic fields of 5 Tesla [22]. Standard APDs have a relatively small ratio of sensitive area to physical area, limiting the usable solid angle when arranged to form large detector planes. We are using therefore LAAPDs from RMD [23] which are fabricated by a novel planar process resulting in a square–shaped sensitive area surrounded by only thin borders of inactive material [24].

20 LAAPDs (each with 13.5 mm$\times$13.5 mm sensitive area) are mounted on top and bottom of the target vessel, in two face–to–face rows of 10 devices, at a vertical distance of only 8 mm from the muon beam center. The 20 LAAPDs are cooled down to -30^o C to achieve an optimal energy resolution and signal–to–noise ratio. The typical bias voltage is around 1600 V and the corresponding gain of order 400. The signals are amplified and stored in an 8-bit waveform digitizer operated at 140 MHz. This allows an optimal suppression of background signals with non–standard shape and the separation of two consecutive superimposed pulses in the offline analysis.

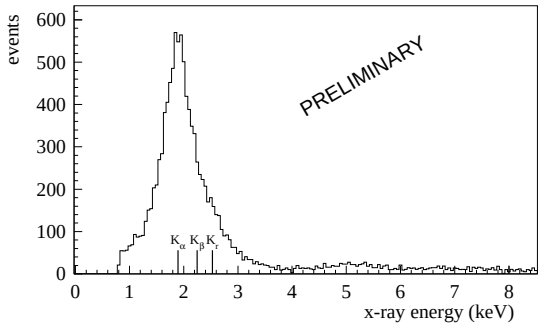

Fig. 2. Energy spectrum of muonic hydrogen K-line transitions measured at 0.6 hPa H_2 gas pressure for a typical run of 1.2 hours. The energy resolution is approximately 30% (FWHM) at 2 keV. The small peak at 5 keV is muonic carbon.

Data were taken during the 2003 beam period. Fig. 2 shows the sum of the energy spectra measured with the LAAPDs for a measuring time of 1.2 h. The energy resolution is $\Delta E/E \approx 30\,\%$ (FWHM) at 2 keV.

The corresponding time spectrum measured for x-rays with energies in the interval 1.4-2.2 keV is shown in Fig. 3. The background at delayed times is quite low. In particular, there are only 1-2 events/hour in the time interval 1.3-1.5 μs where the laser–induced signals will occur. A further reduction of the background is expected from more restrictive cuts. The number of "good" laser events on resonance is expected to be also 1-2 per hour, i.e. the effect/background ratio will be of order 1.

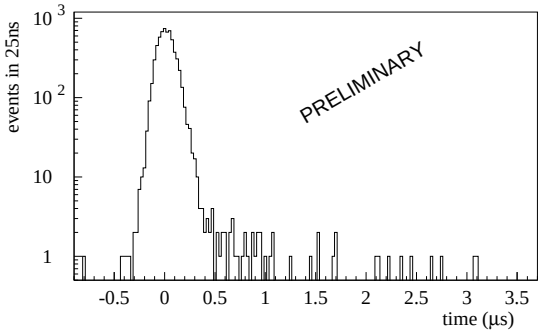

Fig. 3. Time spectrum measured **without laser** at 0.6 hPa H_2 gas pressure. Selected are x-ray energies between 1.4 and 2.2 keV. The "prompt" peak contains 6233 events, 11 events occurred in the time interval [1-2 μs]. The measuring time was 1.2 h.

3. The laser system

The muonic hydrogen Lamb shift experiment puts severe requirements on its laser system. The most stringent one is caused by the time structure of available muon beams. At PSI there are only continuous muon beams, whereas pulsed muon sources available elsewhere are not intense enough. The laser has therefore to be triggerable on the muons entering the apparatus at stochastic times, with a short delay of the order of 1 μs (due to the 1.3 μs lifetime of the $2S$ state at 0.6 hPa pressure), and with a dead time as short as possible.

The scan–range required for the laser is from 6.00 to 6.03 μm according to the uncertainty in the proton radius. The laser bandwidth has to be small compared to the natural $2S-2P$ transition line width of 18 GHz, i.e., of the order of 1 GHz. The energy density needed to saturate the $2S-2P$ transition is 16.5 mJ/cm^2, a density obtained in the mirror cavity where the μp atoms are formed, if the 6 μm pulse has an energy of ~ 0.2 mJ at the cavity entrance. Reliability of the whole system during the measuring time of several weeks is essential.

No tunable and fast triggerable laser which can provide sufficient energy in the 6 μm region is commercially available. A home–built system was therefore developed whose main components are shown in Fig. 4.

Two high power XeCl excimer lasers provide the pump energy (350 mJ each) for the whole system. Their pulses have a delay of ~ 1 μs relative to the trigger signal. Each excimer is pumping a two–stage multimode non–tunable dye laser which converts the 308 nm excimer laser pulses to green light pulses of 45 mJ at 540 nm. Coumarin 153 dissolved in ethanol is used since it is the laser dye with the longest lifetime in the blue–green spectral region. Methanol was also used as solvent but it caused a formation of a white layer on the Bethune cell tube walls of the oscillator which dramatically reduced the output energy. A further factor of two enhancement of the dye lifetime is achieved by dissolving a triplet quencher (DABCO) in the dye solution. 30 liters of this solution are used per day during data taking.

The dye lasers pump an injection–seeded oscillator–amplifier titanium sapphire (Ti:Sa) laser operated at 708 nm. The wavelength tunability and bandwidth of the Ti:Sa oscillator, and therefore of the subsequent amplifier and 6 μm light, is controlled by a single–mode cw–Ti:Sa laser stabilized on a calibrated Fabry–Perot (FP) cavity. The short length of the Ti:Sa oscillator cavity (7 cm) results in a pulse width of 7 ns with a delay of 56 ns and a pulse energy of 1.2 mJ. The amplifier is an eight pass system which provides TEM_{00}-pulses with 12 mJ output energy and 6 ns width.

The wavelength is then converted from the visible to the infrared using a third–Stokes Raman shifter operated with 14 bar H_2 gas [25]. The frequency of the 708 nm photons from the Ti:Sa laser is shifted three times via exciting H_2 molecules from their vibrational ground state $v=0$ to $v=1$,

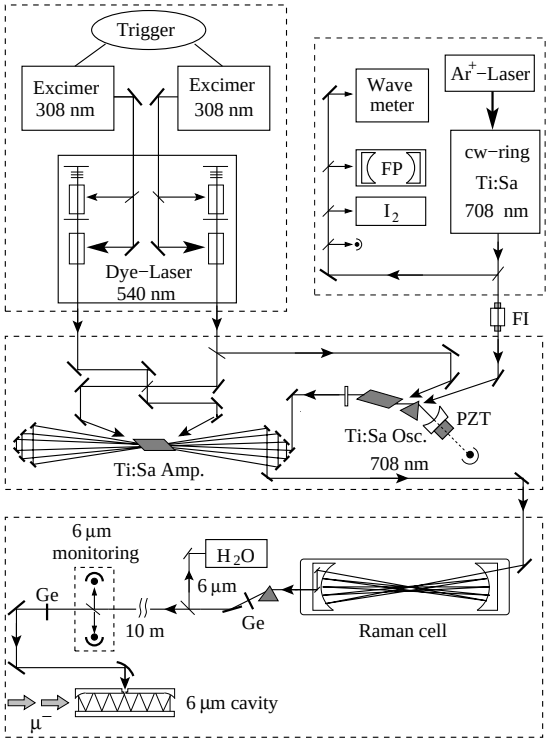

Fig. 4. Schematic view of the laser system. The main components are a pulsed excimer–dye laser system, a tunable cw Ti:Sa laser, a pulsed oscillator–amplifi er Ti:Sa laser, a Raman cell, and a 6 μm mirror cavity with its diagnostic system. FP: Fabry–Perot, I_2: iodine absorption cell, H_2O: water absorption cell cell, PZT: piezo transducer, FI: Faraday Isolator.

passing through 1.00 μm (first Stokes), 1.72 μm (second Stokes) to 6.02 μm. To enhance the conversion efficiency the laser light is reflected 33 times between two spherical copper mirrors (1 m radius of curvature, with 1.93 m spacing) which have a measured reflectivity of 97.7 % at 708 nm. At our conditions, the Raman process is optimal with ~ 4 ns long TEM_{00} mode input pulses. The 6 ns Ti:Sa output pulse length reasonably matches the requirements of the Raman process. The Raman shifter yields 0.2 mJ at 6 μm for 12 mJ input pulses.

The infrared light is transported over a 12 m long path to the mirror cavity inside the 5 Tesla solenoid where the muons are stopped. The 6 μm beam line was flushed with dry N_2 gas to avoid absorption by water vapor. Two mirrors located on the left and right side of the muon stop volume are forming a non–resonant 6 μm cavity. One of the mirrors has a hole of 630 μm diameter, where the laser light enters, and also partially exits the cavity. This leaking light is guided to an infrared detector which gives a diagnosis of the light circulating inside the cavity.

4. Frequency calibration of the 6 μm light

Calibration of the 6 μm laser wavelength is performed via measuring a water absorption line. The line at 6.014 μm (1662.80968(7) cm^{-1}) labeled “37” in Ref. [26] is scanned by tuning the cw–laser at 708 nm. This measurement allows a direct wavelength calibration at 6 μm regardless of possible systematic shifts in the various stages from the 708 nm cw–light to the 6 μm region. The cw–laser is referenced to a Fabry–Perot cavity with a free spectral range of 1.5 GHz and a long term stability of

better than 10 MHz. A wavemeter is used to unambiguously determine the FP fringe number.

The 6 μm light traverses a 37 cm long cell filled with air at 55 hPa and H_2O at a partial pressure of 1.0(5) hPa. Additional measurements were performed at 20 and 3 hPa. Figure 5 shows the transmitted 6 μm laser beam intensity versus the cw–Ti:Sa laser frequency referenced relative to a FP fringe. The

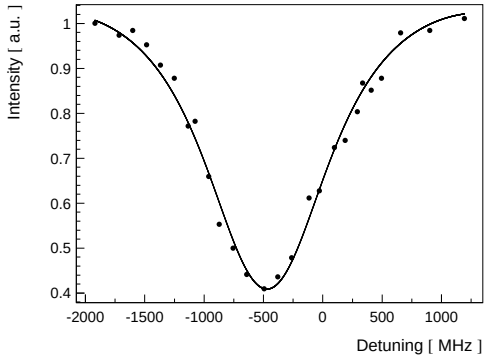

Fig. 5. Wavelength calibration of the 6 μm light by means of a water line absorption measurement. The intensity transmitted through a 37 cm long cell filled with 55 hPa air is plotted versus frequency relative to a Fabry–Perot fringe at 708 nm.

absorption line is fit taking into account saturation effects and pressure as well as Doppler broadening, leaving as free parameters the position and amplitude of the line and the spectral bandwidth of the laser light.

The resulting position is (-470 ± 50) MHz relative to the FP fringe and the laser bandwidth about 700 MHz (FWHM). For the Lamb shift measurement the resonance is scanned by locking the cw–laser on various FP fringes. The laser has to be tuned by less than 100 FP fringes from the water calibration line to cover the whole anticipated $2S - 2P$ resonance region. The FP free spectral range is known with an accuracy of about 1 kHz at 708 nm. Therefore, the uncertainty of the 6 μm wavelength over the whole scanning region is about 50 MHz.

5. 6 μm multipass cavity

The 6 μm light is coupled into an intensity enhancement cavity, placed inside the hydrogen target for the excitation of the $2S - 2P$ transition. Fig. 6 shows the geometry of the mirror cavity. The design considers the muon stopping volume ($15 \times 7 \times 170\,\mathrm{mm}^3$) and the location of the x-ray detectors at only ± 8 mm vertical distance (y-direction) from the muon beam axis. The full stopping volume has to be illuminated quite homogeneously.

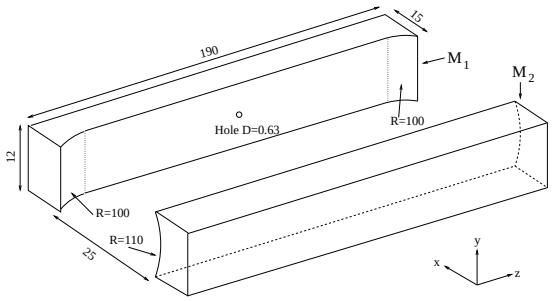

Fig. 6. Cartoon of the 6 μm multi–pass cavity. Dimensions are given in mm.

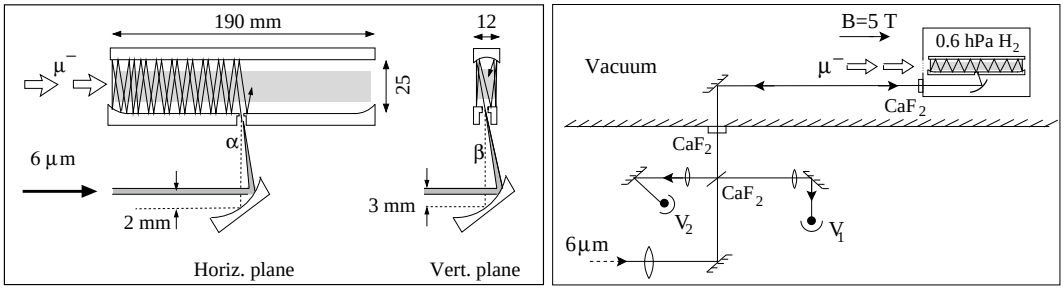

Fig. 7. *(Left)* Off–axis coupling into the 6 μm cavity with $\alpha = 40$ mrad and $\beta = 60$ mrad. The 2-inch focal length of the parabolic gold coated mirror focuses the 6 μm beam to the center of the 0.63 mm diameter hole.
(Right) Monitoring system for the 6 μm cavity. Before entering the vacuum system 5% of the 6 μm light is reflected by a 45 $^\circ$ CaF_2 plate and focused on a fast infrared detector V_1. The transmitted pulse crosses the CaF_2 vacuum and target windows and enters the cavity. Part of the light escaping from the entrance hole travels back on the same axis as the incoming light and is detected with a second infrared detector V_2. V_1 and V_2 are monitoring respectively the input pulse (6 μm production) and the time distribution inside the cavity.

Laser light enters the cavity through a 0.63 mm diameter hole (Fig. 6) and is reflected between the two mirrors on the order of a thousand times. The cylindrical mirror M_2 confines the light in the vertical direction, whereas the two cylindrical pieces added to the flat mirror M_1 guarantee the confinement in the horizontal direction. Calculations show that the radius of curvature R_1 has to be four times the mirror spacing d ($R_1 = 4d = 100$ mm), in order to avoid an increase of the mean horizontal reflection angle. Simultaneously, the radius of curvature R_2 of the cylindrical mirror M_2 has to be different from R_1, to avoid undesired resonant effects. R_2 is chosen to be 110 mm. The substrate material used is fused silica, and a broadband reflectivity of 99.97% at 6 μm is achieved using a dielectric coating of ZnSe and ThF_4 with 26 layers [27].

The 6 μm light is guided by Cu mirrors and CaF_2 lenses to the multi–pass cavity (see Fig. 7). To optimize the illuminated volume and minimize the losses through reflection from mirror M_2 back out the injection hole, the light is injected off–axis at an angle of 40 mrad with respect to the horizontal and 65 mrad with respect to the vertical direction.

Our approach of a non–resonant hole–coupling cavity reduces the constraints on the overall system alignment. It allows for relative simple alignment procedures and lowers the sensitivity to vibrations and misalignment. No servo alignment elements operated in vacuum and high magnetic fields are needed. A simulation of the cavity based on a geometrical–ray approach shows that mirror tilts as large as 7 mrad (vertically) and 0.5 mrad (horizontally) are tolerable. The resulting spatial intensity distribution shows a 30% non–uniformity in the transverse direction whereas it is nearly uniform longitudinally, satisfying the requirements of the Lamb shift experiment.

The main cavity losses are given by the non–ideal reflectivity of the mirrors and by the light escaping from the coupling hole. This light can be used to monitor the time distribution of the intensity inside the cavity, allowing an overall alignment of the system. It is separated with a tilted CaF_2 plate from the entering light and focused on a fast infrared detector (Hg-Cd-Zn-Te semiconductor [28]) as shown in Fig. 7.

The measured intensity time distribution is shown in Fig. 8. An average lifetime of 140 ns for the light in cavity can be deduced. This corresponds to 1700 reflections between the two mirrors which is in good agreement with the simulations.

Since the time integrated spatial intensity distribution is about homogeneous, the fluence is approximately given by $E_{\rm in}^{\rm laser} n_{\rm refl}/A_{\rm cav}$, where $E_{\rm in}^{\rm laser}$ is the pulse energy entering the cavity, $n_{\rm refl} = 1700$ the measured average number of reflections, and $A_{\rm cav} = 17 \times 0.7$ cm^2 the illuminated transverse cavity

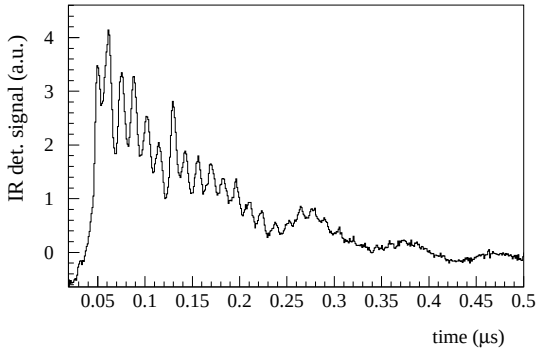

Fig. 8. Measured signal of the light leaving the cavity. An average lifetime of approximately 140 ns corresponds to an average number of 1700 reflections.

area. A 6 μm laser pulse energy of 0.12 mJ is therefore sufficient to saturate the $2S - 2P$ transition (corresponding to a fluence of 16.5 mJ/cm^2). Taking into account various losses on the beam path from the Raman cell to the cavity, about 0.2 mJ are required at the Raman cell exit to saturate the transition.

6. Conclusions

Data were taken in the last 3 weeks of the 2003 beam time. A total of 2×10^7 laser shots was achieved. The laser was operated at 14 different wavelengths corresponding to values between 0.85 and 0.91 fm for the proton radius. Analysis of the data is underway.

Acknowledgments

This work was performed at the Paul Scherrer Institute, Switzerland. We acknowledge support from the Swiss National Science Foundation, the Swiss Academy of Engineering Sciences, BQR de l'UFR de physique fondamentale et appliqu´ee de l'Universit´e Paris 6, the program PAI Germaine de Sta¨el n°07819NH du ministère des affaires ètrang´eres France, Portuguese Foundation for Science and Technology (FCT), and the US department of energy.

The authors would like to thank: L. Simons and B. Leoni for setting up the cyclotron trap and Z. Hochman for technical support; T. Gerber with his Reaction Analysis Group, and R. Bombach for providing us laser components and helpful advice; H.-J. Kluge and W. N¨orthersh¨auser of GSI Darmstadt for providing us dye pumps, excimer and Ar$^+$ lasers; R. Zenobi and A. Renn of the Department of Chemistry at Swiss Federal Institute of Technology in Zurich (Switzerland) for providing us a dye pump and an Ar$^+$ laser; and H. van Den Bergh of the Swiss Federal Institute of Technology in Lausanne (Switzerland) for an excimer laser.

The principle design of the laser system was proposed by H.P. von Arb. We thank also the PSI accelerator division, the workshop, Hallendienst, and other support groups for their valuable help.

References

1. B. de Beauvoir et al., Eur. Phys. J. D **12**, 61 (2000).
2. M.I. Eides, H. Grotch and V.A. Shelyuto, Phys. Rep. **342**, 63 (2001).
3. R. Rosenfelder, Phys. Lett. B **479**, 381 (2000).
4. I. Sick, Phys. Lett. B **576**, 62 (2003).
5. K. Pachucki, Phys. Rev. A **53**, 2092 (1996).
6. K. Pachucki, Phys. Rev. A **60**, 3593 (1999).

7. T. Kinoshita and M. Nio, Phys. Rev. Lett. **82**, 3240 (1999).
8. J.L. Friar et al., Phys. Rev. A **59**, 4061 (1999).
9. P. Indelicato et al., in *Proc. of the Int. Workshop on Exotic Atoms (EXA02)*, ed. by P. Kienle et al. (Austrian Acad. of Sciences, Vienna 2003), p. 61.
10. E. Borie and G.A. Rinker, Phys. Rev. A **18**, 324 (1978).
11. A.P. Martynenko, preprint hep-ph/0409107 (2004).
12. S.A. Srartsev et al., Phys. Atom. Nucl. **23**, 1233 (1976).
13. R. Rosenfelder, Phys. Lett. B **463**, 317 (1999).
14. R.N. Faustov and A.P. Martynenko, AIP Conf. Proc. **564**, 277 (2001).
15. F. Kottmann et al., in *Proc. of the Int. Workshop on Exotic Atoms (EXA02)*, ed. by P. Kienle et al. (Austrian Acad. of Sciences, Vienna 2003), p. 159.
16. R. Pohl et al., Hyperf. Int. **138**, 35 (2001).
17. J. Wallenius et al., Hyperf. Int. **138**, 285 (2001).
18. P. de Cecco et al., Nucl. Instrum. Meth. A **394**, 287 (1997).
19. M. Mühlbauer et al., Hyperf. Int. **119**, 305 (1999).
20. M. Boucher et al., Nucl. Instrum. Meth. A **505**, 136 (2003).
21. L.M.P. Fernandes et al., IEEE Trans. Nucl. Sci. **51**, 1575 (2004).
22. L.M.P. Fernandes et al., Nucl. Instrum. Meth. A **498**, 362 (2003).
23. *Radiation Monitoring Devices (RMD), Inc.*, Watertown, MA 02472, USA.
24. R. Farrell et al., Nucl. Instrum. Meth. A **442**, 171 (2000).
25. P. Rabinowitz et al., IEEE J. Quant. Electr. **22**, 797 (1986).
26. R. Poth et al., J. of Mol. Spect. **190**, 379 (1998).
27. *LohnStar Optics*, Escondido, CA 92029, USA.
28. *VIGO Systems*, PL-01-318 Warsaw, Poland.